A study of turbulent flows and curved jets including application of the laser Doppler anemometry technique.

Marion Joyce Hawkins

A STUDY OF TURBULENT FLOWS AND CURVED JETS INCLUDING APPLICATION OF THE LASER DOPPLER ANEMOMETRY TECHNIQUE

by

MARION JOYCE HAWKINS
B.Sc.(Dunelm), C.Eng., M.I.Mech.E., M.R.Ae.S.

School of Engineering and Applied Science
University of Durham

A thesis submitted for the degree of Doctor of Philosophy
of the University of Durham

OCTOBER 1988

Dedicated to my dear sister,

NANCIE

ABSTRACT

This project concerns the successful application of a laser Doppler anemometry system to two highly turbulent flow situations. A sudden expansion in a circular pipe and an axisymmetric convex curved wall jet have been investigated.

The subsystems of the LDA, data acquisition and data processing sections were fully investigated to identify and quantify or eliminate all sources of error and bias. Particular attention was paid to arrival rate (*velocity*) bias and signal amplitude bias. The experiments, all performed in the sudden expansion situation, provided inconclusive results on these effects but showed the most significant feature to be the sampling mode employed. The use of hardware windowing ensured that truly ergodic sampling was attained and maintained. This had the additional advantage of eliminating arrival rate bias. The optimised system subsequently provided highly repeatable data, scatter held to within 2%.

Velocity and turbulence intensity profiles were obtained at six axial locations downstream of the sudden expansion. These and the derived stream function contours agreed well with previously published comparable data, confirming the system and operating techniques used.

A model Coanda flare measurement rig was designed and commissioned. A detailed survey of this example of a convex curved jet flow was completed, providing measurements of streamline, radial and transverse velocities, normal and shear stresses. Full use was made of the versatility of the LDA system and the flow rig thereby providing a certain amount of data redundancy. This offered the opportunity for a rigorous statistical analysis of the data. The resulting confidence intervals for the 95% limit confirmed the high quality of the LDA measurements. The influence of streamline curvature and divergence on the flow structure was noted by the three-fold increases in normal and shear stress values compared to the equivalent plane wall jet.

The measurements were used as test cases for the commercial computer package PHOENICS. The standard k-ε and mixing-length models were run and modifications were introduced to the latter to account for streamline curvature and divergence features of the Coanda flare configuration. The sudden expansion k-ε predictions showed reasonable agreement with experimental data. Poorer predictions were obtained for the curved jet flow but they served to illustrate the potential of PHOENICS to be tuned for a specific physical situation, via modifications to the basic models.

ACKNOWLEDGEMENTS

Inevitably, in a long-term project of this nature, there are a great many people who have contributed to its success and to whom I am indebted.

Especial gratitude is due to my supervisor, Dr. Gregory-Smith, for his invaluable and unfailing encouragement and support throughout the project. To Dr. King, also, go thanks for sharing his great store of knowledge on LDA.

I am grateful to the Science and Engineering Research Council for providing the funding for the project and to SEAS for supporting my attendance at conferences in Manchester and Lisbon.

Much help was provided by Terry Brown and the technicians of the School's workshop; notably David Jenkins and Stewart Watson for their fabrication of, and rapid repairs to, the Coanda flare flowrig. Thanks are also due to Ray Mand and Mike Page of the thermo-fluids laboratory and to Trevor Nancarrow of the computer laboratory.

Fellow-postgraduates have provided technical and moral support.

Finally, for my parents' totally-biased affection I have unlimited gratitude. They have shared in both the traumatic stages and also the rewarding aspects of the research.

CONTENTS

Page No.

LIST OF FIGURES

NOMENCLATURE

A	cross-sectional area
a_1	$\overline{u'v'}/\overline{q^2}$
a,b	constants
C_f	skin friction coefficient
d_G	spacing of grating
f	focal length of lens
f_D	Doppler frequency
H	shape factor (ratio of displacement thickness to momemtum thickness)
I	laser beam light intensity
I_0	peak laser beam light intensity
k	turbulent kinetic energy $= \frac{1}{2}\overline{q^2} = \frac{1}{2}(\overline{u'^2} + \overline{v'^2} + \overline{w'^2})$
k	order of diffracted beam
ku	kurtosis of probability density function
l	mixing length
m	mass flowrate
N	number of samples
N	number of grating lines
N	LDA data from x-y $-45°$ orientation
N1	LDA data from y-z $-45°$ orientation
p	static pressure
P	LDA data from x-y $+45°$ orientation
P1	LDA data from y-z $+45°$ orientation
r	streamwise radius of curvature
R	axisymmetric radius of curvature
R_{uv}	structural parameter
Re_t	slot Reynolds number
Ri	Richardson number
s	fringe line spacing
sk	skewness of Gaussian distribution

t	slot width
U,$\overline{u}$	mean velocity x-direction
u'	fluctuating velocity x-direction
$\overline{v}$	mean velocity y-direction
v'	fluctuating velocity y-direction
w	width of laser beam
$\overline{w}$	mean velocity z-direction
w'	fluctuating velocity z-direction
x	streamwise coordinate along or parallel to surface
y	coordinate perpendicular to x-direction
$y_{1/2}$	value of y where U = $U_m/2$
z	circumferential coordinate

Greek Symbols

α	intersection angle of laser beams
α_1, α_2	constants
β	angle between velocity vector and fringes
ε	turbulent energy dissipation rate
θ	momentum thickness
λ	wavelength of illuminating radiation
μ	viscosity
ν	frequency of shifted beams
ν_T	turbulent kinematic viscosity = μ/ρ
ξ	non-dimensionalised distance parameter = y/$y_{1/2}$
ρ	density
σ	standard deviation of Gaussian distribution
σ_b	standard deviation of laser beam intensity distribution
σ	constant
τ	shear stress
τ_w	wall shear stress
ϕ	angle of diffracted beams

ψ	stream function = (ρ V A / m)
ω_r	grating radial velocity

Subscripts

a	ambient conditions
D	Doppler
G	grating
i,j	tensor components
m	maximum
m/2	at $U_m/2$
s	slot
s	surface conditions
w	wall
x	grid position x
xy	xy - plane
yz	yz - plane
0	stagnation conditions

DECLARATION

The work contained in this thesis has not been submitted elsewhere for any other degree or qualification and, unless otherwise referenced, it is my own work.

STATEMENT OF COPYRIGHT

CHAPTER 1

FLOW OVER CURVED SURFACES

1.1 INTRODUCTION

There are diverse important engineering applications where turbulent flows over longitudinally curved surfaces are encountered e.g. turbomachinery blade passages, wings and intakes of aircraft, propeller hubs, rocket nozzles and Coanda flares.

Such flows are of basic importance in the development of generalised calculation methods for turbulent shear flows. Traditionally, their characteristics have been calculated by ignoring wall curvature and using turbulent models appropriate to flat-wall jet flows. Bradshaw (1973), however, showed that the behaviour of the turbulent boundary layer is very sensitive to streamline curvature. He showed that even a very mild wall curvature can cause a significant effect on the structure of the flow and its development.

In order to use the potential benefits of the flow fully, investigations into the details of the flow structure are important. The basic properties of curved wall jets - effects of curvature on the skin friction, the law of the wall, turbulent shear stress at the maximum velocity and other turbulence properties - need to be determined as a basis for predicting more complicated flow situations.

1.2 THE COANDA EFFECT

The effect whereby a fluid attaches itself to an adjacent surface is usually associated with Coanda, who exploited aspects of this phenomenon in his numerous inventions, especially applying it to aircraft thrust augmentation devices. Wille & Fernholz (1956), however, quote as the first documentation of the effect a paper by Young as early as 1800. Newman (1961) also references Reynold's (1870) observations on the stable equilibrium exhibited by a ball resting on top of a vertical axisymmetric jet of water. Similarly, flow of fluid around a *Coanda flare* is stably adhered to its surface, the necessary centrifugal force being produced by the low-pressure region immediately adjacent to the surface.

The term *Coanda Effect* is often applied as a blanket term to the phenomenon of a wall jet on a convex surface, without distinguishing certain important features. Fernholz (1971), Wille & Fernholz (1956) and Bradshaw (1973) distinguish between phenomena all labelled under this same title :-

a. the tendency of a fluid to remain attached to a curved surface due to inviscid flow properties (e.g. for a liquid jet, surface tension promotes attachment);

b. the viscous flow properties whereby acceleration of the ambient fluid - entrainment - produces a low-pressure region if the jet is adjacent to a wall;

c. the effect of streamline curvature on a mixing layer which causes a marked increase in growth rate of the jet.

Bradshaw (1973) suggests that the latter phenomenon should be the one reserved for the term Coanda Effect.

1.3 COANDA FLARES

Flaring in the energy industry is a necessary consequence of having to safely dispose of tail gases produced in various industrial processes and also toxic gases which have to be completely burned. Coanda flares are in widespread use by BP at oil installations and on off- shore production platforms in the North Sea.

The design of these flares is becoming increasingly specialised. They must not only provide a stable smokeless flame, but also be able to cope with a wide range of flow rates, from low purge through continuous flaring to emergency disposal, while operating in hostile environments such as the North Sea.

The basic principles of the Coanda flares are shown in Fig. 1.1 and outlined below :-

A high pressure gas exits from a narrow slot at the base of the flare as a jet and follows a curved surface. The jet entrains the surrounding quiescent fluid and thus the maximum velocity decreases and width of flow increases downstream. Skin friction also has a minor effect. Pressure on the surface is lower than ambient and rises only slowly, so that the jet remains attached - the Coanda effect.

The gas entrains up to twenty times its own volume of atmospheric air which ensures the gas is thoroughly pre-mixed before combustion to ensure a

smokeless flame. The jet is ignited on its outer edge, at the maximum diameter of the flare. It burns inwards so that there is a protective layer of unburned gas which insulates the lip of the flare against flame impingement. Thus, the flare tip can be made of conventional steel alloys and be manufactured by normal welding methods.

Another major advantage of the flares is that the radiation levels are much lower and the flame lengths shorter, than the traditional pipe flare. The boom or tower that holds the flare can thus be made shorter and a considerable reduction in the cost of the flare, plus its installation, is achieved.

The INDAIR (Induced - Air) flare is an axisymmetric flare whose cross-section has the same shape as above. The entrainment properties of the jet are so good that gas at near atmospheric pressure can be added into the jet at the top of the Coanda surface, via an axial duct, without producing any smoke.

It was developed by Professor D.H.Desty and a group of researchers at B.P. Research Centre, Sunbury-on-Thames during the early 1970s. Kaldair Ltd., established as a wholly owned B.P. subsidiary in March 1978, are responsible for the manufacturing and marketing of these and other flare designs. Many oil production platforms now operate them in such diverse locations around the world as the North Sea, Alaska, Brazil, India and Kuwait.

The performance of these flares has been researched at B.P.'s Research Centre and also at both Durham and Exeter Universities. The latter's work has concentrated on the noise production levels. The researchers at B.P. and Durham have looked at various flare geometries and studied the undesirable situation of 'breakaway', which has not been considered in the present project.

Robinson (1982) carried out work on the discharge coefficient of various nozzles. He also investigated surface pressure distribution for a 2-dimensional model of the flare in an incompressible flow regime.

Gilchrist (1985) extended this work and looked at high- speed flows to study the separation criteria for several nozzle profiles.

Current work by Senior (1988) is aimed at further extension of the high-speed studies.

Morrison (1982) acquired experimental data for a half-model idealised Indair Coanda flare with hot wire and 3-hole pressure probes in low speed air flows. He studied the surface pressure distributions and measured mean velocity profiles and the turbulence structure of the jet. He also developed a calculation method using a simple mixing length model with empirical corrections for the effects of streamline curvature and divergence to close the solution. By deduction of the Reynolds stresses, studies were made of the high turbulence levels caused by the combined effects of streamline curvature and divergence.

1.4 LASER DOPPLER ANEMOMETRY

The development of the high intensity coherent light sources known as LASERS (Light Amplification by Stimulated Emission of Radiation) has made it possible to introduce many optical measurement techniques previously impracticable. The technique is not a general replacement for other methods such as hot wires or pitot tubes; optical access, essential for laser Doppler work, is not always available and LDA equipment is expensive. Laser Doppler

does, however, permit measurements of velocity and turbulence to be made in situations otherwise impossible or unobtainable.

The technique of using the Doppler shift of laser light to determine velocities was first demonstrated in 1964 by Yeh & Cummins when they observed the shift of light scattered from particles carried in a water flow. Lasers produce a very intense monochromatic light ideally suited for this type of measurement.

There are a number of variations of the technique which may be broadly described as laser Doppler anemometry, commonly abbreviated to LDA. For LDA situations, there is no relative movement of the source and receiver; the shift is produced by the movement of a particle or larger body that reflects light from the source to the receiver. In the application to optical velocity measurement, Doppler shifted light is heterodyned, either with scattered light obtained directly from the original source, or further scattered light, having a different shift due to scattering through a different angle, or from a different point.

LDA provides an ideal tool for the experimental investigation of turbulent flows. It is a high resolution, fast response technique and, in the field of turbulence, fully realises its potentialities. LDA is non-intrusive and capable of monitoring all components of velocity, and hence can provide information on Reynolds stresses.

1.5 OBJECTIVES

The main aim of this project was to investigate the jet structure around a convex curved surface using a plane model of the axisymmetric Indair flare. This then provides comparability with the airflow survey of Morrison (1982) and a useful test case for the application of the LDA technique. The results can be compared to Morrison's hot wire and three-hole pressure probe results.

In addition to the extensive measurement collection programme, a small amount of theoretical computer modelling has been completed. The theoretical work has included models of both the sudden expansion situation and the curved jet flow. The results have been compared with those obtained experimentally.

The work reported falls naturally into 4 sections :

Chapter 2 describes the LDA system and data acquisition technique and

Chapter 3 its verification and preliminary application;

Chapters 5 & 6 describe the experimental work undertaken to provide the comprehensive study of the turbulent structure of the Coanda flare jet;

the theoretical modelling work undertaken is detailed in Chapter 7, including comparisons between experimental results and computer predictions.

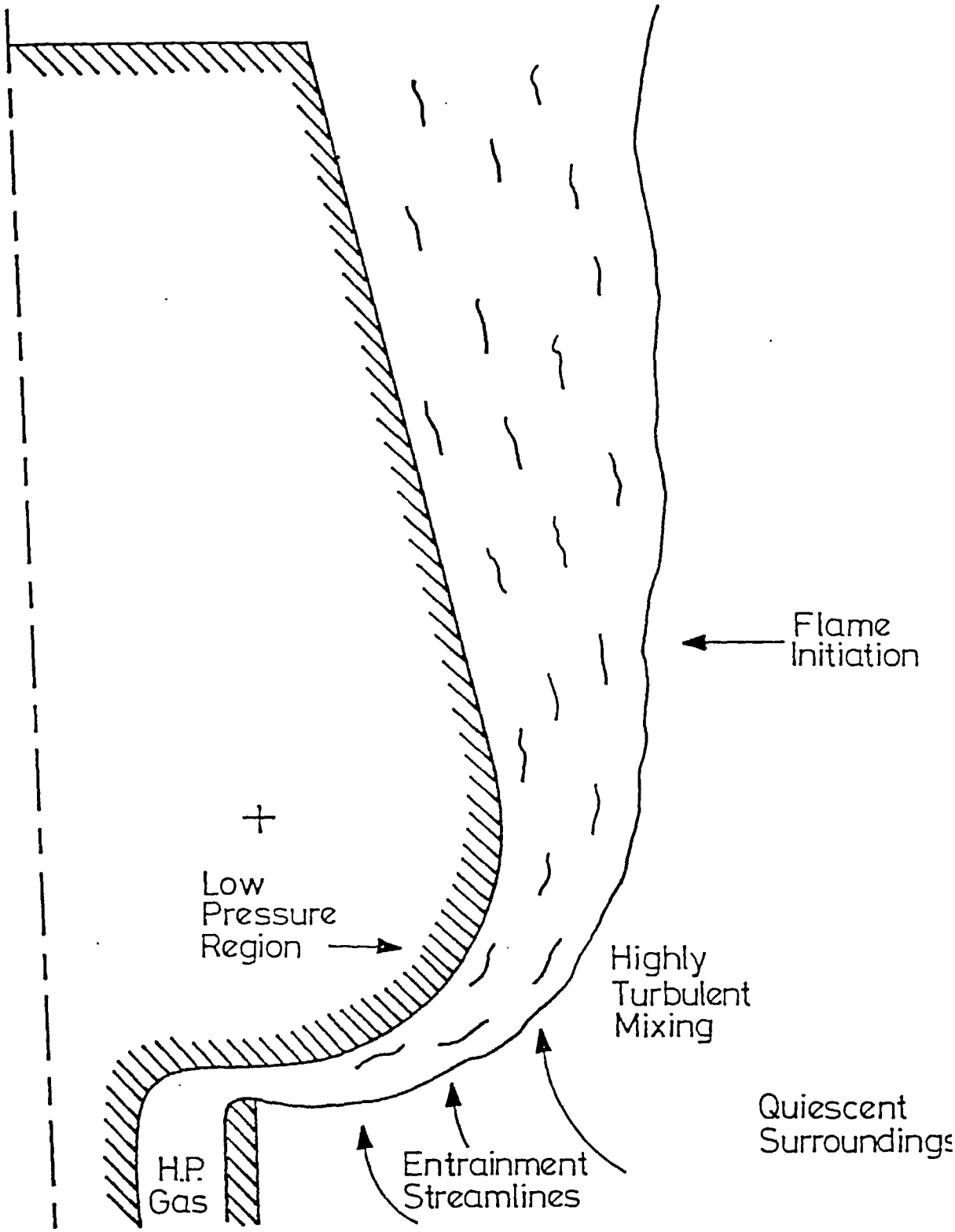

Fig. 1.1 Principles Of The Coanda Flare

CHAPTER 2

LASER DOPPLER ANEMOMETRY TECHNIQUE

2.1 INTRODUCTION

Flow measurement is a fundamental requirement for the extension of understanding in all areas of fluid mechanics. Mean velocity and parameters statistically describing turbulence are of great significance.

Velocity cannot be measured explicitly; all forms of velocity measurement measure some other variable and infer velocity from it. The implicit nature of anemometry means that all flow velocity measurement systems require some degree of data processing and all have some drawback.

From its invention in 1960 and its first application to fluid flow measurement in 1964 by Yeh and Cummins, the *LASER* has shown significant advantages in certain applications.

Laser Doppler Anemometry (LDA) or Laser Doppler Velocimetry (LDV) has gained wide acceptance as a measuring instrument. It is unique among flow measurement techniques in being capable of meeting all six of the requirements suggested by Hinze (1975) for making accurate turbulent measurements :-

1. Probe must cause minimal disturbance to the flow.

2. Probe must be smaller than smallest turbulent structure.

3. Instrument must have a fast response time.

4. Instrument must be sensitive enough to record small velocity changes.

5. Calibration of the instrument must not change over the time required to make a series of measurements.

6. Probe must be strong enough to withstand forces exerted by the flow.

Standard local velocity measurement techniques e.g.pitot probes, hot wire anemometry, require insertion of an object into the flow, cause flow disturbances, are sensitive to particulate content of the flow and some have the capability to monitor only mean rather than instantaneous values. LDA is at the other exteme of sophistication and expense from pressure probe techniques. In contrast to these, LDA does not disturb the flow and, within limits, takes advantage of particulate content; it does, however, require that light paths are available into and out of the flow.

2.2 THEORY

Comprehensive details of the LDA technique are given in Drain (1980) and Durst, Melling & Whitelaw (1981) but the essentials are outlined below.

2.2.1 Laser

A laser works by taking the photon emitted from an electron and using this energy to stimulate emission of more photons from other electrons and thus amplify the original light.

In a given laser system there are usually a number of modes of oscillation possible. These differ in the distribution of light across the beam (transverse modes) or in the number of wavelengths in the laser length (longitudinal modes). The spatial mode produced by a gas laser is determined by its construction and the type of gas present in the tube. In particular, it is dependent upon the mirror radii within the cavity and the wavelength of operation.

The dominant transverse mode is the uniphase Transverse Electro–Magnetic mode TEM_{00}. This has circular symmetry and a Gaussian power profile across the beam. The relationship for the intensity distribution of such a Gaussian laser beam is given by :–

$$I = I_0 exp\left(-\frac{1}{2}\left(\frac{w}{\sigma_b}\right)^2\right) \qquad 2.1$$

In almost all LDA applications the laser is operated in this fundamental transverse mode which provides the smallest beam diameter and divergence angle. It can be focused to a single spot (of the order of microns) at the point where the velocity measurement is required and it is this feature which makes it most desirable in LDA.

2.2.2 LDA Systems

There are basically two main types of LDA configuration, the reference beam mode and the dual beam or differential Doppler mode of operation. In any LDA system, laser light is transmitted to the point of interest in a

flow. In both modes of operation, the basic principle is the detection of the Doppler shift in the laser light frequency caused by scattering by the particles moving in the flow. The presence of particles in the flow is fundamental to the operation of the technique.

The reference beam mode of operation involves the mixing of scattered light with a reference beam whose light intensity is a fraction of the laser source intensity. A typical arrangement is shown in Fig. 2.1(a). Optical beating between the unshifted reference beam and the Doppler shifted beam is detected by the the receiving optics. The intensity of the scattered light collected is small since only a small aperture can be used. The limit on signal–to–noise ratio set by the intensity of the scattered light means that increasing the reference beam intensity provides no improvement of this ratio. A major disadvantage of the reference beam technique is that the Doppler frequency is dependent upon the angle of detection.

Fig. 2.1(b) shows the basic configuration for the differential beam mode. No reference beam is used; instead, optical heterodyning occurs between two laser beams scattered through different angles.

In this situation, the Doppler frequency is independent of collection angle so a large aperature can be used, providing a considerably stronger signal than that from the reference beam technique.

2.2.3 Beam Splitting

To achieve a Doppler signal, two coherent beams are required. The coherent monochromatic beam emerging from the single laser source must

therefore be split. There are several methods currently available for beam splitting.

(a) Anisotropic mediums : these are materials in which the refractive index varies according to the polarisation of the incident wave e.g.calcite,crystalline quartz. On entering an optically anisotropic medium, an unpolarised beam of light is refracted differently according to its polarization. As a result two beams emerge from the crystal having polarizations perpendicular to each other and being displaced laterally. This property is used in the application of polarising prisms e.g. Rochon or Wollaston.

(b) Part–silvered reflecting surfaces : using appropriately coated surfaces, two beams can be produced. Prisms are most often used and can be configured for equal path length and insensitivity to minor misalignment and tilt.

(c) Bragg cells : these are acousto–optic devices designed to give beam splitting. They require a stable, high frequency voltage supply.

The incident light beam passes through a medium in which acoustic waves are travelling. The intensity of the light in each refracted beam depends on several parameters including the cell dimensions, the acoustic and light frequencies, the absorbing medium, the electrical power used to drive the crystal and the angle between the acoustic wave fronts and the incident beam.

(d) Diffraction gratings : One of the simplest ways to split the laser light beam is to pass it through a moving grating mounted perpendicular

to the direction of the incident light. The light wave is diffracted and the beams emerge at angles corresponding to

$$\phi = \sin^{-1}\left(\frac{k\lambda}{s}\right) \qquad 2.2$$

Optically flat glass with bleached lines are usually used to provide the grating. In the most common arrangement, the laser beam is focused onto the grating, avoiding a difficulty in the use of a radial grating with a beam of significant width. This arises from the variation of the spacing of the grating across the beam and would give rise to different angles of diffraction across the beam. The diffracted beam cross–section would thus become elliptical with increased divergence and lead to a degradation of the optical system performance. The main disadvantage of such focusing is that the light energy is concentrated on a small spot on the grating which could lead to damage if the grating were stopped when using a high power beam. The performance is also more sensitive to dust and imperfections in the grating.

2.2.4 Measurement Volume

The two main beams are then brought to a focus, by the transmitting optics, in the field of interest. One of the features of a Gaussian beam is that once brought to a focus, the beam radius passes through a minimum known as its *waist*, at which point the wavefronts are plane.

Where the beams cross, constructive and destructive interference occurs. This, according to the Fringe Model, can be thought of as producing light and dark interference fringes – see Fig.2.2. The fringe spacing is given by

$$s = \frac{\lambda}{2\sin\left(\frac{\alpha}{2}\right)} \qquad 2.3$$

2.2.5 Particle Scattering

When the laser beams pass through the flow, light is scattered by suspended particles. A particle moving with velocity v at an angle, β, normal to the fringe planes will experience a modulation of light intensity of frequency f_D– the differential Doppler frequency – and its velocity is given by

$$v = \frac{f_D}{2\sin\left(\alpha/2\right)\cos\beta} \qquad 2.4$$

It is not the fluid velocity which is being measured directly but rather the particle velocity, from which the former is inferred. The seeding particles can be considered to be the actual velocity probes and seeding considerations are important in laser anemometry.

The Doppler shift frequency and hence the determination of the velocity is unaffected by the number and optical properties of the particles; the ease of taking measurements and the possibilty of tracking the flow continuously

do, however, depend on these factors. The particles must be small enough to track the flow accurately yet large enough to scatter sufficient light for the proper operation of the receiving optics and signal processor. If there are too few suitable particles present, the time taken to accumulate data may be prohibitive.

Scattered light intensity in the Lorenz–Mie scatter region (where particles are of sizes comparable to the light wavelength) depends on the size and shape of the particles, the intensity of the incident light and is influenced by the ratio of the refractive index of the particles to that of the surrounding medium. They scatter far more light in the forward direction (10^2 or 10^3 times) than in the backward direction. Smaller particles scatter more evenly and larger particles are more unpredictable in their light intensity distribution.

A laser is useful in this application because it produces such a high power density light – when this is concentrated on the scattering particles a strong Doppler signal is obtained. An example of the polar intensity plot for particular scattering is shown in Fig. 2.3. This shows how a large proportion of the light is concentrated in a forward lobe with smaller proportions in a number of secondary lobes at various angles around the particle.

The particle size is determined by its ability to follow the fluid flow i.e.higher mean velocity and tubulence levels need smaller seeding particles.

An identical signal is produced from a particle crossing the fringes from top to bottom or vice versa. In some applications the direction of flow is known and is always the same. In many flow situations where the LDA technique can be most useful, however, reversals of velocity are involved and

a way of discriminating velocity direction is indispensable when dealing with such complex flows.

Most popular techniques for direction determination involve shifting the frequency of the light beams. The choice of frequency shifting technique is a matter of convenience, shift required, availability of equipment – there is no universal best choice.

In order to measure a velocity rather than a speed, an asymmetry is introduced into the system. The asymmetry may be achieved by the addition of *frequency shift* by which an artefact velocity is introduced into the system.

Two methods which introduce not only beam splitting but also frequency shift are :–

(a) Bragg cells : these can be designed to give beam splitting and frequency shifting. The Doppler shift will add to or subtract from the offset frequency shift. If the shift is arranged to be higher than the highest negative Doppler shift, the signal processor will be able to distinguish between negative and positive flow directions.

(b) Diffraction gratings : One of the simplest and cheapest ways to change the frequency of a laser–light beam. Rotating the diffraction grating produces a *moving* fringe system inside the measuring control volume. This is comparable to the frequency shift from a moving particle.

Doppler shift considerations imply that the frequency of each of the split beams will be different from the incident beam by an amount

$$\nu = kN\omega_r \qquad 2.5$$

The two emerging beams are obtained from the +1 and -1 orders of diffraction, shifted by $\pm v_G/d_G$. Other orders of diffraction are stopped off. The frequency shift thus imposed on the Doppler beat signal is $2(v_G/d_G)$ i.e.twice the product of the rotation frequency of the grating and the total number of grating lines.

The maximum frequency shift obtainable from a rotating diffraction grating is limited by the speed of mechanical rotation achievable. Durst & Zare (1974) identify several parameters that influence the spectral purity of the frequency spectrum obtained from the shifted light beams produced by a rotating diffraction grating. These included mechanical vibrations of the rotating grating and the light source; unsteadiness of the rotational speed; imperfections of the optical grating.

In general, the frequency shifts achieved with Bragg cells are much higher than those with a rotating diffraction grating.

The probe volume is defined as the volume within the contour corresponding to a fringe amplitude of $1/e^2$ of its maximum modulation. The measuring volume, however, is defined as the region in space from which Doppler signals are received and detected by the signal processor. The probe volume is not, therefore, necessarily equal to the measuring volume. The size of the measuring volume is determined by a number of factors including velocity direction, particle size and shape, detector optics, amount of frequency shift and overall gain of the system (see Buchhave (1979)).

2.2.6 Signal Detection

The detection optics of any LDA system are focused upon the probe volume. The light scattered from the particles moving through the measuring volume is collected by the optics which form an image on a pinhole before detection. The pinhole acts as a spacial filter to remove optical noise from the focused light before it impinges on the photocathode of the tube. It is the scattered light which contains the Doppler frequency information and it is this which is extracted from the total signal by means of optical heterodyning on the photodetector surface.

An essential element in any laser Doppler equipment is the light detector. It converts changes in light intensity into electrical signals which are required for most methods of analysis. High sensitivity and fast response are desirable. The main criteria in the selection of photodetectors for LDA include quantum efficiency – the ratio of the number of electron emmissions or other events to the number of incident photons; current amplification – the amplification of the photocurrent produced by secondary emission at the intermediate dynodes; frequency response – the frequency range over which operation is satisfactory; noise introduced by the detector and cost.

There are basically two types of detector available, photomultipliers and photodiodes.

Photodiodes are semiconductor devices in which light is detected by the production of electron–hole pairs in the junction region of a p–n diode. Illumination by light of an appropriate wavelength range generates electrons and hole carriers which produces a leakage current proportional to the intensity of the incident light.

Photomultipliers are vacuum tubes in which electrons are released by light falling on a special photoemissive surface. Photons hitting the cathode of a PM generate photo–electrons leaving the cathode. Due to the high voltage between the cathode and anode, as well as in the subsequent dynodes, electrons move through the multiplying dynode chain towards the anode – Fig. 2.4.

After chain multiplication, electrons hit the anode, which leads to a current at the anode. The appropriate choice of terminating resistor of the electrical circuits allows conversion of the anode current – the current containing frequency information relating to the velocity to be measured – into an output voltage as the output signal of the PM.

The photodiode is most suitable for strong signals e.g. for use with a reference beam LDA configuration. Ordinary photodiodes do not have a built–in current amplification and thus much more external amplification is required than with photomultipliers. However, in the 'avalanche' type of photodiode, operated near the junction breakdown point, some multiplication of carriers can be produced and these have many of the advantages of both photodiodes and photomultipliers. The photomultiplier is of benefit for a system producing weaker signals i.e.a differential Doppler system.

The time response characteristics of the PM tube are important in pulse applications, particularly involving accurate time measurements or high count rates. The time characteristics are a function of the level of light at the cathode and a weak function of the wavelength of illumination (due to initial energy effects of the photoelectrons). Commonly specified measurements include :– Rise Time : the time taken for the output pulse to rise from 10% to 90% of its peak value.

Full Width at Half Maximum Height (FWHM) : the full width of the output pulse measured at half its maximum amplitude.

Overall Electron Transit Time : the time interval between the arrival of a flash of light at the photocathode and the instant when the pulse output is maximum. The transit time is of less interest, comprising a 'fixed' delay, than is the variation in transit time from pulse to pulse – the Transit Time Jitter or Fluctuation.

The primary result of a laser anemometer measurement is a current pulse from the photodetector. In common with all light detectors, a photomultiplier (PM) is a square–law device i.e.it is sensitive to light intensity (this being the square of the light amplitude).

The current pulse from the photodetector contains frequency information relating to the velocity to be measured. It also, however, contains noise, the primary source being photodetection shot noise, a fundamental property of the detection process. The interaction between the optical field and the photo–sensitive material is a quantum process which unavoidably impresses a certain measure of fluctuation on the mean photocurrent. In addition, there is a mean photocurrent and shot noise from undesired light reaching the photodetector. Further noise sources include secondary electron noise from the photomultiplier dynode chain and preamplifier noise in the signal processor.

2.2.7 Signal Processing

The velocity information is present in the Doppler signal as a frequency modulation of the detector current, Fig. 2.5. The signal processing electronics

function essentially as a frequency demodulator. Some of the factors affecting the choice of signal processing are – signal to noise ratio of the input signal; the required measurement accuracy; the type of information required e.g.power spectrum, average velocity, instantaneous velocity etc.

The d.c. part of the input, which is removed by a high–pass filter, is known as the *Doppler Pedestal.* The envelope of the Doppler–modulated current shows a Gaussian intensity distribution in the measuring volume.

The principal types of LDA data processors are trackers and counters. A recently introduced LDA signal processor is the burst spectrum analyser. The perfect signal processor has yet to be made and no one type is equally suitable for all situations. A choice has then to be made to suit each individual application of LDA. The main factors to be considered are the type of signal (intermittent, continuous), the signal to noise ratio and the turbulence levels. The proper choice of signal processor and an understanding of its limitations is of major importance in obtaining satisfactory LDA measurements.

An LDA tracker is a frequency tracking filter which locks on to the Doppler frequency and continues to track the instantaneous frequency as long as the internal servo loop stays locked. Its operation is shown in Fig. 2.6 and is briefly as follows:– The signal is first cleaned by removing frequencies outside the range of interest. It is then amplified and mixed with the output of a local oscillator, the frequency of which can be controlled by an applied voltage. The difference frequency is amplified and then applied to a discriminator (a circuit whose response is strongly frequency dependent). This usually consists of a balanced tuned detector circuit designed to give zero output when the frequency of the applied signal is exactly on tune. The output of the discriminator is then amplified and used to control the frequency

of the variable oscillator. When the system is tracking, the feedback loop is locked to the signal and the variations of the local oscillator frequency are the same as those of the signal. An analogue output representing the Doppler frequency may be obtained from the input voltage to the voltage controlled oscillator.

Frequency tracking demodulators thus provide real time demodulation of the Doppler signal continually proportional to the component of the local fluid velocity to which the optical system is sensitive. Due to the random amplitude of most Doppler signals, the circuit must be protected from *drop–outs* – periods when the signal is insufficient to lock the circuit. The frequency of the voltage controlled oscillator is usually *frozen* during these periods. The performance of the tracker is satisfactory if these periods are not too long. However, if the time interval between the bursts is too long or there are large velocity changes between bursts, the tracking principle does not work and it is not possible for a signal processor to follow the velocity fluctuations.

Spectral analysis of LDA signals has potential advantages over schemes based on zero crossings. It enables a considerable reduction of laser power and measurements with smaller particles are feasible. Lading (1987) gives details of one such commercially–available system. The burst spectrum analyser (BSA) digitizes the photodetector output signal at a high fixed rate and determines the Doppler frequency through the use of a discrete Fourier transform. The basic structure of such a processor comprises :– the filtered input signal activates a burst detector when it exceeds a preset threshold level. The burst detector measures the time of occurrence and the residence time and initiates the Fourier transform process. The post–processor validates the measured spectrum and estimates the Doppler frequency from the spectral samples collected.

For steady, laminar flow, or if the turbulence level is low, almost any type of processor is suitable. Trackers, with their superior signal to noise ratio performance, are generally preferred to counters. Trackers are designed, however, for continuous signal detection and are not well–suited for high resolution, fine-scale turbulence measurements. The laser Doppler technique is often required to investigate flows in which the velocity is varying rapidly due to, for example, turbulence. Counters can be used in sparsely– or highly– seeded flows, they have a wide range of operation and are particularly suited for measurements in highly turbulent flows. In situations where signal characteristics vary greatly during a single measurement e.g.oscillatory flows in I.C. engines, where boundary conditions lead to variation of signal to noise ratios e.g.turbomachinery, or where there is a wide distribution of particle sizes, the BSA could prove to be advantageous.

A counter processor is basically a timing device or 'electronic stop–watch'. Its operation is illustrated in Fig. 2.7.

It measures the time taken for a particle to cross a known number of interference fringes in the measuring volume. The distance between the fringes is known from the system's geometry and the wavelength of the laser light. An LDA counter is designed to accommodate the burst–type Doppler signal with relatively long periods of no signal between bursts and when the velocity may change appreciably between bursts.

The counter consists of a high–frequency clock oscillator whose pulses are counted in two counter registers, the High and Low Count Registers. The signal is band–pass filtered to remove high and low frequency noise. It is then amplified and allowed to trigger a Schmitt Trigger. The presence of a measureable Doppler signal is detected by the Trigger which has one or more

fixed thresholds set, at different levels, symmetrically about zero volts. The Trigger controls a flag which is raised and lowered by the crossing of the threshold by positive value, positive waveforms and by negative value, negative waveforms respectively. A measurement is initiated when the signal exceeds the fringe counter predetermined threshold level. The first zero–crossing then enables the counter and counting continues through the following N zero–crossings. New measurements continue, based on N zero–crossings, throughout the burst as long as Doppler signals exceeding the Schmitt trigger level are available.

Measurement checks are performed by making two readings of the period of the Doppler signal using different numbers of cycles. The data is entered into the High and Low Count Registers. If the two measurements of the Doppler period agree to a specified degree of precision, they are 'validated' and accepted for output or further processing. If an error condition is detected by the validation circuits, the counter is immediately reset and the data point rejected. It is preferable to use cycle numbers that have no common factor e.g. a 5:8 comparator circuit is commonly used, as illustrated in Fig. 2.8.

2.2.8 Data Acquisition

When making measurements in fluid flows it is often useful to be able to control the data gathering process. This may entail taking readings at some specific instant relative to a previous reading or to some aspect of the behaviour of the flow. This conditional sampling is particularly important where the flow field is time varying in a cyclic manner since it permits the selection of data from a fixed point in the cycle. Movement of this fixed point around an interval of the cycle then allows the reconstruction of the

flow field pattern over that interval. In aperiodic flows, the ability to control the sampling process can permit the decoupling of the sampling aspect from the signal. Any bias generated by correlation between the signal and the sampling process is thus eliminated.

Control of the LDA data acquisition process can be achieved by the use of either software in the data analysis section e.g.microcomputer, or by selectively interrupting the signal in the hardware chain. There are several methods which can be used to define a window in an LDA system.

The main advantage of *software windowing* methods is that the analysis and checking procedures are not performed in real time, allowing additional features to be incorporated in the software. Its main disadvantage is the large amounts of data storage required of the microcomputer system. 'Hardware windowing' avoids this difficulty but does require real time definition of the window. Such methods involve the use of timing circuitry to interrupt the data collection process. The timing function which defines the window has two elements; the delay from the cycle start and the duration of the window. The delay and the duration both depend on the cycle period so the timing function must be controlled.

Control of the sampling process is possible, when using a counter, by allowing the counter to operate only during that period of time when signals are required. The data may be sampled at regular time intervals by the use of some windowing technique.

2.3 BIAS EFFECTS

Concurrent with the increasing adaptation of LDA to a variety of fluid flow measurement situations, has been the recognition of limitations of data collection, analysis and interpretation. An awareness of the quantity actually being measured and the systems' inherent errors are fundamental to progress.

In this section each subsystem within the LDA is reviewed individually to assess the potential sources of error, inaccuracy or effects which could bias the values of velocity recorded. They must all be identified for the particular hardware used to ensure the acquisition of reliable data.

Some sources may be avoided or eliminated by judicious choice of equipment or operational technique. Others may be reduced to insignificant levels ; yet others must be accepted and, in certain cases, allowance made by numerical correction of the measurements.

Thompson and Flack (1976) identified 10 sources of potential signal biasing which may occur in an LDA measurement. Their suggestions are identified '*' among the others discussed below.

2.3.1 Laser Subsystem

i)* Directional Ambiguity – when the laser beams forming the probe volume are at the same frequency, the same Doppler frequency is detected for a given particle velocity whether flowing in a positive or negative direction perpendicular to the fringes. The discrimination of the direction of a velocity or velocity component is a fundamental problem in LDA measurements.

A selectable offset frequency (higher than the highest Doppler shift in the system) is introduced, via a Bragg Cell or rotating diffraction grating, to which the Doppler shift adds or subtracts. This then gives a zero velocity component with a finite frequency difference and allows determination of direction.

ii) Frequency Broadening – this may result if the two beams do not cross at their waists. In this situation, spherical rather than plane wavefronts interfere and the resulting fringe surfaces are distorted and are no longer parallel planes. Particles with the same velocity, but crossing different parts of the probe volume, will therefore produce different Doppler frequencies. Care must, therefore, be taken to ensure a correctly aligned system.

iii) * Incomplete Signal Bias / Fringe Number Effect – when a particle crosses the probe volume at an angle to the fringe normal, it may not cross enough fringes to produce the N cycles required by the counter processor. Its velocity data is therefore lost. Generally, such particles would have a velocity component normal to the fringes which is lower than the mean velocity. These incomplete and uncounted signals result in the ensemble average mean velocity being biased towards a higher value. Frequency shifting significantly reduces this error by increasing the number of fringes seen by a particle crossing the probe volume.

2.3.2 Flow Field

i) * Particle Lag – an LDA does not measure fluid velocity but the velocity of particles in the flow. These particles must, therefore, be small

enough to track the flow accurately whilst large enough to scatter sufficient light for the proper operation of the receiving optics.

If these conditions are not fulfilled, an insufficient signal could be obtained from particles that are too small or an incorrect velocity reading could be measured from particles that are too large. Seeding considerations are very important in the correct operation of an LDA system.

ii) * Particle Distribution Bias – this results from non–uniform seed distribution in the flow; this often occurs in mixing or reacting flows. Adequate mixing lengths upstream of the measuring section help avoid this error.

2.3.3 Receiving Subsystem

i) Misalignment – errors can occur if the pinhole aperture of the PM tube receiving optics is not coincident with the crossover point of the beams. Efforts must, therefore, be made to ensure a properly designed and aligned system to eliminate this effect.

ii) Signal Amplitude Bias – this was first proposed by Durao and Whitelaw (1980). Slower moving particles have a longer residence time in the probe volume and, they argued, are thus more easily detected than are faster moving particles. More slow–moving particles will, therefore, be likely to be monitored. This results in the observation of a proportionately larger number of lower velocity signals and biases the mean velocity calculation towards these low velocities.

iii) Noise – for most measurements, noise defines the lower limit of signal detectability and determines the accuracy of the results. A primary source is

photodetection shot noise – a fundamental property of the detection process. Interaction between the optical field and the photo–sensitive material is a quantum process which unavoidably impresses a certain measure of fluctuation on the mean photocurrent. In addition, there is a mean photocurrent and noise from undesired light reaching the photodetector. A further noise source is secondary electron noise from the PM dynode chain.

2.3.4 Data Acquisition System– Counter Processor

i) * Velocity Bias – if the sampling is coupled with the velocity, the average velocity can be biased and needs correction depending on the particle arrival rate in order to give the correct value. One of the first studies on statistical bias was done in 1973 by McLaughlin and Tiederman. They postulated that, for a fluid with a uniform distribution of scattering particles, more fluid volume and hence scattering centres pass through the probe volume per unit time at high velocities than during periods of lower velocity. Thus, for an ensemble average, a weighting of the calculated mean velocity towards the high velocities will exist.

ii) * Comparator Tolerance – in signal processing a comparator check is made to eliminate poor signals, usually due to signal dropout or electronic noise. Signals may also be rejected due to particle acceleration within the probe volume. This is most likely to occur in significant proportions in flows with high turbulence intensity and disproportionately more slow particles are rejected than faster particles. A bias of mean velocity towards higher than actual flow value would therefore be incurred. It can be significantly mitigated by selection of a higher value of tolerance on the comparator which will ensure the rejection of fewer legitimate signals.

iii) * Particle Acceleration – when a particle accelerates, or decelerates, while passing through the probe volume, the average velocity calculated will depend on the averaging technique used. This biasing is a result of the same particle behaviour as the Comparator biasing above but is distinct from it because biasing may occur independently of the comparator setting. The use of time averaging techniques rather than spatial averages should alleviate this error. Thompson & Flack (1976) found this to become significant only for clock frequencies below 50 MHz.

iv) * Clock Accuracy – when frequency measurements are made by counting techniques, time measurements are made by counting pulses generated by precision oscillators of constant frequency. Devices of this kind have a finite time resolution which sets a limit to the accuracy with which signal frequencies can be monitored by counters. Biasing may occur due to the finite accuracy of the clock, accurate to within one pulse. The clock frequency of an electronic counter should be high compared to the measured signal frequency to prevent reduced accuracy due to timing errors. High speed clocks reduce this effect to insignificant levels in most cases.

v) * Frequency Cut-off – if the spectral bandwidth of the Gaussian pedestal overlaps the Doppler spectrum, the effectiveness of the high pass filter can be seriously diminished. When some of the signals are lost, the measured results may be biased since the lost signals may all be from one end of the velocity histogram. Any frequency cut–offs which eliminate valid data will change the measured mean as well as the other average quantities. If the frequency cut–off is at the low end, the measured mean will be high and vice versa. Should overlap occur, it may be eliminated by frequency shifting; optical removal of the pedestal is also possible.

vi) * Multiple Particle Bias – signal rejection due to one or more particles entering the probe volume while another signal is being received may result in biasing. Roesler et al (1980) state that this error results from a lack of synchronisation of the gating of the clock with the beginning and end of the Doppler burst. Wang (1975) investigated this problem and showed its successful elimination by the use of a 5:8 comparator circuit operated with a high speed clock.

2.3.5 Data Processing Subsystem

i) Ergodicity Assumption – an ergodic process is one in which a single sample function carries the same statistical information as any other sample function. Hence, one sample function can provide all the statistics of the entire process i.e.time averages are identical to ensemble averages. If this condition is not in fact true for an LDA sampling system, a biased estimate of the flow measurements will result since data will be recorded from only one part of the turbulence spectrum.

2.3.6 Previous Work

The bias controversy was initiated by McLaughlin & Tiederman (1973) who postulated that the mean velocity obtained from an ensemble average of Individual Realisation LDA data points in a steady turbulent flow will be biased to higher values than the true mean. The original proposal of arrival rate bias (commonly, but somewhat ambiguously, referred to as velocity bias) stimulated discussion of other bias error mechanisms inherent in LDA systems.

Amplitude bias can further complicate the task of obtaining correct velocity measurements from individual realisations (Doppler bursts). The signal amplitude of high velocity particles may be smaller than that of low velocity particles. In systems where signal validation criterion depends on the amplitude, Durao et al (1975,1979) and Durao & Whitelaw (1980) claimed that this error mechanism provides a compensating effect for velocity bias.

Much research has been undertaken over the last decade to attempt a conclusive end to the debate on these two opposing effects. Durao et al (1982) include a Table, lucidly summarising a review of notable theoretical and experimental published works related to the bias controversy.

Several data reduction algorithms have been proposed to negate arrival rate bias effects. The technique proposed by McLaughlin & Tiederman (1973) to compensate for arrival rate bias, used weighting factors applied to the individual data samples before determining the average. The weighting factor was the inverse of the numerical value of the measured velocity component for each particle. A deficiency of this velocity weighting is that it approaches infinity as the velocity approaches zero.

Buchhave (1975) extended McLaughlin & Tiederman's one–dimensional weighting to study a three–dimensional case, when he took into account the velocity probability distributions in three directions.

Subsequent suggestions for weighting factors utilise the particle transit time across the LDA measurement volume to correct for velocity bias. The concept of residence–time weighting was developed by George (1976), who expressed the time as a function of the velocity and the probe volume size.

Such corrections have also been used by McDougall (1980) and Buchhave (1979). This method has the advantage of not producing infinite weights and is claimed to work equally well for one and two component LDA systems. Buchhave (1979) completed an extensive analytical and experimental bias study, including measurements by hot–wire and LDA in a free jet using tracker and counter processors. He concluded that a residence time weighting provided correct statistical results in uniformly seeded flows.

Hoesel & Rodi (1977) proposed two alternative approaches– the residence time weighting was suggested suitable for flows with uniform seeding; for flows with non–uniform seeding, they preferred the particle interarrival time as a more appropriate weighting factor. They provided some experimental results to support their theory but, as no comparison was made with independent measurements, no definite conclusion on the validity of the correction scheme was possible. Barnett & Bentley (1974) also used the time between samples as their correction method.

Residence time correction is very difficult to implement in general practice, necessitating the recording of the total length of each Doppler burst.

It has been emphasised that indiscriminate application of all correction schemes in situations where the extent, or even the existence, of bias is unknown, can lead to significant errors. Buchhave (1979) indicates that the schemes may, in certain cases, even introduce more error than they eliminate! He highlighted the situation of a system which incorporates frequency shifting, thereby eliminating incomplete signal bias. This bias partially compensates for velocity bias effects and if a non–dimensional correction is then applied, the measurement error may actually be increased. He found that the McLaughlin

& Tiederman correction over–corrected counter–processor data from a flow with turbulence intensities of 10% to 20%.

Petrie et al (1988) produced a two–dimensional extension of the McLaughlin & Tiederman velocity inverse weighting algorithm. They made comparisons between biased and weighted statistics for data obtained with a coincident two–component LDA system. They concluded that velocity bias effects can be substantial, changing the mean velocity and Reynolds stress terms appreciably. A two–dimensional correction was found to work well in compensating for these effects and produced apparently reasonable velocity probability distributions.

Barnett & Bentley (1974) showed, analytically, velocity bias to be dependent on particle arrival rate (seeding density) in contrast to McLaughlin & Tiederman (1973) who had concluded that arrival rate bias was independent of particle arrival rate. Barnett & Bentley found it theoretically to decrease as the sampling rate increased relative to the flow frequency. Their results implied that the bias is proportional to the Turbulence Intensity $(T.I.)^2$.

Roesler, Stevenson & Thompson (1980) endorsed the existence of velocity bias in data from comparator counter processors. They agreed with Barnett & Bentley in its proportionality with T.I. They suggested its elimination by use of high seeding levels and equal time interval sampling.

Johnson et al (1984) state that, from their data, at low particle arrival rates velocity bias is independent of sampling rate. Also, it only becomes significant for $T.I. > 20\%$ and is proportional to $(T.I.)^2$. They claim that

their results support Barnett & Bentley's (1974) proposal that no bias will occur if the particle arrival rate is much less than the turbulence frequencies.

Bogard & Tiederman (1979) found, in direct conflict with Barnett & Bentley (1974), velocity bias in their data to be unaffected by particle arrival rate. They also found no evidence of signal amplitude bias to compensate for velocity bias effects.

Giel & Barnett (1978), however, found no clear evidence of velocity bias in comparisons of LDA data with pitot and hot wire probes within a free jet. They concluded that significant statistical bias does not exist in all velocity measurements. They suggested the use of heavily seeded flow with very slow sampling rate to avoid biased results.

Petrie et al (1988) found a linear relationship between bias and T.I., when they made measurements in a flowfield with tubulence levels in excess of 40%.

Analytical studies have generally assumed that velocity bias is dependent upon T.I. and one or more characteristic time scale. Erdmann & Tropea (1981) concluded that the three important frequency scales are particle arrival rate, f_p, sampling rate, f_s, and turbulence frequency scale, f_t. They confirmed the qualitative trends predicted by a limited set of measurements in a backward–facing step water flowrig. Stevenson et al (1982) obtained data for a similar flow configuration, varying particle arrival rates and sampling rates and their results agreed with Erdmann & Tropea (1981).

Adams & Eaton (1985) postulated that, if $f_p >> f_s$, unbiased data

should be attained while if f_p and f_s are of similar magnitude, velocity bias would result. Edwards & Jensen (1983) statistically modelled LDA systems and found that bias vanished when f_p/f_t exceeded 10.

Durao et al (1982) and Stevenson et al (1984) show experimentally that, for sampling time scale high compared to particle arrival rate and to turbulence time scale, velocity bias may be avoided. Durao et al (1982) maintain, however, that signal amplitude bias is always present. In their study, velocity bias was detected for a range of turbulence intensities from 5 – 25%.

Experimental sampling techniques have been proposed to eliminate velocity bias during data acquisition. These require high seeding densities, however, which are not always achievable in practical situations.

Durao & Whitelaw (1975) suggested using random sampling to reduce arrival rate bias. They postulated that such sampling destroys the correlation between the particle arrival rate and the flow. They presented artificially generated data which confirmed the effect of random sampling, reducing the measured mean velocity. Their measured Doppler signal data, however, produced inconclusive results.

Edwards (1981) statistically analysed velocity bias and concluded, from probability considerations, that a particle arrival rate bias exists in counter–type detectors. If the detector samples the data at regular intervals the bias becomes a function of the particle density. He suggested that the bias could be made negligibly small in many practical situations.

Erdmann & Tropea (1981,1982) statistically modelled the LDA sampling process for two–dimensional flows. Their analysis predicted a shift from fully velocity biased to bias–free results as the sampling process changed from a free–running processor to a processor controlled system. The former is able to process and transfer data from every particle that generates a validated signal; the flow determines when particles are sampled. If, however, the maximum sampling rate of the processor is much less than the validated particle data rate, the processor constantly samples at its maximum rate and the processor then controls the sampling process. They predicted the velocity bias to be proportional to $T.I.^2$.

The reduction of the arrival rate bias between free running and processor–controlled sampling was observed experimentally by Johnson et al (1984), Craig et al (1984) and Stevenson et al (1982). From these studies, unbiased data was obtained when the sampling rate was at least fifty times less than the validated particle data rate. Conversely, completely biased data was recorded when the mean validated particle data rate was significantly smaller than the processor sampling rate.

Edwards & Jensen (1983) showed that the data–handling system strongly influenced the results of an experiment. From their rigorous mathematical analysis, they suggested that velocity bias vanished when the counter ran at its maximum rate, effectively sampling the data at equal time intervals.

A panel of accredited experts on LDA convened in September 1985 to create a consensus document on their understanding of the statistical bias problems. Edwards (1987) reported their discussions in which they stress

that the importance of statistical bias errors lies not in their magnitude but in the fact that they are systematic. Bias errors remain even when there is no statistical error. Also, since the bias errors are a function of the flow velocity and the turbulence intensity, the measured results may contain apparent trends that are artifacts of the measurement process. The panel conclude that a given experiment will not be interpretable unless the relevant parameters are known, recorded and reported.

Recent studies by Gould et al (1988) are reported to be in general agreement with the Bias Panel's findings. They report a study in which turbulence intensity, time between samples and turbulence time scales were independently varied in an effort systematically to quantify bias effects. Their experiments were carried out in a sudden expansion flowrig and they concluded a linear variation of bias with T.I., in contradiction to the square law dependence proposed by Barnett & Bentley (1974) and Erdmann & Tropea (1982), but in agreement with the findings of Petrie et al (1988). Of the correction methods which they investigated, they found a two–dimensional McLaughlin & Tiederman appeared valid up to 35% T.I. but overcorrected at higher turbulence levels. Approximately equal time sampling provided nearly unbiased results.

It is apparent from the literature reviewed that a definitive quantification of these biases still remains to be achieved. The studies provide so much conflicting opinion that the bias question continues unresolved.

2.4 RESEARCH OBJECTIVES

At the commencement of the present research, having surveyed all evidence on LDA system problems, and gained sometimes conflicting opinions from the authors, a number of fundamental questions were posed. If bias effects do exist in the hardware being used –

1. On what do they depend ?

2. How large are they ?

3. How can they be reduced or eliminated ?

The aims of the initial section of the project therefore, were to undertake a systematic programme to quantify whatever bias effects exist for whichever reasons in this particular hardware and LDA system arrangement. A reliable datum should thereby have been established for all future LDA measurements with the laser and data acquisition system used here. The work also, innately, involved a certain optimisation of operating techniques to minimise any errors recognised.

Table 2.1 presents a summary of the souces of error and bias identified from the literature and indicates methods available for their elimination or reduction. It also shows their importance in the existing apparatus.

Subsystem	Error/Bias	Relevance To Present Rig
(a)Laser	Frequency Broadening	Ensure alignment of optics to maintain crossover at beam waists.
	Directional Ambiguity	Frequency shift via a rotating diffraction grating.
	Incomplete Signal / Fringe No. Effect	Frequency shift.
(b)Flow Field	Particle Lag	5micron filter ensures particles small enough to follow flow.
	Particle Distribution	Long mixing length before measuring section.
(c)Receiving Subsystem	Misalignment	Care taken to ensure pinhole/crossover coincidence
	Signal Amplitude	Investigation to discover significance in present application
	Noise	Inherent & unquantifiable
(d)Data Acquisition	Velocity Bias	Under investigation for the present system
	Comparator Tolerance	Suitably high value chosen
	Clock Accuracy	High speed clock (500 MHz) minimises this problem
	Frequency Cut-Off	Suitable filter setting chosen & frequency shift applied
	Particle Acceleration	Time averaging technique used in this system
	Multiple Particle	Counter Processor uses 5:8 comparator circuit and high speed clock
(e)Data Processing	Ergodicity Assumption	Investigated for present regime

TABLE 2.1 SOURCES OF BIAS IN LDA

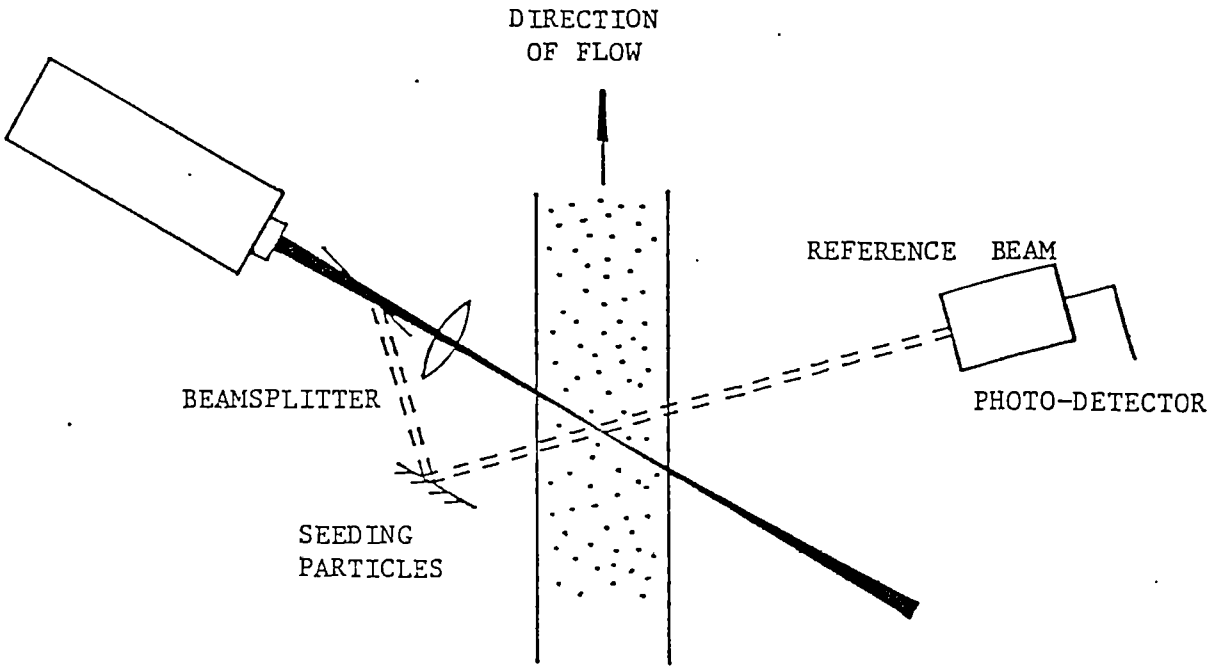

(a) SIMPLE REFERENCE BEAM ARRANGEMENT

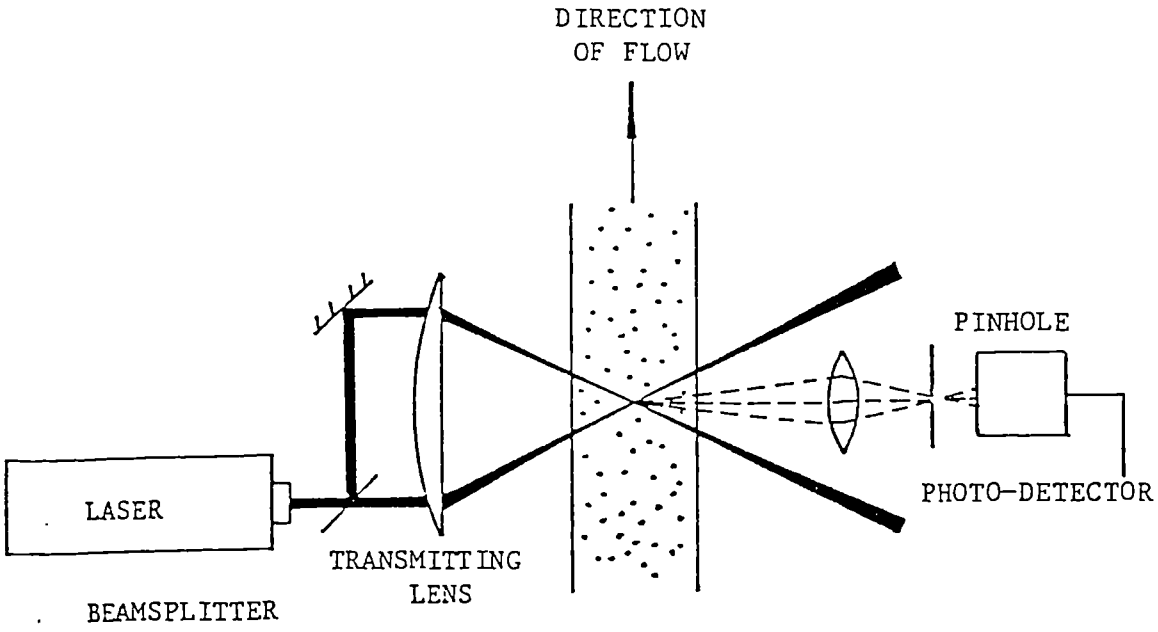

(b) SIMPLE DUAL BEAM ARRANGEMENT

Fig. 2.1 LDA Configurations

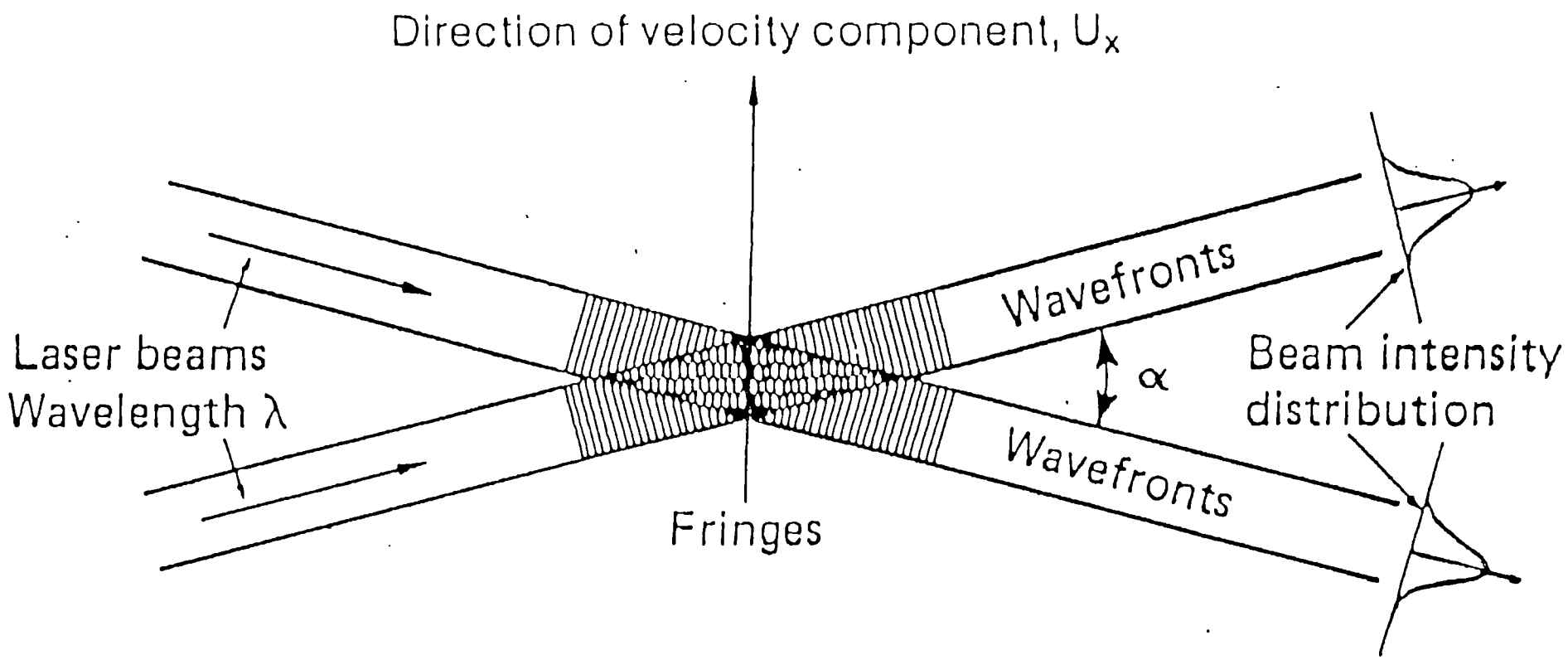

$$\text{Fringe spacing} \quad s = \frac{\lambda}{2 \sin \frac{\alpha}{2}}$$

Fig. 2.2 Interference Pattern For Beams Crossing At Their "Waists"

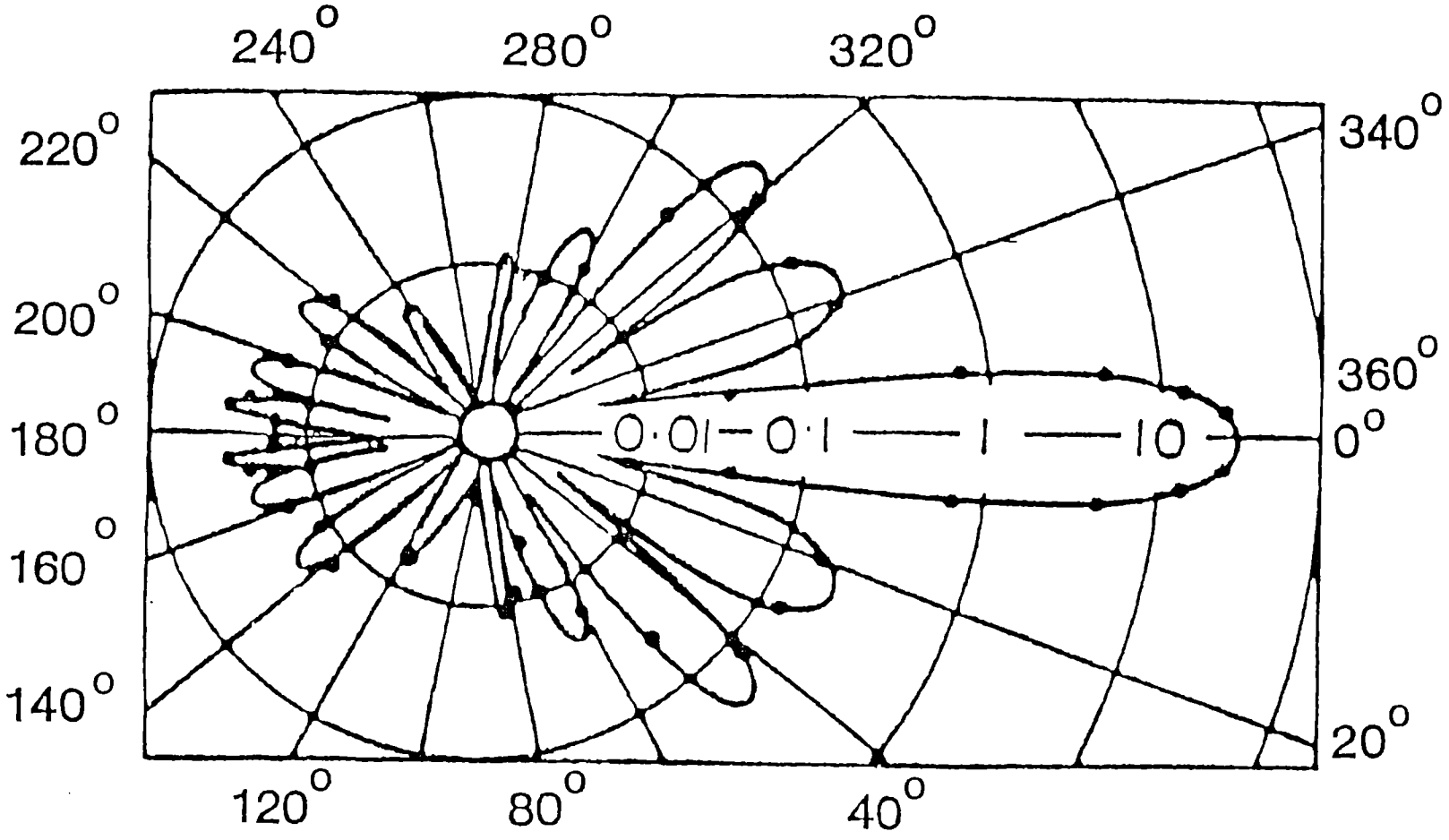

Fig. 2.3 Variation Of Light Intensity Scattered By A Single Particle

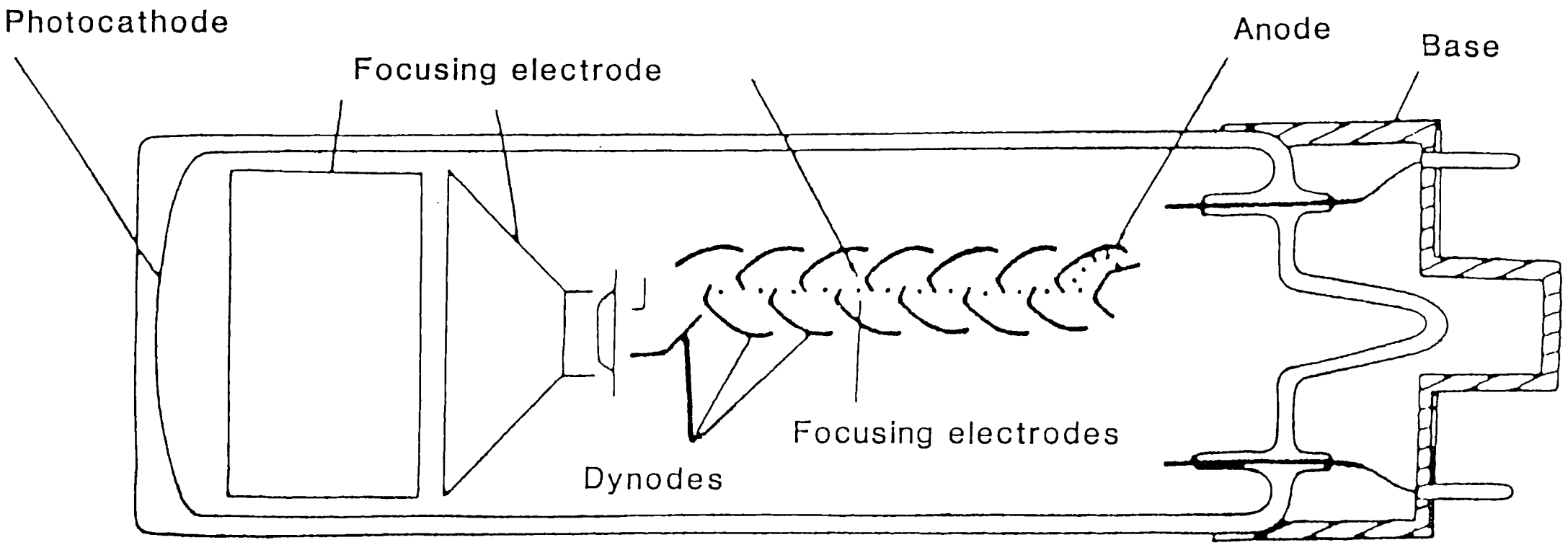

Fig. 2.4 Components Of Photomultiplier Tube

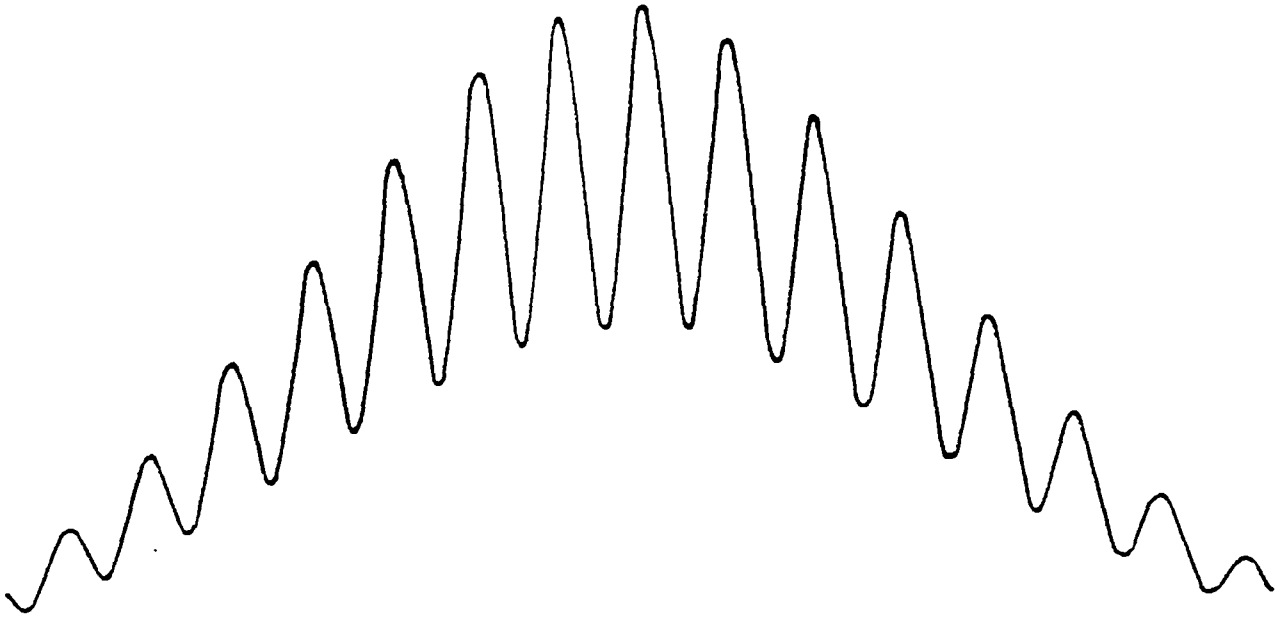

a With pedestal

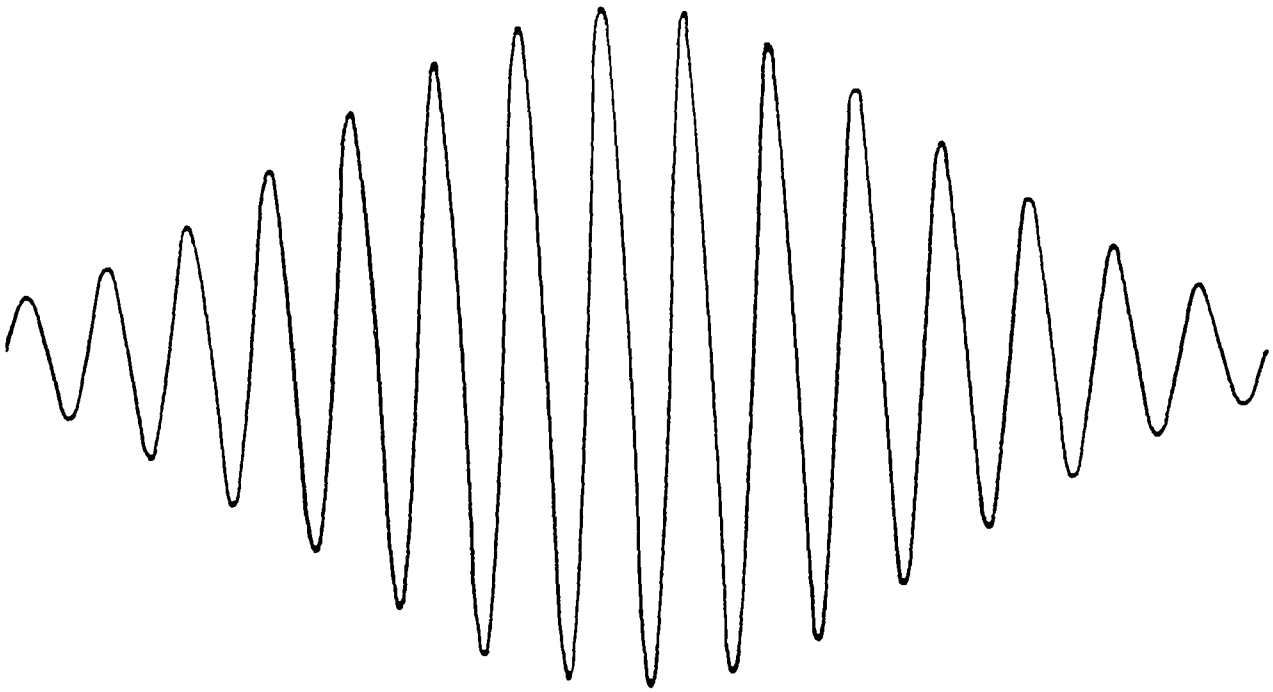

b Without pedestal

Fig. 2.5 Typical Doppler Signals

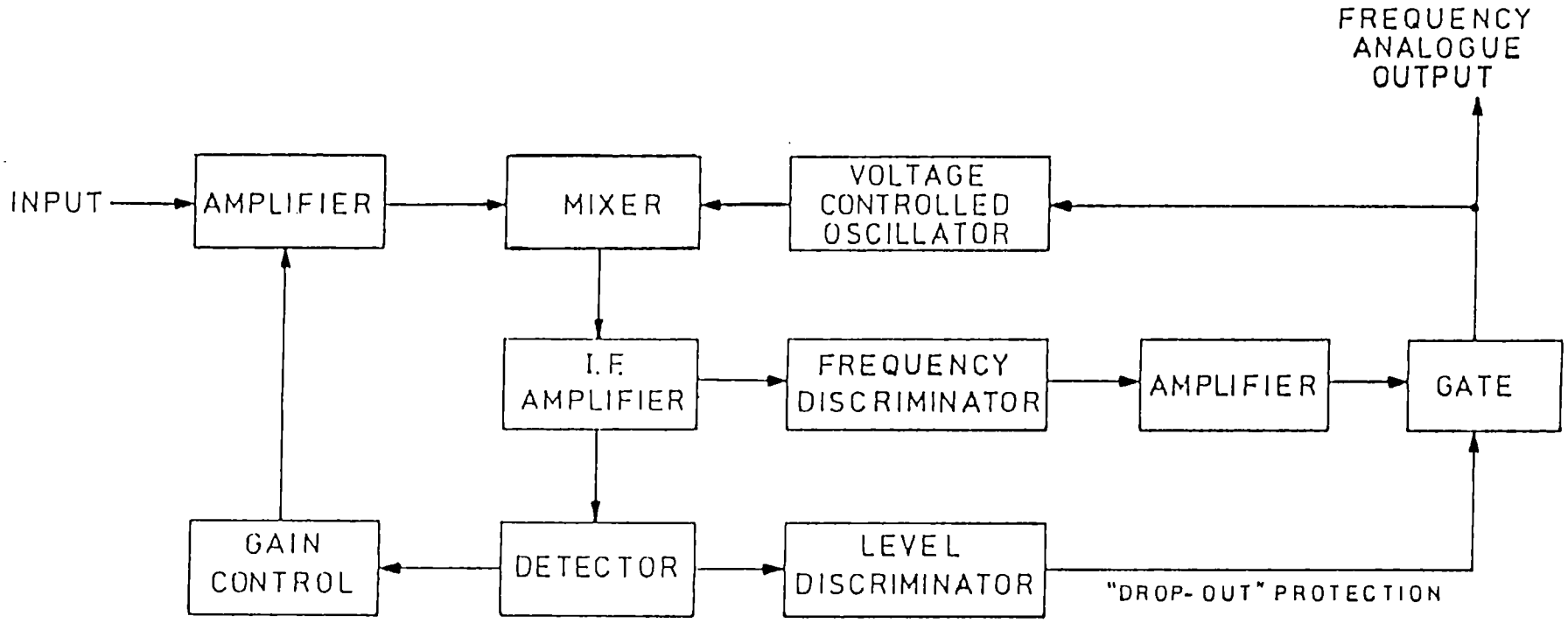

Fig. 2.6 Block diagram of a frequency tracker

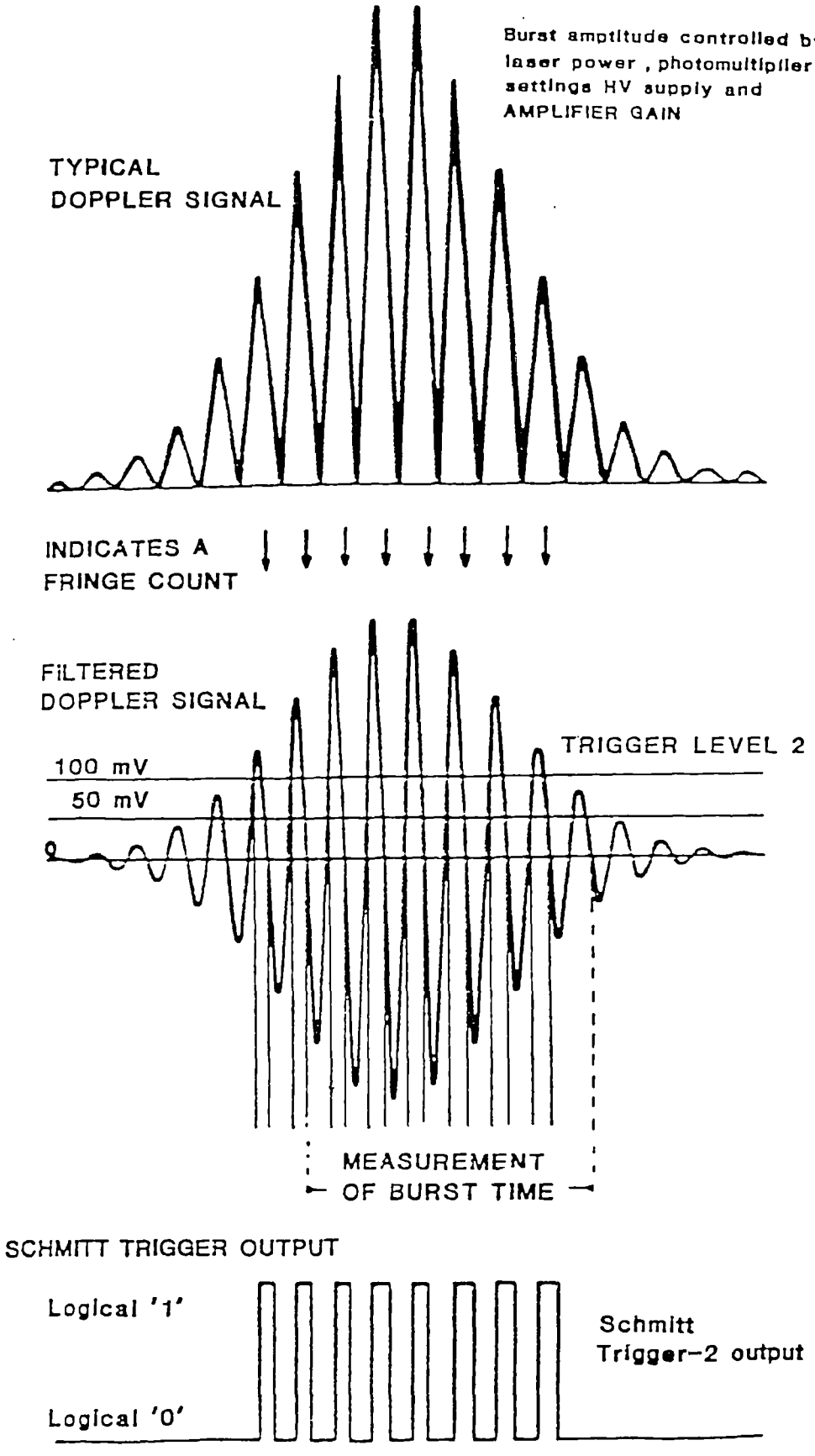

Fig. 2.7 Doppler signal from a signal scattering particle and the Schmitt Triggers, of a Counter Processor

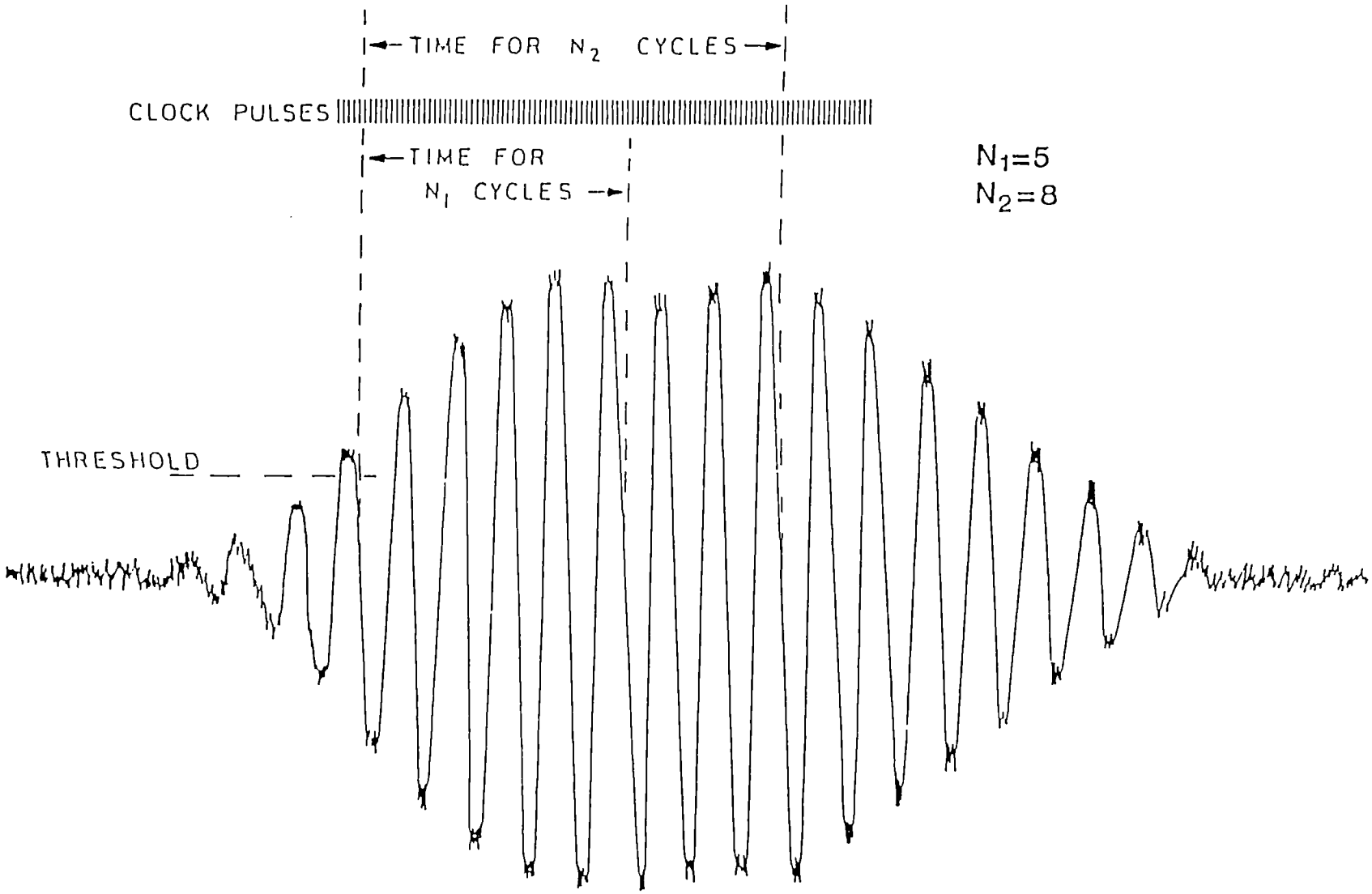

Fig. 2.8 Timing cycles of a Doppler burst for frequency measurement and validation in a counter processor

CHAPTER 3

BIAS INVESTIGATION

3.1 EXPERIMENTAL APPARATUS

The system may be divided into four subsystems :-

LDA.

The flow system.

Data acquisition.

Data processing.

The Laser Doppler Anemometry system used throughout this project was designed and built within the Department during 1982-1985 by G.Hartis and A.Wright (Ref. Hartis & King 1983).

3.1.1 LDA

Monochromatic and coherent laser light for the system was supplied by a Lexel 95, 2Watt Argon-ion laser, operating in the TEM_{oo} mode using the 514.5nm line.

The general layout of the LDA is shown in Fig. 3.1.

Figs. 3.2 - 3.5 show details of the LDA optical system arrangement and hardware.

Two plane mirrors aligned the laser output beam with the axis of the transmission optics. The mirror mounts had rotational adjustments, allowing the laser head and the optical bench to be firmly bolted down without need of complex adjustment arrangements.

The single beam from the laser was then focused onto a rotating radial diffraction grating. This provided beam splitting and variable frequency shift.

The grating (with 21600 lines) was produced by a bleaching process on a 160mm diameter plate glass disc and was designed so that the even order beams were suppressed. The first order beams thus contained a large proportion of the input laser power, essential for operating the differential beam technique.

The grating disc was mounted on the shaft of a 1/15 h.p. 200V d.c. motor whose speed might be varied and displayed on a digital readout.

The motor was mounted, as shown on Fig. 3.4, on a tube whose axis defined the bench optical axis. The motor could be rotated about the tube and provided the facility for rotating the plane of the beams. The tube also acted as a slideway for the first lens mount. This biconvex lens (f=200mm) was used to form a beam waist close to the grating plane. Adjustment of the beam waist position, to ensure its coincidence with the intersection volume, was thus possible.

The fringe number effect – due to the fact that the LDA signal processor requires a minimum number of fringes for processing – was eliminated by frequency shifting. The rotational speed of the grating was chosen to ensure the elimination of directional ambiguity.

A mask was placed after the grating to stop the higher order beams. The beam divergence was then increased by a biconcave lens (f=20mm). Parallel first order beams were produced by a plano-convex lens (f=140mm). This combination of lenses greatly reduced the overall length of the optical bench. A mask was then used to blank the zero order beam and a final plano-convex lens (f=200mm) converged the first order beams, which crossed at the intersection volume.

Altering the spacing of this combination of positive and negative lenses allowed a variation in parallel beam separation and hence fringe spacing. The arrangement maintained optical path length equality.

The three lens mounts were all similar in construction. They were fully adjustable and allowed careful alignment. The components were mounted on an optical bench which enabled easy removal and reassembly to a rigid structure.

The laser and transmission optics were all mounted on an extended milling machine bedplate. This provided full 3–D traversing and a very rigid foundation for the optics, with virtually vibration-free movement of the whole system. The extent of traverse available was 480mm vertically and 520mm x 330mm horizontally. There was a turntable on top of the traverse gear which provided angular rotation of the laser/ optical bench hardware. It was scaled in 1degree divisions and the full extent of rotation was limited only by the extent to which the milling machine bedplate and the laser physically interfered. The 2 beams of equal intensity emerging from the transmitting optics were brought to a focus within the flow rig.

3.1.2 Flow System

The flow rig designed, built and used for all bias investigation measurements is described by Simpson (1985). Its design aims were to be simple and provide a flow situation in which high turbulence intensities are obtainable and which is fairly common and well–documented elsewhere. The rig chosen consists of a closed loop water system, incorporating a sudden expansion. It had to be suitable for LDA measurements and to fit in with the existing laser system.

Its use in this project was appropriate due to its ability to provide a flow situation encompassing comparable Reynolds numbers and turbulence frequencies to those anticipated for the curved jet flow study.

The general layout is shown in Fig. 3.6. Its main elements are :– pump, settling section, test section and exhaust section.

The water used in the rig was first filtered through a 5micron filter and the system was then able to use naturally–occurring seeding particles as its scattering centres. The use of a water system thus avoided the problems of introducing some form of artificial seeding. A closed loop system has the advantage of recycling the working fluid and thus maintaining a constant seeding level. The particles were large enough to provide an adequate Doppler signal, but were small enough to avoid particle lag bias problems.

Particle distribution bias was avoided by the inclusion of an adequate length of pipe – 90 small pipe diameters – between the pump and the expansion section.

The pipework for the test section was constructed from Perspex tubing, providing the optical access essential for LDA purposes. Its only restriction was the common problem of *lensing* – the effect of the cylindrical surfaces, which also cause flare.

Its flexible design allowed measurements over a wide range of flowrates and turbulence intensities. Flowrate was controllable by a simple ball valve. The pump selection was governed by flowrate versus headloss considerations and non-corrosion requirements. In order to maintain an adequately constant water temperature, a heat exchanger, comprising a copper tubing coil fed with mains water, was included in the reservoir.

3.1.3 Data Acquisition

The system operated in forward scatter mode (the light collection system was on the opposite side of the measuring section to the transmission system) with an independently mounted, fully adjustable photomultiplier(PM) tube assembly. The detector system was mounted on a photographic tripod, providing easy adjustment for optimum positioning relative to the beams and the crossover.

Scattered light from particles crossing the beam intersection was collected by a commercial camera zoom lens (Tamron 80-210mm). The optical assembly was fitted with a hood and incorporated a variable aperture, which could be used to restrict the size of the cone of scattered light reaching the detector. The receiving optics thus prevented backround illumination reaching the photomultiplier surface. The zoom lens projected an image of the intersecting beams onto a plane which included a pinhole.

The variable focal length lens enabled the image of the measuring volume on the pinhole to be enlarged or reduced to improve the signal. Its main advantage was its ability to control the image size and thus project only that part of the crossover containing the cleanest signal.

A special adaptor, shown in Fig. 3.5, housed the pinhole mount and bolts onto the PM housing. The zoom lens screwed onto the front of this mount. The pinhole mount was secured between two adjustable screws, which enabled the centre of the pinhole to be aligned with the image of the intersection volume. The effective measuring volume size could be varied using the adjustable magnification of the zoom lens in conjunction with three pinhole sizes (25, 50 and 100micron). The 50micron size pinhole was used throughout the present investigation and subsequent curved jet flow study.

An integral pinhole viewer, comprising a microscope objective and eyepiece was used to aid focusing the intersection upon the pinhole. A coarse adjustment of the lens position moved the image of the measuring volume over the pinhole. The fine adjustment screws were then used to yield the optimum signal strength and quality.

The light passing through the pinhole was then detected by a photo-multiplier tube (Thorn EMI Type 9871B). The optics were mounted on a camera tripod, allowing easy adjustment and optimum location.

The photomultiplier output signal, carrying the sum of the Doppler frequency and grating frequency, was fed to a commercial, DISA (Dantec Electronics Ltd.) Counter Processor, Model 55L90a. The PM signal was continuously monitored on a dual trace oscilloscope.

The DISA processor comprised a counter unit, data rate display and indication of % validated signals, and mean velocity computer to display velocity or Doppler frequency.

Signals from the photomultiplier were input to the processor's signal conditioner. The Counter Module contained low and high pass filters for removing noise and the Gaussian pedestal from the Doppler signal. It also contained an amplifier which varied the amplitude of the filtered signal and attenuated the preamplifier output when the signal level was too high.

The DISA counter was operated in its 'continuous' mode. The timer module determined the Doppler frequency from 8 cycles. Signal validation was performed with a 5:8 cycle comparator with a tolerance adjustable from 1.5 to 12%. This was maintained at the lowest value for all present measurements.

The Doppler frequency of a burst was determined using a high speed digital clock (500MHz) in conjunction with a zero crossing detector and a Schmitt trigger. The Schmitt trigger produced a square wave from that proportion of the signal which exceeded a pre-set theshold (200mV).

Optional settings of the *Theshold Window* were possible on the Counter. These set the upper amplitude for the incoming Doppler signal. If this was exceeded, all Counter circuits were reset and signals from large scattering particles were thus rejected.

The Mean Velocity Computer Module provided an *Ensemble Width* selector switch which determined the number of validated velocity calculations used in the evaluation of the mean velocity before display. The options ranged from 1 to 4086 samples, the choice of which depended on the current data rate. The Velocity display could provide data in the form of velocity

or frequency; it was maintained in the Doppler frequency mode throughout the project and thus gave an output in MHz.

Finally, the *Data Rate Module* displayed continual updates of both the data rate (in the range .000 - 999 kHz) and data validation rate (as %o).

To investigate the time-varying nature of turbulent flows, the discrete digital output of a counter was preferred to the analogue output of a tracker (Hartis & King (1983)).

Gating of the data might be achieved on a DISA 5590a Counter, using TTL logic voltage levels applied to either or both of the ARM and INHIBIT lines, accessed from the rear counter plate (Ref. DISA manual). Both these lines are held at logic level high under default conditions. Holding the INHIBIT line to logic level low by some external circuit inhibits the counter from processing further input signals, while allowing it to remain high permits the counter to continue to process all incoming signals.

Fig. 3.7 displays the principles of the operation. The counter remains enabled while the ARM line is high. When the ARM line falls to logic level low, a single measurement may be completed and, if validated, recorded. The counter is then disabled until the ARM line returns to high. A short pulse on the ARM line thus allows the counter to make a single measurement from the first valid data point to arrive after the pulse. This can occur at any time until the INHIBIT line falls to low. The two lines therefore permit a simple windowing process to be achieved under the control of external circuitry.

Two forms of hardware data windowing can be achieved. If the ARM line is held high while the INHIBIT line changes from low to high and back to low after an interval τ, a window of length τ is defined, during which every

valid data point will be processed. Alternatively, if, while the INHIBIT line is high, a short pulse to high is given on the ARM line, the next one valid data point will be processed and recorded. If no valid data is received before the INHIBIT line falls, no measurement will be recorded for that window.

If an external circuit, which is strobed by the flow, controls the opening and shutting of the window, measurements may be made at fixed points in a flow cycle. Alternatively, the rate of sampling may be controlled by using a fixed frequency clock to strobe the windowing circuit.

A block diagram, shown in Fig. 3.8, illustrates the operation of the windowing circuit designed and built by Simpson(1985). It consisted of a high frequency clock, whose output was fed to a frequency dividing circuit (giving frequency division up to 999999) to provide pulses of the required frequency. Then, to obtain pulses of the correct duration, the signal was input to a monostable (which detects rise in waveform and produces only a short pulse). In order to obtain an input compatible with the ARM socket, the monostable signal was fed through 2 Hex Schmitt inverters.

3.1.4 Data Processing

A microcomputer system had been developed to read and process the data from the DISA counter. Data acquisition and short term data storage was performed by a purpose-built interface and a CIFER terminal with Ithaca CP/M computer and twin 8" floppy disc drives.

A maximum of 4000 samples could be stored for a single reading. After acquiring the requested number of data points, the data was processed by

the computer either immediately or later. A number of FORTRAN programs were written to process and display the statistical results.

The CIFER FORTRAN programs already in existence proved to be either inappropriate or unusable for their present application. Work was, therefore, directed towards modifying, expanding or re-writing the data collection, analysis and storage programs.

Data collection was initiated by DTEXP (which, when *disc* or *console* options were chosen, called up subroutines DTITD or DTITC respectively). This defaulted to filing data on its own disc in VELDATA.DAT or, if requested, onto a specified file on disc drive B (the specified file need not have existed already – if it did, the contents were overwritten).

The appropriate file was then accessed by the program TRANS, whose storage capacity had been increased from 2000 to 4000samples/reading. This performed the data analysis, including options to reject data outside 3 standard deviations, view the probability density function (P.D.F.) and transfer the resulting statistical data onto the other disc, suitably formatted for transmission to MTS.

An attempt was made to remove the analysis stage from the CIFER system and onto the Durham NUNET MTS mainframe computer system. This, although successful, was an unattractive alternative since the raw data took a considerable time to transfer between discs and each disc, in its MTS-compatible format, could store only one, or part of one, file when the data had also been suitably formatted.

The first three moments of the data were computed using standard formulae (Wright 1984). Mean velocity, turbulence intensity, standard de-

viation, skewness and kurtosis were among the parameters computed. The assumption was made of ergodic turbulence i.e. it was assumed that the statistical properties of the turbulence were invariant with time (the turbulence is 'stationary') so that the time mean was identical to the ensemble mean. The mean velocity of a sample was calculated from

$$\overline{u} = \frac{1}{N}\sum_{i=1}^{N} u_i \qquad 3.1$$

From the calculation of the mean, a probability density function for the fluctuating velocity could be established. By definition, the mean of this sample should be zero :-

$$u' = \frac{1}{N}\sum_{i=1}^{N}(u_i - \overline{u}) = 0 \qquad 3.2$$

The other statistical parameters are the second, third and fourth moments about the i=0 axis :-

The VARIANCE

$$\sigma^2 = \frac{1}{N}\sum_{i=1}^{N}(u_i - \overline{u})^2 \qquad 3.3$$

The SKEWNESS

$$sk = \frac{1}{N}\frac{1}{\sigma^3}\sum_{i=1}^{N}(u_i - \overline{u})^3 \qquad 3.4$$

The KURTOSIS

$$ku = \frac{1}{N}\frac{1}{\sigma^4}\sum_{i=1}^{N}(u_i - \overline{u})^4 \qquad 3.5$$

Skewness and kurtosis are used to quantify the departure of real turbulence statistical properties from those given by the 'normal' or Gaussian P.D.F., for which sk=0 and ku=3. Skewness is a measure of the asymmetry of the fluctuating velocity distribution : a positive value for skewness implies a distribution with fewer large negative values than large positive values. Kurtosis is a measure of the flatness of the distribution : a large value infers a high probability of obtaining a value in the 'tail' of the P.D.F. An example of the significance of the statistical data is shown in Fig.3.9. The *turbulence intensity* is defined as the ratio of the standard deviation of the instantaneous fluctuating velocity to the mean velocity

$$T.I. = \frac{\sigma}{\overline{u}} \qquad 3.6$$

Data more than 3 standard deviations away from the mean was not automatically rejected – the results were displayed and a judgement was made as to where to set the rejection limit. The moments could then be recalculated and were finally stored.

Collection of data points continued until a superpopulation of approximately 30000 samples had been collected at any one condition.

3.2 INITIAL EXPERIMENTS

3.2.1 Initial Problems

Giel & Barnett (1978) emphasise that in order to measure statistical bias experimentally, the precision uncertainty in the LDA measurements must be less than the bias.

Consistent values were unobtainable initially due to electrical interference between the flow rig pump and adjacent equipment. Installation of an induction motor driven pump solved this problem.

To establish a datum and gain understanding of what it might be reasonable to expect for repeatability of readings, a point on the large diameter tube centre-line, approximately 40mm. above the sudden expansion, was located. Here the T.I. was of the order of 4% and all subsequent subsystem experiments were carried out at this position.

A. System Stabilisation

With the laser on *current control* setting and the PM voltage fixed, the PM current fluctuated by over 1% and this was reflected in the range of mean velocities recorded. Changing to laser *light control* reduced the variation to .3% and, hence, the scatter in u readings. All further LDA measurements were obtained with the laser set to the **light control** option.

It was also noted that time must be allowed for the system, and especially the laser, to settle – typically 1/2hr. – both when initially turning on and again after changing any system parameter.

B. Processor Problems

During a sequence of readings, the data rate, validation rate and frequency indicated by the DISA processor showed a sudden inexplicable step change in levels with a concomitant fluctuation in mean velocity values. A malfunction in the hardware was indicated since alteration of the filter settings restored the levels. The DISA processor was finally returned to the manufacturers and updated with their latest standard of filters and processing equipment and this problem was then successfully eliminated.

3.2.2 Subsystem Investigation

It was considered expedient to split the system into its constituent components and attempt to isolate and measure the scatter inherent from various sources. Such isolation should identify the major contributors to the observed variation in measurements, which might then be minimised by their modification or removal.

The sections identified for study and the experiments performed on the divided LDA system are as follows :-

A. Laser beam

A laser power meter was used to investigate the calibration of the laser power supply and the day to day fluctuation of the beam power.

The meter was inserted into the beam path 'upstream' of the diffraction grating. A variety of power settings were chosen and a calibration of the laser power supply was obtained.

The calibration was subsequently repeated over a number of days to assess laser beam power variations.

In order to investigate the conditions of the crossover, the beams were focused onto the wall. The fringes at the probe volume are then detectable by eye since this, like the PM tube, is a square law detector. The beams are plane parallel only if they cross at their waists; deviation from this situation produces fringes that are not parallel and their spacing thus varies through the probe volume.

The calibration obtained with the laser power meter showed the measured power to be approximately 30% lower than that displayed on the power supply dials but no day to day variation was detectable.

With the crossover projected onto the wall, the beams appeared coincident and crossed at their waists, with parallel fringes and, hence, equidistant fringe spacing.

B. Photomultiplier Tube

To eliminate variations due to the flow field and thus study only the performance of the PM tube, the laser beams were focused onto a Perspex block. The signal from the PM tube was then monitored.

Two different Brandenburg power supplies were also tested for their effect upon PM tube performance, as indicated by the PM current and DISA data rate displays. Firstly, using only one of the supplies, a particular PM voltage was selected by a number of different combinations of 'buttons'. Differences between the two supplies was also studied: by applying the same

voltage by the same combination of 'buttons', the PM tube current output and DISA data display values were compared.

When focused on the beam crossover within a block of Perspex, the data recorded showed a 13% variation. There was, however, a much higher fluctuation ($\pm 15\mu$A) of PM current than normally registered during flow rig running ($\pm 2\mu$A) and the processor filters were not at their 'normal' values. No explanation for this inconsistency was discovered.

When using only one of the supplies, a particular PM voltage was selected by a number of different combinations of 'buttons'. The different permutations resulted in a PM current variation of $\pm 15\%(\pm 5\mu$A) and $\pm 7\%(\pm 5$ kHz) on data rate. When returning to a previous value of PM voltage, therefore, care was always taken to use the identical combination of voltages in its production.

When differences between the two supplies were studied it was found that similar data rate and current values were achieved by similar values of applied voltage. It was, however, considered advisable to use one supply only for all subsequent measurements. This avoided the introduction into the system of any further variability.

C. Processor

To isolate the processor from the errors introduced by the other LDA system components, a frequency generator was applied directly to its input. This simulated a Doppler frequency output from the PM tube with negligible noise and provided a test of the processor alone.

A range of frequencies was applied directly from the generator to the DISA processor. The data collection and analysis programmes were run to study the scatter in the data thus generated.

Only small variations in the computed mean velocities were recorded over the range of applied frequencies. It is difficult, however, to put the results into context since the filter settings required to obtain satisfactory signals were somewhat different from those used for normal rig running.

D. Flow rig

In order to monitor the fluctuations in the flow introduced within the flow rig itself, a pressure transducer was mounted across the sudden expansion section. Its output was fed to a voltmeter and to an oscilloscope.

The calibrated pressure transducer showed negligible variation in pressure difference, and hence flowrate, over a period of running, or between runs, when monitored by a voltmeter. When connected to an oscilloscope, however, the existence of low frequency fluctuations was indicated. It was difficult to isolate flow variations, but if they do exist in the flow they would contribute to the recorded scatter on velocity readings.

3.3 BIAS INVESTIGATIONS

Reported studies by Giel & Barnett (1978), Bogard & Tiederman (1978), Roesler et al (1980), and Durao et al (1982) were examined to establish the parameters to which arrival rate bias is related -

a. Turbulence persistence time, the time–scale of the energy–containing turbulent fluctuations, as quantified by the Kolmogoroff length scale (Davies 1972), whose range is limited by the flowrates available.

b. Turbulence intensity, a range of values are available across the flow, downstream of the sudden expansion.

c. Particle arrival rate, dependent upon the level of seeding but also affected by the laser intensity and PM sensitivity.

d. Sampling rate, variable by using the DISA processor alone or by insertion of an external timing circuit.

Factors which were identified by Durao, Laker & Whitelaw (1979) and by Durao & Whitelaw (1980) as of importance in the investigation into LDA signal amplitude bias are:-

a. PM tube sensitivity – varied by changing the applied voltage.

b. Laser power – a range between 0.075 and 0.6W is available.

c. Turbulence intensity – a range of values are available by traversing the beam crossover position across the flow, at a variety of locations dowstream of the sudden expansion.

d. Frequency shift – this is always present in the existing configuration to eliminate other bias effects.

To quantify bias effects and their dependence on these various parameters, attempts were made to produce a carpet plot of velocity and turbulence data for a wide variety of conditions. By keeping constant all but one variable, the effect of that variable upon velocity measurements could be

studied.The intention was to separate and quantify their individual influences on bias effects.

3.3.1 Arrival Rate Bias

A sequence of readings comprised

e.g. for a constant flowrate (constant Kolmogoroff frequency),

constant turbulence intensity (at one point in the flow),

fixed sampling rate,

and constant laser power,

the PM tube sensitivity was varied.

At each value of PM tube applied voltage, groups of 4000 samples/point were collected until a superpopulation of at least 30000 samples was obtained. For each sub-group of 4000 samples, the values for mean velocity, U, and the turbulence statistics were calculated and recorded.

Throughout the arrival rate bias study, data was collected with no sample interval control on the collection process. The variables were systematically studied and measurements were taken for a wide selection of conditions.

3.3.2 Signal Amplitude Bias

Arrival rate and signal amplitude bias effects are acting simultaneously within the data acquisition process.

To study signal amplitude bias in isolation, one must therefore operate in a regime totally free from any arrival rate bias. Arrival rate bias is effectively eliminated by hardware windowing the data. In this situation, hardware windowing was achieved by applying the windowing circuit to the DISA counter ARM line thereby ensuring that the signal and the sampling process were uncorrelated.

The identification and quantification of arrival rate bias was then attempted by taking velocity measurements with constant PM voltage and various levels of laser power and then with constant laser power and a variety of PM voltage settings.

3.3.3 Ergodicity Investigation

The effect of sampling rate and hence ensemble integration time upon measurement scatter was then studied.

The hardware windowing circuit designed and built by Simpson (1985) was again used for this work. In conjunction with the DISA counter it provides the facility for varying the time between sample acquisitions, obtaining 1 sample only per window (thus, in effect, varying the apparent data rate).

At a point approximately 40 mm above the sudden expansion, traversing the pipe diameter provided a range of local turbulence intensity from 11% to 46%. Lower values of turbulence intensity were found approximately 10mm downstream of the expansion. Here a region of 5% T.I. was located.

Consecutive experiments were performed over the range of turbulence intensities where, at each position, the sample interval value was varied over

several orders of magnitude, from $1\mu s$ to $10^4\mu s$. The time taken to acquire the requested 4000 samples comprising each data point thus varied widely.

3.3.4 Sudden Expansion Velocity Profiles

Using the windowing technique to ensure repeatability of data within 2%, traverses were made across the large diameter tube. Profiles were measured up to 5 diameters downstream, including one at the inlet section, approximately 2mm downstream of the expansion, to check velocity and turbulence levels at entry. Measurements were taken across the full pipe diameter in order accurately to assess the position of the pipe and/or flow centre-line.

These profiles were used to compare the flowfield with that obtained by other authors working with similar flow geometries (Freeman (1975), Szchepura (1985)) and hence validate the LDA system and measurement technique.

3.4 RESULTS & DISCUSSION

3.4.1 Arrival Rate Bias

Having identified the factors affecting bias and performed the sequence of experiments to establish their individual significance, the data from all permutations of flowrate, T.I., laser power and PM tube sensitivity investigated were studied for repeatable trends.

Fig. 3.10 shows just one example, typical of the results obtained. It is a plot for the effect upon velocity measurements of varying the laser power.

The scatter in the range of $\overline{u}$ obtained at any one condition, however, repeatedly outweighed any variation in the level of the mean $\overline{u}$ of the 30,000 sample superpopulations. The precision uncertainty in the readings produced such a large level of scatter at all conditions investigated that it was impossible to identify indisputably any influences of bias upon recorded velocities.

3.4.2 Ergodicity Study

The ergodic hypothesis states that finite samples of a time series have the same statistics as the infinite time series. For this to be true, the length of a finite sample must be long in comparison with the wavelength of the lowest frequency present in that time series. For a discrete sampling system such as an LDA counter system, this means that the ensemble must be built up over a time period long by comparison with the period of the lowest frequency in the turbulence. The Doppler frequency at the test condition was of the order of 2.5MHz and thus the shortest sample interval of the uncontrolled acquisition was 3.5μs i.e. 2.5 μs to obtain 10 cycles of Doppler frequency plus 1μs counter reset time.

The dramatic effect upon scatter, in $\overline{u}$ and T.I. estimates, of varying the time taken to acquire the 4000 samples, comprising each data point, was repeatedly seen - just one example is shown in Fig. 3.11 for a local turbulence intensity of 40%. Each data point represents 4000 samples and indicates the effect upon velocities and T.I. of increasing the sample interval time by orders of magnitude from 10 to $10^4\mu$s whilst maintaining all other system parameters constant.

The data for all sample intervals at all levels of turbulence intensity

were statistically analysed. An overall mean velocity value was computed for the superpopulation of 30000 data points collected at each condition and the limits for 2 standard deviations was obtained. The results from all these experiments are shown in Fig. 3.12 as scatter of data, expressed by 2 standard deviations, plotted against sample interval.

Except at very low turbulence levels (5%), the scatter in the readings drops significantly as sample acquisition time increases. To operate in a situation with a sufficiently low level of scatter, the sample interval must be long in comparison with the turbulence length scale. This then ensures that the sampling process is completely uncorrelated from the signal and hence a truly ergodic sampling regime is attained and maintained.

The Kolmogoroff frequency of the flow in the small pipe was calculated from the relationship

$$f_k = 0.06 V_m \frac{(Re)^{.56}}{d} \qquad 3.7$$

and found to be 3 x 10^4 Hz. The expected lower frequencies in the turbulence are around 10 Hz, based on larger pipe diameter of 40mm and a mean flow velocity of 0.3m/s. Thus it would be expected that an ensemble time extent of 1s should eliminate variations in mean velocity measurements. Fig. 3.12 shows that, for 4000 samples at $10^3 \mu$s sample interval (an ensemble time extent of 40s), the variation in $\overline{u}$ is still of the order of 3%. Further extending the sample interval to $10^4 \mu$s (and the ensemble time extent to 400s), reduces this variation to less than 2%. This infers that there may be some significant lower frequency components in the flow, of order 0.1 to 1Hz

as previously indicated by the pressure transducer. Szczepura (1986) reports similar low frequencies in a sudden expansion flow situation.

3.4.3 Signal Amplitude Bias

The attempt to identify signal amplitude bias involved operating with a long sample interval time to ensure no arrival rate bias, as shown in Fig. 3.13. The PM voltage was maintained while the laser power was varied and then vice versa, whilst all other parameters were held constant. The results are displayed in Figs. 3.14 & 3.15.

Results from both tests gave no clear indication of any trend larger than the measurement scatter. According to Durao, Laker and Whitelaw (1980), signal amplitude bias and arrival rate bias are of a similar magnitude. The work of Johnson et al (1984) quantifies *arrival rate bias.* From their work, Fig. 3.16 suggests that, for the present study at 46% T.I. a 10% overall change in mean velocity could be expected going from a biased to an unbiased state.

Here the scatter was 3.5% maximum and the variation was only 3% maximum and not monotonic with either laser power or photomultiplier tube voltage.

Alternative explanations for this result include

(a) bias does not exist,

(b) amplitude bias effects only exist at other conditions i.e.even at the minimum laser power and PM voltage used, all particles are already adequately illuminated.

(c) the photodetector integration time is the dominant factor in the identification or elimination of amplitude bias.

The technical literature for the PM tube used in the current survey (Thorn EMI 9871B) quotes characteristics of 35ns for transit time and 2.2ns for anode pulse rise time. These values are closely similar to those of one of the tubes used by Durao & Whitelaw (1980) in their study. The anode pulse FWHM is, however, very different, being 5.5ns and 32ns respectively. The other PM tube used by Durao & Whitelaw was model Thorn EMI 9558. This had significantly different characteristics from those mentioned above. These differences may be sufficient to explain the present inability to confirm the existence of signal amplitude bias.

3.4.4 Velocity Profiles

The velocity data obtained from across the full large pipe diameter was examined and mean 'half-pipe' values were produced.

All the mean axial velocities were normalised with respect to the centre–line inlet mean velocity. The plots in Fig. 3.17 show profiles at inlet, at 0.5 large pipe diameters downstream of the expansion and at 1D intervals thereafter.

The profiles display certain general characteristics of flow at abrupt axisymmetric expansions, as shown in Fig. 3.18. The flow can be divided into three distinct regions; a core, a shear layer and a reverse flow. An annular shear layer grows from the step edge. In the core region, which reduces in size as the the shear layer grows, upstream pipe conditions persist. Between the shear layer and the pipe wall lies an area of recirculating flow.

A trapezium rule integration of (ρ V A / m) was performed using the velocity profiles to produce normalised stream functions. This was performed at the various locations downstream at which velocity measurements were recorded. Fig. 3.19 shows the contour plot of the stream function values thus obtained.

The separating streamline reattaches to the wall at a distance of approximately 11.5 step heights downstream. The eye of the recirculation bubble is 0.5 large pipe diameters downstream and 0.25D from the centre–line.

The results of Freeman (1975) with a 2:1 expansion ratio system (and finer measurement grid) were used for comparison and are shown in Figs.3.20-21. Freeman's 2:1 expansion flow reattaches approximately 9.2 step heights downstream and the eye of the recirculation bubble is 0.83D downstream and 0.37D from the centre-line. The maximum reverse velocity for the 3:1 expansion situation is about 5% of the inlet centre–line velocity compared to 12% from Freeman, both occurring 1D downstream.

Fig. 3.22 shows the corresponding profiles of turbulence intensity. Maximum values were recorded at 1D and 2D downstream where values, based on the inlet centre-line velocity, of 22% were measured. The region of the separating streamline shows levels of turbulent fluctuations that are very much higher than in the recirculating region or on the pipe centre-line. In the recirculating region close to the wall, the absolute level of turbulence remains fairly constant whereas a rapid rise is shown on the centre–line after 1D. The turbulence intensities show close similarities both in distribution and level in the shear layer and on the centre–line to Freeman's data (not shown).

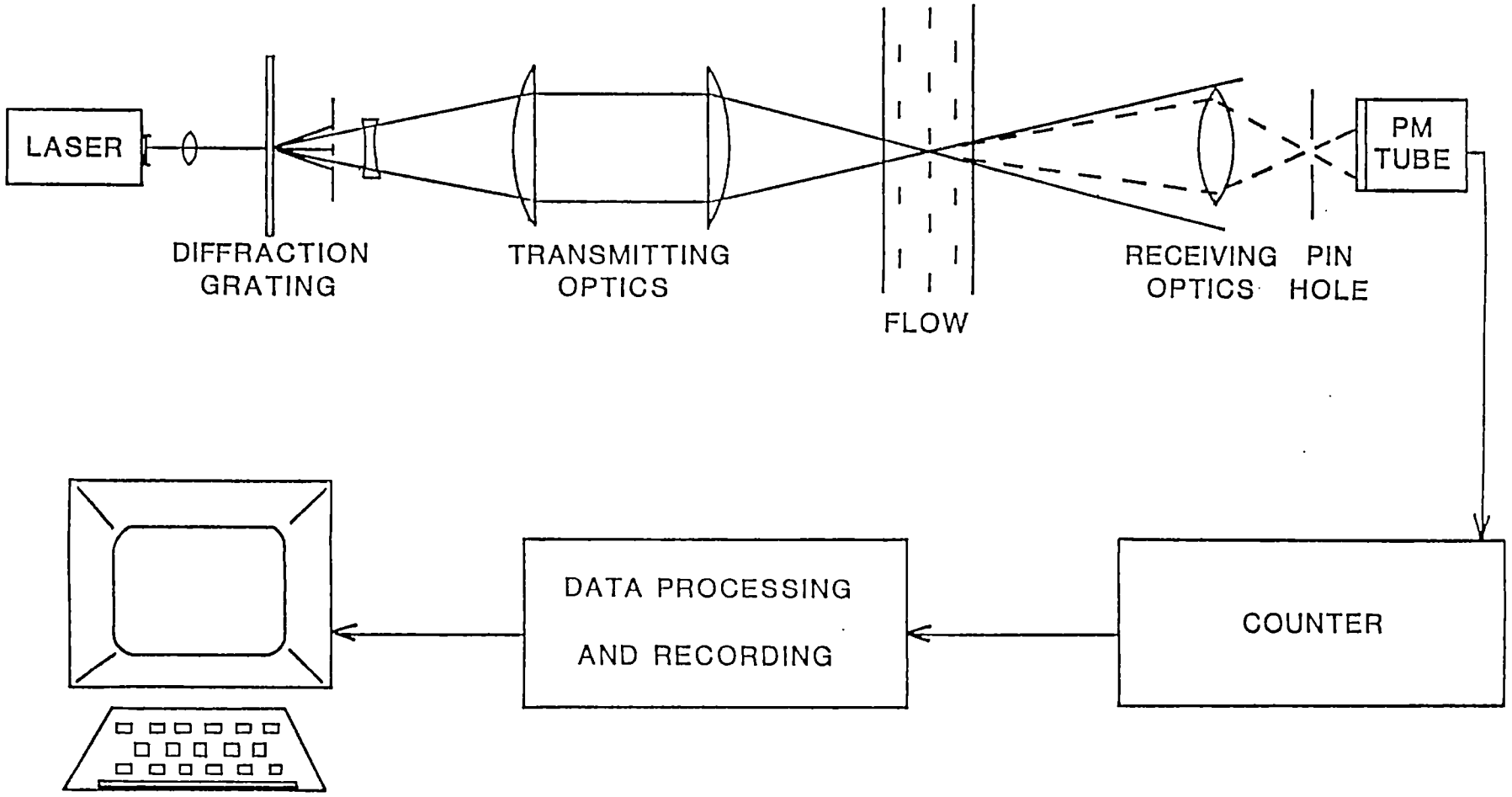

Fig. 3.1 LDA System Components

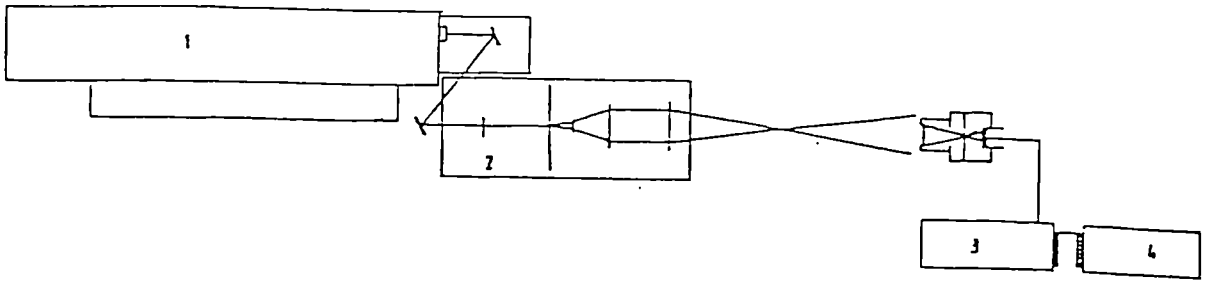

1 - Laser, 2 - Transmission Optical Bench,
3 - Counter, 4 - Microcomputer

Fig. 3.2 LDA System Component Details

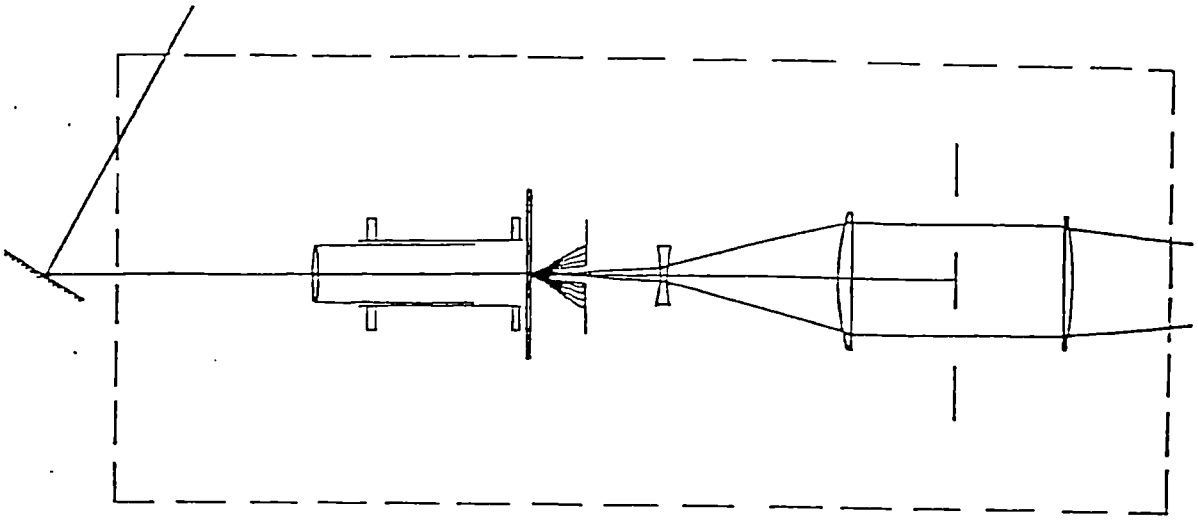

Fig. 3.3 Optical Transmission Bench

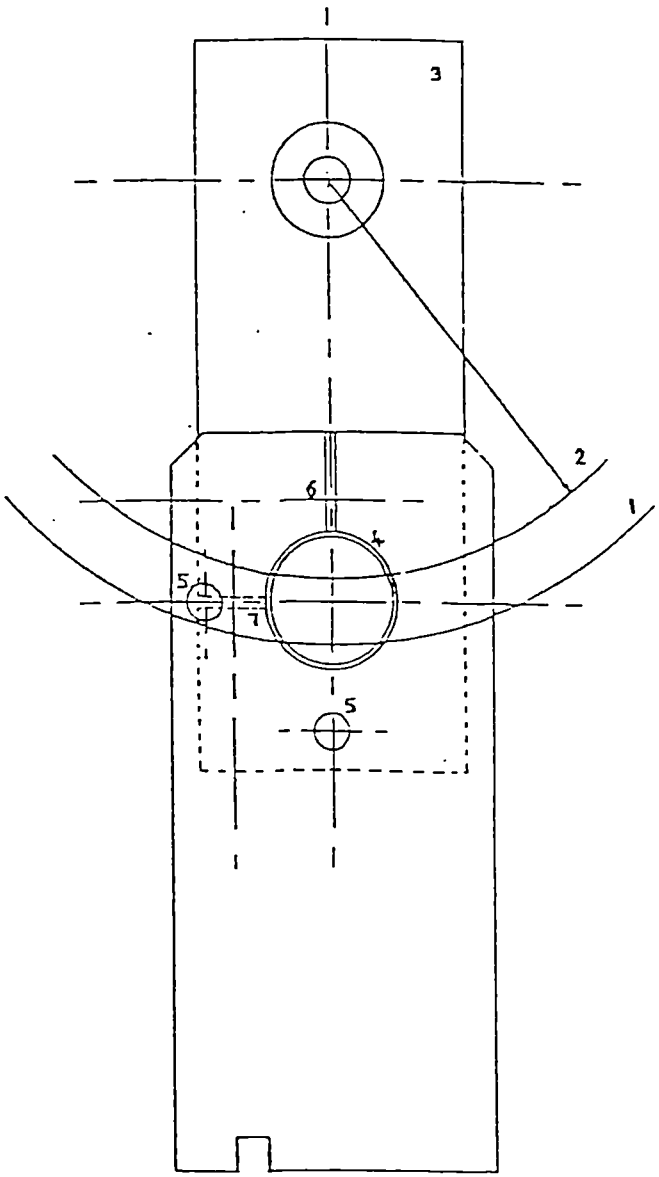

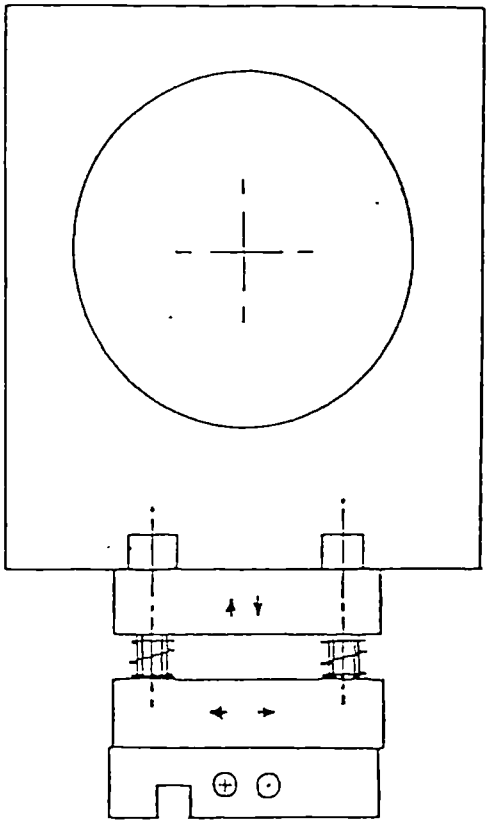

Radial Diffraction Grating Mount
1 - edge of grating disc,
2 - inner limit of bleached grating
3 - motor mount, 4 - tube,
5 - Indexing pin positions,
6 - 'Slot and Screw' clamp; tube to carrier, 7 - 'Slot and screw' clamp: motor mount to tube.

Lens mount. The arrows show the direction of linear adjustment for each layer.

Fig. 3.4 LDA Harware Details

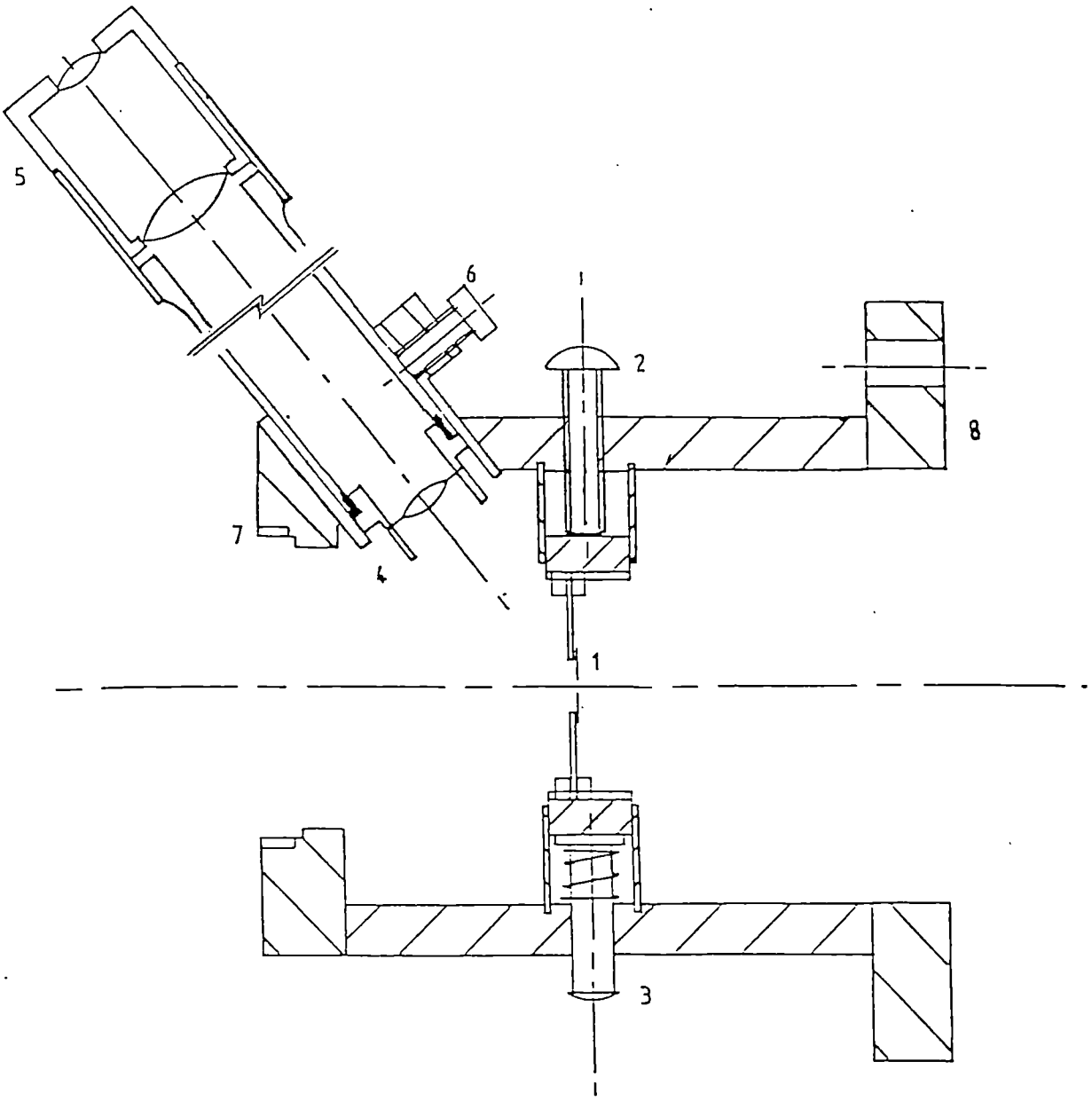

Pinhole mount 1 - Pinhole, 2 - adjusting screw,
3 - pusher and spring, 4 - objective,
5 - eyepiece, 6 - microscope focus adjustment,
7 - mating thread for zoom lens,
8 - flange for photomultiplier housing.

Fig. 3.5 Receiving Optics Details

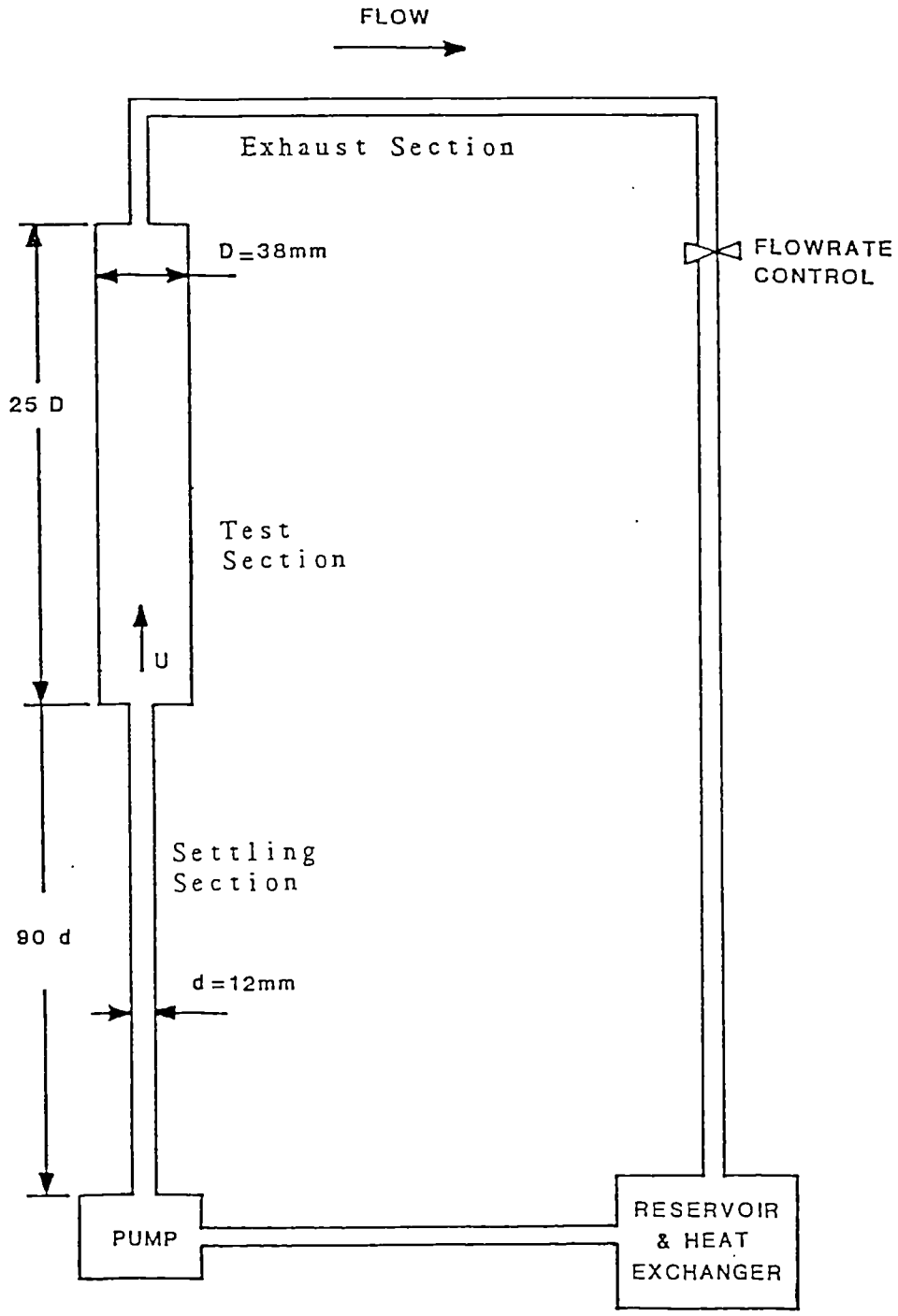

Fig. 3.6 WATER FLOW RIG

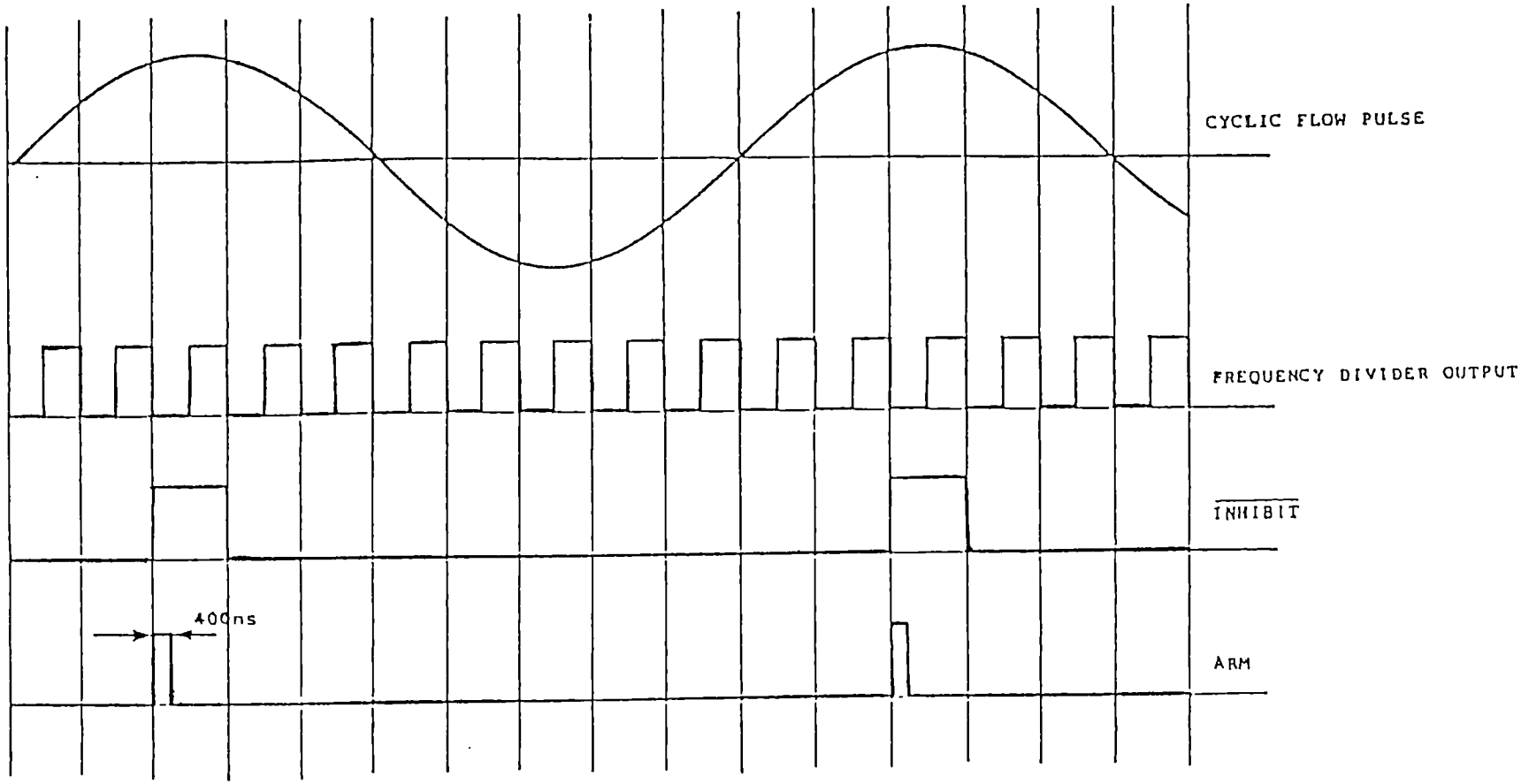

Fig. 3.7 Input and Output Waveforms for Windowing Circuit

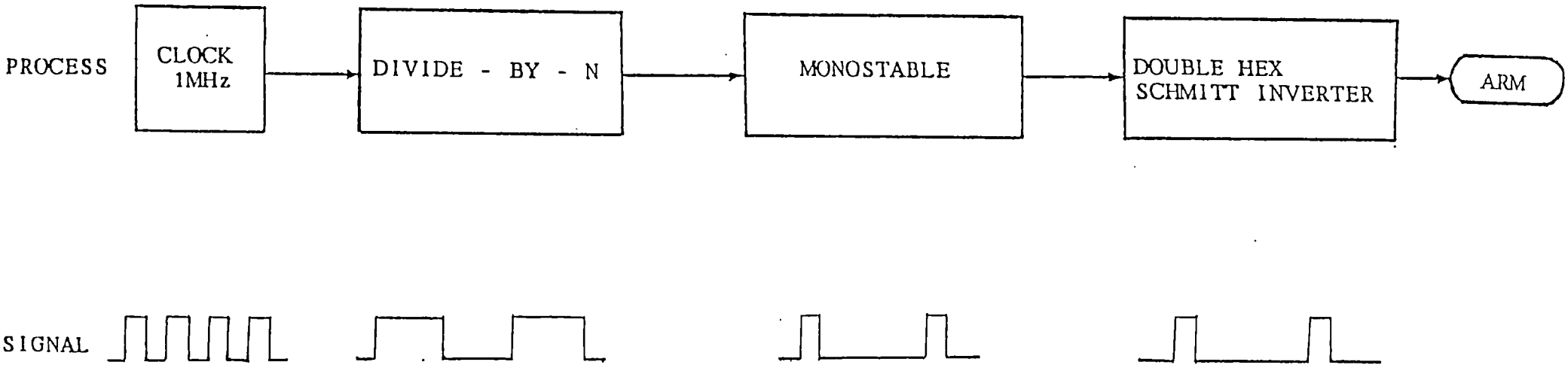

Fig. 3.8 BLOCK DIAGRAM OF WINDOWING CIRCUIT

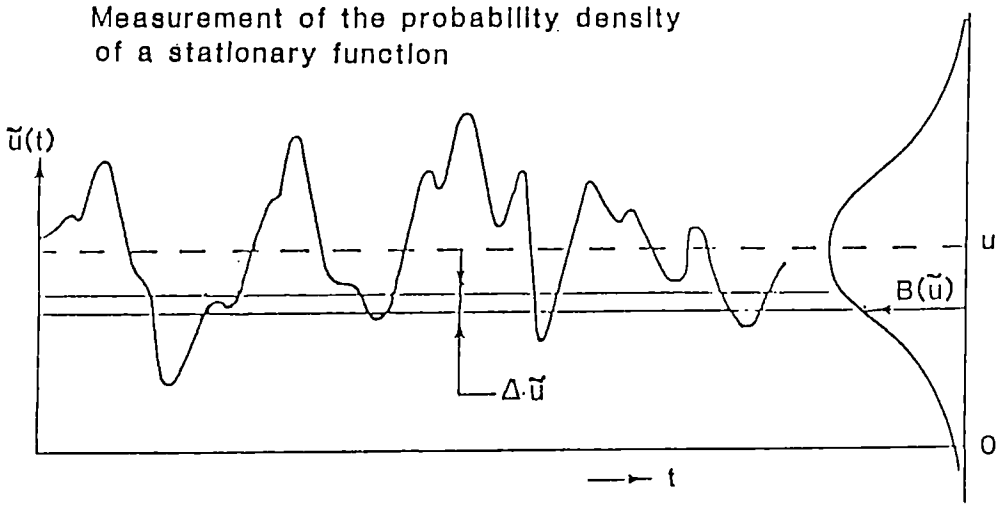

Fig. 3.9 The statistical description of turbulence

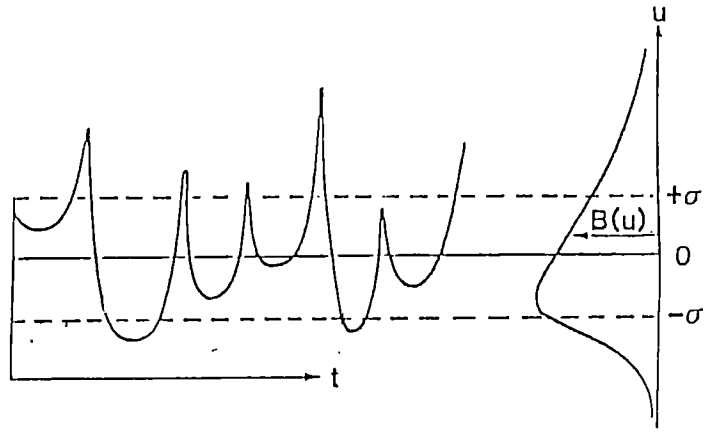

A function with negative skewness

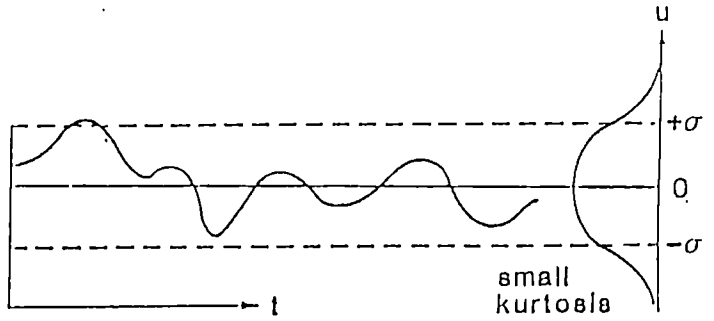

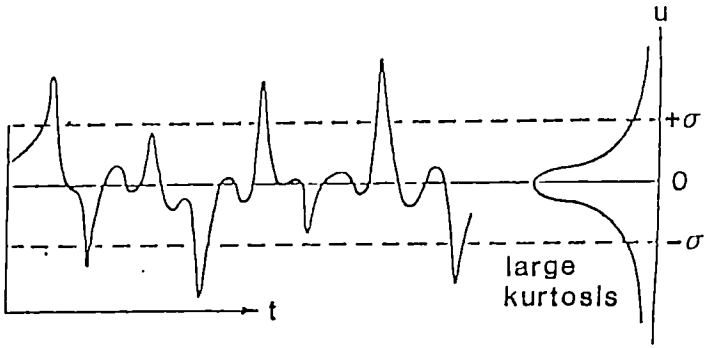

Functions with small and large kurtosis

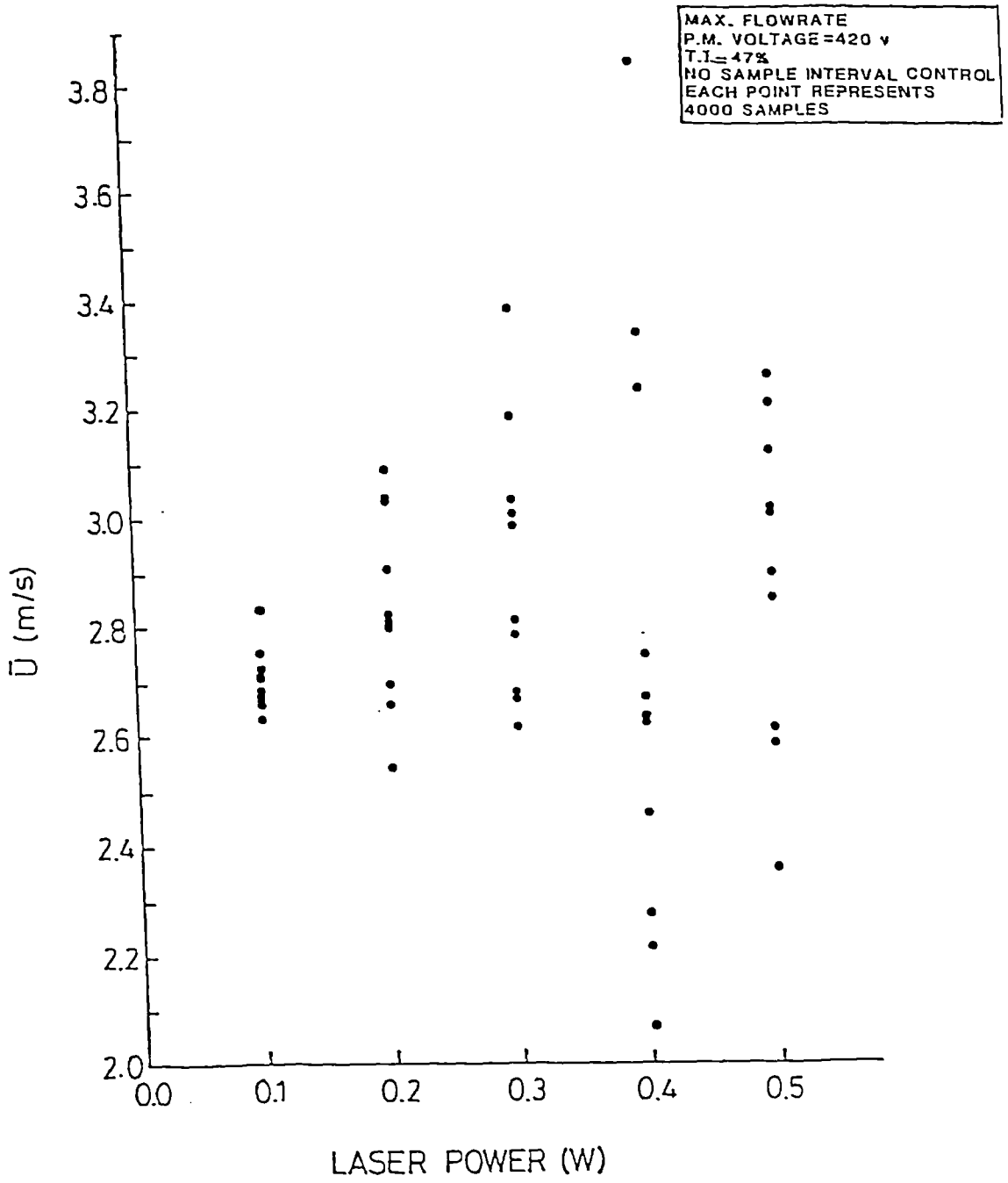

Fig. 3.10 Ū vs. LASER POWER

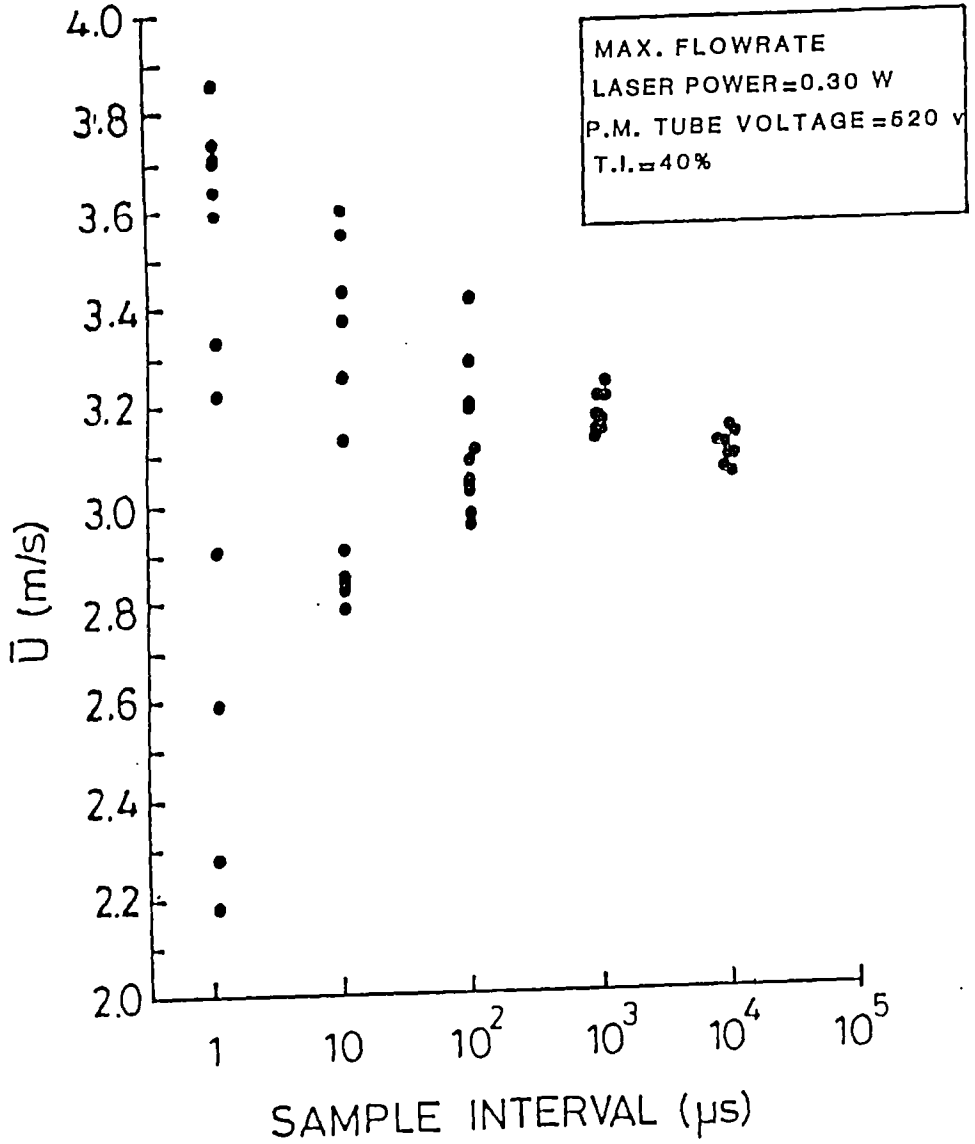

Fig. 3.11(a) Ū vs. SAMPLE INTERVAL

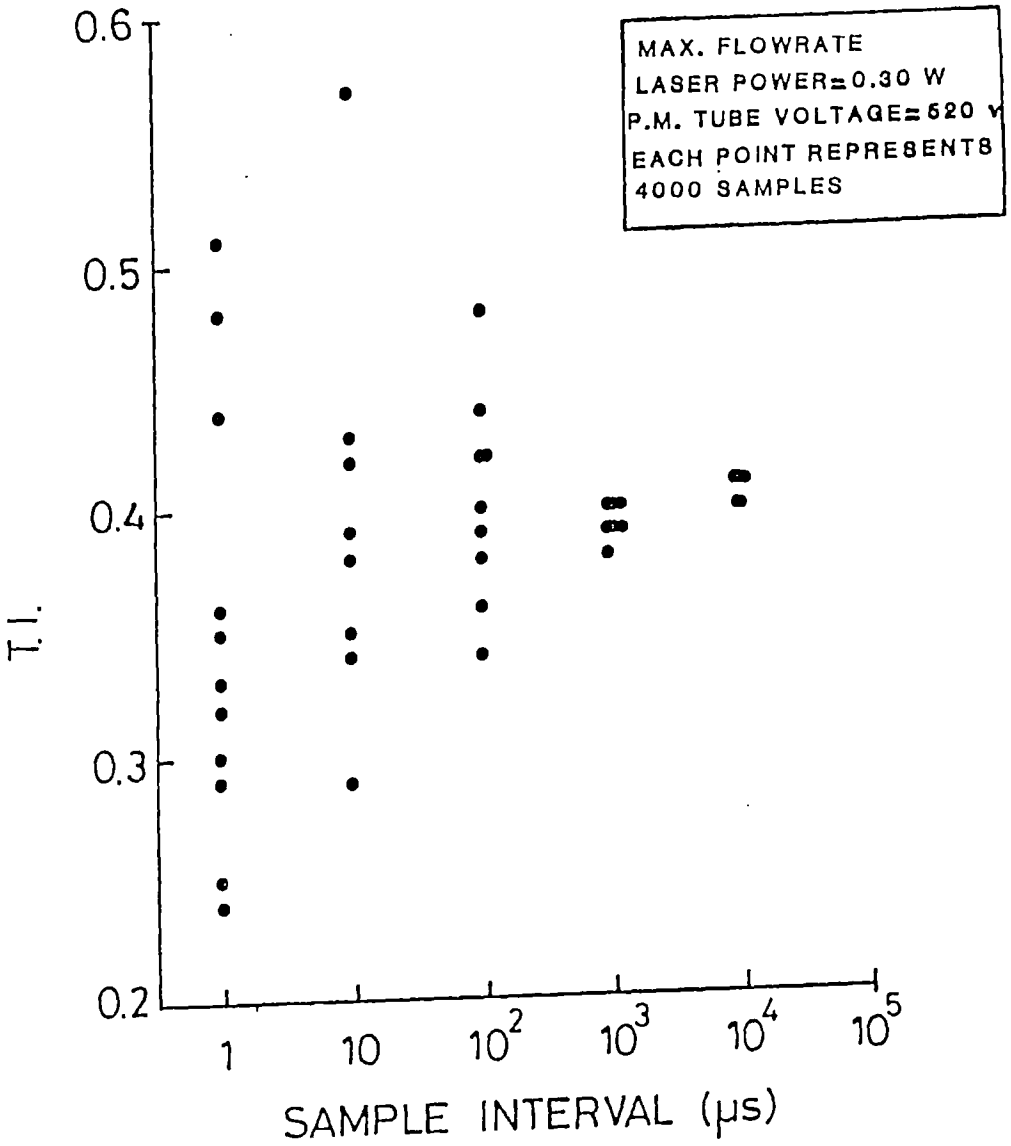

Fig. 3.11(b) T.I. vs. SAMPLE INTERVAL

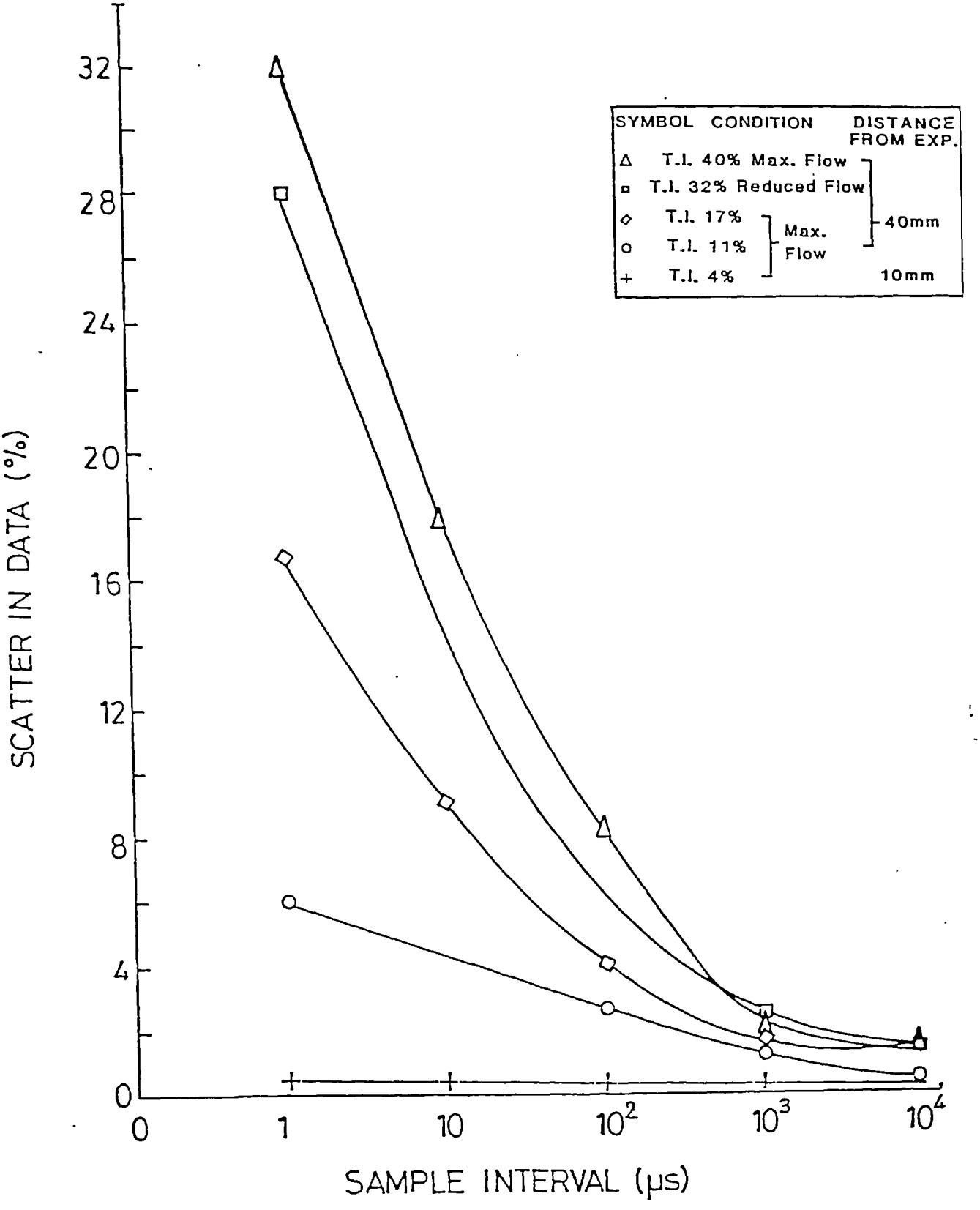

Fig. 3.12 SCATTER IN VELOCITY DATA vs. WINDOW LENGTH

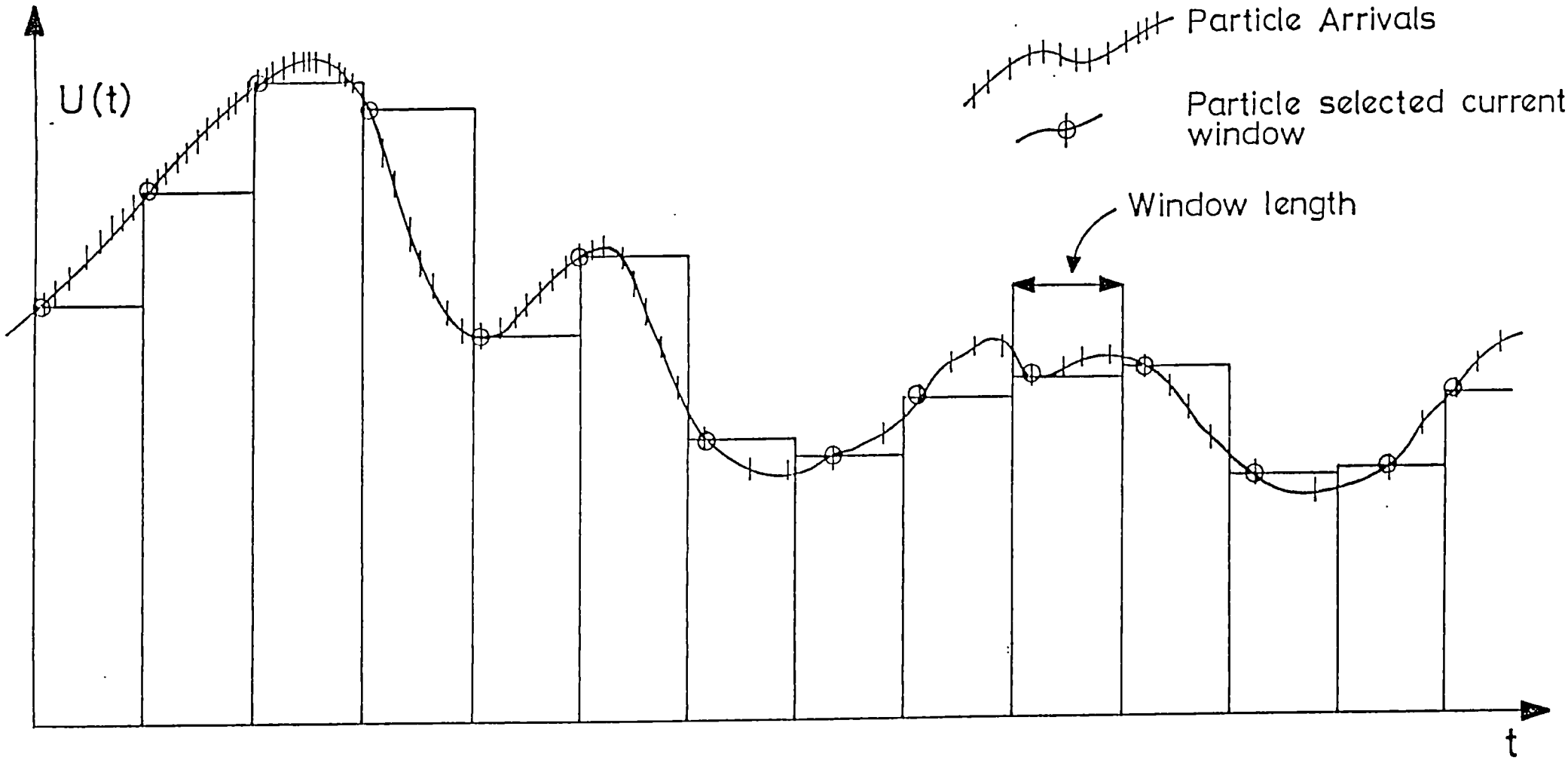

Fig 3.13 Elimination of arrival rate bias by windowed sampling

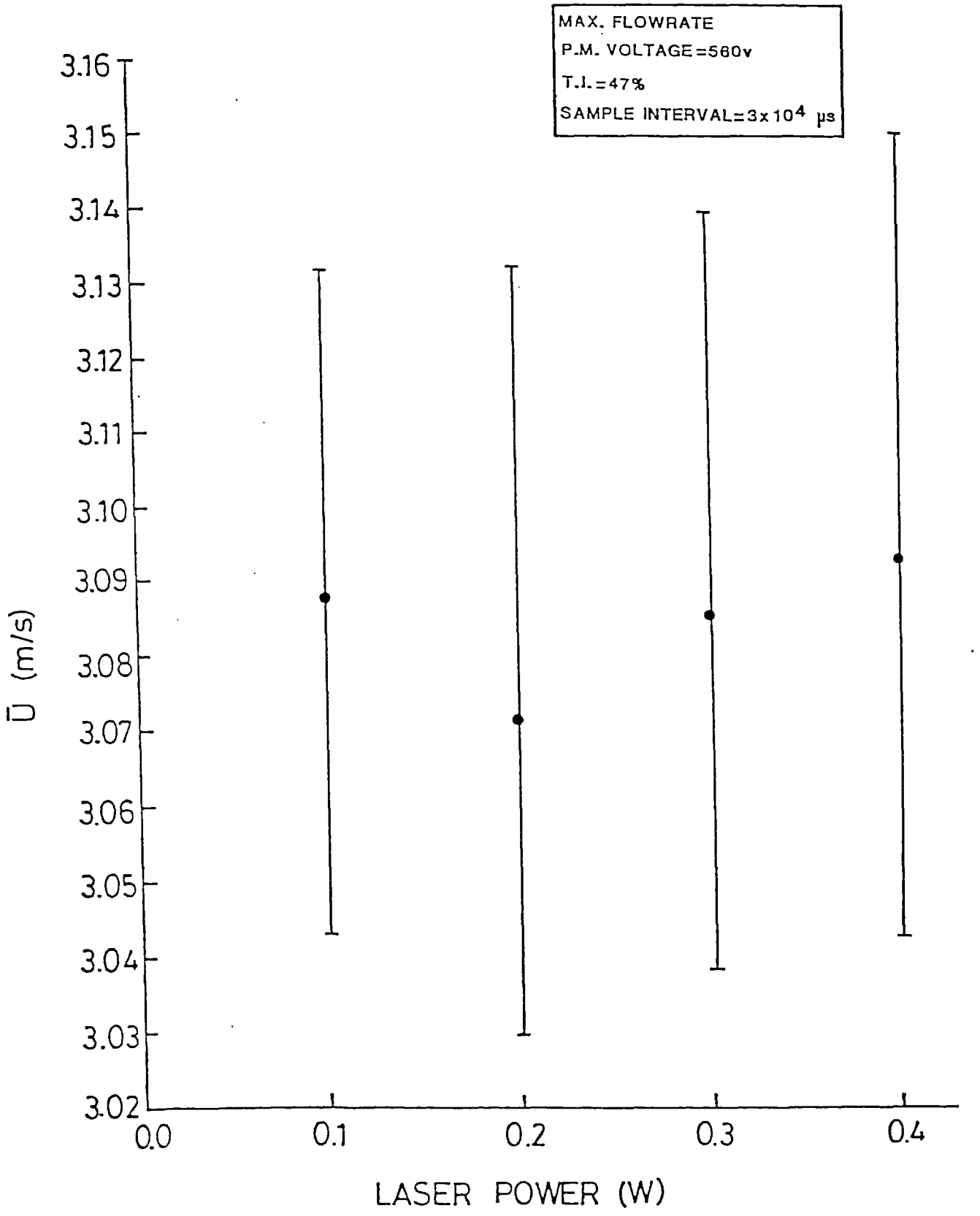

Fig. 3.14 Ū vs. LASER POWER

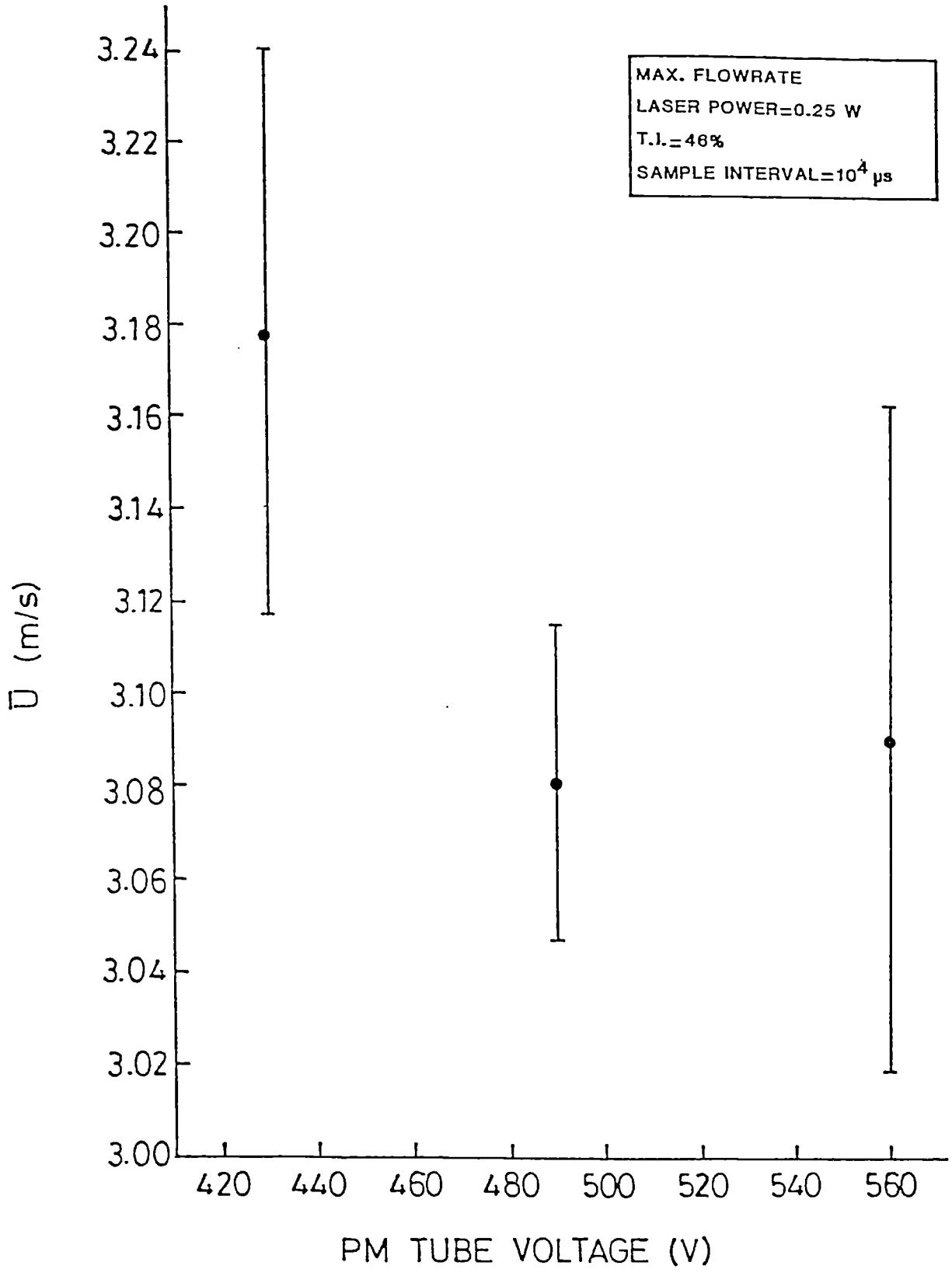

Fig. 3.15 $\bar{U}$ vs. P.M. TUBE VOLTAGE

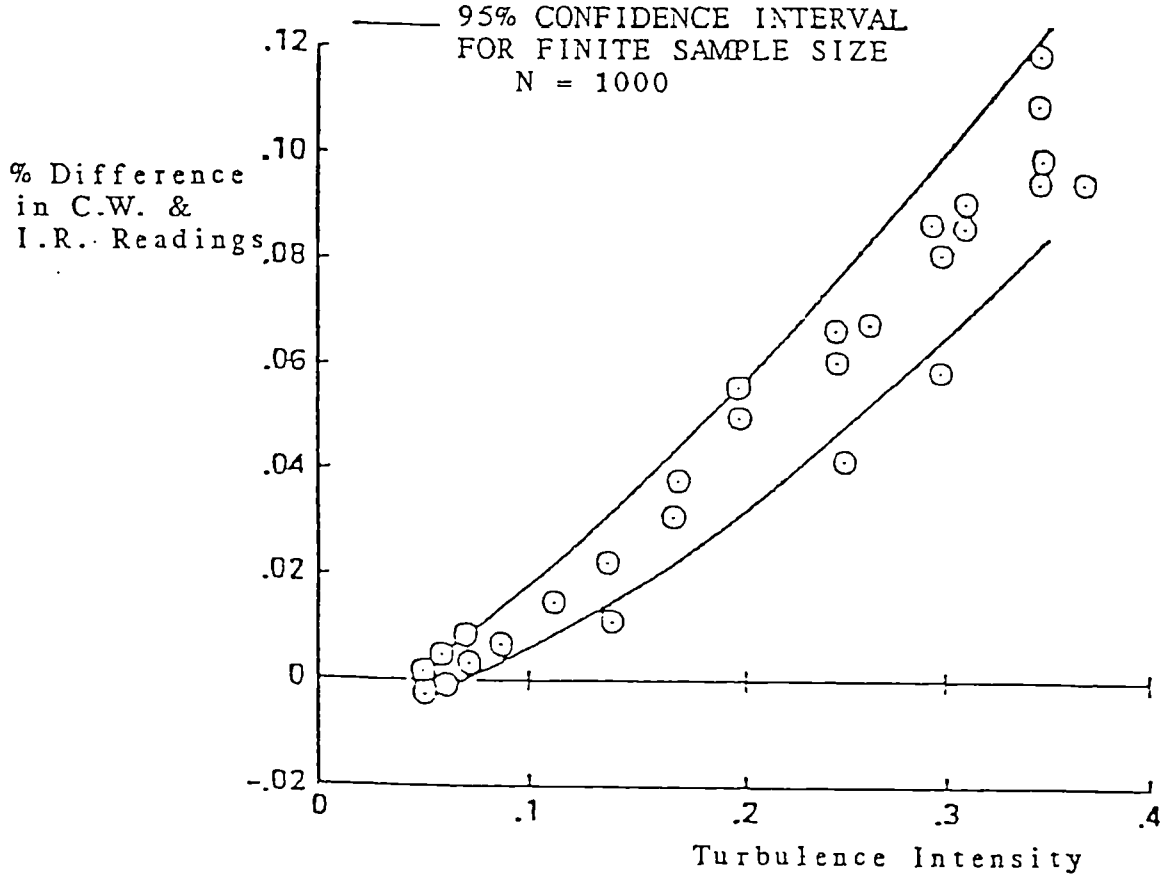

Fig. 3.16 DIFFERENCE BETWEEN 'CONTINUOUS WAVE' & 'INDIVIDUAL REALISATION' READINGS vs TURBULENCE INTENSITY LEVEL
(From Johnson et al (1984))

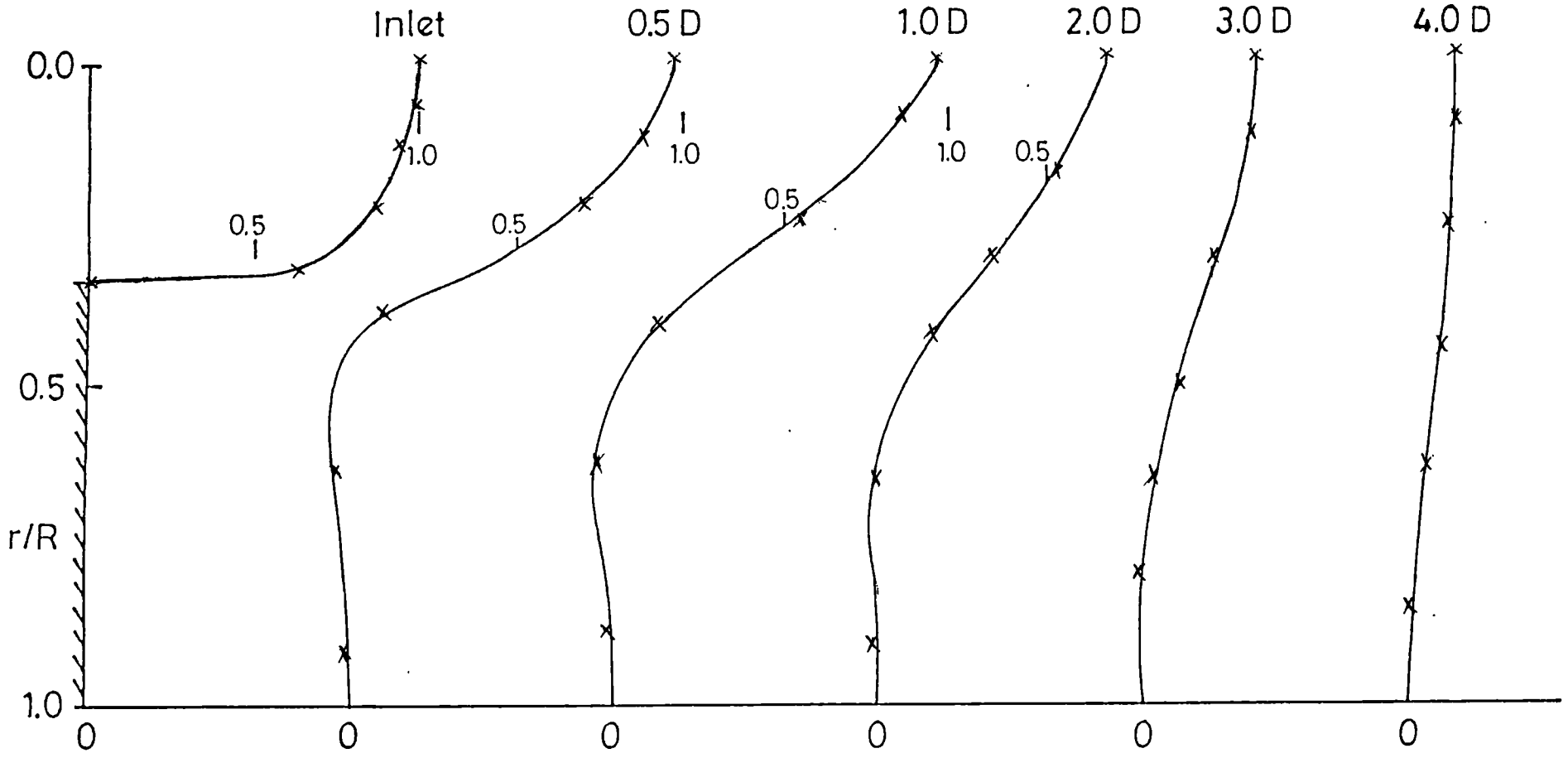

Fig. 3.17 NORMALISED MEAN VELOCITY PROFILES

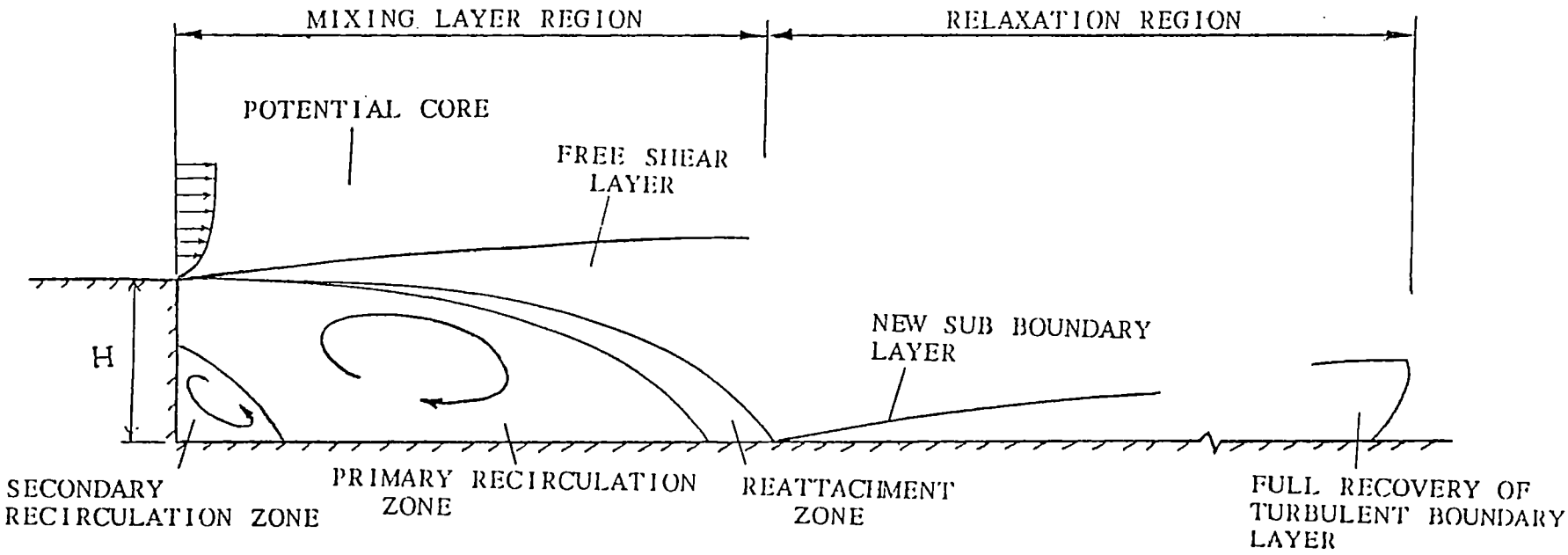

Fig. 3.18 FLOW REGIONS IN A SUDDEN EXPANSION

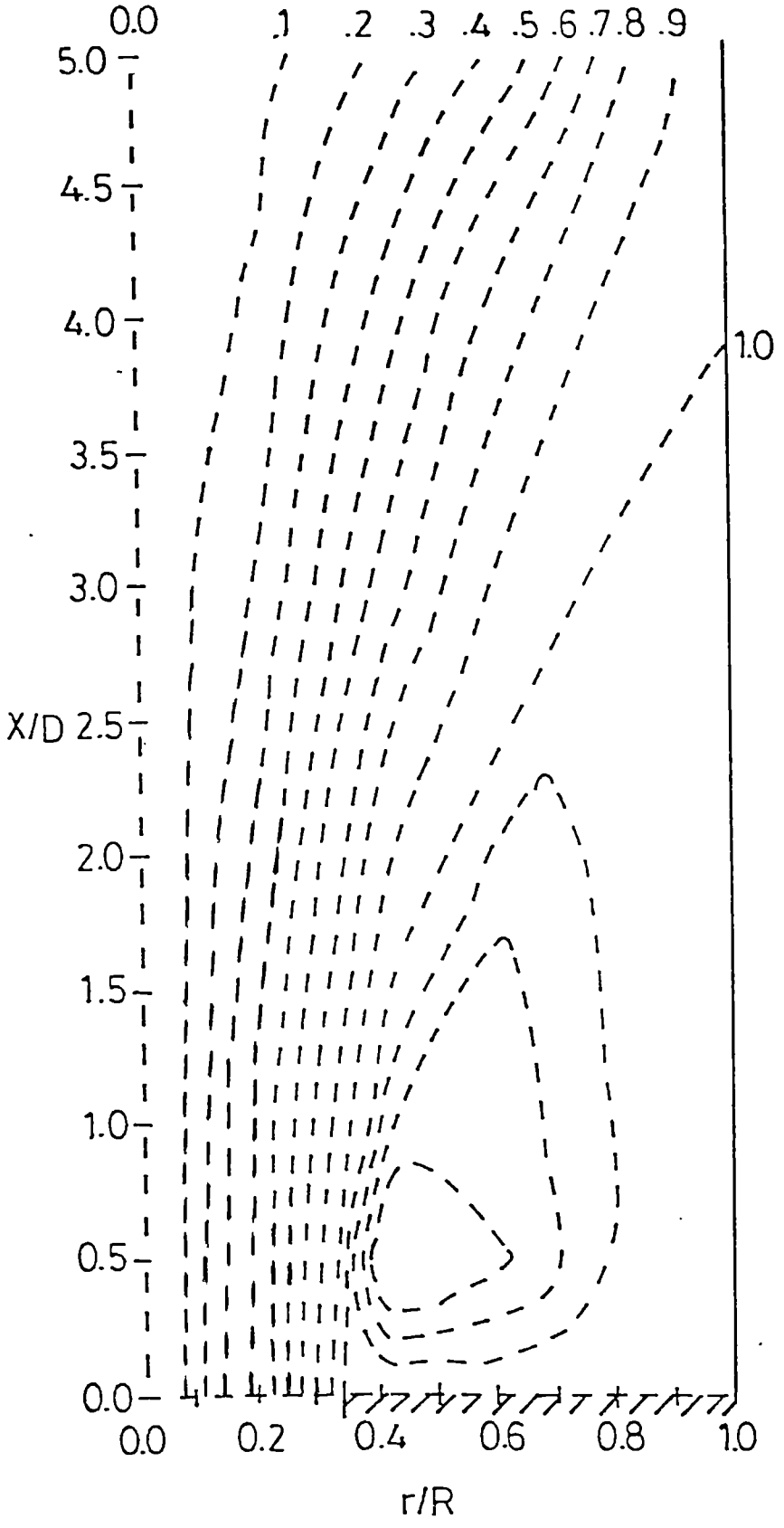

Fig. 3.19 STREAM FUNCTION CONTOURS

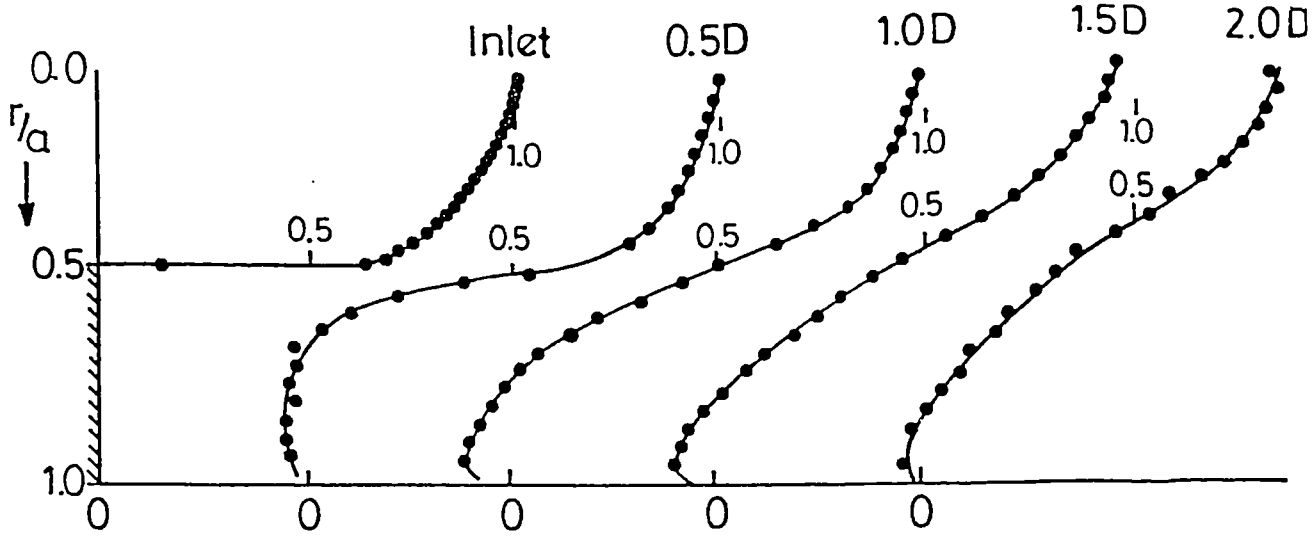

Fig. 3.20 NORMALISED MEAN VELOCITY PROFILES

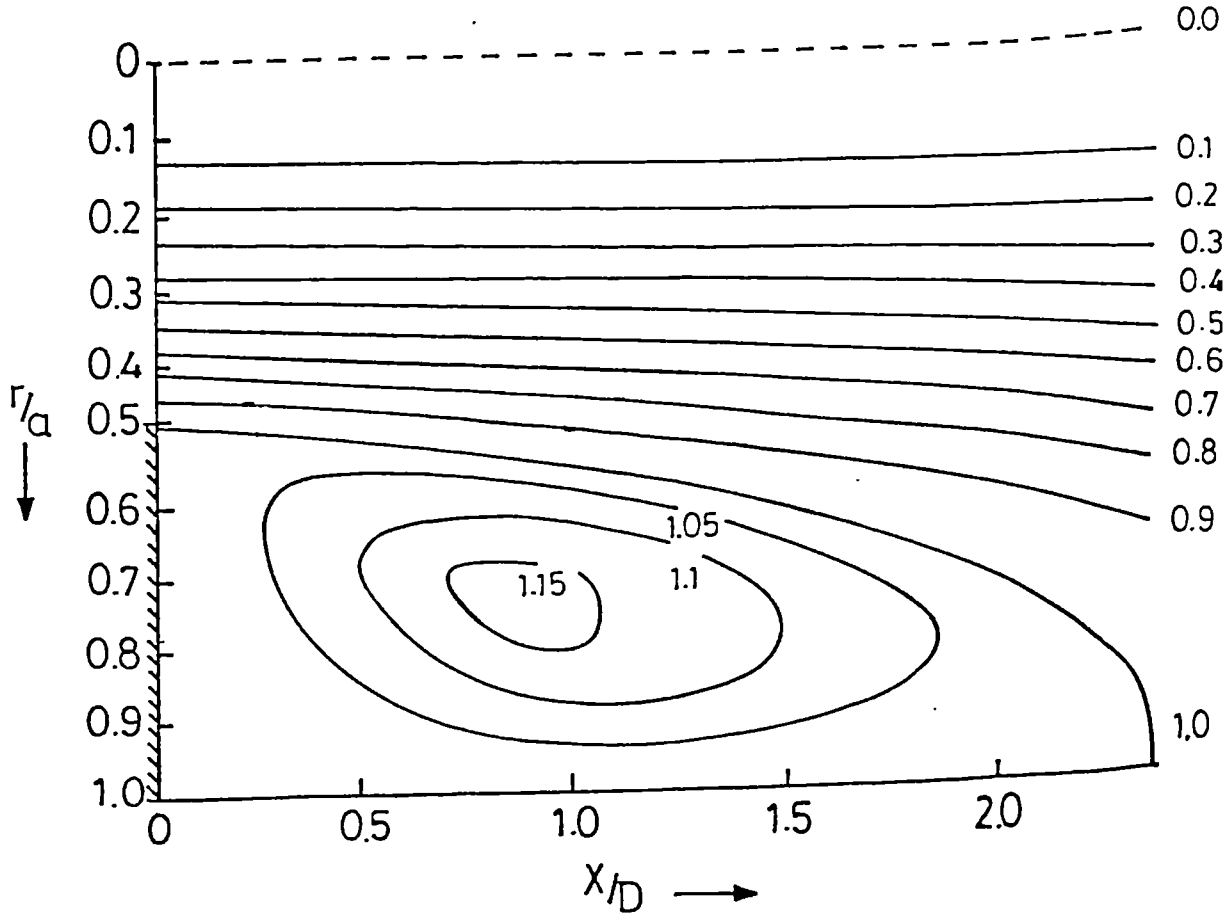

Fig. 3.21 NORMALISED STREAM FUNCTIONS

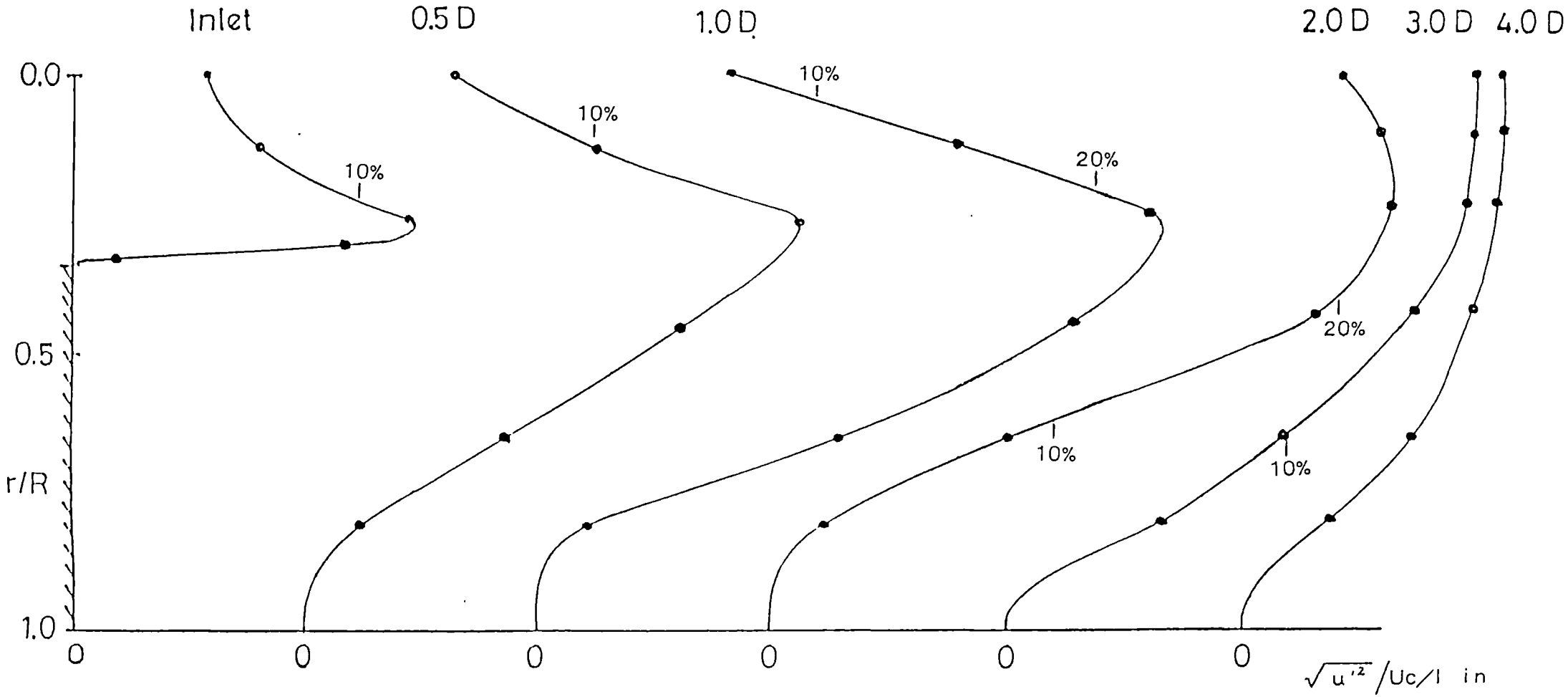

Fig. 3.22 TURBULENCE INTENSITY PROFILES

CHAPTER 4

THEORETICAL BACKGROUND OF TURBULENCE

4.1 BASIC TURBULENT FLOW RELATIONSHIPS

Hinze (1975) suggests that a suitable definition for turbulent fluid motion might be formulated as 'an irregular condition of flow in which quantities show a random variation with time and space coordinates, so that statistically distinct average values can be discerned'.

At any point in a flow, of Reynolds number greater than some critical value, the instantaneous velocity vector varies with time in both magnitude and direction.

The randomness of the flow properties is the essential characteristic of turbulence. Turbulence can be generated by the shear strain rate produced by velocity gradients, such as exist in the vicinity of fixed walls, or by the flow of layers of fluids with different velocities past or over one another.

A qualitative description of turbulence employs the concept of eddy or vortex stretching. Turbulent eddies have both translational and rotational motion; if a fluid element rotating about one axis is under the influence of linear strain normal to that axis, the element is stretched in the direction of strain. An extension in one direction can decrease the length scales and increase the velocity components in the other two directions. These in turn stretch other elements of fluid with vorticity components in those directions. An initial stretching in one direction produces nearly equal amounts of smaller–scale stretching in each of the three directions after a few stages of the process.

Energy enters the turbulence by interaction of the larger eddies with the mean flow field and is passed down to the smallest scale of eddies where it is dissipated in viscosity. Turbulent flow of real fluids is thus of a dissipative nature; if there was no continuous external source of energy for the continuous generation of the turbulent motion, the motion would decay.

The larger eddies carry most of the turbulent kinetic energy and the *energy cascade*, down which this energy is transmitted, is independent of viscosity until the final stage.

The distribution of the eddies must be considered with respect to direction at a point, to space throughout the flow field and to time at a point. These three conditions provide assessment of flow isotropy, homogeneity and stationarity respectively.

When the turbulence has quantitatively the same structure in all parts of the flow field, it is said to be homogeneous.

If perfect disorder exists, when the statistical features of the turbulence have no directional preference, it is called isotropic. In this situation, the mean velocity is constant throughout the field and has no gradient and no average shear stress can occur. The distribution of the middle-sized (energy transferring) and small (energy dissipating) eddies can be considered independent of direction and are statistically locally isotropic. The largest eddies, however, depend on the flow boundary conditions and cannot be isotropic in a flow displaying velocity gradients. The term *shear-flow turbulence* is often used since the mean velocity gradient is associated with the occurrence of an average shear stress. This class encompasses wall turbulence and anisotropic free turbulence.

The assumption that the turbulence is stationary is often necessary for the purposes of statistical analysis of the flow. This is reasonable in a fully developed flow situation.

The energy cascade is an essentially random process, implying no directional preferences. The small-scale dissipating motions fluctuate in space and time in response to the large-scale fluctuations. They can, however, be approximated to locally statistically isotropic turbulence ($\overline{u'^2} = \overline{v'^2} = \overline{w'^2}$), generally valid for high Reynolds number flows. The turbulent energy dissipation rate is then expressed by

$$\varepsilon = \nu \overline{\left(\frac{\partial u_i}{\partial x_j}\right)^2} \qquad 4.1$$

It should be noted that ε is determined by the energy transfer rate in the cascade and therefore by the large energy-containing eddies. The minimum size of eddies is determined by the viscosity.

Townsend (1961) showed, from dimensional considerations, that

$$\varepsilon = \frac{k^{3/2}}{L_\varepsilon} = c\frac{k^{3/2}}{l} \qquad 4.2$$

assuming the turbulent kinetic energy is proportional to the turbulent shear stress; ε is therefore represented by a single length and velocity scale i.e.L_ε, eddy dissipation length scale and k, the turbulent kinetic energy.

The fully turbulent flows of practical interest remain mathematically intractable. Even if it were possible to determine complete solutions, only the

average behaviour, in terms of mean velocity fields and turbulent stresses, are needed in the majority of cases. The statistical description of the flow and the subsequent modelling of the terms which appear in the equations need experimental verification and determination of empirical constants is required for their closures.

4.1.2 Statistical Description

The turbulence velocity is still a continuous function of space and time. Statistical correlations between the motions at different points can be distinguished, but the probability distribution of the velocity at a given point is nearly the Gaussian or normal probability distribution.

Turbulence can, therefore, be treated in terms of statistical properties. Hinze (1975) notes one of the original suggestions to be given by Taylor. Such techniques have subsequently been developed by many authors, Hinze (1975) again noting the notable contributions made by Kolmogoroff, Heisenberg, Von Karman and Townsend.

The instantaneous values of turbulent flow properties e.g.velocity, pressure, temperature, are conveniently expressed in terms of the sum of the mean value and the fluctuation from the mean.

Thus the instantaneous velocity vector (in three dimensions) can be defined as composed of a mean velocity describing the general magnitude and direction of the flow, and a fluctuating component which describes the magnitude and direction of the departure from the mean.

$$u_i = \overline{u_i} + u_i' \qquad 4.3$$

where necessarily the mean of the fluctuation is zero

$$\overline{u_i'} = 0.$$

Time correlations (autocorrelations) of data recorded at a single point, with a time lag, provide information on the extent of the eddies. A discrete function can be formed by the mean product of two fluctuating velocity components measured at the same point at times t and (t + T).

$$C_{uu}(k) = \frac{1}{(n-K)} \sum_{i=1}^{N-K} (u_i', u_i + k) \qquad 4.4$$

Spatial correlations (covariances) are a measure of the strength of eddies whose length in direction s is greater than s. The shape of the correlation function as s changes size gives information about the eddy structure of the flow.

The statistical function most used to examine the spatial structure of the turbulence and its evolution in time is the double velocity correlation function, defined as

$$R_{ij}(x, s, t) = \overline{u_i(x, t) u_j(x + s, t + T)} \qquad 4.5$$

$R_{ij} = 0$ as s or T approaches infinity.

Integral length and time scales are measured in terms of the normalised form of the double correlation function:

$$\mathbf{R}_{ij}(x,s,t) = \frac{R_{ij}(x,s,t)}{R_{ij}(x,0,0)} \qquad 4.6$$

then

$$ij_{L_l}(x) = \int_{-\infty}^{\infty} Rij(x,s,0)dr_l$$

$$ij_T(x) = \int_{-\infty}^{\infty} Rij(x,0,t)dt \qquad 4.7$$

The longitudinal integral scale u_l(x) is most used, giving an indication of the mean eddy size in the longitudinal direction. It can, therefore, be used as a length scale typical of the energy–containing eddies.

The double velocity correlation provides a complete description of turbulent flow only if the probability distribution function for the velocity field is joint-normal i.e. at each point in the flow field, the probability of having a fluctuating velocity component u' is given by

$$P(u) = \frac{1}{\sqrt{2\pi\overline{u}^2}} exp(-\frac{1}{2}\frac{u'^2}{\overline{u}^2}) \qquad 4.8$$

implying that the flow is homogeneous. However, of more practical use is the single-point distribution.

Departures of the actual probability distribution function from the normal form give information about the turbulence. The skewness of the distribution is connected with the convection of turbulent energy by turbulent movements, transferring energy from regions of high intensity to regions of lower intensity. The effect of inhomogeneity of turbulent intensity makes the kurtosis or flatness factor of a fluid property e.g. its velocity, exceed its *normal* value of three. Definitions of these statistical quantities are given in Chapter 3.

4.2 CALCULATION METHODS

It is impossible to attack the problem of turbulent fluid flow rigorously; even if the mean motion is steady and two–dimensional, the associated turbulent motion is three–dimensional and unsteady. It is necessary to resort to semiempirical methods that are characterised by the description of the random, unsteady, three–dimensional motion of turbulence in terms of statistical mean quantities. The statistical quantities are related to each other by a set of differential equations. Empirical assumptions, closure conditions, have to be introduced to establish such a set of differential equations.

A thorough examination and classification of turbulent shear flows are dealt with in the standard texts of Bradshaw (1971), Hinze (1975) and Townsend (1976).

A detailed review of boundary layer flow theory, wall jets and turbulence modelling is covered in Bradshaw's monograph (1973). Turbulence models are also reviewed by Launder & Spalding (1974), Mellor & Herring (1973) and Reynolds (1976).

Solution techniques are classified as hyperbolic, parabolic, and elliptic. The one chosen for any model depends upon the physical situation being considered and any simplifying assumptions made. In supersonic flow, disturbances cannot be propagated upstream; the region of influence of a point is thus confined to an area downstream from that point. The whole flow field may be solved by a single sweep downstream, by a hyperbolic form of the turbulence model. In subsonic flow, the region of influence of a point is unbounded; the equations of motion are then elliptic. Solution must be obtained by an initial guess and an iterative process over the whole flowfield to achieve convergence. The elliptical equations can, however, be approximated to parabolic under certain conditions e.g. classical boundary layer assumptions.

There are basically two groups of calculation methods for turbulent boundary layers, as shown in Table 4.1. Early models concentrated on the solution of the 'integral' forms of the boundary layer equations. The advent of increasingly fast computers has made the alternative, differential methods practicable and attractive; only relatively recently have differential methods been applied to curved flows.

A comprehensive comparison of both types of calculation method was provided by Kline et al (1969), reviewing work up to 1968 and more recent studies have been included in the report by Bradshaw (1972).

4.2.1 Integral Methods

These are based on the solution of the ordinary differential equations obtained from weighted integrals of the x–component Navier–Stokes equation.

They work because of the adequacy of a boundary-layer, or thin shear layer assumption. In a thin shear layer, an extra strain rate affects the turbulence but not the mean flow. Therefore, static pressure differences across the layer and normal stress gradients are negligible. This avoids the necessity of solving highly non–linear boundary layer equations in their partial differential form.

For a two–dimensional, incompressible flow with no mass transfer, the momentum integral equation can be written as:-

$$\frac{d\theta}{dx} + \frac{\theta}{U}(2 + H)\frac{dU}{dx} = \frac{C_f}{2} \qquad 4.9$$

The shape factor, H, contains information about the mean velocity profile, and the skin-friction coefficient, C_f, contains information about the Reynolds shear stress.

To obtain a closed system of equations to solve for the three unknowns, two further relations are needed between θ, H and C_f. The accuracy of the solution depends on the assumptions made for these relationships. Head (1960) obtained a successful method by using Ludwieg & Tillman's skin–friction formula and an empirical expression for the entrainment rate into the boundary–layer as the two auxilliary relations.

Cebeci & Smith (1974) and Bradshaw (1972) reviewed integral methods and found that they have been shown to give accurate solutions for simple flow cases such as a turbulent boundary layer on a smooth flat plate. Integral methods cannot, however, give solutions for each point in the flow field because an ordinary differential equation for integral quantities is solved. Different ways of describing the mean velocity profiles, skin-friction and shear stress

profiles are required if extra effects, such as surface roughness, are to be included.

Large curvature effects cause great difficulties due to the variation across the shear layer width of turbulence terms. Patel (1969a) investigated flows with large cross-stream static pressure variations i.e. with significant streamline curvature. He found it necessary to redefine the usual integral parameters δ^* and θ and that the flat-surface momentum integral equation failed when used in this situation. Patel, therefore, incorporated extra terms in the momentum integral equation to account for the effects of the cross-stream pressure gradient. It was pointed out by So (1975a), however, that both H and C_f have also to be modified to account fully for the effects of curvature.

Morrison (1982) noted an integral method developed by Titcombe (1980) specifically for the Coanda flare. Effort was directed to the inclusion of refinements to simulate radial pressure gradients and the effects of streamline curvature and divergence upon the entrainment rate. It failed, however, to give good agreement for the jet growth rate data, and such methods have not been considered further for this application.

4.2.2 Differential Methods

These methods all approach the problem by solving the Navier–Stokes equations directly using a suitable numerical technique.

The set of equations comprising a transport equation, the Reynolds averaged Navier–Stokes and continuity equations do not provide a closed set of

equations if the flow is turbulent. The problem of closing this under–specified set of equations has taxed researchers in this field for almost a century.

A good turbulence model, suggest Launder & Spalding (1974), has extensive universality and is not too complex to develop or use. Universality implies that a single set of empirical constants or functions, inserted into the equations, provides close simulation of a large variety of types of flow. Complexity is measured by the number of differential equations which the model contains, and the number of empirical constants and functions which are required to complete them. Increase in the former complicates the task of using the model, increase in the latter complicates the task of developing it.

The main obstacles to model development are the difficulty of selecting which set of differential equations is most capable of providing universality and the difficulty of then providing, from experimental knowledge, the required constants and functions. Many proposals have been made for closing the Reynolds stress equations and they form the bases for numerous prediction methods applied to complex shear layers (with varying degrees of success).

Schlichting (1979), Cebeci & Smith (1974) and Bradshaw et al (1981) discuss the methods of closure. There are two main approaches to the solution of the differential form of the two–dimensional Navier–Stokes equations for boundary–layer type flows, identified by the assumptions they use to obtain closure, as shown in Table 4.1.

A. Mean–Flow Methods

The first approach , the mean–flow methods, obtain closure by making assumptions that relate the Reynolds stresses to the properties of the mean field.

In the latter part of the nineteenth century, Boussinesq suggested replacing turbulent shear stress with a laminar flow of greatly increased viscosity (termed an eddy viscosity), the value of which should be determined from experiment. Boussinesq's concept, that the eddy viscosity has a scalar value, is followed by Patankar & Spalding, obtaining the turbulent kinematic viscosity from the local level of the *mixing–length* i.e. the mean free path between collisions, and the mean velocity gradient

$$\nu_t = l^2 \frac{dU}{dy} \qquad 4.10$$

Many models include the use of Boussinesq's eddy–viscosity concept e.g. Prandtl's mixing–length hypothesis. Three of the mean–flow methods which have been applied to a wide range of turbulent shear flows are those of Patankar & Spalding (1970), Cebeci & Smith (1974) and Mellor & Herring (1973).

The first attempts to calculate wall jets with a differential method, used by Patankar & Spalding (1970), made use of Prandtl's mixing–length hypothesis. The mixing–length approach of Patankar & Spalding transforms the y ordinate into a non–dimensional stream function. It uses upwind difference mode for the simultaneous solution of all points at a given value of x.

Launder & Rodi (1983) reviewed work on curved flows and found a limitation of this type of method to be that, the secondary strain associated with the curvature had to be empirically augmented, by an order of magnitude, to obtain reasonable agreement between predictions and measurements. The precise value required for the empirical coefficient varied from flow to flow.

Irwin & Smith (1975), using the model of Launder et al (1975), from Patankar & Spalding (1970), first used the method to calculate curved flows. They limited the calculation to shear layers with mild longitudinal curvature. They produced results for curved–wall jets, boundary layers and a curved free jet. They were unable to make very detailed comparisons with measurements of turbulent quantities since, at that time, there was not a great selection of experimental results. The method did, however, produce good agreement with the values of jet growth rate obtained by Smith (1973).

Morrison (1982) selected the calculation procedure of Patankar & Spalding (1970) as a basis for his predictions. It was suitable for predictions of shear layer flows with significant cross-stream pressure gradients. Corrections were introduced to account for the effects of streamline curvature and divergence; their combined effects were assumed to be simply additive. The constants in the correction expressions were tuned individually for the flow situation considered. An allowance was made for the effects of variable pressure in the flow field. The model is adaptable for use with different types of turbulence model.

Cebici & Smith's (1974) eddy–viscosity approach transforms the equations into a rectangular grid and the governing equations are written in the form of a first order system.

B. Transport–Equation Methods

The second approach to obtain closure uses the transport equations for the turbulent quantities, together with the mean momentum equations,as indicated in Table 4.1.

There are two separate routes adopted by users of the transport- -equation methods. The first considers the solution of the mean–continuity and mean–momentum equations, together with the turbulent kinetic energy equation. The second considers the solution of the mean–continuity and mean–momentum equations together with the Reynolds stress–transport equation. Both these approaches involve assumptions that all the third–order turbulence products can be expressed in terms of second–order products and that there are certain relations between the second–order products.

In order to close the system, it is necessary to make assumptions for the unknown terms.

The first route uses one of two different methods for its closure assumptions for the pressure–velocity term and the form of the relation between the Reynolds stress and the turbulent kinetic energy.

Bradshaw et al's (1967) model uses a system of hyperbolic equations. It models shear stress as proportional to kinetic energy and has been applied to boundary layers and shear layers where cross-stream pressure variations were considered negligible. The model has been thoroughly investigated for a wide variety of flows and been found accurate. The original model encompassing incompressible flow only has subsequently been extended by

Bradshaw & Ferriss (1971) to include compressible flow as well as unsteady and three–dimensional flows.

Within this group of models is the 'k-ε' model. This title is used to designate the turbulence model in which two differential equations are solved, the dependent variables of which are the turbulent kinetic energy k and the dissipation rate of turbulence energy ε. Launder & Spalding (1974) present the differential equations and auxiliary relations which define their k-ε model and their solutions. The turbulent viscosity ν_t is obtained from k and ε via the Boussinesq eddy viscosity relationship

$$\nu_t = c_\mu \frac{k^2}{\varepsilon} \qquad 4.11$$

In the elliptic solution form of this widely used model, a velocity field is initially assumed, production and dissipation of the turbulent kinetic energy are then calculated, based on the gradients in the assumed field. This provides an eddy viscosity value for each spatial location. The eddy viscosity values are then used in the numerical solution of the conservation of momentum equation which, in turn, gives the mean velocity and pressure fields. The new velocity gradient results are then used in the turbulent kinetic energy calculations. The process continues to iterate between the kinetic energy calculations and the momentum equation calculations until a converged solution for the velocity and pressure field is obtained. In the k-ε model, as in other eddy-viscosity models, it is assumed that the turbulence is isotropic and that for every spatial location there is a single eddy viscosity.

Launder & Spalding (1974) summarise the findings of a number of studies, including those by other researchers in which the k-ε model has been applied. They aimed to convey a representative impression of the k-ε model's capabilities and, hence, an indication of its limitations and development requirements. They concluded that it is the simplest kind of model to permit prediction of both near–wall and free–shear flow phenomena without adjustments to constants or functions. It was found to account successfully for many low Reynolds number turbulence features and accurately predict flows with recirculation and those of the boundary–layer kind.

The k-ε model of turbulence has been one of the most extensively used methods. A primary defect of all existing k-ε models, noted by Nagano & Hishida (1987), was their inability to reproduce the 'law of the wall' which had been observed experimentally over a range of pressure gradients. They produced a model which, while not claimed to be perfect, provided considerable improvement for near–wall and low Reynolds number flows.

Among the methods that follow the second route for using Reynolds stress transport equations are those of Donaldson et al (1972) and Hanjalic & Launder (1972). Gibson & Rodi (1981) reported on a Reynolds stress calculation method which reproduced the main features of a turbulent shear layer subjected to a strongly stabilizing curvature.

4.3 WALL JET FLOWS ON FLAT SURFACES

A thorough knowledge of the fluid mechanics of the wall jet, including the turbulence field that it generates, can materially improve the design of

any device in which it is employed. Much of the literature reviewed so far has been of benefit in gaining an insight into the background of turbulent flows in general and specifically in the curved jet situation and a qualitative understanding of the mechanisms involved.

Newman (1961, 1969) reviews turbulent jets in general and, both he and Fernholz (1971), report on the *Coanda Effect.* Love at al (1959) look at free jet structures. Launder & Rodi (1981, 1983) present excellent, comprehensive articles on turbulent wall jets.

Glauert (1956) introduced the term *wall jet* to describe the flow that develops when a jet, consisting of a fluid similar to that of its surroundings, impinges on a plane surface and spreads out over the surface.

The first theory of the laminar and turbulent wall jets, for plane walls, developed by Glauert, was based on the model which considers the flow to comprise two regions divided by the line of maximum velocity. In the inner region (from the wall to y_m i.e. y at U_m), the flow is assumed to be dominated by wall effects and to behave rather like a boundary layer – governed by Blasius' formula. The flow in the outer region (from y_m to the outer edge of the flow), although influenced by the wall, is assumed to behave more like a free jet. Entrainment of quiescent fluid occurs near the outer edge of the flow. A solution for the outer region is obtained using an eddy viscosity which is constant across the region.

This two–layer model of the wall jet provides a basis for detecting unexpected features in the shear flow, of which there are many since the two regions strongly interact.

Glauert obtained a near similar solution using this model. A solution ignoring viscous effects in the inner layer was sought in which the mean velocity profile varied according to :-

$$U_m \propto x^a \qquad\qquad y_{1/2} \propto x^b \qquad\qquad 4.12$$

The eddy viscosity of the outer layer was assumed to be constant and that of the inner layer assumed to vary as U^6. The inner layer velocity profile was assumed to conform to Blasius' pipe flow formula, varying as $y^{1/7}$.

The two layers were patched at the velocity maximum, at which point the shear stress is assumed to be zero. The values of the constants were found by Glauert to be dependent on the matching procedure used for the inner and outer layer solutions but are given as approximately

$$a = -0.5$$

$$b = 1.0.$$

Experimental determination of these constants by Schwarz and Cosart (1960) found that values of a ranged from -0.5 to -0.6 and quoted a=-0.555 and b=1.0.

Glauert's two–layer model forms the basis for an approximate solution by Fernholz where the outer region is regarded as a free shear layer with similar velocity profiles; the inner layer is treated as a turbulent boundary layer with transverse pressure and the appropriate momentum and energy

equations derived. He found good agreement for a wide range of slot height to radius ratios, for angles around a convex surface between 40° and 180°.

An extensive review of over two hundred experimental studies was carried out by Launder & Rodi (1981). They used the momentum integral equation to check two–dimensionality of the flows wherever there was sufficient data. Where significant departure from two–dimensionality was indicated, the results were excluded from further consideration.

When the experimental mean velocity results were plotted non–dimensionally, as U/U_m against $y/y_{1/2}$, Launder & Rodi (1981) showed the profiles to be satisfactorily similar and in close agreement with the predictions from Glauert's theory. The normal velocity profiles measured by Wilson & Goldstein (1976) were also shown to be similar when plotted non-dimensionally as U/U_m against $y/y_{1/2}$.

Launder & Rodi (1981) found that the growth rate of the wall jet's outer layer also agreed with Glauert's theory. They showed that the growth rate of the outer layer of a wall jet developing in stagnant surroundings may be characterized by

$$\frac{\partial y}{\partial x} = 0.073 \pm 0.002 \qquad 4.13$$

This growth rate is over 30% below that for the plane free jet. They postulated that the difference is due to the damping of turbulent velocity fluctuations in the direction normal to the wall by the turbulent pressure reflections from the wall.

Two discrepancies, however, were noted by Bradshaw & Gee (1960) between Glauert's theory and real flow.

1. Blasius pipe flow surface friction formula underestimates the wall shear stress by 25%. Launder & Rodi (1981) show wide variation in the value of wall shear stress measurements, the alternative methods for which all have their problems. They adjudged the data of Bradshaw & Gee (1960) to be one of the most accurate, from which they quote the relationship

$$\frac{\tau_w}{1/2\rho U_m^2} = 0.0315\left(\frac{U_m y_m}{\nu}\right) \qquad 4.14$$

Launder & Rodi (1981) suggest this relationship to be valid only for the range 3E3 $< U_m y_m/\nu <$ 4E4. In two–dimensional turbulent boundary layers in zero or modest pressure gradients, the mean velocity variation near the wall is describable by

$$\frac{U}{U_\tau} = A log\left(\frac{yU_\tau}{\nu}\right) + B \qquad 4.15$$

Although virtually all works reviewed by Launder & Rodi (1981) report such a semi–logarithmic relationship, there is a wide variation in the values of A and B deduced from the measurements. This arises from two main causes:-

a. errors in measuring the wall shear stress

b. the extent over which the relationship is applied. Launder & Rodi (1983) suggest that authors have attempted to apply the formula over too large a portion of the inner region.

The most accurate results appear to be those of Patel (1965) from which A = 5.5 and B = 5.45.

2. The two kinds of turbulence interfere everywhere but especially where the velocity is a maximum. One result of this interaction between the regions is that the positions of zero shear stress and maximum velocity are no longer coincident (as for a laminar wall jet).

The shear stress is no longer simply related to the local mean velocity gradient and the point at which it changes sign is displaced towards the wall, inside the maximum velocity point. Any theory modelling shear stress in terms of the first derivative of velocity i.e. eddy viscosity is therefore incorrect, but may prove to be adequate in some situations.

Launder & Rodi (1981) note that large scale eddies from the outer layer, bearing shear stress of opposite sign to that of the wall, encroach into the inner layer. This not only reduces the range of validity of equation 4.15 but is also the reason for the shear stress zero lying within the inner layer, inside the velocity maximum.

There is an abundance of data, including observations by Wilson & Goldstein (1976) and Irwin (1973), which shows that the shear stress falls to zero at about 60% of the distance to the velocity maximum. It also shows that, at ym the shear stress is of the same magnitude as, but of opposite

sign to, that at the wall. They found the velocity maximum to lie at $\xi = 0.2$, whereas zero shear stress occurred at $\xi = 0.1$.

The strong influence of the outer region on the inner is equally evident in the distributions of turbulent kinetic energy – the energy decreases smoothly from a maximum as the wall is approached with no evidence of the near–wall peak found in a boundary–layer.

4.4 CURVED WALL FLOWS

4.4.1 Boundary Layer Studies

Investigations have been carried out into the effect upon turbulent boundary layers of various degrees of wall curvature, both concave and convex.

Hong and Murthy (1986) cite work done by Ramaprian and Shivaprasad (1977,1978), So and Mellor (1972), and Gillis et al. (1981).

The principal findings comprise the following :-

Even mild curvature has a significant effect upon both the mean flow structure and development of the turbulent boundary layer.

For mild wall curvature, the mean velocity distribution in the fully turbulent region close to the wall still obeys the flat–plate log law, but the extent of the region where this is valid is affected by the curvature. The outer section of the boundary layer is affected significantly by wall curvature.

CONVEX	CONCAVE
Inhibits turbulence => reduces wall shear stress	Promotes turbulence => increases wall shear stress
Turbulence tends toward greater anisotropicity for strongly convex (nearly 2x that for strongly concave)	Turbulence tends toward reduced anisotropicity for strongly concave
Rotation of principal axes of stress decreases	Rotation of principal axes of stress increases
Log law region reduced	Log law region increased
Increased relative strength of the wake component	Reduced relative strength of the wake component

Meroney & Bradshaw (1975) observed steady longitudinal vortices, consistently reproducable. So & Mellor (1972) also established the presence of such vortices and Smits et al (1979) found them persisting indefinitely downstream in their measurements on a concave wall. All such longitudinal vortices gave rise to crest and trough spanwise locations of wall shear stress.

4.4.2 Wall Jet Flows

When a wall jet develops on a longitudinally curved surface, some of the wall jet properties are emphasized by the curvature effect.

Young (1800) first noted the deflection of a plane jet by an adjacent convex surface.

In 1916, Rayleigh determined, by balancing centrifugal and pressure forces on a fluid element, that decreases in angular momentum with distance from the centre of streamline curvature, would generate unstable flows. Conversely, flows in which angular momentum increased from the centre of curvature would be stabilised. The outer region of a wall jet on a convex surface will thus, by Rayleigh's criterion, be unstable.

Only since about 1960 have studies of sufficient detail been made to warrant consideration as possible test cases for turbulent flow calculation schemes. At this time, motivated mainly by the aeronautical industry, there was increased interest in the flow of turbulent jets over convex surfaces.

Most studies concentrated on incompressible jet flow over constant radius convex surfaces. The principle points of interest were the surface static pressure distribution around the surface, the structure of the turbulent flow field, the increase in jet growth rate and the separation of the jet from the surface.

Catalano et al (1977) measured mean velocities on 3–dimensional wall jets on flat and curved surfaces. They produced data on turbulence intensities autocorrelations and power spectral densities for an axisymmetric jet exhausting into a moving airstream. All the work reported below, however, concentrates on two–dimensional cases, being of greater relevance to the present study.

For a curved wall jet issuing into still surroundings at pressure p_a, air is continuously entrained from the surroundings. There is a pressure drop across the flow, the surface pressure being lower than that of the surroundings. The pressure force is related to the centrifugal acceleration associated with

the curved flow and keeps the jet attached to the wall. As the jet proceeds around the curve, the entrained fluid reduces the jet velocity. Thus, even though the jet width increases, the surface pressure gradually rises to p_a. This produces an adverse pressure gradient and can finally lead to the separation of the jet from the surface.

Newman (1961) describes the flow of an incompressible jet over a surface of constant radius. The radial momentum equation can be integrated across the jet to give a non-dimensional surface pressure

$$C_p = \frac{p_s - p_a}{p_o - p_a} \qquad 4.16$$

Newman (1961) and Bradshaw & Gee (1960) first noted the increased growth rate of a jet on a curved surface and used a qualitative representation to explain it. Most work studying the effect of increased strain rate on turbulent flows previously concentrated on boundary layer measurements.

A distinct group of jet flows exist where the flow may be considered to be in local equilibrium or self–preserving. Self–preserving shear layers must have dynamically similar profiles; that is, not only the mean velocity profiles but also profiles of Reynolds stress and other turbulence quantities must be representable by a single velocity and length scale. Truly self–preserving flows are rare. Certain shear layers, however, can attain near–similar profiles of mean velocity when fully developed.

A flat wall jet requires a tailored pressure gradient for self–preservation as investigated by Irwin (1973). He established the criterion for flow to be self–preserving. Irwin (1973) made pitot–tube and hot wire traverses to

obtain mean velocity, turbulence shear and normal stress profiles. He also emphasised the problems of ensuring two–dimensional flow. Turbulence energy was plotted in its component parts of advection, production, diffusion and dissipation and they were compared with various models. The mean velocity profile in the region close to the wall was shown to be logarithmic. The zero shear stress position was closer to the wall than the velocity maximum.

For a curved wall jet, Sawyer (1963) and Guitton & Newman (1971) demonstrated that for self–preserving flows the surface must take the form of a logarithmic spiral. This is a configuration where the local radius of curvature is proportional to the distance from the flow origin. When the ratio of jet width to radius of curvature is thus maintained constant along the jet, the outer part has a turbulence eddy structure which is related non–dimensionally to local parameters. These parameters do not change significantly with downstream distance. Few engineering systems follow this restrictive surface shape requirement and the flows are not then self–preserving since they develop significantly over the section length.

Launder & Rodi (1981) reviewed a vast number of papers of experimental investigations into jet flow situations. In their subsequent paper, Launder & Rodi (1983), they included consideration of radial wall jet studies. They rigorously tested the published data for two–dimensionality, using momentum–balance considerations as their criteria. Later surveys are included and reviewed by the present author without any comparable critical assessment of their two–dimensionality; any statements on the situation made by the researchers themselves have been accepted in good faith with no specialist knowledge of their shortcomings.

A major problem encountered by Guitton & Newman (1977) and other researchers was the establishment of two–dimensional flow. Non–two–dimensionality can be attributed to two effects - secondary flows occurring in the corners with the end walls. These have a significant effect on the displacement thickness of the end wall boundary layers and cause divergence or convergence at centre–span. The other effect causing non two–dimensionality was found to be extreme sensitivity of the flow to initial disturbances - non–uniformity in initial flow or slot geometry.

Guitton & Newman (1977) reporting on Guitton's PhD exploration emphasised that exceptional care was taken to ensure uniformity of flow. This was done by maintaining thin boundary layers at the slot and end–wall and thus impeding their generation of secondary motion. Launder & Rodi (1981) calculate a discrepancy of 18% between the shear stress maximum measurement and the momentum balance (in their own report, Guitton & Newman set this discrepancy at 25%). This was the smallest inconsistency of all those studied by Launder & Rodi and confirms that Guitton & Newman were the most successful in approaching two–dimensional conditions. The streamwise and normal mean velocity profiles were similar at all downstream stations. All four non–zero Reynolds stresses also generally displayed close similarity in shape and magnitude between stations and the position of zero stress was found to be inside the inner layer.

Two detailed studies on the turbulence structure of an incompressible jet flowing over a convex surface of constant radius were reported by Wilson & Goldstein (1976) and by Alcaraz et al (1977).

Wilson & Goldstein (1976) collated data for plane and curved wall jets in order to assess the effects of curvature. Their slot width to downstream radius ratio (t/r) was 0.0605 and they reported reasonable agreement between their mean flow development data and that of Fekete (1963) and a jet growth of

$$\frac{y_{1/2}}{t} = 0.0787\left(\frac{x}{t} + 6.0\right)\left(1 + 2.956\left(\frac{y_{1/2}}{r}\right) - 0.1559\left(\frac{y_{1/2}}{r}\right)^2\right) \qquad 4.17$$

where a simple linear fit was adequate for y until 180° round the cylinder, at which point the quadratic term was required. The comparable relationship for velocity decay rate was given as

$$\left(\frac{U_m}{U_s}\right)^2 = 0.0359\left(\frac{x}{t} + 6.0\right)^{1.05}\left(1 + 3.354\left(\frac{y_{1/2}}{r}\right)\right) \qquad 4.18$$

For the apparatus used, Launder & Rodi suggest that the flow ceases to be two–dimensional by the 180° location.

Wilson & Goldstein found that the mean velocity profiles, plotted as U/U_m against $y/y_{1/2}$, appeared to be similar with the position of maximum velocity close to that of the flat plate wall jet. They demonstrated the non–preserving nature of the flow by reference to profiles of V/U_m which were not similar for the curved case, but were for a wall jet on a flat plate. Profiles of U/U_m were too insensitive to show the degree of similarity. They observed a large increase in turbulent mixing caused by the centrifugal instability for

a wall jet on a convex surface and the Reynolds stresses were several times higher than the corresponding plane flow–values.

Alcaraz et al (1977) made very detailed hot wire measurements in a plane wall air jet over a constant radius convex surface of small curvature. The flow issued from an 18mm slot over a surface of radius 5800mm (t/r = 0.0031), with most extensive data for a slot Reynolds number of 4E4. Effort was directed towards achieving a two–dimensional flow situation. They reported that the jet growth rate started at the flat–plate value but rose 25% by the end of the 20° test section.

From the longitudinal and transverse velocity fluctuations Alcaraz et al produced estimates of the Reynolds shear stresses and they calculated skin friction coefficients. Their studies are adjudged by Launder & Rodi (1983) to provide one of the best sets of wall jet measurements to test calculation methods for turbulent shear flows. Launder & Rodi suggested that the main shortcomings were the lack of Reynolds stress data in the initial region of the test section and that the effect of curvature was limited to only 20° of arc.

Alcaraz et al found the maximum turbulent shear stress to increase from 0.012 to 0.017 as the wall jet develops, while the position of stress reversal shifted from 0.54 y_m to 0.35 y_m. Each component of Reynolds streamwise and cross-stream normal stress displayed a similar increase in the maximum value of approximately 25% between 30 and 90 slot heights, mainly in the region inside $y_{1/2}$.

Wilson's (1976) measurements, however, showed little variation in streamwise turbulence intensities between 60° and 130° and the radial com-

ponent showed a 35% augmentation. The main reason postulated for this disagreement is the large difference in the value of y/R in the two experiments. For Alcaraz, this was of the order of 10^{-3}, while for Wilson it was 0.4 at the 130° station. Fluctuating pressure reflections from the wall act as an important damper of the radial fluctuations, hindering the transfer of energy from u' to v' (their influence is the main factor in making the plane wall jet values of $\overline{v'^2}$ so much smaller than those for a free jet). For Alcaraz, y is so small compared with R that pressure fluctuations act as though the surface was plane. For Wilson's experiment, the wall–reflection mechanism is less effective in impeding energy transfer than in a plane wall case.

A more recent experiment by Dakos et al (1984), while principally directed towards obtaining heat transfer data, also provides useful comparative turbulence field information. They considered theirs to be the most extensive turbulence measurements attempted in this type of flow to the date of reporting. They used pressure–tube and hot wire techniques to study data on mean velocities, the non–zero Reynolds–stress tensor components and the triple–velocity products in a plane and a convex curved wall jet, of t/R = 0.04.

They found that the turbulent diffusion of turbulent energy and shear stress, associated with the triple velocity products, was dominated by the large–scale motion. This was not affected by longitudinal curvature. Profiles of $\overline{u'^2v'}$ and $\overline{v'^3}$ show turbulent–energy transport from the two high–shear high–intensity regions close to the wall in the inner layers and at approximately ξ = 0.8 in the outer layers, to the regions around the zero–shear–stress points.

The triple products passed through zero at, or very close to, the zero–shear–stress points - thus dividing the outward and inward energy transports.

The correlation $\overline{u'v'^2}$ is associated with the turbulent transport of shear stress.

The physical interpretation of these triple–velocity products is, they suggest, the same : outward transport of negative shear stress from the near-wall production zone and inward transport of positive shear stress from the outer–layer / high–shear / high–intensity region. The zero–shear–stress point marks the boundary between these opposing processes.

4.4.3 Axisymmetric Curved Jets

An early investigation into an axisymmetric jet was performed by Bakke (1957) who made pitot–tube measurements in a turbulent, low–speed jet spreading radially over a smooth plane surface. Traverses were made perpendicular to the plate and, by assuming the static pressure to be atmospheric everywhere, velocity profiles were deduced.

The profiles were found to be similar and to agree with Glauert's theory (1956) : the eddy viscosity distribution near the wall was consistent with the Blasius power–law velocity profile and a constant eddy viscosity could be used in the outer part of the flow. The similarity constants for equation 4.12 were found to be a=-1.12 and b=0.94 i.e. the velocity decay rate is about twice that of a corresponding plane wall jet, and the jet growth rate is approximately the same.

Starr & Sparrow (1967), investigating a cylindrical wall jet, found that the outer layer velocity profiles were similar but the inner layer profiles were not. They noted that the position of zero shear stress did not coincide

consistently with the velocity maximum and hence the shear stress was not proportional to the mean velocity gradient in the outer layer.

Sharma (1981) collected pitot tube measurements in the flow field around a conical wall jet to compare with previous investigations. The apex angle, a, of the cone varied from 0° to 90°, the limits representing a cylindrical wall jet and a radial wall jet respectively. The accuracy of the data should be regarded with caution since there was no indication of corrections applied to the pitot readings for turbulence effects, and the ratio of jet width to outer diameter of pitot tube was small.

The jet growth rate was found to be independent of the apex angle and of the initial slot width. For a slot width t, the jet growth rate could be expressed by

$$\frac{y_{1/2}}{t} = 0.120\left(\frac{x}{t}\right)^{0.91} \qquad 4.19$$

The velocity profiles were independent of slot width and there was a close similarity between profiles for varying angles of **a**. At each value of **a**, the velocity profiles proved to be similar in both the inner and outer layers. Sharma suggested that this discrepancy with the findings of Starr & Sparrow (1967) was due to curvature effects; the ratio of slot height to rod diameter used by the latter was more than four times greater than that of Sharma.

Sharma's data showed the inner layer profiles could be described by equation 4.15, the log law of the wall, with A=4.17 and B=7.6 for the range of distances $yu_\tau/\nu < 200$.

Morrison (1982) acquired data for an idealised Coanda flare with hot wire and 3–hole pressure probes in low speed air flows. He studied the flow over a half model of an Indair flare with two values of slot width to downstream radius ratio of 0.167 and 0.066 and corresponding stagnation pressure ratios 0.98 and 0.94.

Measurements of surface static pressure showed an initial drop, due to the jet curvature, followed by a gradual increase in pressure up to atmospheric as the jet flowed around the Coanda curve. The experimental data was limited to mean flow and Reynolds stress measurements outside the log–law region of the inner layer.

The three hole probe and hot wire measurements of mean flow properties were recorded at various angular locations around the flare. Streamwise velocity profiles up to 75° around the Coanda appeared to be similar, as was noted by Wilson & Goldstein (1976) in their study of a plane convex surface. Thereafter, the similarity of profiles around the Coanda broke down in the outer layer, due to the influence of the flat portion of the surface further downstream.

The non–similarity of the flow was shown by the normal velocity profiles. With increasing distance downstream, the non–dimensionalised velocity increased at a constant value of $y/y_{1/2}$. This feature was also noted by Wilson & Goldstein. The growth rate of the jet from the smaller slot was similar to that of Wilson & Goldstein's (1976) study of a plane wall jet. The jet flow from the larger slot produced a larger potential flow region and the jet did not fully develop. The resulting jet growth rate was consequently found to be below that found by Wilson & Goldstein.

A study was made of the high turbulence levels caused by the combined effects of streamline curvature and divergence. Detailed hot wire analysis for the larger slot configuration showed normal turbulence intensities of up to 45% on the curved portion of the Coanda. The maximum values were recorded at $(y/y_{1/2}) = 0.6$, corresponding to the maximum negative gradient of the streamwise velocity. The normal and shear stresses at locations up to 75° were generally greater than those from Wilson & Goldstein's data, due to the effect of divergence in addition to that of streamline curvature.

As found on plane and curved wall jets, the position of zero shear stress was shown to lie within the inner layer, i.e. inside the position of the velocity maximum. The interaction of outer and inner layers is emphasised by the zero shear stress position moving further towards the wall with increasing distance downstream.

Similarity was shown between Morrison's data for the structural parameter $a_1 = \overline{u'v'}/q^2 = 0.13$ and the results of Wilson & Goldstein (1976). However, the non–dimensional turbulence parameter $\overline{v'^2}/\overline{u'^2}$ showed peak values far higher than those recorded by Guitton (1970) due, Morrison suggested, to the effects of divergence upon the flow field. Morrison's data further showed that both the turbulence structure and the mean flow were distorted by the sudden change in surface curvature experienced when the flat portion of the flare was reached. The structural parameters and individual stress components recovered non–monatonically, in direct contrast to the data of Castro & Bradshaw (1976) and Smits et al (1979a) who noted the monatonic return to equilibrium of a_1.

Morrison (1982) also performed tests on a full scale 8" Indair flare. The velocity profiles measured with a three hole probe were found to be similar. A jet growth rate similar to that of Wilson & Goldstein was also displayed.

Gilchrist (1985) extended this work to encompass high speed flows. Special attention was paid to the mechanism of breakaway, the phenomenon whereby the jet leaves the surface tangentially. Gilchrist used interferometric, Schlieren and shadowgraph techniques in his study as well as surface oil flow visualisation. Total pressure traverses were performed within the underexpanded jet and surface static pressure measurements established the existence of a separation bubble. No further consideration of compressible jet flows is given since it is not directly relevant to the present investigation.

4.4.4 Extra Rates Of Strain

Bradshaw's (1973) thorough discussion of extra rates of strain primarily concentrates on the effects of streamline curvature, but also reviews the effects of divergence, dilatation and longitudinal acceleration. The effect on any turbulent flows' structure of an extra rate of strain is an order of magnitude greater than that predicted by the extra terms in the Reynolds stress transport equations. In addition to the explicit changes to the production and transport terms, higher order correlations are also changed, implicitly changing the sizes of all the terms. These latter, implicit changes are generally more important than the explicit changes.

Studies involving divergence effects have often also included the effects of other extra rates of strain. One study concerning pure divergence effects is that of Smits et al (1979b). This involved a detailed survey of a boundary–layer on a cylinder–flare body. A fully developed boundary–layer was subjected to lateral divergence on a cone. Identical measurements were made to those in a previous study , Smits et al (1979a), to allow a qualitative assessment of the isolated effect of divergence on the flow structure.

Their results highlighted the following points :-

no longitudinal vortices were detectable;

the Reynolds stress profiles did not collapse after the removal of curvature;

divergence effects were of the same order as those of streamline curvature e.g. shear stress data maintained values for the whole test section, falling gradually with the extra rate of strain, the peak of the profiles moving steadily outwards with increasing downstream distance;

the structural parameter a_1 increased from 0.15 and then returned to the value of 0.15;

the triple products were magnified by a factor of at least five.

4.5 CONCLUSIONS

All measurements made in boundary layers on convex surfaces show an increase in turbulent activity, specifically large increases in second and third order correlations. These result in an increased shear layer growth rate. There is also evidence of the existence of steady longitudinal vortices. For wall jets on convex surfaces, there is a similar increase in turbulence activity reported, but no evidence of vortices.

For all unstably curved wall shear layers, it is very important to establish the initial flow conditions as near two-dimensional as possible.

Previous studies have concluded that, for convex streamline curvature, the extra strain thus introduced tends to reduce turbulent mixing and shear stress in the near-wall layer (where the angular momentum of the flow increases in the direction of the radius of curvature). Conversely, it tends to increase it in the jet-like layer outside the velocity maximum region. The large eddy length scale and the lateral turbulence intensity are increased over a convex surface and thus entrainment is increased. This preferential amplification increases the distance between the positions of zero shear stress and maximum velocity. The reverse applies for a concave surface.

The effect of streamline divergence on turbulent shear layers appears to be an increase in turbulence activity. Although there are far fewer reports on this aspect, its effect appears to be of the same order as that of streamline curvature.

TABLE 4.1 CALCULATION METHODS

INTEGRAL	DIFFERENTIAL
Based on the solution of the integral equations of motion. To obtain a closed set requires additional relations between unknowns.	Based on the solution of the partial differential equation form of the boundary layer equations. Classified via closure assumptions :-
	Mean-Flow Methods Closure obtained via eddy-viscosity or mixing-length approaches
	Transport Equation Methods Closure obtained via I. Solution of mean momentum + mean continuity + turbulent K.E. equation (a) Eddy viscosity from turbulent energy eqn. (b) Reynolds shear stress from turb. energy eqn. II. Solution of mean momentum + mean continuity + Reynolds stress transport equation

CHAPTER 5

COANDA EXPERIMENTAL APPARATUS AND INITIAL EXPERIMENTS

5.1 EXPERIMENTAL APPARATUS

5.1.1 Flowrig

The design, construction and commissioning of the original flowrig was undertaken by A.Wright (1982-1985) as part of a project for applying LDA to swirling flow studies.

It comprised a closed loop water flowrig. The present work maintained the major sections of pipework routing, accompanying hardware and rig layout as its basis and only adapted the remaining sections where necessary to be appropriate for the current survey. The general arrangement of the revised system is shown diagrammatically in Fig. 5.1.

The water flowrig was operated with chlorinated water which had first been filtered from the mains supply through a 5micron filter. The chlorination imposed constraints of corrosion resistance on the choice of pump.The pump (model SIHI–Ryaland RYAXF 65/16) operated with a 2bar delivery head and a maximum capacity of 20litres/sec.

The output from the pump could be routed to a bypass circuit or around the main pipework to the Coanda Tank. The proportion of water that went to the bypass was varied by a control valve on this branch of the network. The water fed to the flowrig piping flowed along a section

of pipe of diameter=100mm. The pipe then divided, one branch comprising lengths of d=50mm pipe, the other D=100mm pipe. Water could be routed to either or both alternative paths, control valves on the two sizes of feed pipes providing variation of the flow distribution through the system. Orifice plates were situated along each pipe, with bores=60mm and 30mm for the large and small diameter pipes respectively, designed to BS 1042.

The pipes rejoined into d=50mm pipe, approximately 20 diameters upstream of the Coanda Tank. Water then flowed into the tank through a 50mm pipe breaching one of the side walls of the tank near the top. It was pumped out through a 100mm pipe in the tank base.

There was a further control valve on the return pipe and water was routed out of the test cell to a heat exchanger, situated in the main thermodynamics laboratory. The heat exchanger was an air cooled radiator, using the relatively cool air of this laboratory and the water was thus maintained at a fairly constant temperature of approximately 20°C. The return pipe was also connected to the drain system via an isolating valve. This was then used to empty the whole flowrig.

Where the tubes entered and left the Coanda Tank they were sealed by suitably-sized 'O' rings (to BS 1806 (1962)) compressed by flanges onto the walls.

The pipework was rigid unplasticised poly-vinyl chloride (uPVC) linked to segments of flexible piping to accommodate the water surges imposed when starting up the rig.

5.1.2 Water System

Air vents were located on the radiator, the top of the measuring tank and along the top inlet feed pipe. To fill the rig, the mains tap was opened and the bleed valves were all opened. After partially filling, chlorine was added via the inlet pipe and then further water added, closing successive valves as the rig filled. The mains tap was gradually closed as filling neared completion. The rig was left to settle when the top bleed valve was reopened and all air expelled by adding a further amount of water until water began to exit the valve.

The design of the pipework and the various control valves allowed flexibility over a wide range of flowrates. The length of pipework upstream of the tank measuring section of the rig was designed to ensure that any flow distortions introduced by the pump had been eliminated. Steady state pipe flow velocity profiles should, therefore, have been established before entry to the test section.

Throughout the curved jet flow work, the entire pump delivery was fed through the larger (100mm diameter) pipe. An accurate and precise measure of the flowrig operating conditions was achieved by monitoring a water manometer. This was connected to the orifice plate situated in the 100mm diameter pipe, upstream of the measurement section of the system. All data was corrected to a standard orifice plate pressure drop.

The system used naturally–occurring particles as the LDA scattering centres.

5.1.3 Tank Section

The tank section of the water flowrig was constructed entirely from 2"thick plates of Perspex. Its internal dimensions were 400mm x 400mm x 950mm. It allowed the full optical access vital for LDA purposes.

Careful sealing at every joint was required. Silicone rubber sealant was applied to all mating surfaces before the final assembly and the walls were bolted tightly together.

5.1.4 Coanda Design

The basis for the design was the axisymmetrical 18-H-AS flare, marketed by Kaldair Ltd. This Coanda flare consists of a small flat section upstream of the slot, followed by a constant radius convex curve through 100°, ending in a tangentially conical section.

A 3/5 scale half-axisymmetric solid model of this Indair flare was constructed in Perspex. Features of the design are shown in Fig. 5.3. It was located onto a Perspex backing plate by 3 threaded studs. Stainless steel nuts clamped it into position. The back plate had slots milled which allowed movement to provide the opportunity for changing the slot width at the base of the flare. A slot in the backing plate allowed water to flow into a feed passage and thence out of the slot.

In their study of an incompressible self-preserving wall jet over a convex surface, Guitton & Newman(1975) identified two main causes for the departure from two-dimensionality. One cause was related to the conditions

in the plenum chamber and, in particular, at the slot lip; the other cause was due to secondary flows in the boundary layers on the sidewalls dowstream of the slot.

In an effort to avoid such problems in establishing two–dimensional flows, the rig's feed system included a plenum chamber and a suitable length of flow in the feed passage. The plenum chamber and feed pipe were included so that upstream non-uniformities likely to cause three–dimensional effects in the jet were damped out and thus the feed system should have produced a reliably steady feed condition. The lip of the feed tube at the slot was manufactured with particular care, attention paid to achieving consistent curvature and a high quality surface finish.

To avoid secondary flows induced by the proximity of the tank sidewalls, the scale and positioning of the flare was designed so that, when located within the tank, wall effects were minimised. Fig. 5.2 shows the positioning of the Coanda in its tank, 100 mm from the sidewall and 400 mm from the top of the tank. This provided a situation in which the Coanda was effectively mounted in isolation, unaffected by the relatively distant tank.

The plenum chamber was fabricated from a Perspex tube, mounted across the tank width. This also provided the support for the backing plate, feed tube and Coanda assembly.

The annular slot at the base of the flare was set to 5mm to provide comparability with Test Case A in Morrison's work (1982). In order accurately to set this slot width, slip gauges were placed on the feed tube lip and the Coanda lowered onto them. After locking the flare into position the gauges

were again used to check the dimension which was estimated to be accurate to within 0.1mm.

In order to obtain measurements at a variety of angular positions, relative movement between the model and the laser beams was necessary. This was possible by movement of either the laser and optics, or the tank and model or the model only. In order to obtain measurements at a variety of angular positions of all three velocity components, further relative movements were necessary.

The laser and optics were located on the milling machine bedplate and this imposed severe limitations on their manoeuvrability. Physical limitations dictated that the only feasible and realistic option was to design the rig to enable

(a) rotation of the model to provide access for measurement over the required range of angular positions ,

(b) a combination of this rotational capability with a repositioning of the tank and model to enable the measurement of all three velocity components at all angular locations. Figs. 5.4, 5.5 show the laser beam to model orientations which fulfilled these design criteria.

Acquisition of full three-dimensional LDA measurements i.e.all velocity components, demanded an adjustable assembly. The rig design therefore enabled rotation of the model to provide such access.

It was necessary to be able to assess the position of the crossover relative to the model surface with a sufficiently high degree of accuracy to

ensure three–dimensional measurement capability – after moving the model and realigning the beams.

The plenum chamber feed tube was attached to the backing plate and hence the Coanda model as shown in Fig. 5.3. It formed the support for the model within the measurement tank. The feed tube was freely supported at one side of the tank by the feed pipe. At the opposite tank wall it was screwed onto a solid Perspex handle which protruded from the side wall. When the handle was rotated, therefore, the feed tube, backing plate and Coanda model assembly all rotated together. A pointer on the handle allowed careful and accurate alignment with a protractor scale mounted on the tank's outer wall. When the required angle had been attained, the assembly could be locked into position with three bolts positioned around the circumference of the handle's flange.

5.1.5 LDA System

The LDA system used for the curved jet flow survey was exactly the same as that used previously for the bias studies and sudden expansion flowrig measurements. The details of the arrangement were given in Chapter 3 but the essential elements are included here for completeness and ease of assimilation.

The 2Watt Argon–ion laser operated in the TEM_{00} mode on the 514.5nm wavelength. The monochromatic and coherent light was focused on a rotating diffraction grating which provided beam splitting and frequency shifting. The fringe number effect was eliminated by frequency shifting.

The rotational speed of the grating was chosen to ensure the elimination of directional ambiguity.

The grating and its associated motor could be rotated about the tube which defined the bench optical axis as shown in Fig. 3.4. This provided the facility for rotating the plane of the beams. The assembly was secured by locating a pin through a hole in the motor mounting into one of a number of matching holes in the tube mounting. The locating holes were spaced at 45° and thus the plane of the beams could be orientated at four angles, designated 0°, 90° and ±45°.

The system optics brought the two first order beams of equal intensity to a focus within the test section. The entire laser system was carefully aligned and rigidly mounted on the traversing table. The assembly operated in forward scatter mode with signal collection performed by the independently–mounted, fully adjustable photomultiplier(PM) tube assembly. The PM output was monitored on a dual trace oscilloscope and was also fed to the DISA counter processor, operated in *continuous* mode with a 5:8 crossing comparator operation.

Data collection and initial analysis was performed on the Ithaca CP/M computer.

The analysis programmes converted the Doppler shift information, from the PM tube and counter system, into a mean velocity and the first four moments of the signal probability density function (PDF).

From all component measurements, information was obtained on velocities, streamwise and radial turbulence intensities (normal stresses) and shear stresses.

The reduced data was then passed to the mainframe computer for further analysis and display. A number of FORTRAN programmes had been written for the purpose of data reduction and graphs were produced via the graphics package, GHOST80.

5.2 INITIAL EXPERIMENTS

Throughout the Coanda flow study, a curvilinear coordinate system was used : the distance downstream being the positive x–direction and the distance perpendicular to the surface the positive y–direction. Fig.5.4 shows the angular positions around the Coanda at which data was collected. Also shown is the sign convention adopted throughout the present study. Radial traverses were performed at each of these locations.

5.2.1 Traverse Details

It was necessary to adopt a measurement technique that ensured a high degree of positional accuracy and repeatablility. This was especially necessary in order to relocate the probe volume when the rig had been turned. The Coanda had been aligned with a protractor scale outside the chamber. It could be tipped to the appropriate angle for measurements.

A traverse was set up as follows :–

the Coanda model and its feed system assembly were rotated by the protruding handle. The pointer was carefully aligned with the protractor

scale. When the required angle had been achieved, the assembly was then locked into position with the three bolts on the handle flange.

The laser beams were projected in an orientation ensuring that they are tangential to the model surface. The milling machine bed traverse mechanism was used to wind in the beams until they just impinged upon the flare surface. The beams were moved horizontally and vertically until the crossover was accurately located on the surface of the Coanda. The beams must then have been at the widest point of the surface and this ensured correct location and reliably repeatable alignment. To eliminate errors from the backlash of the traverse mechanism, the beams were then wound into the model and repositioned by winding back out. Repeatability was checked for each traverse and repositioning was achievable to within 25micron.

All traverses were performed by winding out away from the surface, along a normal to the Coanda for that specific angle of inclination. The rotation of the model provided opportunity for performing a traverse by using one axis only of the traversing mechanism, thereby reducing positional inaccuracy.

The beam crossover relative to the model could be located within 1degree for all streamline (X–Y) traverses. Relocation for the transverse (Y–Z) measurements was less precise. Each traverse was zeroed by positioning the crossover just touching the surface, repeatable to within 50 micron. The positions on a single traverse were then accurate to within 25 micron relative to its zero.

In order to minimise positional errors, all velocity component information was collected at a traverse point before moving to the next radial location on that traverse.

A physical limit was set on the measurement position attainable nearest to the surface by the impingement of the beams (on their approach to or exit from the crossover) with the Coanda. Generally, greater access was possible in the X–Y plane; streamline values in the X–Y plane could be collected closer to the surface than other components i.e. other beam orientations. These differences were solely due to the physical limitations set by the rig.

The radial spacing of the readings was varied at each position; the distances were determined by careful study of Morrison's (1982) data to estimate the areas expected to be of greatest interest. The traverses were thus tailored to the location to ensure that most data was recorded in these areas.

5.2.2 Sampling

Due regard was paid to the findings of the previous work into the bias existing in the LDA system as detailed in Chapter 3. All the initial work on the ergodicity of sampling had been performed on the sudden expansion water flowrig. It was, therefore, necessary to study this aspect of the LDA system and data acquisition technique in the Coanda flow situation. It was not the intention to reproduce an equally extensive survey as that for the sudden expansion rig, but rather to confirm that truly ergodic data sampling was employed throughout the curved jet studies.

The window circuit was applied to the counter processor ARM line and hardware windowing of the data was performed with a variety of window lengths of varying size to study the sampling of the data and ensure ergodicity.

Firstly, in the X–Y plane, at the 45° angular position around the Coanda, data was collected at y=3mm and 9mm. These were the two radial positions approximately corresponding to the expected position of the maximum streamwise velocity,U_m, and the radial position at which the steamwise velocity had fallen to half this maximum value, $y_{1/2}$. Streamline velocities and turbulence data were recorded for sample intervals of $10^3\mu$s and $10^4\mu$s. A check was also performed on the cross-stream data by collecting samples with the beams in their $-45°$ orientation, at y=3mm for a sample interval of $10^4\mu$s only.

When the model had been turned and Y–Z plane data obtainable, further checks were made. In this orientation, the 45° traverse was inaccessible so data was collected at the 90° traverse position. Here data was recorded at radial locations of y=2mm and 10mm for sample intervals of $10^2, 10^3$ and $10^4\mu$s.

5.2.3 Flow Axisymmetry

As detailed in section 5.1.4, design effort was directed to minimising problems of non–two–dimensionality.

In addition to the full jet survey, some measurements were made, in both the x–y and y–z planes, at various circumferential positions to check the axisymmetry of the flow. Several preliminary traverses were performed to test the axisymmetry of the flow as the curved jet developed around the Coanda surface. To perform an initial review on axisymmetry, traverses were completed at the 90° position. Data was collected at 1deg. intervals in the z

direction around the centre–line from +5° through to -5°, both at 4mm and at 10mm from the wall. The Coanda model was locked at its 90° orientation.

The traverse around the 90° 'line of latitude' was conducted by moving the laser system relative to the measuring tank. The laser and optical bench were mounted on a turntable on top of the milling machine bed. The system was rotated in 1degree intervals, locked in position and the readings taken before moving to the next angular location. At each angle, the crossover was repositioned at the surface of the model and, after careful alignment, was then wound out to the required radial distance.

For further confirmation of axisymmetry, complete radial traverses were performed at the 90° location – two on the centre–line, and one at each of +5° and −5° on either side of the centre–line. The crossover alignment for these traverses was similar to that for the previous survey – the turntable was used to reposition the beams at the required angle and the assembly was then wound in until the crossover was just impinging upon the Coanda surface. A radial traverse was then completed by using one axis of the traversing gear.

With the rig turned for transverse–component traverses, further axisymmetry checks were performed. In this orientation, traverses were effected at 90° on the centre–line and at 45° on either side. Difficulties were encountered in establishing the beams at exactly 45° around the Coanda. No direct angular positioning is available for the beams relative to the Coanda. To relocate the beams, geometrical calculations were necessary to estimate the appropriate horizontal and vertical movements required. The milling machine traverse gear was then used to move the laser beam by the correct amounts. It is uncertain how great an error is introduced by deficiencies in respect of the relocation.

The crossover was located at the model surface on the 90° centre–line. The coordinates for the 45° positions were calculated and the x–y traverse mechanism was employed to realign the beams for the off–axis traverses. The usual procedure of 'zeroing' the crossover was then used before beginning a traverse.

5.2.4 Data Redundancy

At each grid point, the beams were placed in two orientations in the X–Y plane to give the streamwise and normal components of velocity. They were also orientated at +45° and −45° to allow the (x–y) turbulent shear stress to be determined. All four readings were recorded at one position before moving to the next radial position. The full complement of readings was recorded at each radial position for each angular location of the X–Y plane radial traverses.

The tank section of the flow rig was turned out of the plane of Fig. 5.4 to provide the necessary model to laser orientation for collecting data on the transverse component. In addition to the z–velocity data, a duplication of radial data was then also possible in this orientation, as shown in Fig. 5.5.

The interaction of hardware and laser beams restricted the traverse positions attainable in this orientation. Attempts at off–axis and even backscatter signal collection were unsuccessful. However, the 75° to 100° + 20mm locations were all studied.

The measurements provide varying degrees of redundancy in determining velocities and higher order turbulence data. There are two orientations of the rig; for each orientation, four configurations of the laser beam and thus probe volume, are attainable. There are, therefore, a maximum of eight readings at each traverse point.

For instance, it is possible to derive the streamwise and radial velocities from the 'direct' measurements or from the beam orientations at $\pm 45°$. Further redundancy is achieved for the locations at which transverse-component traverses were also performed. Here, a repeat of the direct measurement of radial velocities was made, in addition to the other three orientations. Thus from 75° to 100° + 20mm, three velocities (u,v,w) are required from a selection of 8 velocity readings. Similarly, although to an increasingly smaller extent, the second and third order data has been duplicated e.g. five stresses are obtainable from the 8 readings.

Matrix analysis methods were applied to solve for the required parameters from the combination of equations and an error analysis was implemented. This provided 'confidence intervals' on the derived data ; the 95% limit was chosen for all the analysis.

The procedure adopted for statistically analysing the data from the traverses at all angular locations around the Coanda is outlined below :-

1. The basic analysed data comprising mean velocity and the first four moments of the signal's probability density function (PDF) had been tranferred and stored on the mainframe computer.

A FORTRAN programme SUMSx was used to access each traverse location x and scale the data at the discrete radial positions to correct to the standard orifice plate pressure drop. The data for mean, first and second order terms was then written into separate files in matrix form. Each file contained the data appropriate to one angular traverse.

2. Separate, although functionally identical, FORTRAN programmes, MEAN_MATx, SD_MATx and SKEW_MATx, were used to perform the required matrix calculations.

They all contained calls to the NAG library subroutine F04AMF. This calculates the least squares solution of a set of m linear equations in n unknowns with multiple right hand sides.

A solution was sought to

$$\mathbf{AX} = \mathbf{B} \qquad 5.1$$

where

$\mathbf{A}$ = matrix of relationships

$\mathbf{X}$ = matrix of unknowns

$\mathbf{B}$ = matrix of experimental data from '1' above

A sample of the matrices is shown below for the full complement of mean velocity data e.g. at 90°.

$$\begin{pmatrix} 1 & 0 & 0 \\ 0 & 1 & 0 \\ 1/\sqrt{2} & 1/\sqrt{2} & \\ 1/\sqrt{2} & -1/\sqrt{2} & 0 \\ 0 & 0 & 1 \\ 0 & 1 & 0 \\ 0 & 1/\sqrt{2} & 1/\sqrt{2} \\ 0 & -1/\sqrt{2} & 1/\sqrt{2} \end{pmatrix} \begin{pmatrix} u \\ v \\ w \end{pmatrix} = \begin{pmatrix} U \\ V \\ P \\ N \\ W \\ V1 \\ P1 \\ N1 \end{pmatrix} \qquad 5.2$$

All the experimental results were given equal weightings although some data were probably less reliable than others. The addition of weightings would be an added sophistication to the analysis technique. However, without knowledge of a rigorous scientific approach to estimating the appropriate values for such weightings, this could introduce as great an error as it eliminates!

3. The output from the calculations in F04AMF was processed within the corresponding FORTRAN programme to produce confidence intervals on the mean values output. This was accomplished by deriving the computed equivalent of the input signals, B, from

$$\mathbf{S} = \mathbf{A} * \mathbf{X} \qquad 5.4$$

The residuals were then calculated

$$\mathbf{r} = \mathbf{B} - \mathbf{S} \qquad 5.5$$

The 'error' was defined as

$$\mathrm{E} = \frac{\sum_{i=1}^{m} \mathbf{r}_i^2}{no.equations - no.unknowns} \qquad 5.6$$

The confidence intervals were then obtainable from

$$C.I. = \sqrt{\mathrm{E}} * \sqrt{\mathrm{S}_{inv}} * t \qquad 5.7$$

where

$$\mathrm{S}_{inv} = (\mathrm{A}^T\mathrm{A})^{-1} \qquad 5.8$$

and t is a statistical parameter, obtained from tables, and is dependent upon the number of degrees of freedom and the limit chosen, in this situation 95%.

4. The details of the computed mean values of the data from F04AMF and their corresponding confidence intervals were written into files. The data was then accessed by FORTRAN programmes e.g. FITVELx, which contain calls to further NAG library subroutines.

E02BAF computes a weighted least squares approximation to a set of arbitrary points with arbitrary weights by a cubic spline. The cubic spline consists of a number of cubic polynomial segments joined end to end with continuity of first and second derivatives at the joins. The x-values of the joins are called 'knots' or, more precisely, 'interior knots', which are specified by the user.

The routine uses a least–squares criterion which enables an allowance to be made to take account of differing accuracies of the individual data values. The allowance takes the form of 'weights' applied to the data values, so that those known to be more accurate have a greater influence on the fit than others. The weightings used for the present analysis were made inversely

proportional to the confidence intervals corresponding to the individual traverse points.

A second NAG subroutine, E02BCF, evaluates the cubic spline and its first three derivatives from the E02BAF representation. It was used to compute the fit at a large number of points. This provided interpolation between traverse data points and produce a smooth fitted curve to the data.

The first derivative of the curve for the mean velocity data was used to identify U_m and then further FORTRAN programming assessed the value of $y_{1/2}$.

5. The computed values from F02AMF and the fitted curve from E02BCF were read by the appropriate FORTRAN plotting programmes to produce the results displayed in Figures 5.16 - 5.26.

5.3 EXPERIMENTAL RESULTS AND DISCUSSION

5.3.1 Ergodic Sampling

The data from all the sampling studies were analysed in a manner similar to that previously applied to the sudden expansion measurements. Scatter in the mean velocity data, as defined by the 95% confidence limit, is shown in Fig. 5.6. The plots show a similar trend to that observed in the pipe flow, although the levels of scatter are lower. This is despite the measurements being recorded in regions of very high local turbulence intensity.

The aim was to limit scatter to within 2%; it was found that a window length of $10^4 \mu s$ provided a suitable compromise, limiting scatter to an acceptable level while maintaining reasonable data acquisition time. No condition was found where, when operating with this window length, the scatter exceeded the required limit.

5.3.2 Axisymmetry Checks

The results of the surveys performed at the 90° position at y=4mm and 10mm are plotted in Figures 5.7 to 5.11.

Streamwise velocity plots show a variation of less than 0.3m/s while radial velocities are within 0.02m/s. At both 4mm and 10mm traverses although the results show variations over the full 11 degree range of traverse, there are no indications of a systematic variation which could be attributable to slot flow imperfections.

The normal and shear stresses and the derived structural parameters also show a high level of consistency (Figures 5.9 – 5.11). No trends can be identified in the small changes in x or y component normal stresses. The shear stresses show more variation although somewhat exaggerated by the choice of scale on which they have been plotted. No structure is identifiable which could be the result of the existence of longitudinal vortices as identified by the studies of Tani (1975) and Smits et al (1979a).

The plots from the traverses on the 90° centre-line and 5 degrees either side are shown in Figures 5.12, 5.13. A repeat of the X–Y centre–line traverse was completed after the off–axis data was recorded. The original 90° centre–line traverse was the first full set of data to be collected from the Coanda

rig. It was, therefore, considered expedient to obtain yet another check of the acquisition technique and of the traverse mode. There is some variation in the data but, generally, they confirm the axisymmetrical consistency of the velocity field. The normal stresses are closely similar, especially in the inner portion of the jet, $\xi < 0.7$.

With the rig turned for transverse–component traverses, further axisymmetry checks were performed. In this orientation, traverses were effected at 90° on the centre-line and at 45° on either side, since access of these locations was possible in this orientation. They provide an indication of the maximum variation to be found in the flow around the Coanda in the Y–Z plane. Results from these checks are shown in Figures 5.14, 5.15. They do not coincide exactly but, so far off axis, discrepancies are not unexpected. Some effects of the presence of the edge of the half–model may be apparent.

5.3.3 Redundancy Checks

Plotted on Figures 5.16 – 5.18 are the non- dimensionalised velocity plots for the 'best fit' curves. Superimposed are the 95% confidence intervals calculated for the redundant data points. Below 75° only X–Y traverse data was obtainable. This provides four velocity and turbulence data readings, and reduces the extent of the data redundancy. The confidence intervals would, consequently, be expected to be larger. Of the data for the early jet development, the 45° traverse shows the largest error bars but these are still not significantly large.

The additional mean velocity data, for 75° and above, repeatedly show very small error bars. There are erratic variations but even at the highest

angles, 100° and 100° + 20mm, where re-location for the z-traverse was difficult, the results are remarkably consistent.

The normal and shear stress data with the calculated 95% limit bars are shown in Figures 5.19 - 5.23. The shear stresses are plotted as $\sqrt{\overline{u'^2}}/U_m$ so are, in effect, turbulence intensity levels relative to the maximum streamwise velocity. The normal stress error bars are seen to be generally satisfactorily small. The worst results are at 100° + 20mm where relocation for the Y–Z traverse was most difficult. Less explicable are the larger–than–average error bars seen for the 45° data. The data at 90° shows the smallest error bars.

As the number of degrees of freedom (number of equations - number of unknowns) reduce, with higher order correlations, the error bars would be expected to increase. Fortunately, the confidence intervals for the shear stresses, plotted as $\sqrt{\overline{u'v'}}/U_m$, over the first 30° are still very small. The scatter estimates do increase further downstream but the fitted curves look plausible.

Fig. 5.24 is included to illustrate a *before* and *after* comparison. It demonstrates the curve fitting process, for the 90° location. This highlights the improvement obtained from smoothing unrealistic deviations in the raw data.

Fig. 5.25 shows a repetition of the data for 90° but plotted in terms of the square of the velocity maximum. It is included for assimilation with comparable data from those authors who had chosen to so present their results.

5.3.4 Summary

These initial experiments in the curved flow situation tested

1. the quality of the measurement technique, by varying the sampling window length and establishing ergodic data acquisition

2. the quality of two-dimensionality of the flowfield by a number of axisymmetry checks.

3. the quality of the resulting data by undertaking a statistical analysis to compute confidence intervals.

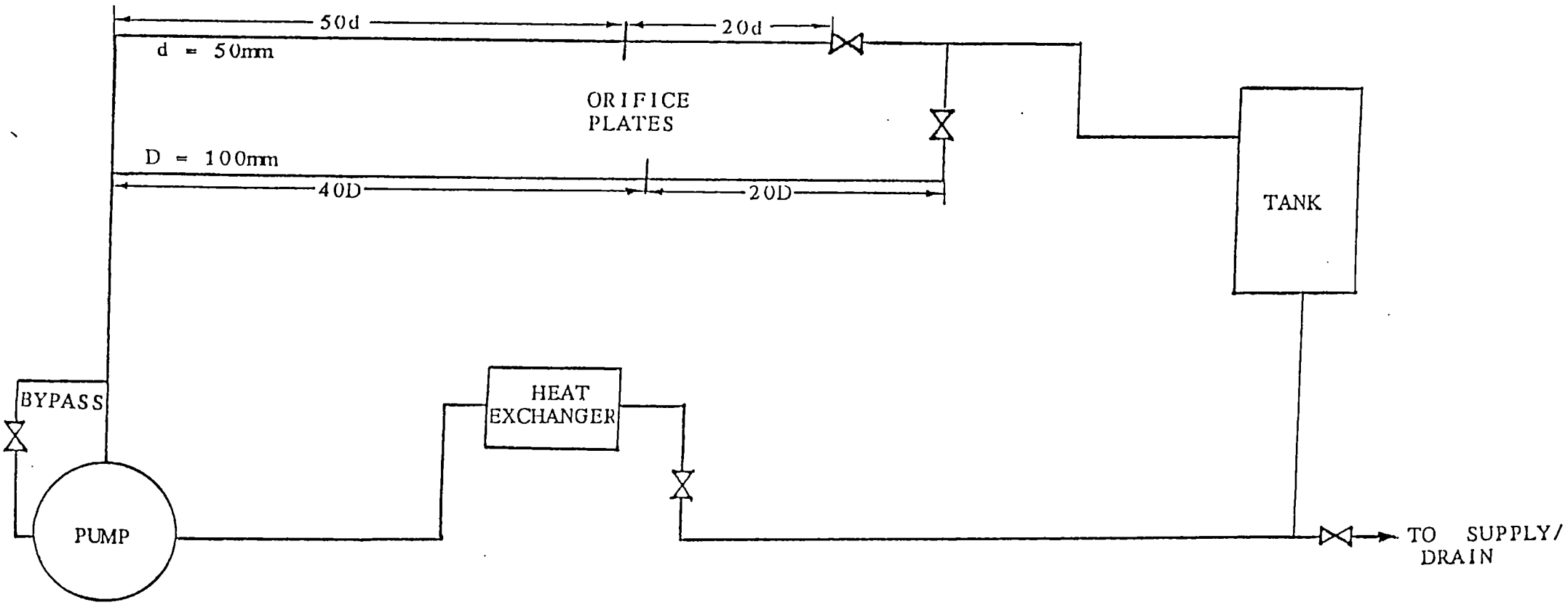

Fig. 5.1 COANDA FLOW RIG GENERAL LAYOUT

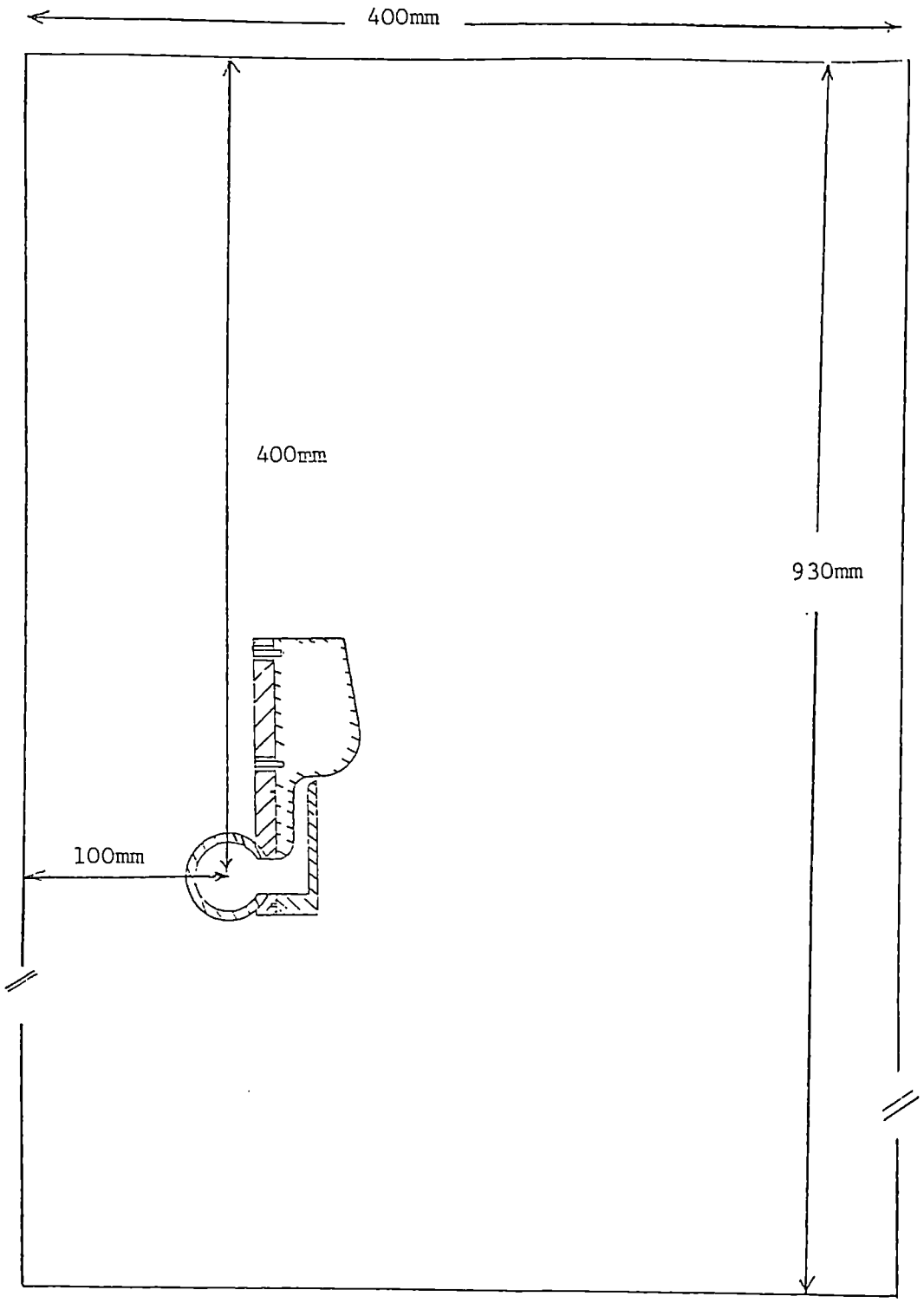

Not To Scale

Fig. 5.2 Model Coanda Flare Rig Details

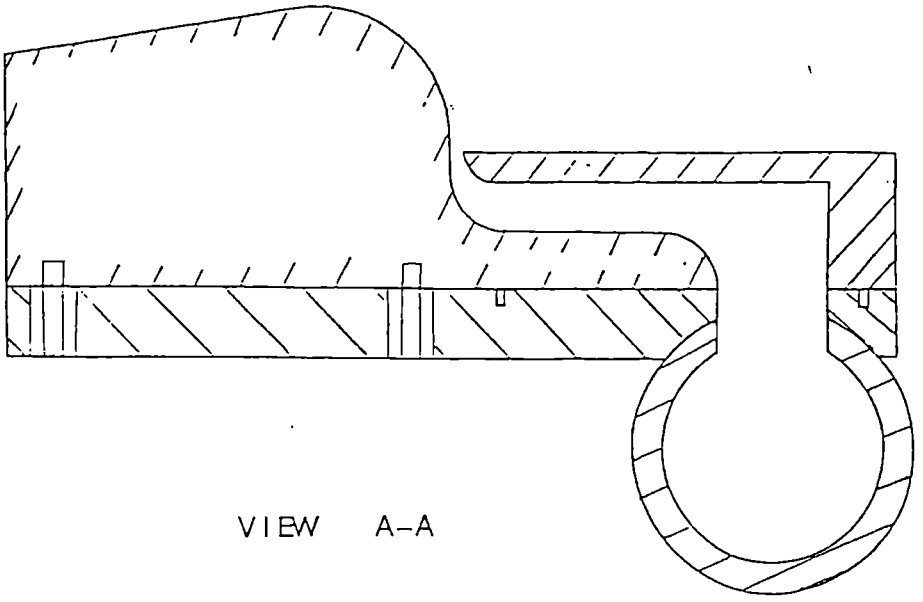

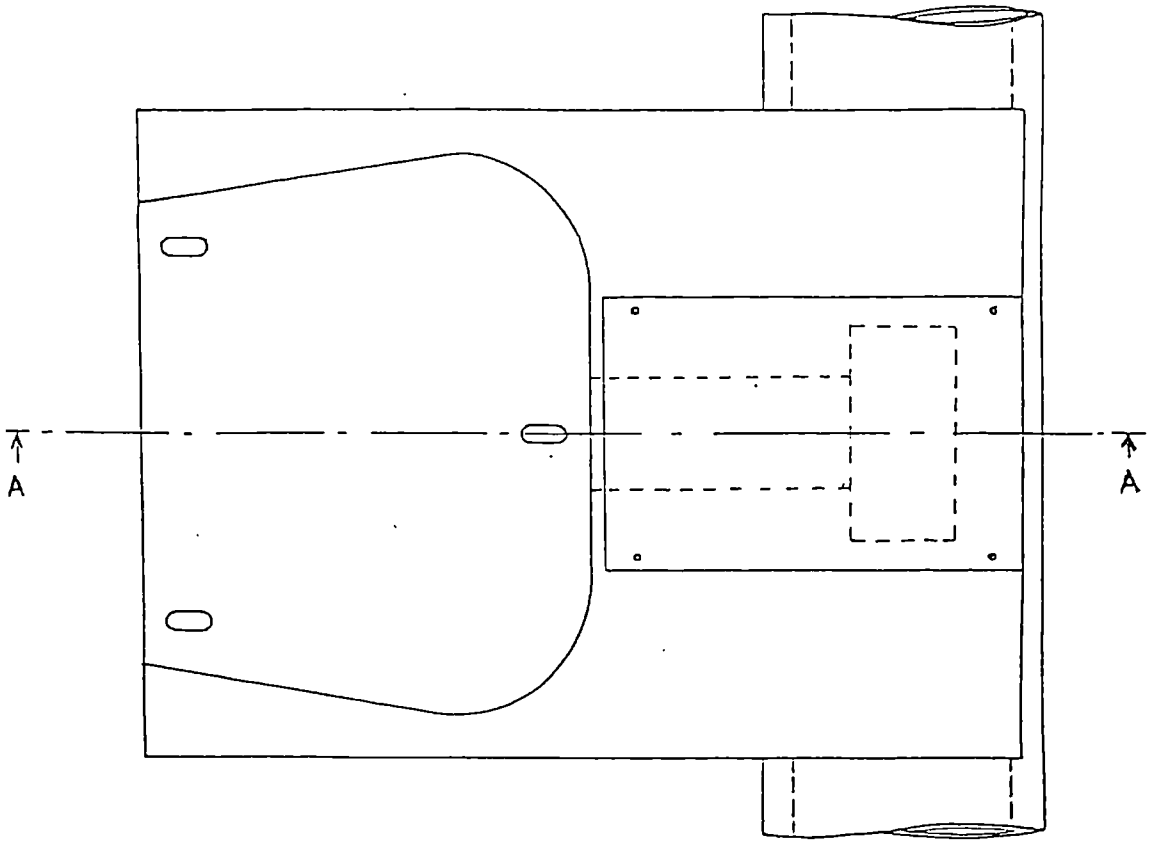

Fig. 5.3 Details Of Coanda Model

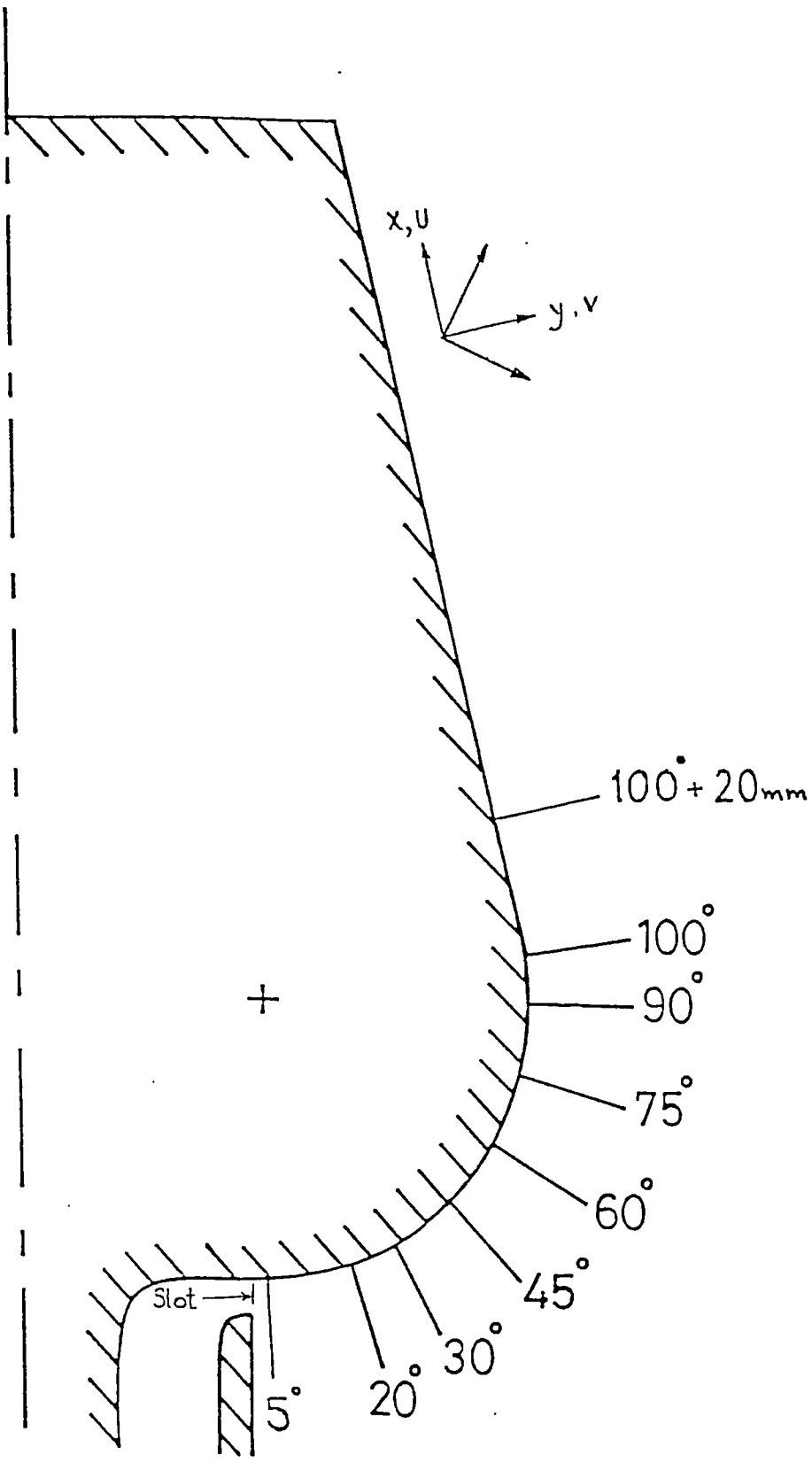

Fig. 5.4 Coanda flare measurement locations

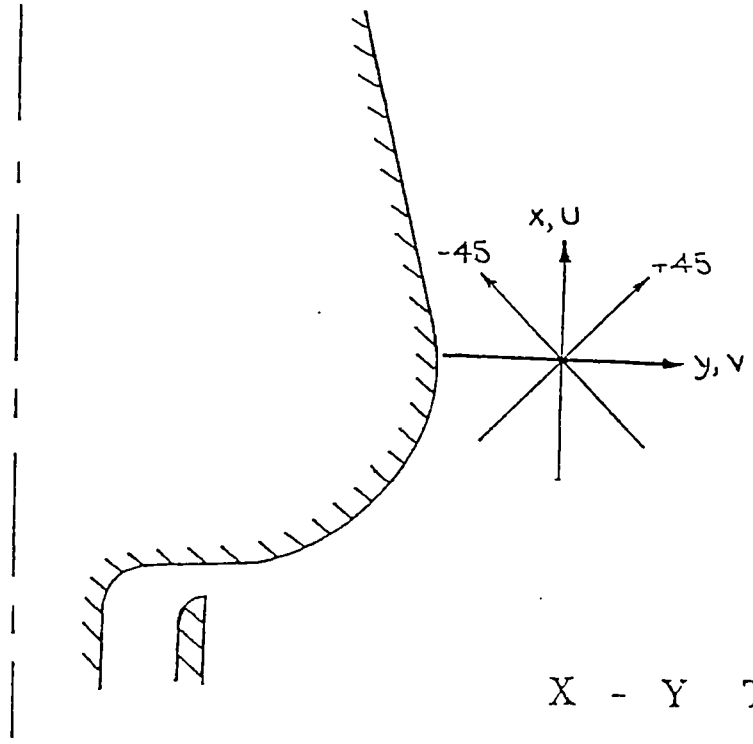

X - Y TRAVERSE

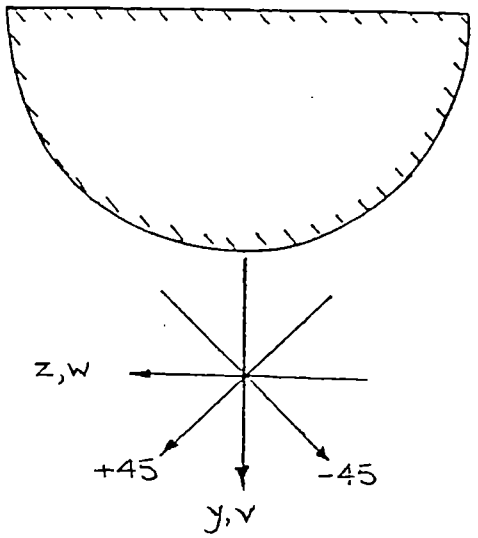

Y - Z TRAVERSE

Fig. 5.5 Coanda Traverses And Nomenclature

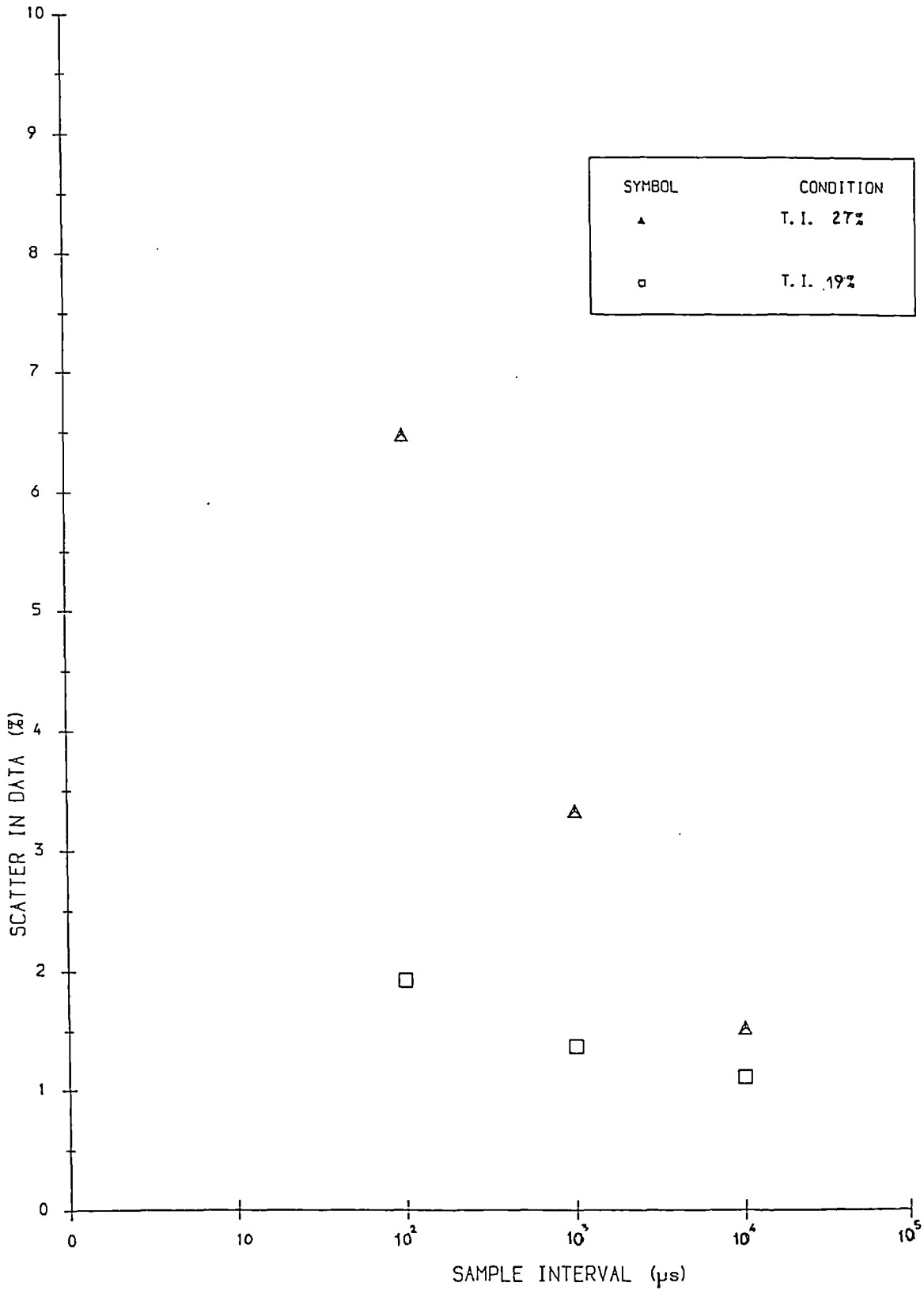

Fig. 5.6 SCATTER IN VELOCITY DATA vs. WINDOW LENGTH

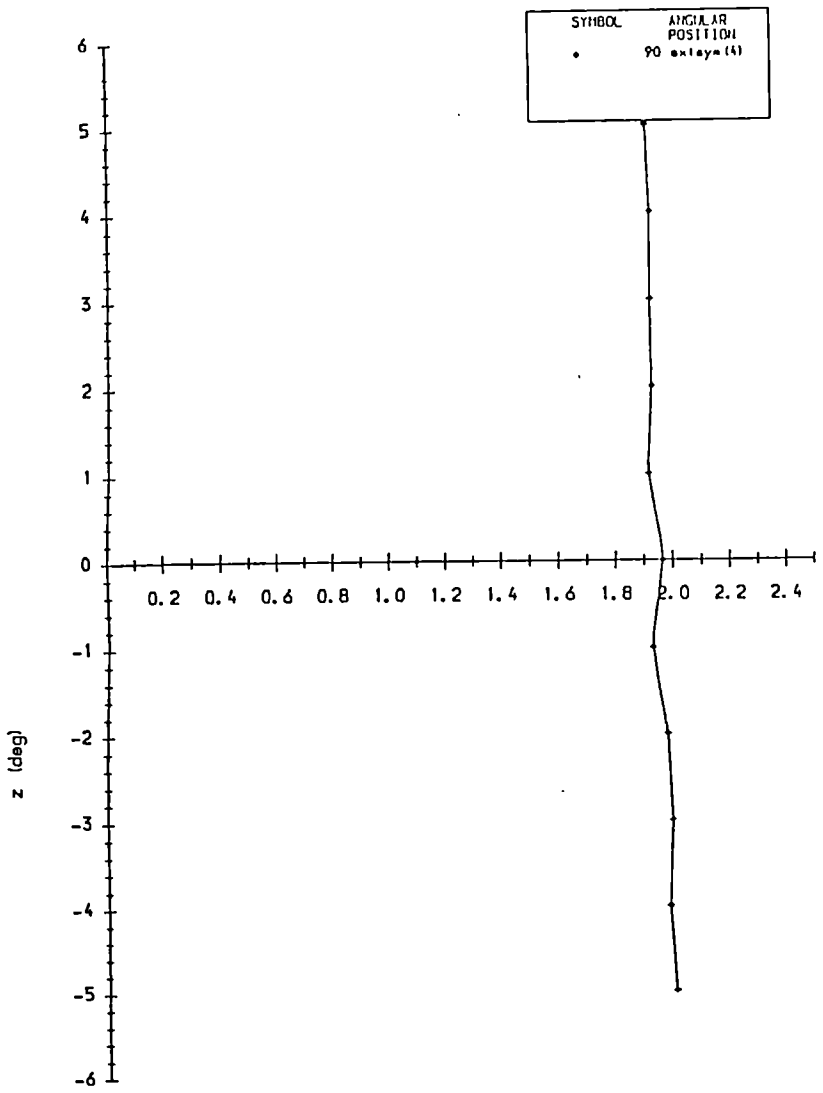
SYMBOL
ANGULAR POSITION
90 exteym (4)
z (deg)
U (m/s)
U vs. z

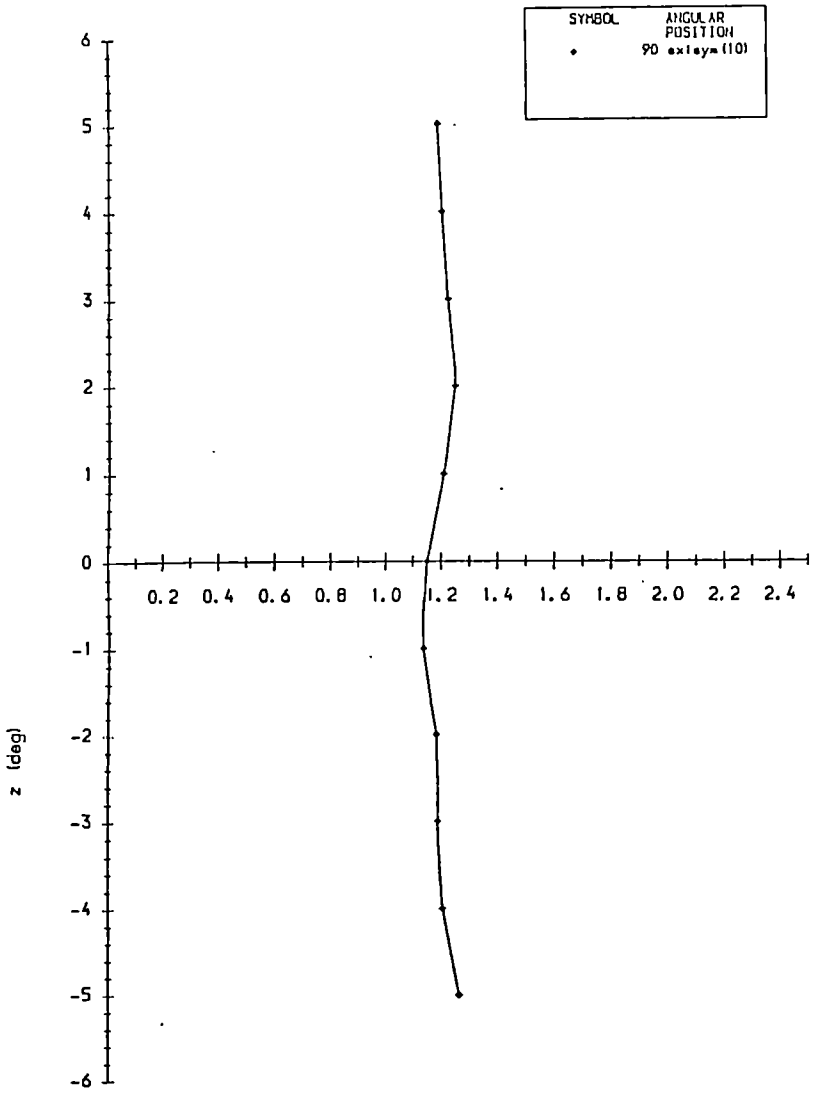
SYMBOL
ANGULAR POSITION
90 exteym (10)
z (deg)
U (m/s)
U vs. z

Fig. 5.7

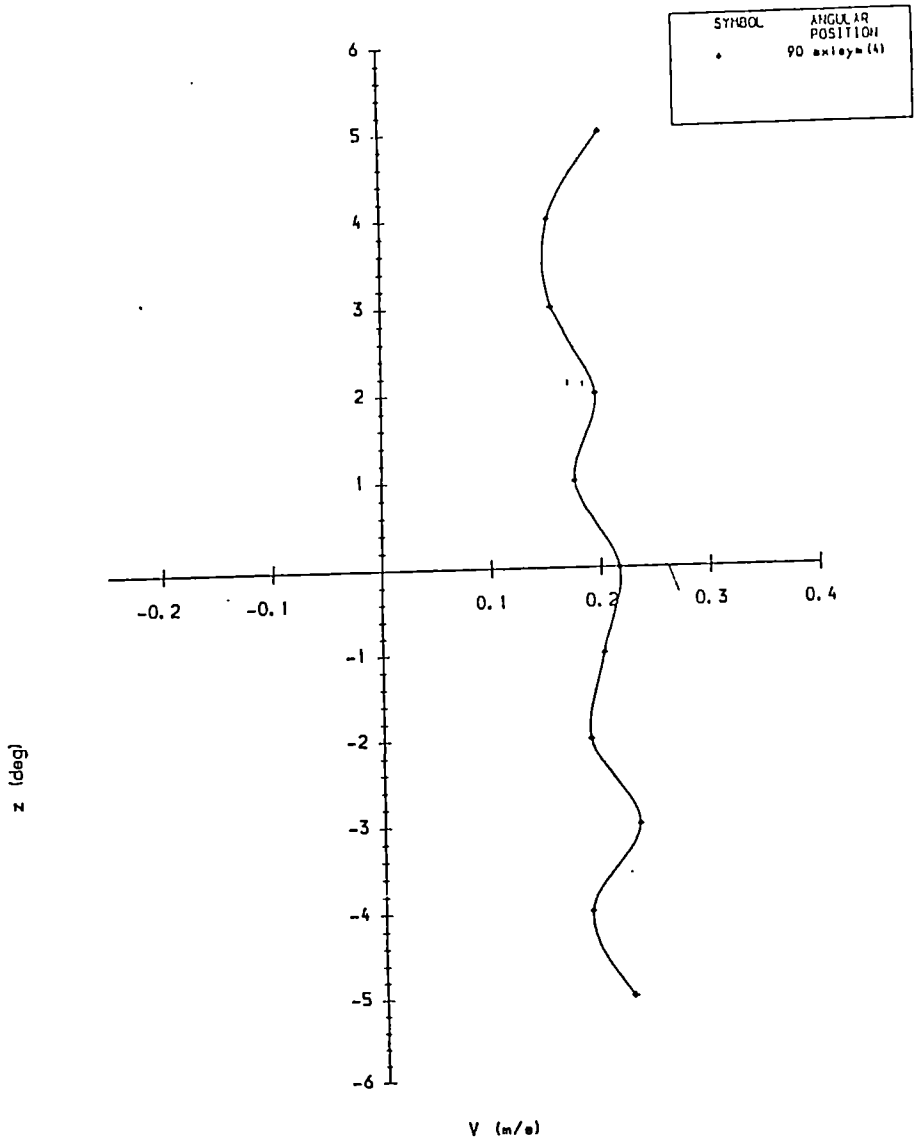

V vs. z

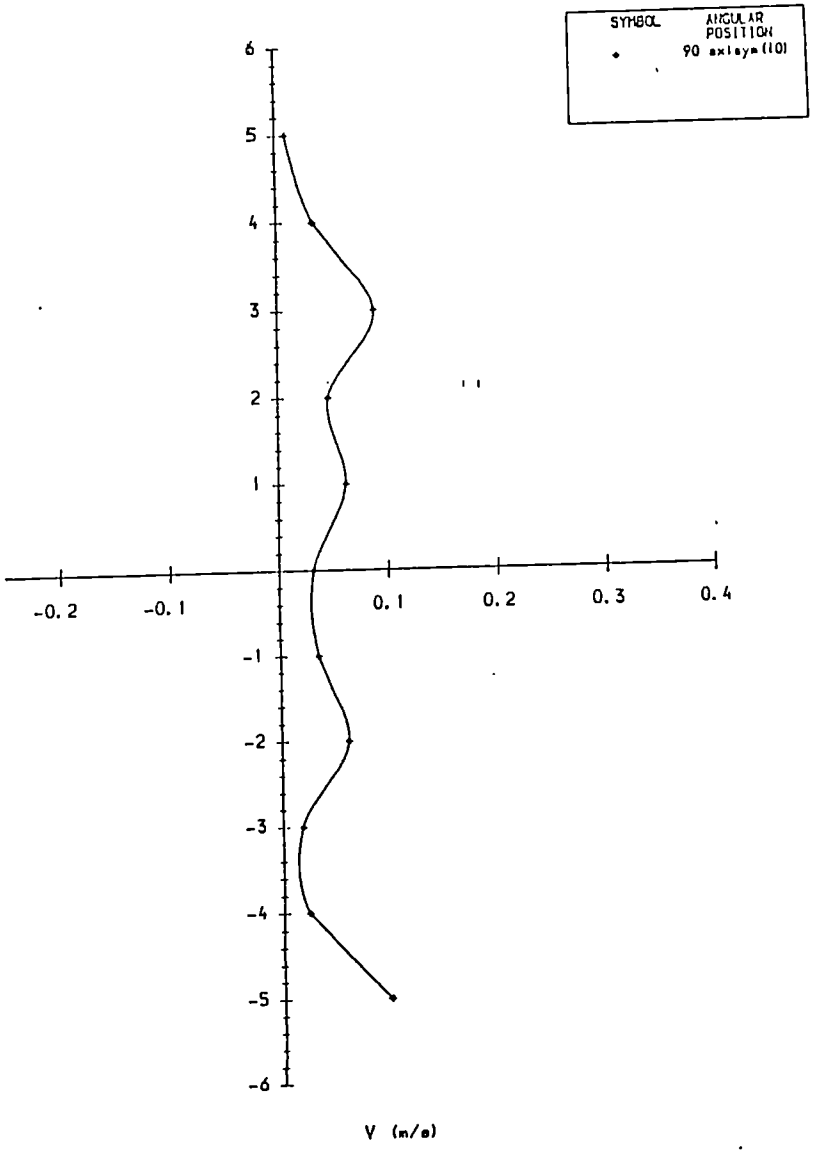

V vs. z

Fig. 5.8

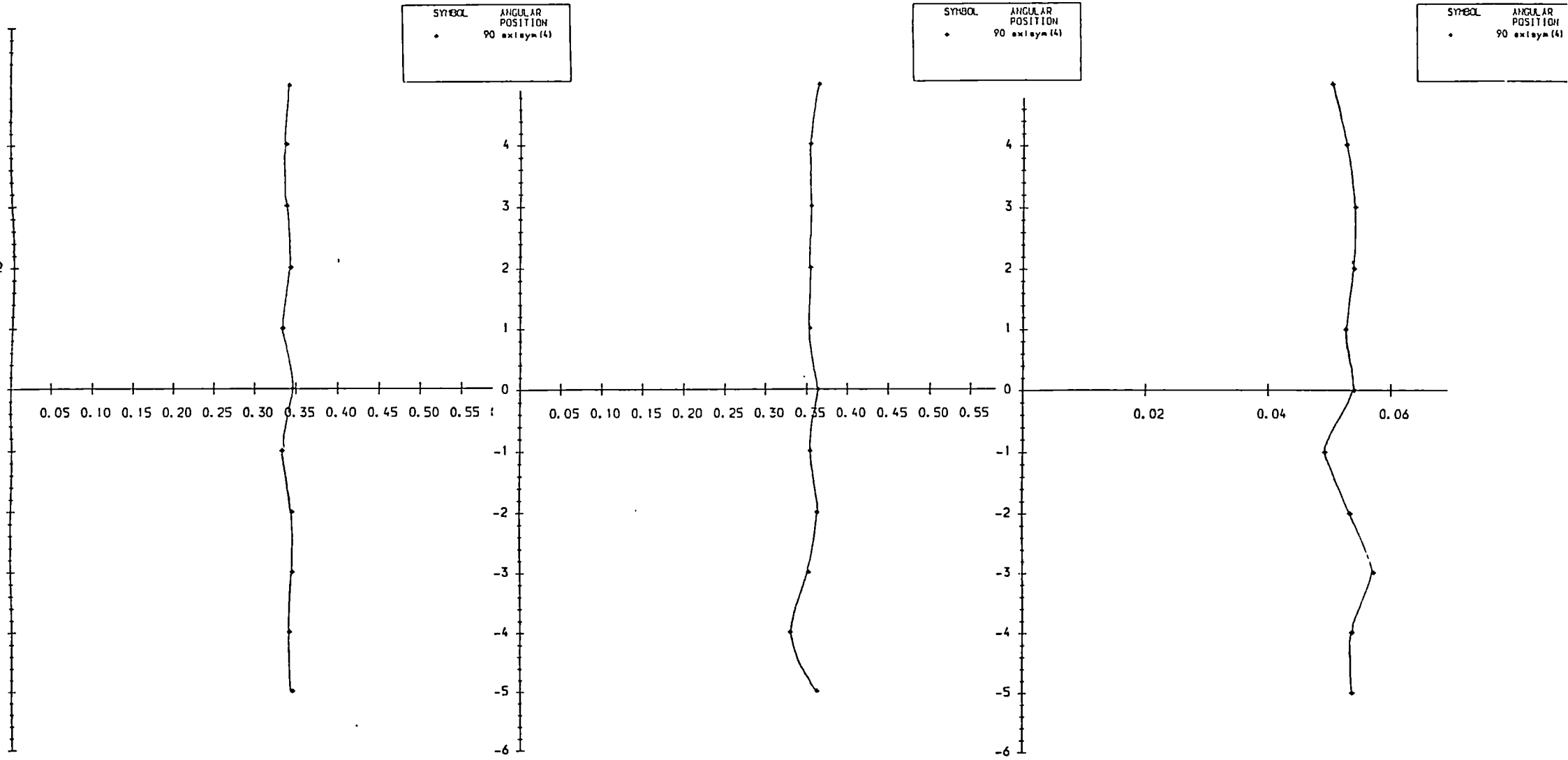

x- Component Normal Stress

y-Component Normal Stress

Shear Stresses

Fig. 5.9

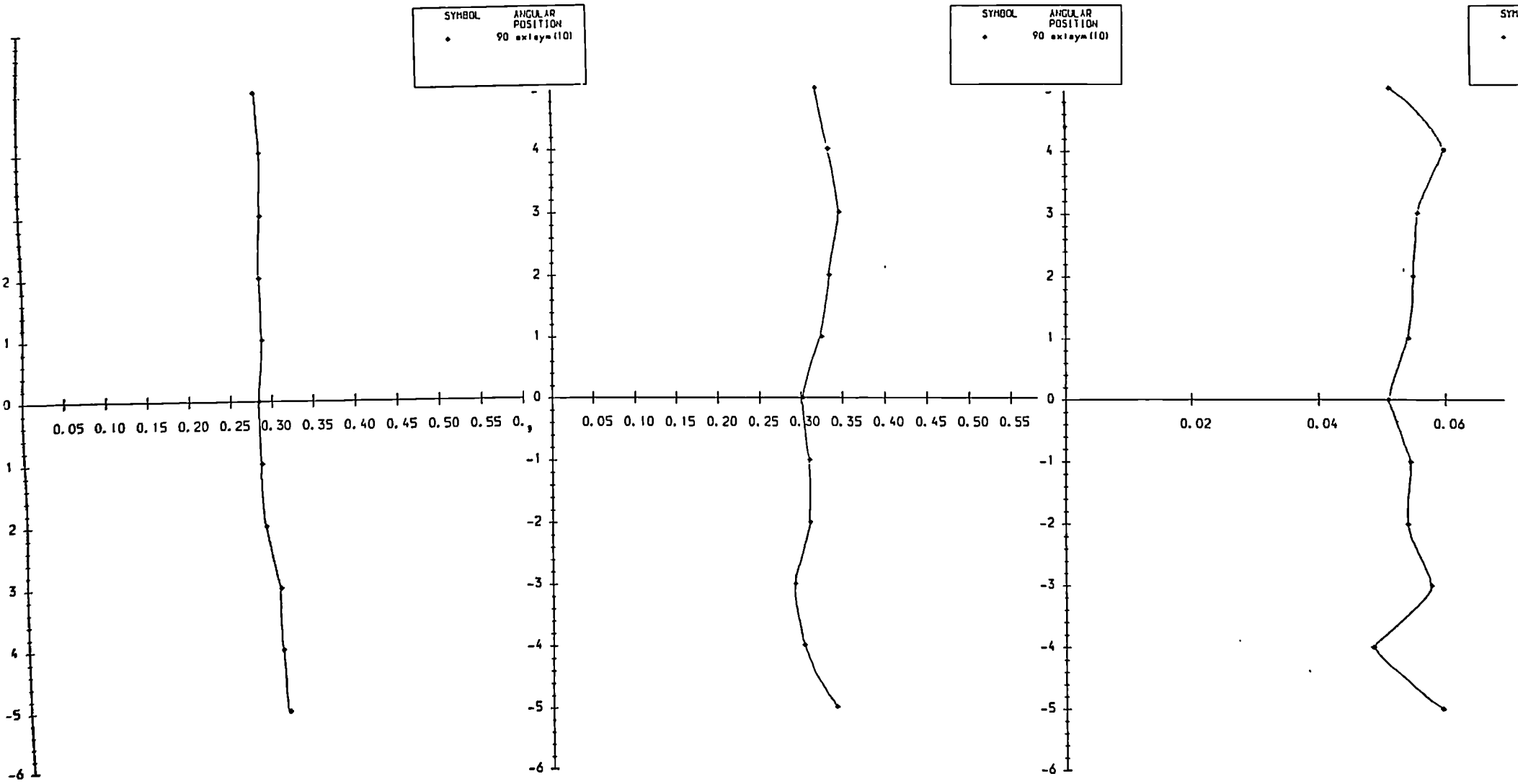

x- Component Normal Stress

y-Component Normal Stress

Shear Stresses

Fig. 5.10

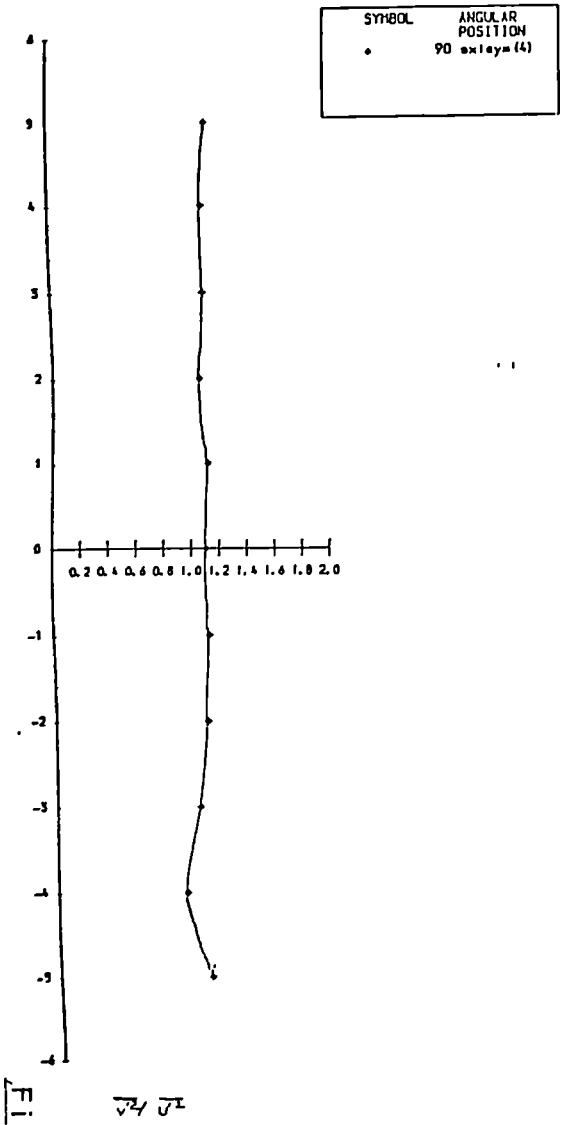

$\overline{v'^2}/\overline{u'^2}$

Structural Parameter $\overline{v'^2}/\overline{u'^2}$

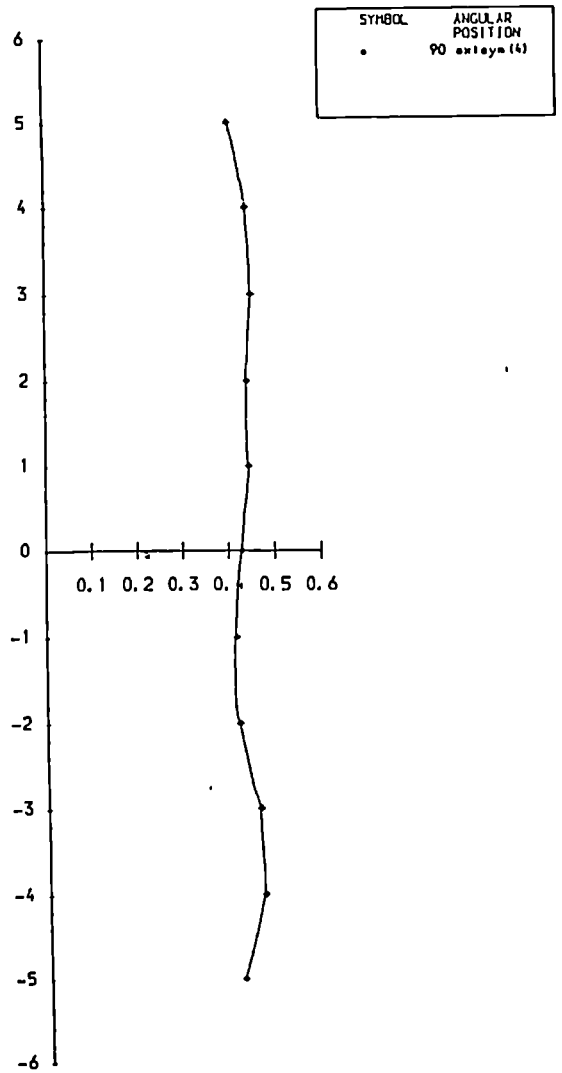

Structural Parameter Ruv

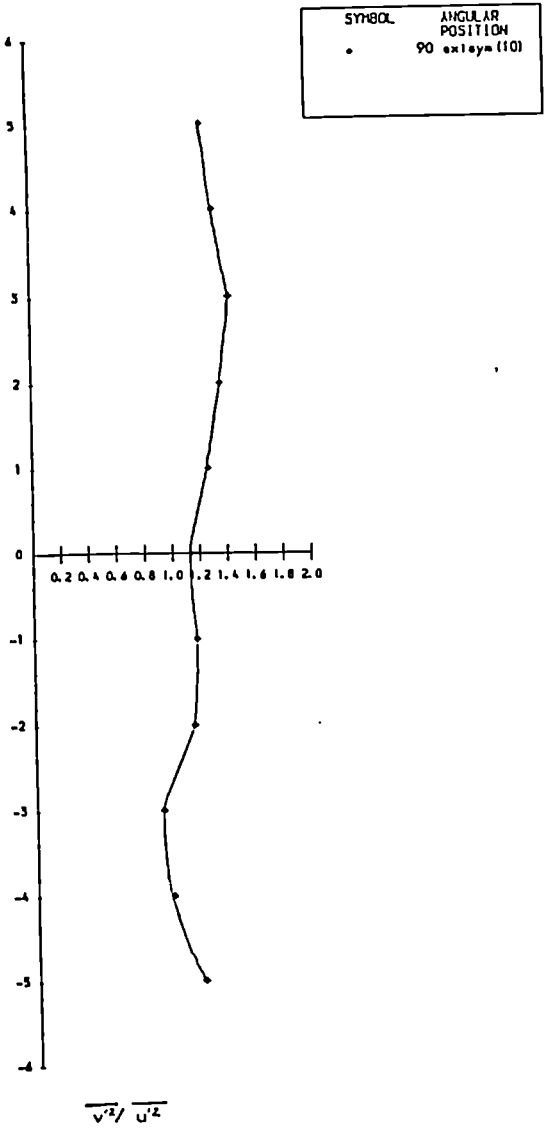

$\overline{v'^2}/\overline{u'^2}$

Structural Parameter $\overline{v'^2}/\overline{u'^2}$

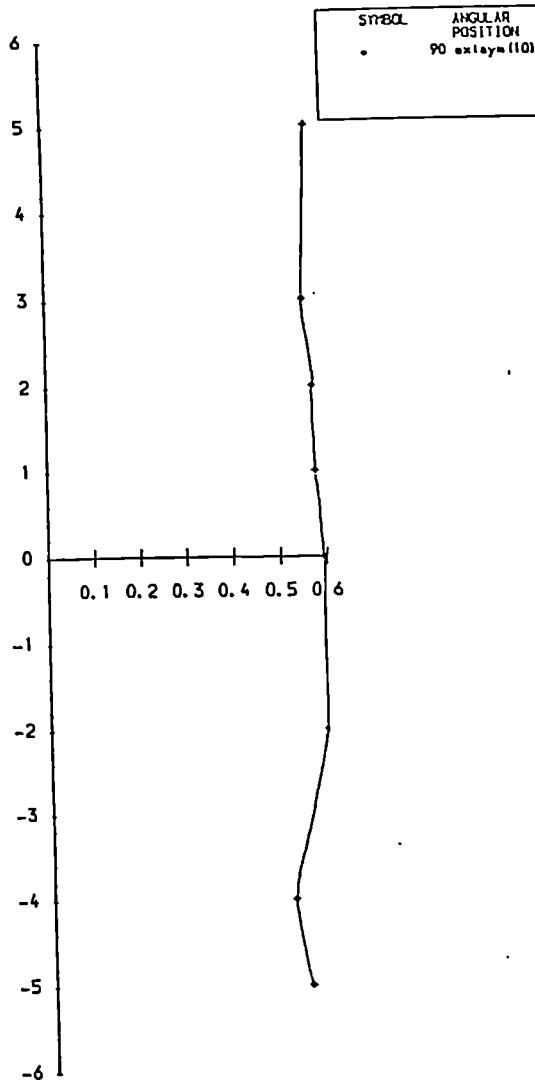

Structural Parameter Ruv

Fig. 5.11

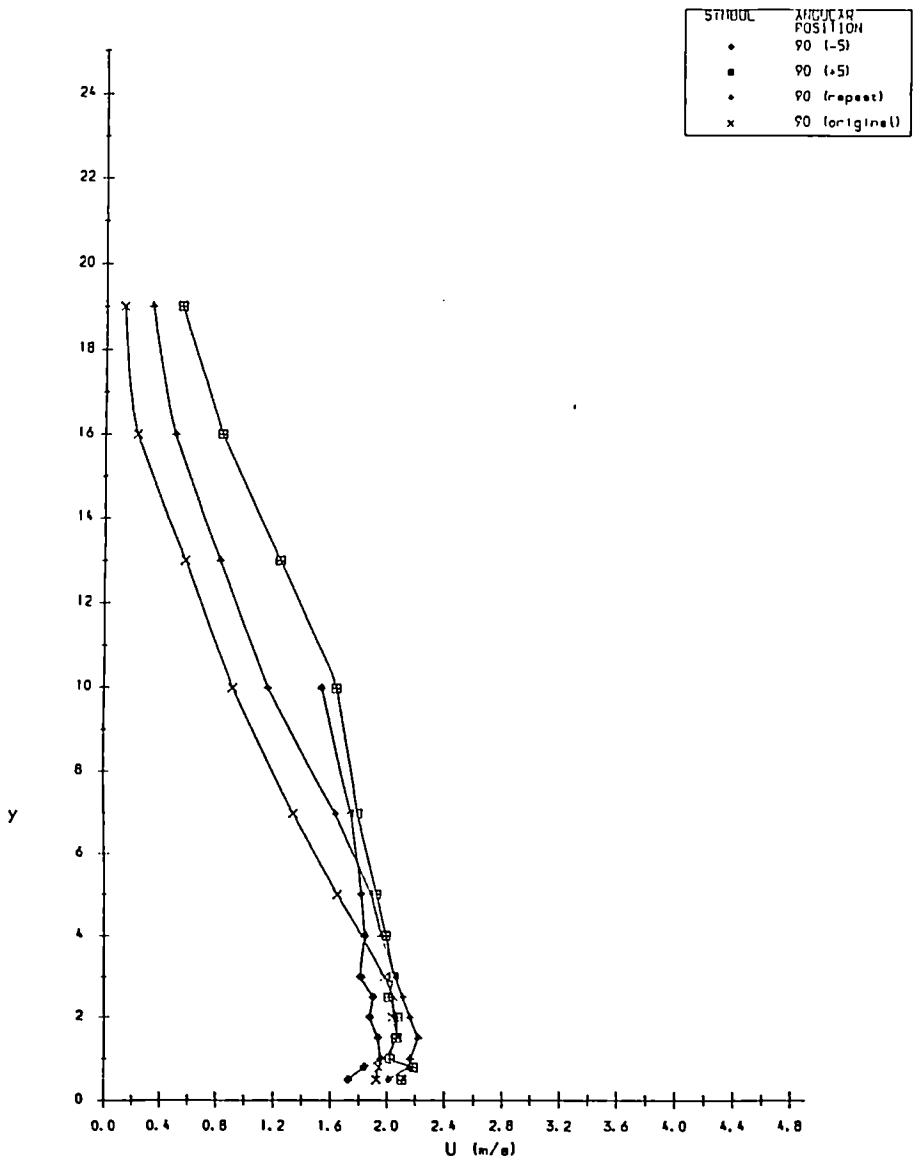

U vs. y

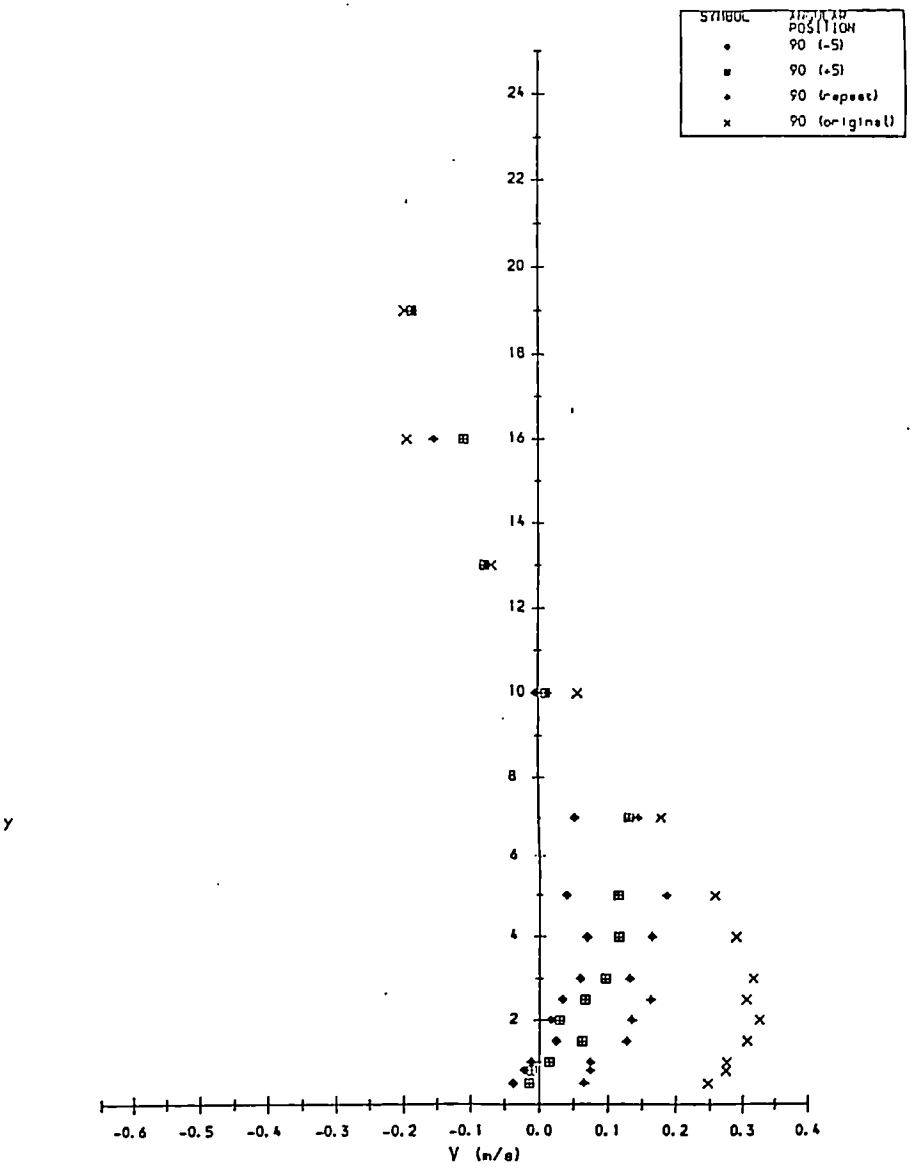

V vs. y

Fig. 5.12

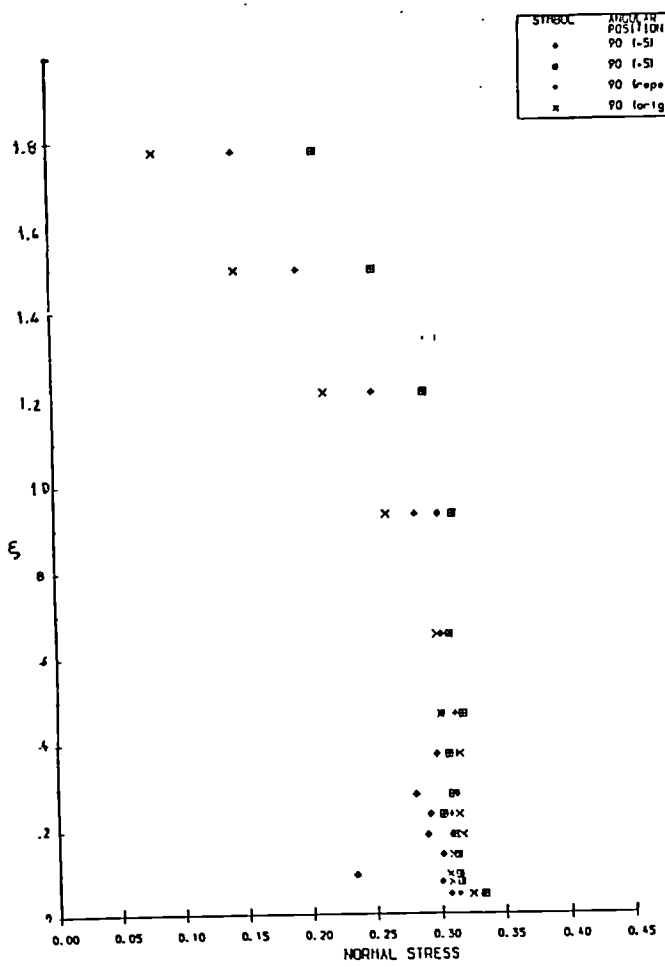

x - Component Normal Stress

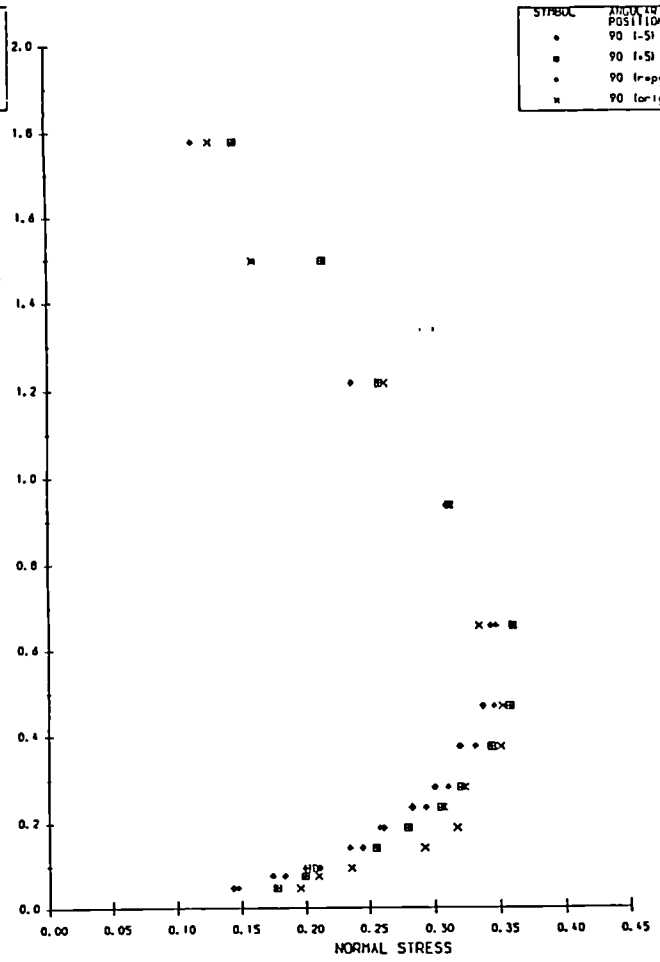

Y - Component Normal Stresses

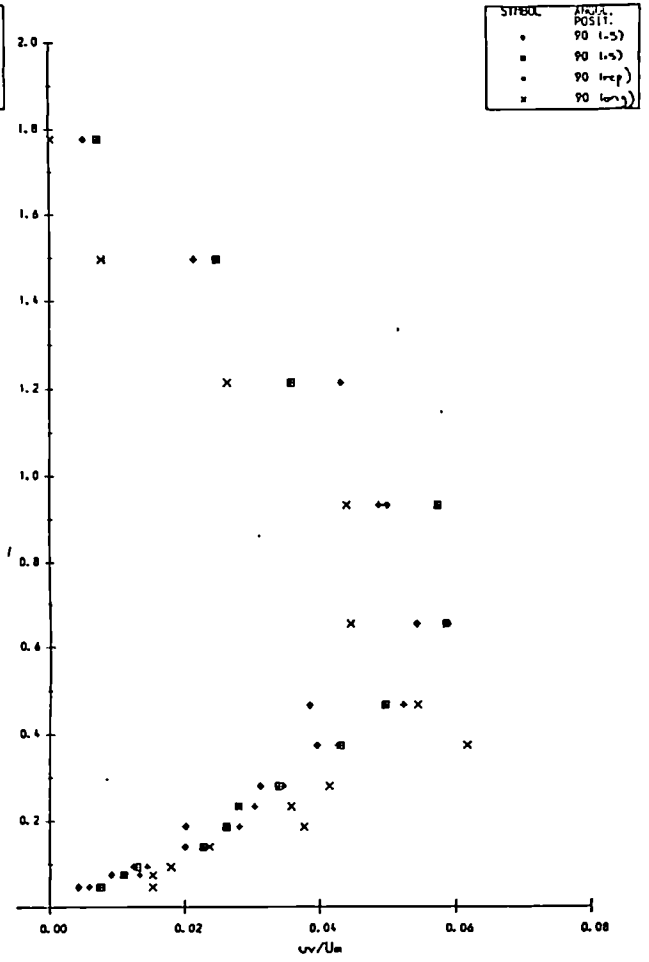

Shear Stresses

Fig. 5.13

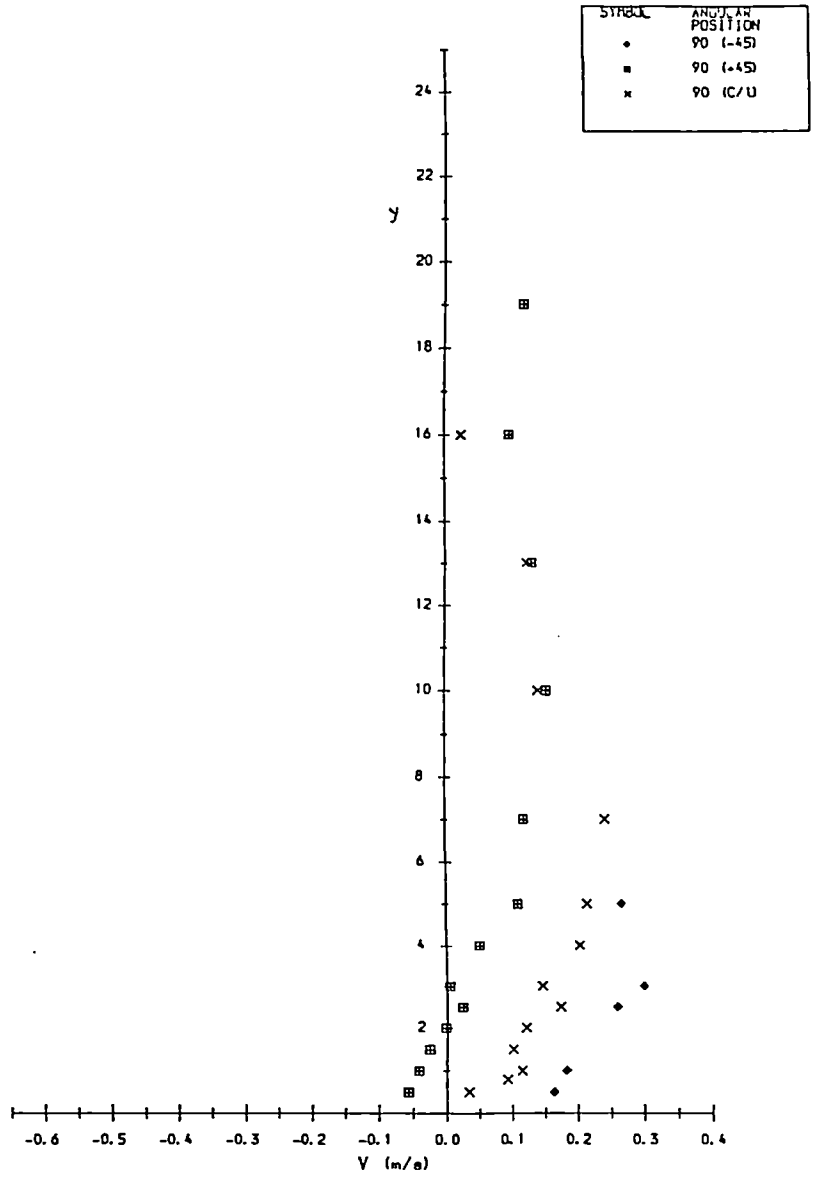

V vs. y

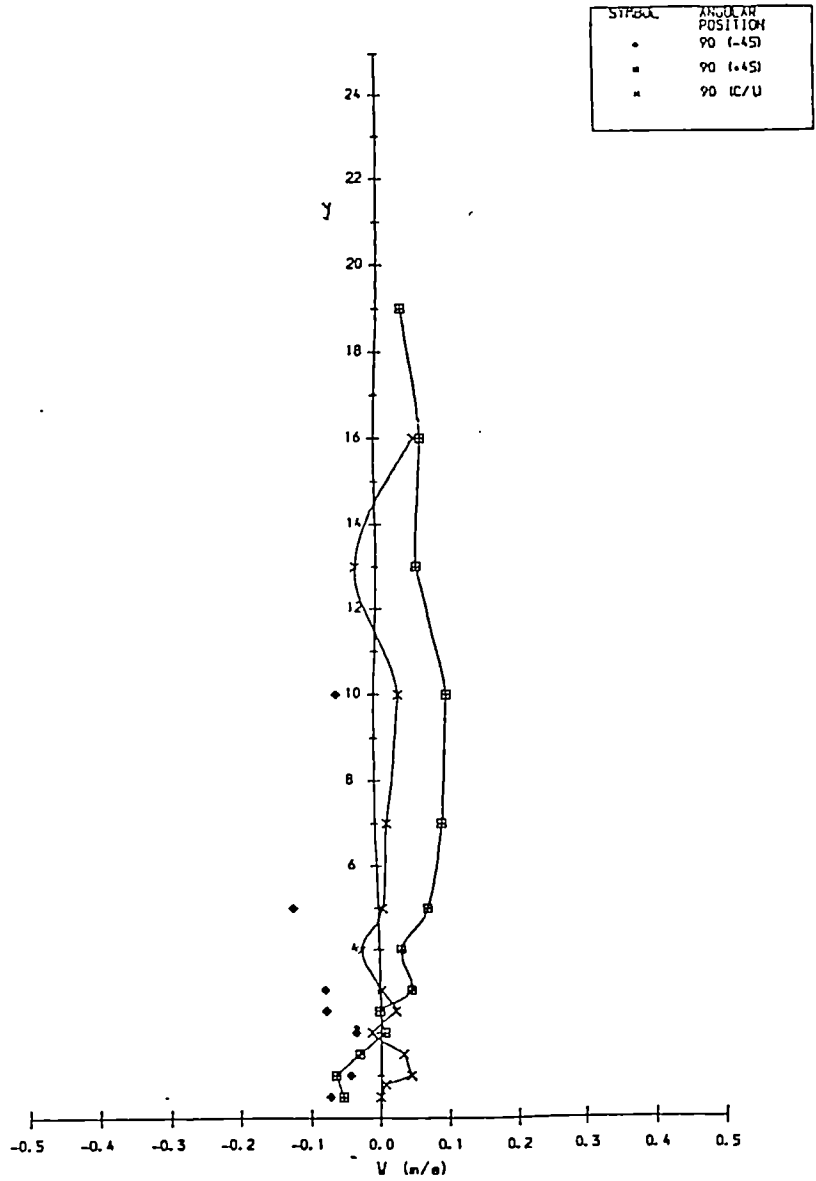

V vs. y

Fig. 5.14

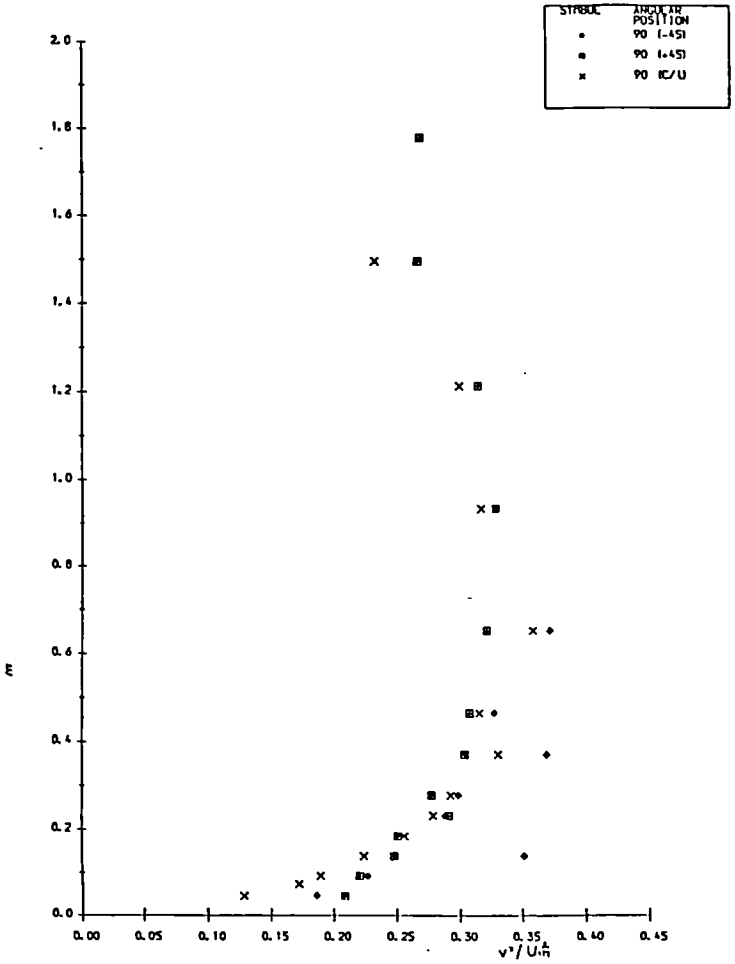

Y - Component Normal Stresses

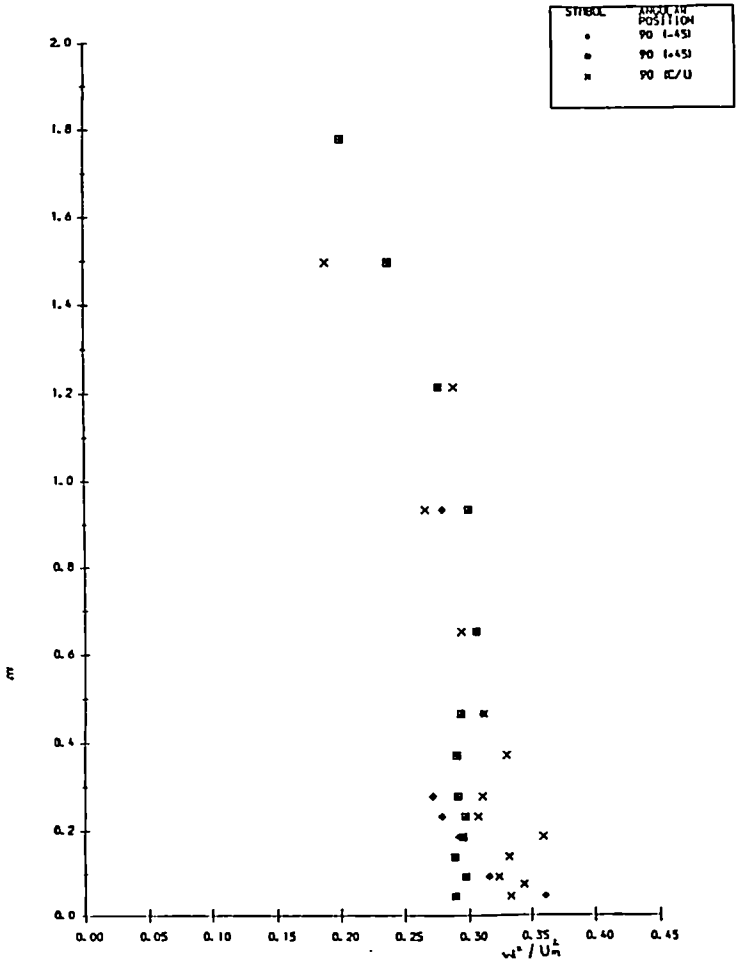

Z - Component Normal Stress

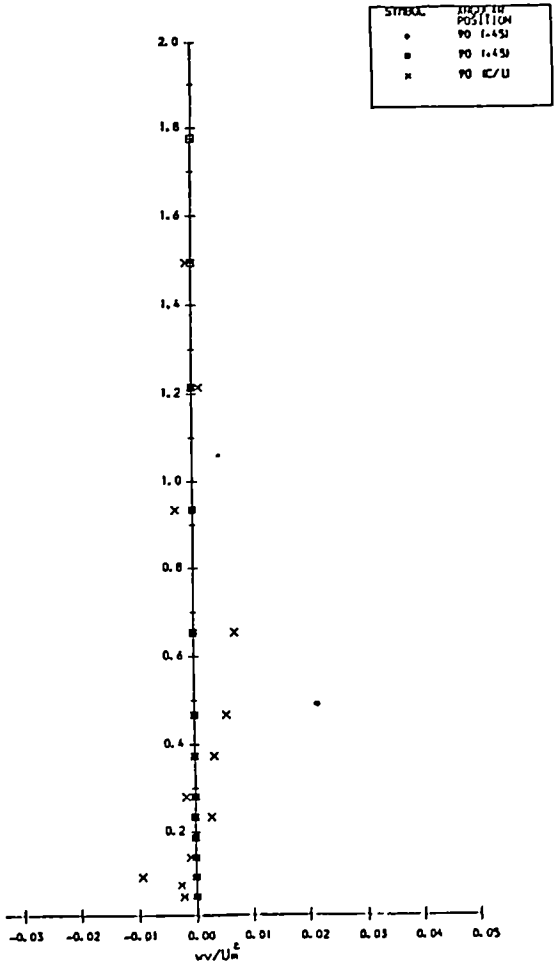

Shear Stresses

Fig. 5.15

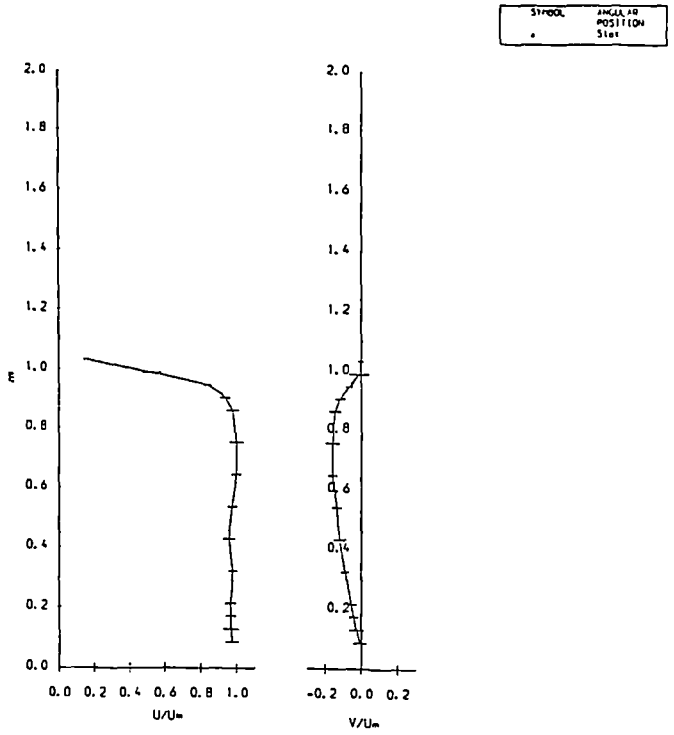

Non-Dimensional Velocities vs. Y/y

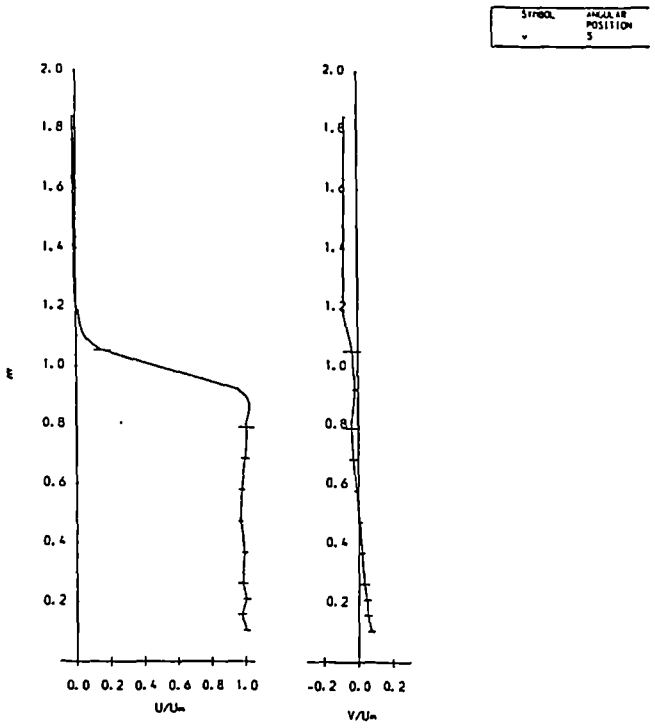

Non-Dimensional Velocities vs. Y/y

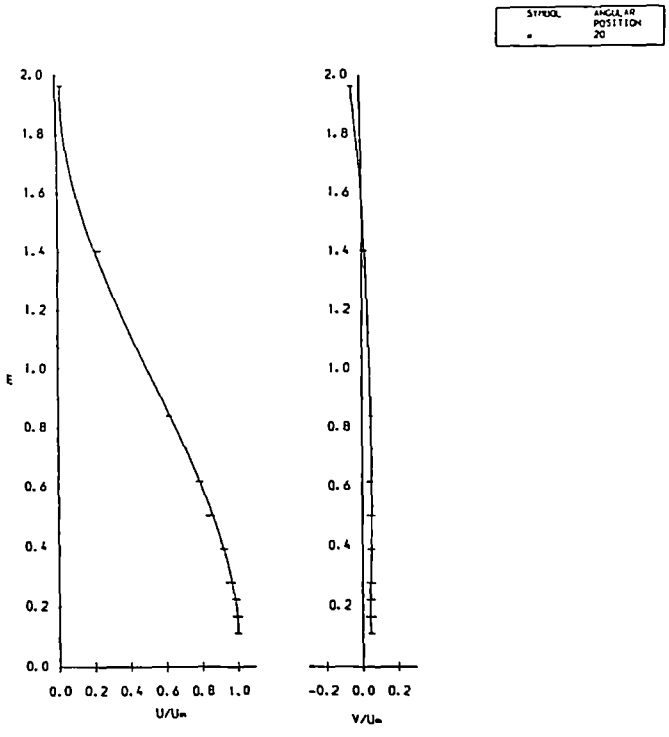

Non-Dimensional Velocities vs. Y/y

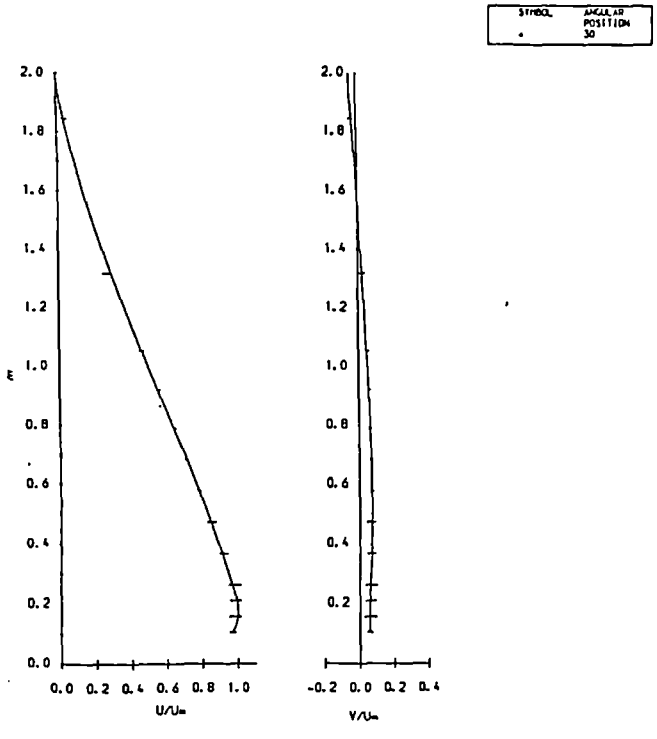

Non-Dimensional Velocities vs. Y/y

Fig. 5.16

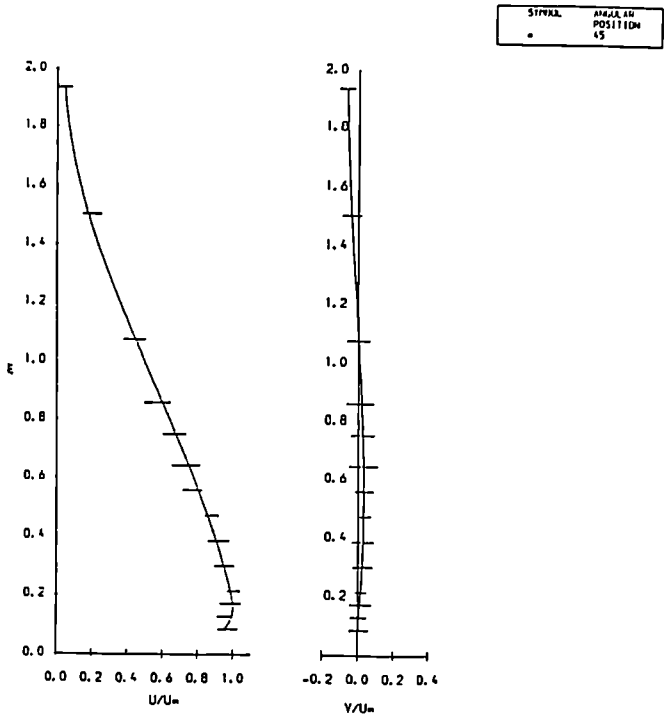

Non-Dimensional Velocities vs. Y/y

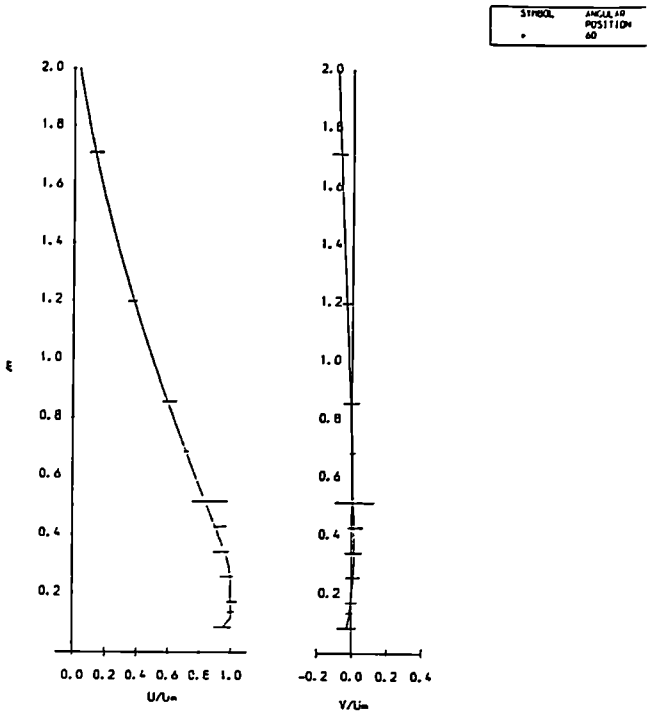

Non-Dimensional Velocities vs. Y/y

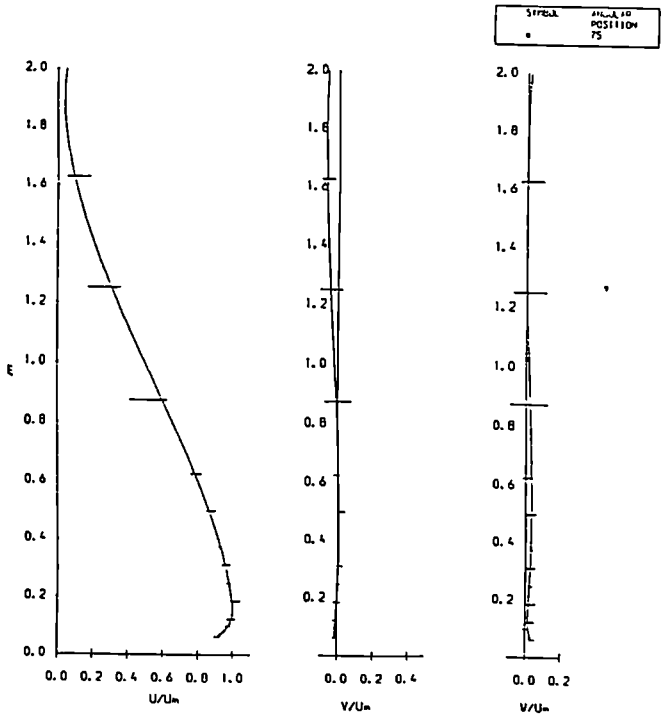

Non-Dimensional Velocities vs. Y/y

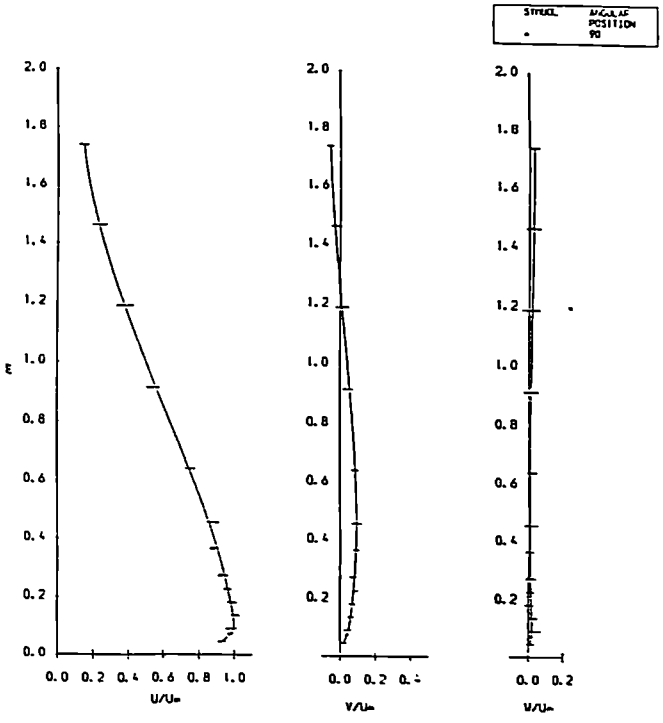

Non-Dimensional Velocities vs. Y/y

Fig. 5.1

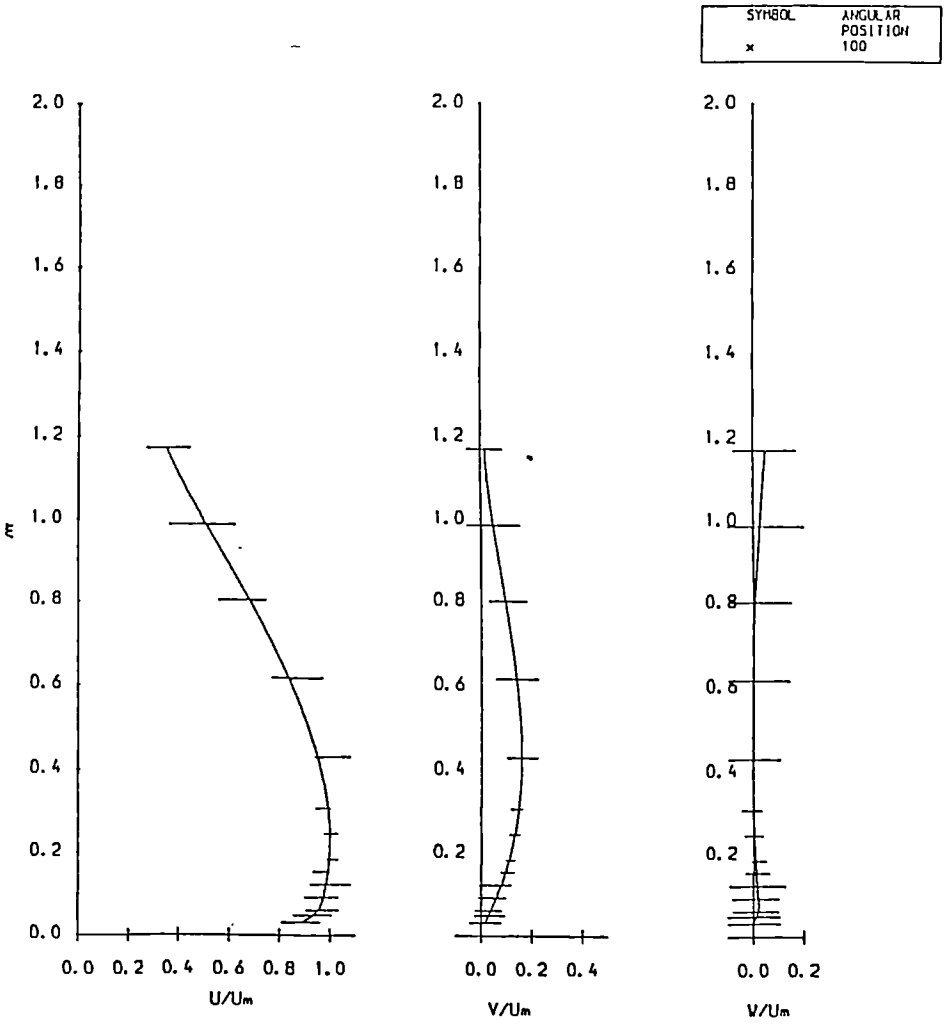

Non-Dimensional Velocities vs. Y/y

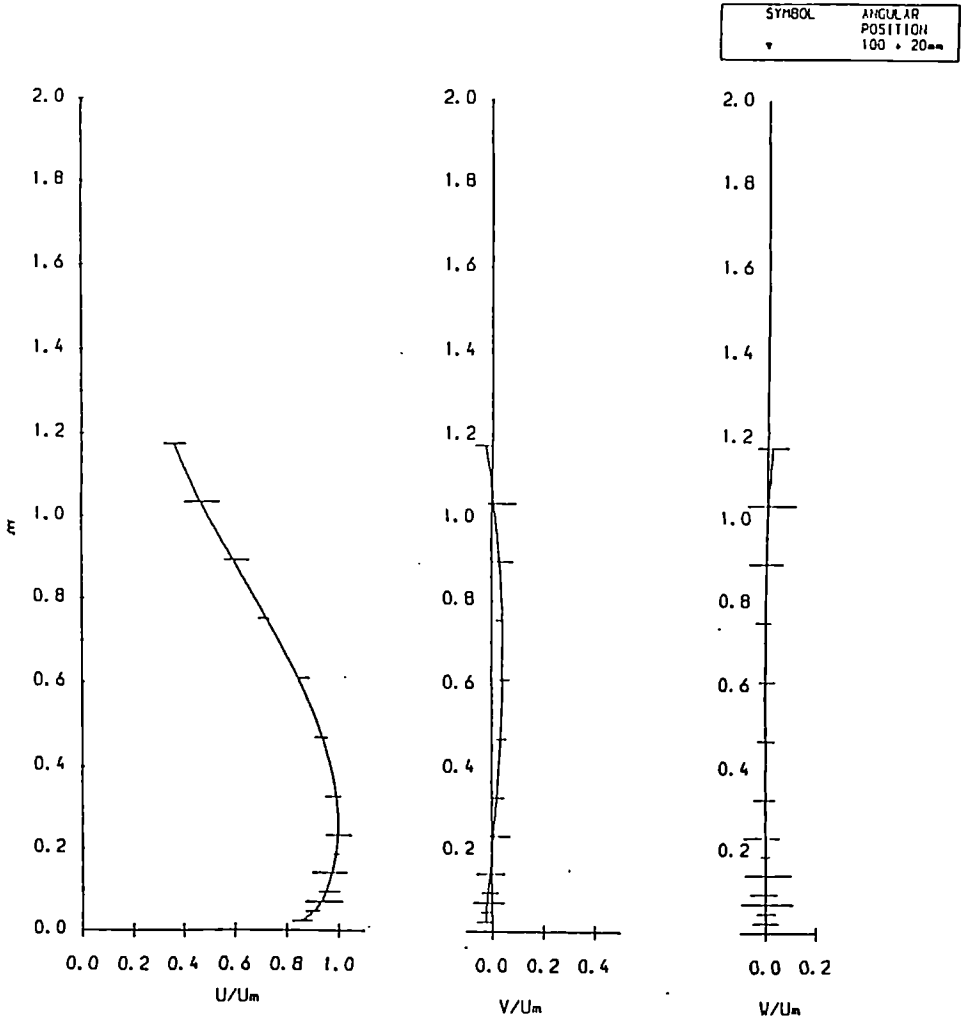

Non-Dimensional Velocities vs. Y/y

Fig. 5.18

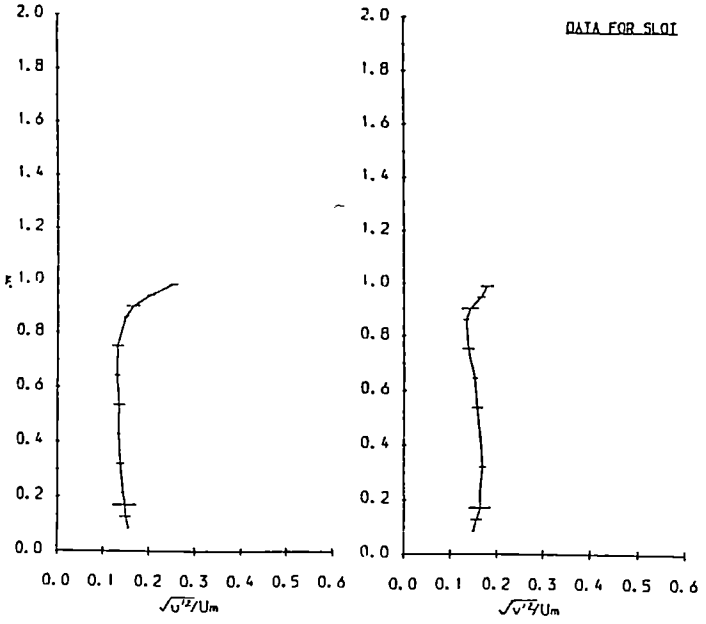

NORMAL STRESSES

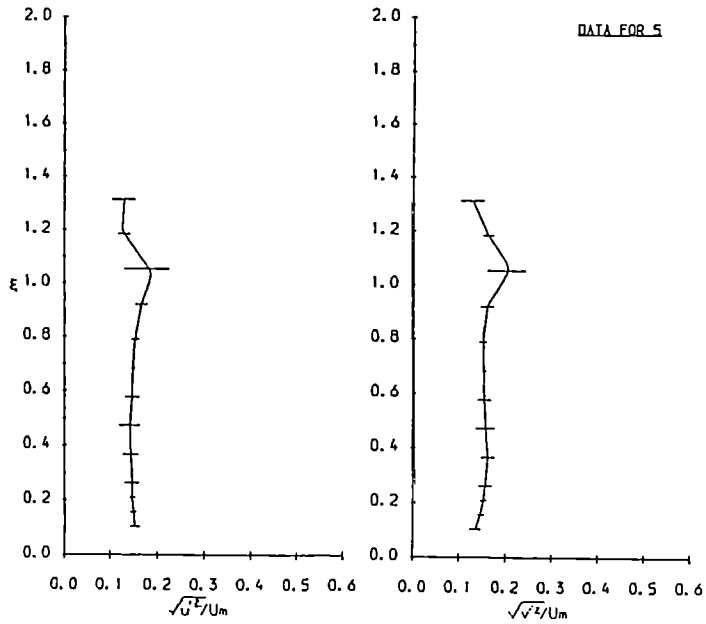

NORMAL STRESSES

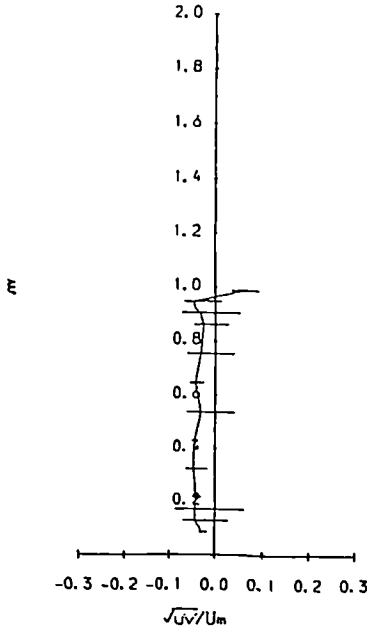

SHEAR STRESSES

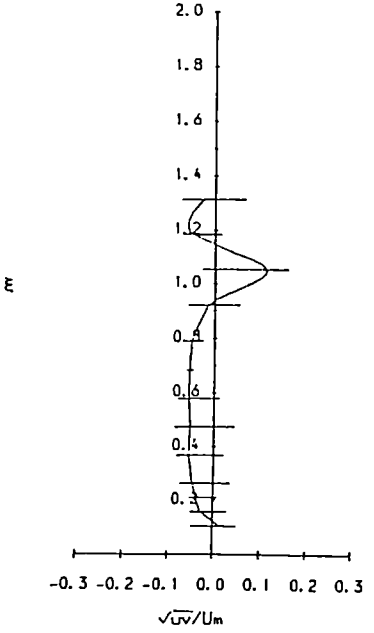

SHEAR STRESSES

Fig. 5.19

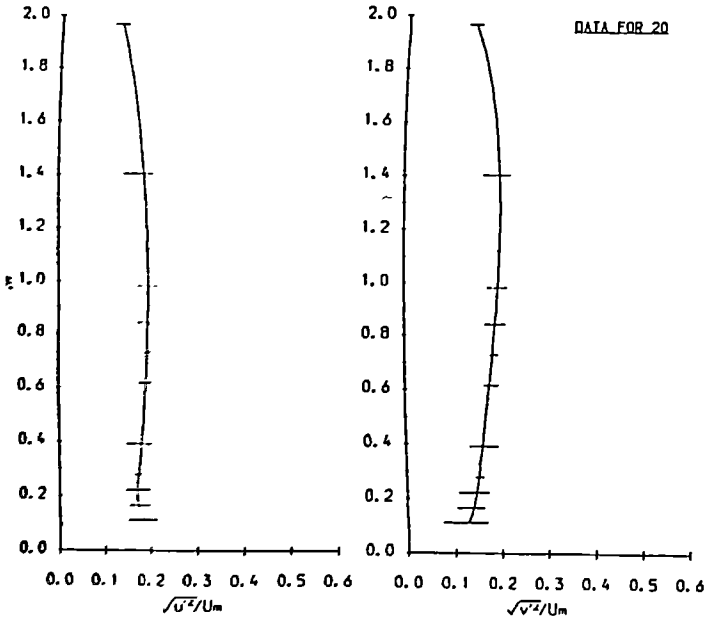

NORMAL STRESSES

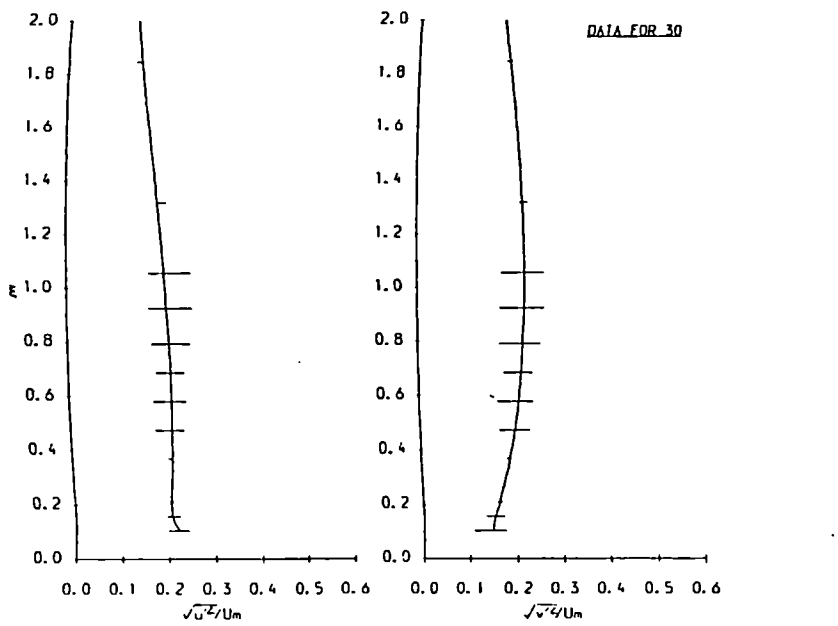

NORMAL STRESSES

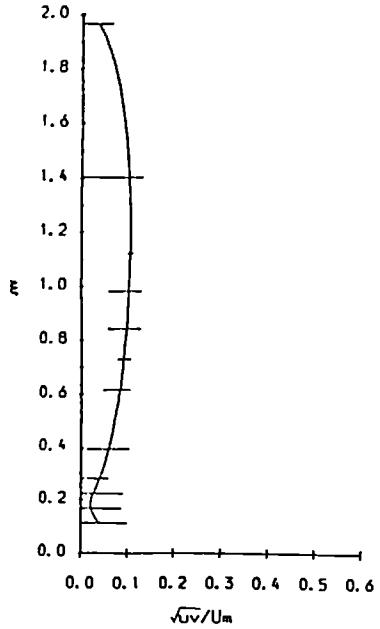

SHEAR STRESSES

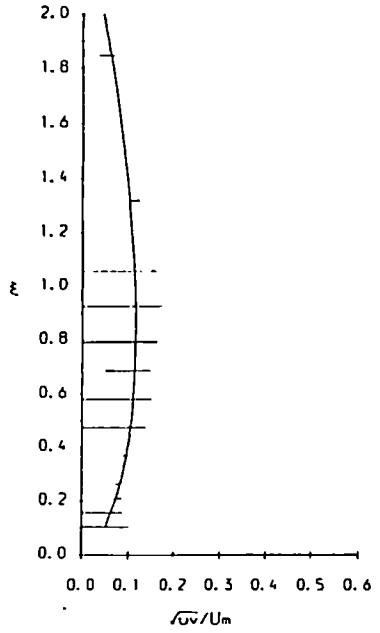

SHEAR STRESSES

Fig. 5.20

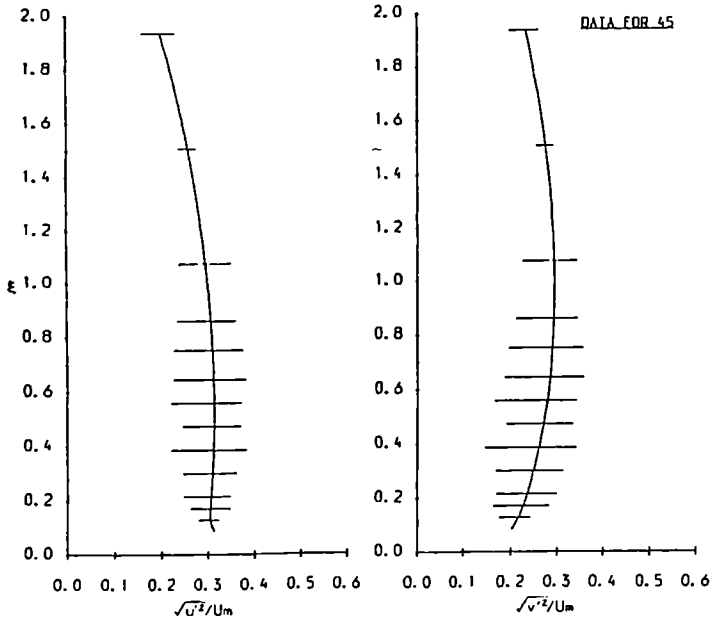

NORMAL STRESSES

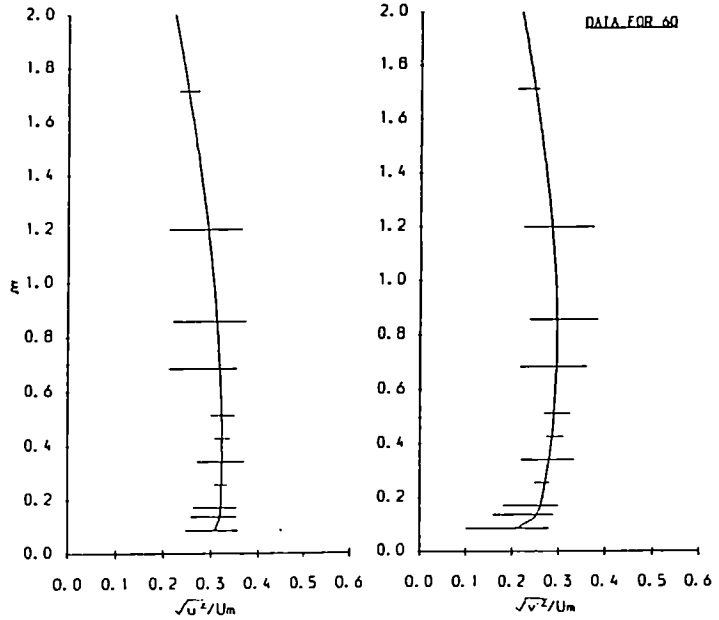

NORMAL STRESSES

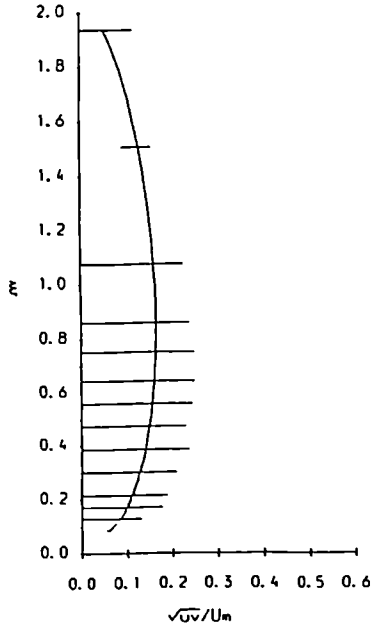

SHEAR STRESSES

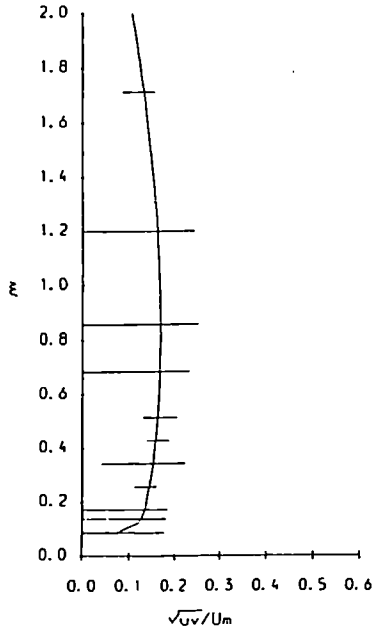

SHEAR STRESSES

Fig. 5.21

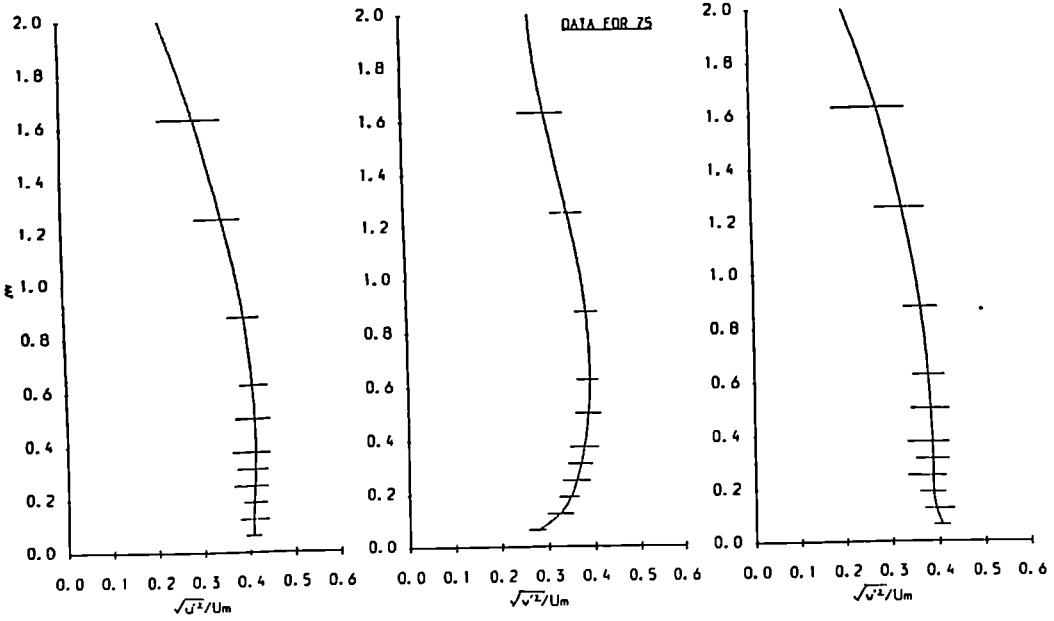

NORMAL STRESSES

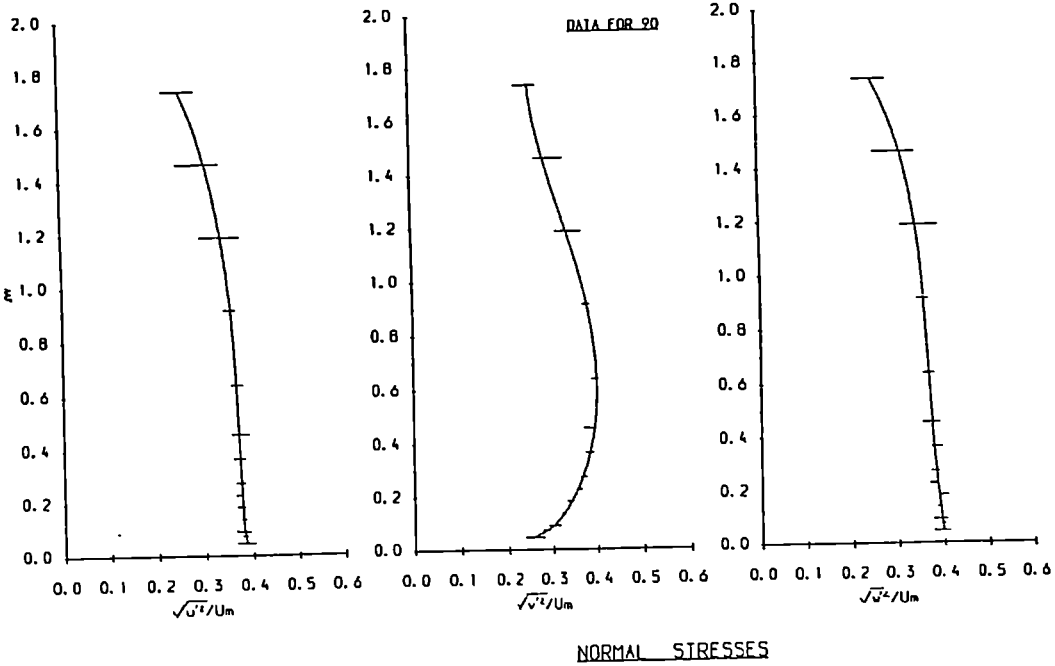

NORMAL STRESSES

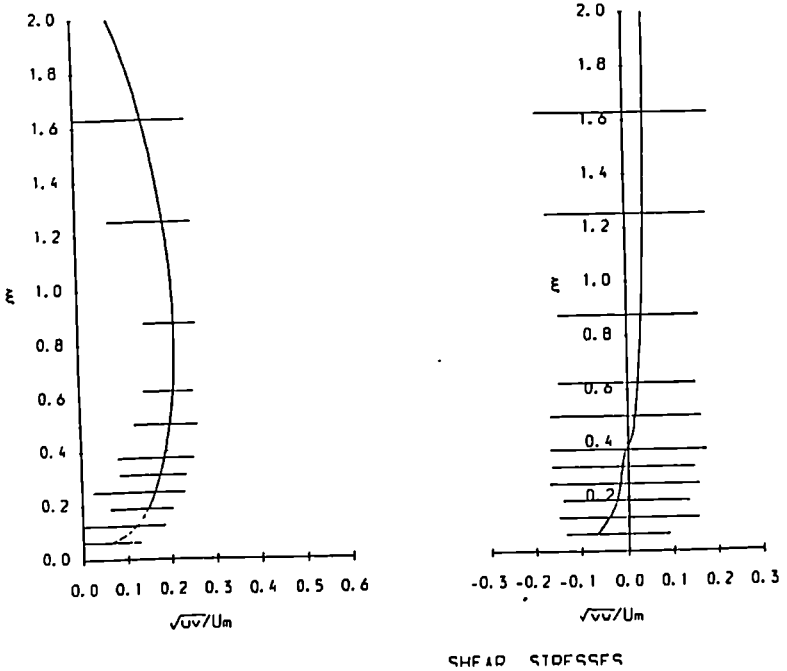

SHEAR STRESSES

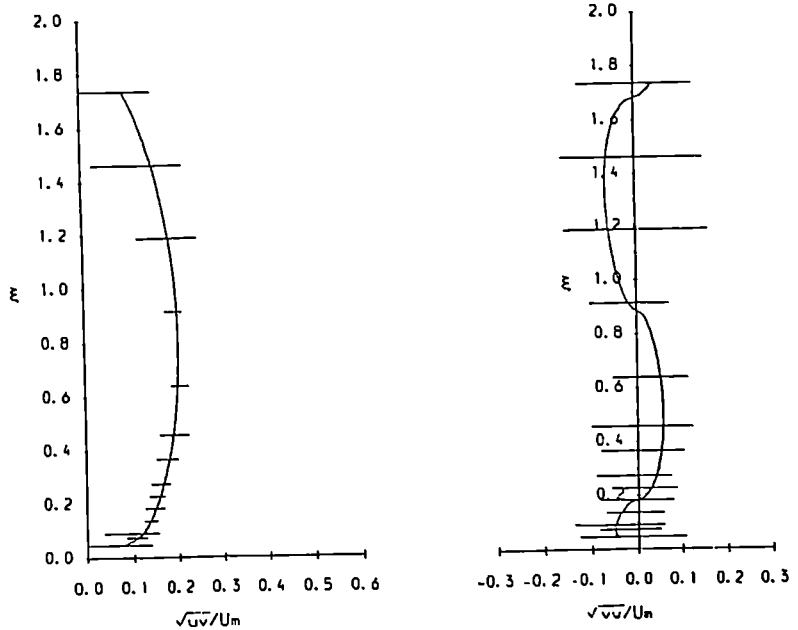

SHEAR STRESSES

Fig. 5.22

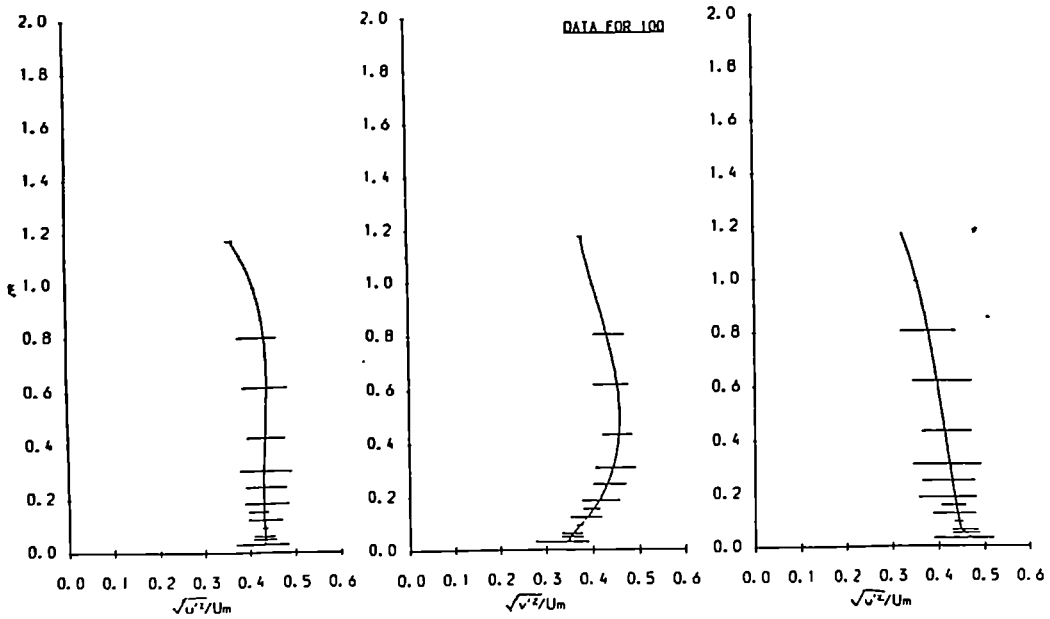

NORMAL STRESSES

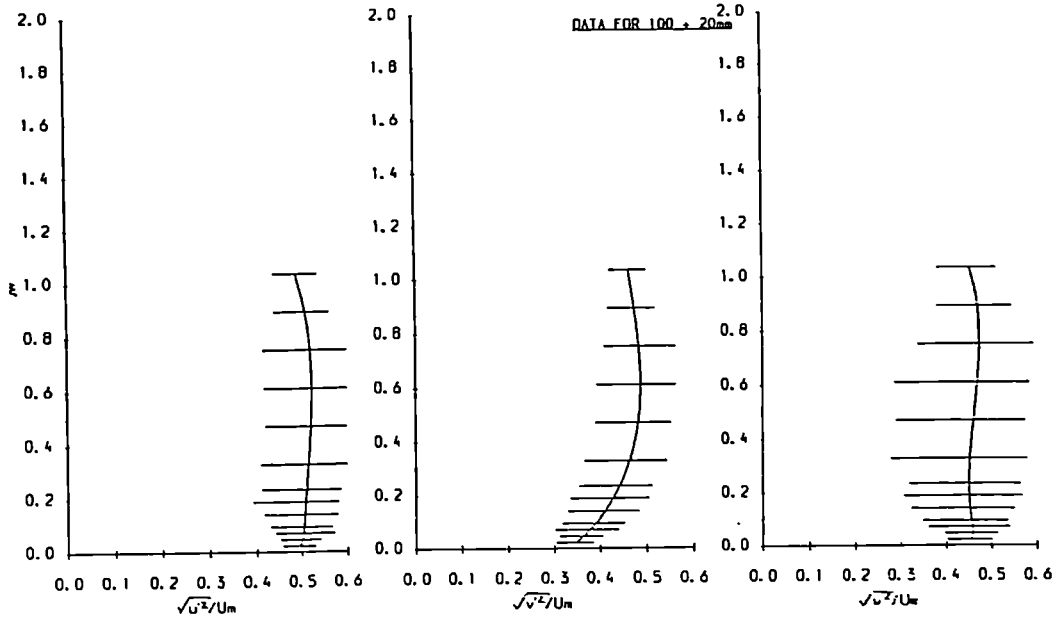

NORMAL STRESSES

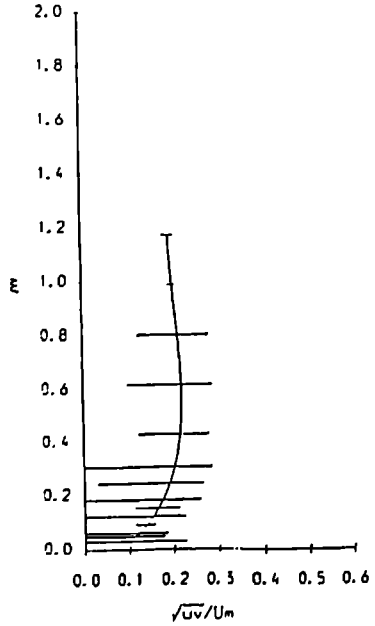

SHEAR STRESSES

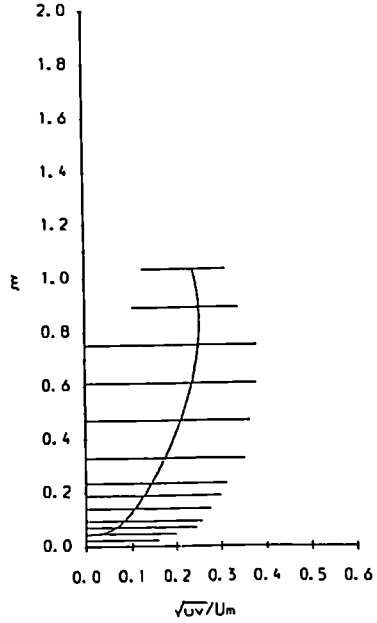

SHEAR STRESSES

Fig. 5.23

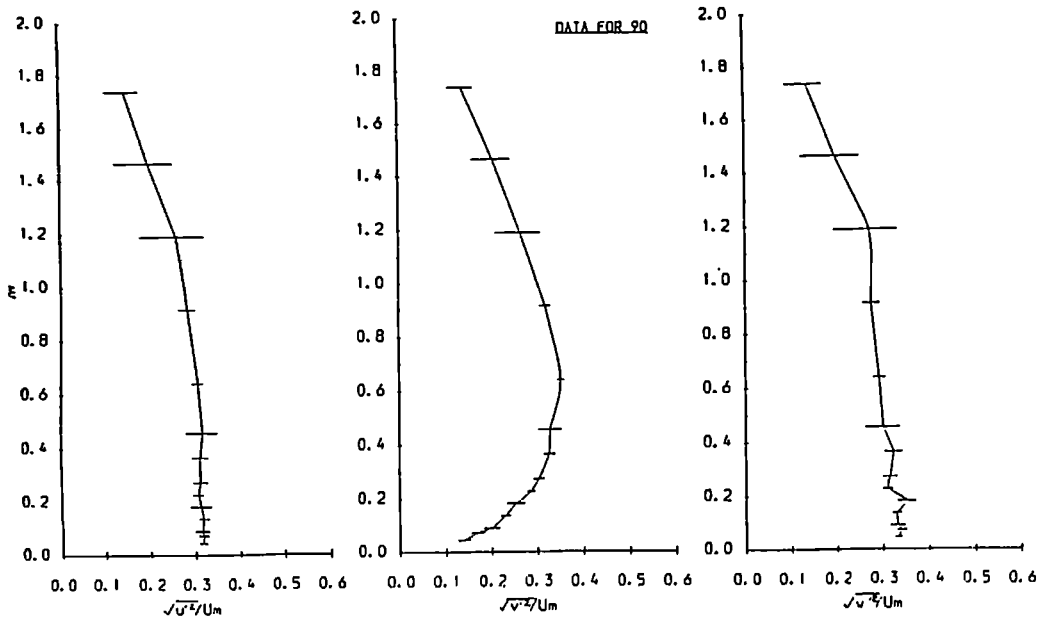

NORMAL STRESSES

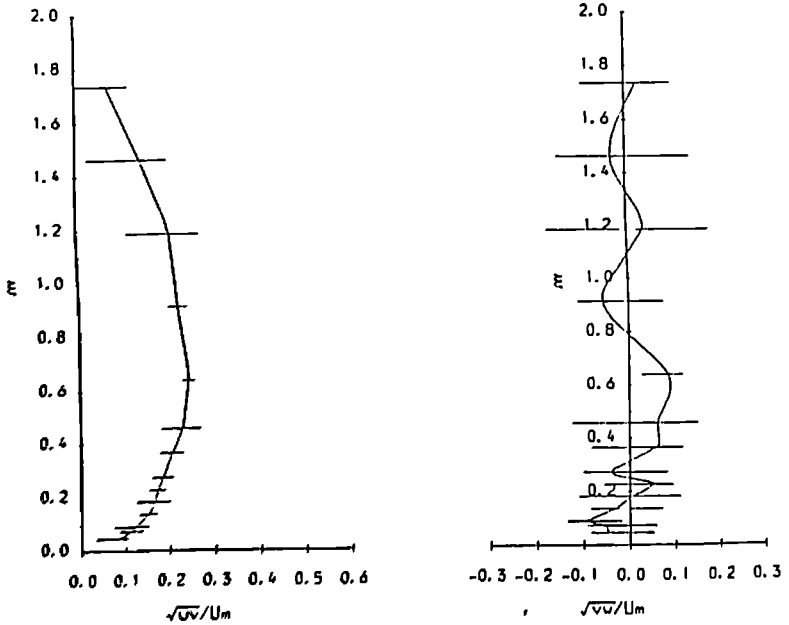

'BEFORE'

SHEAR STRESSES

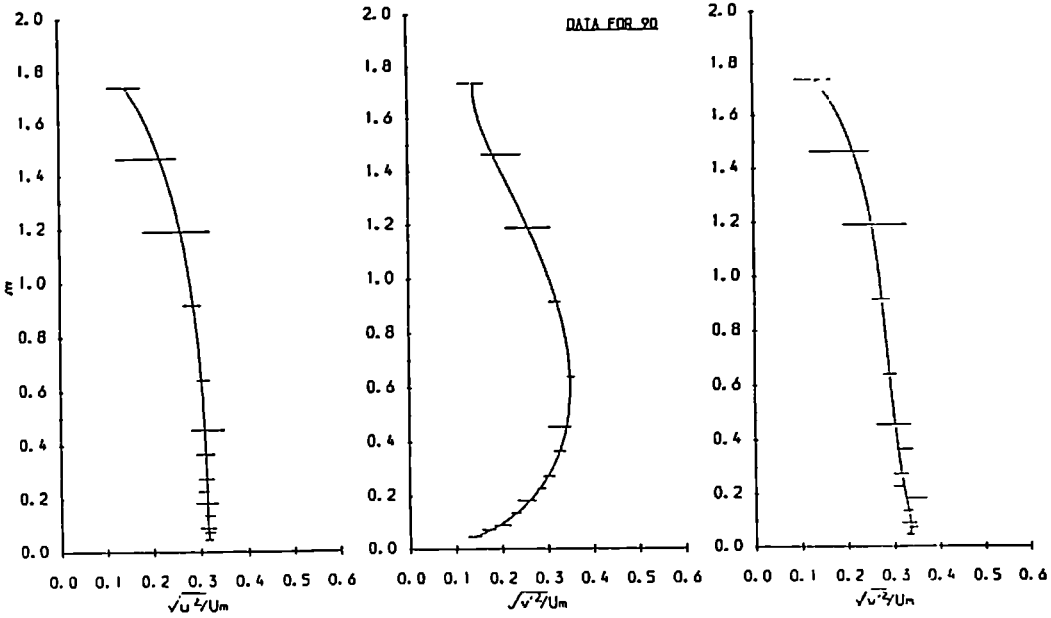

NORMAL STRESSES

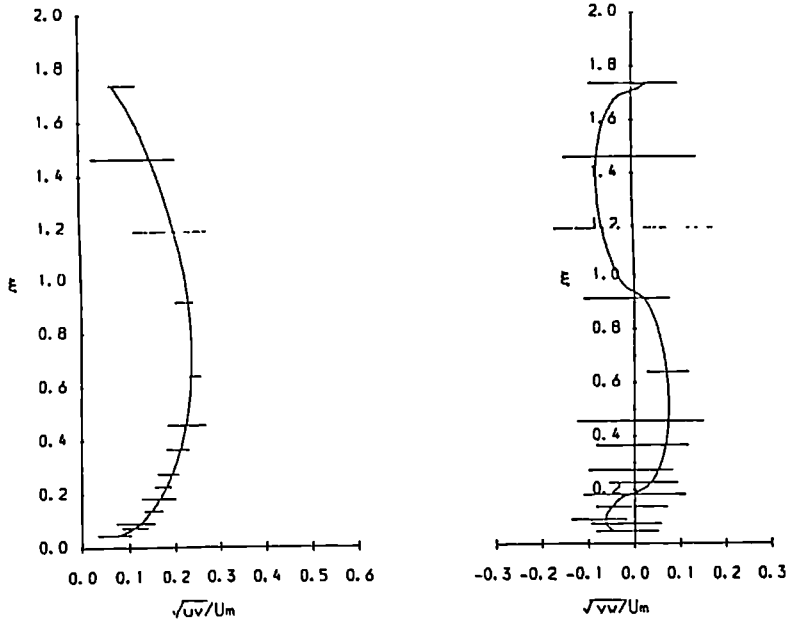

'AFTER'

SHEAR STRESSES

Fig. 5.24

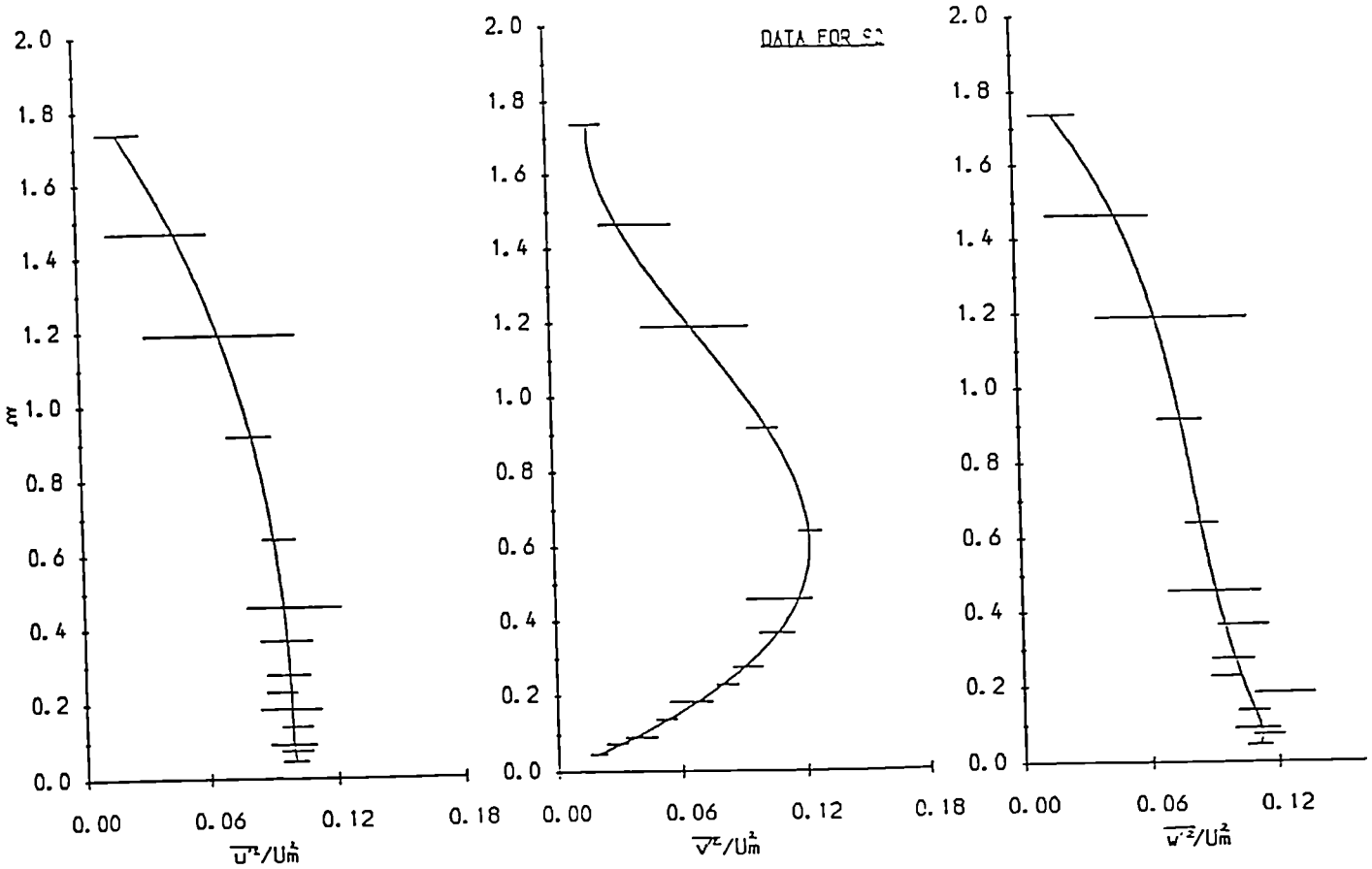

NORMAL STRESSES

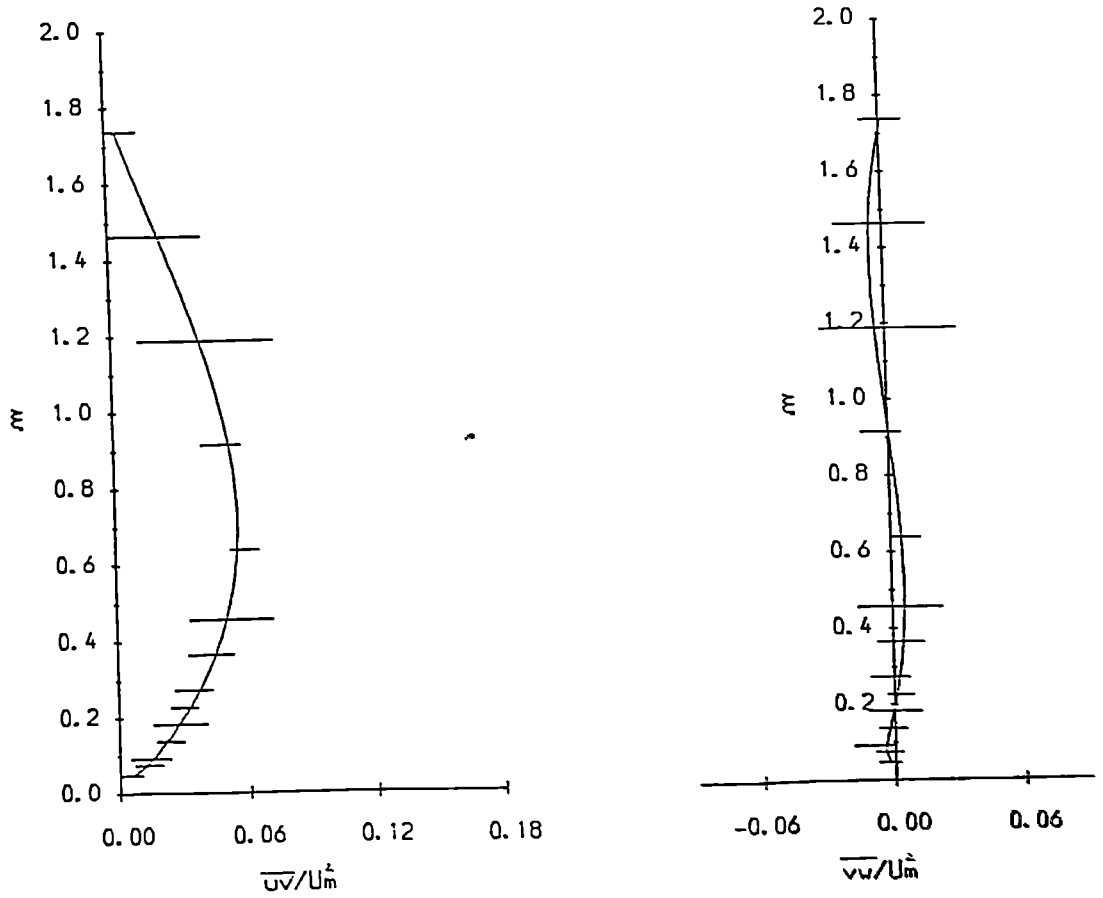

SHEAR STRESSES

Fig. 5.25

CHAPTER 6

CURVED JET SURVEY

6.1 APPARATUS & METHOD

The Coanda had been set with a slot width of 5mm, the accuracy and uniformity of which were checked with slip gauges before and after clamping firmly into position. This provided comparability to Morrison's Case A study using hot wire and three hole probe techniques in a low velocity air flow survey.

The flowrig was carefully filled with chlorinated water and all the air was bled out of the system. For all the traverses, the maximum flowrate was used. This was achieved by feeding all the pump delivery through the large diameter pipe only. The water manometer connected across the orifice plate, upstream of the inlet to the tank was used to monitor the flow input to the model. The results were all corrected to one reference value of pressure drop.

The Coanda flare slot was maintained at 5mm and the slot Reynolds Number was 2.14E5.

The water temperature was held approximately constant at 20° C both during a traverse and between traverses by its passage through the air–cooled radiator heat exchanger. A maximum variation of 5° C is estimated.

It was assumed that the presence of the base–plate, to which the Coanda is attached, would have no detrimental effect upon the flow (e.g. secondary flows) along the centre-line at which all traverses were conducted. The axisymmetry checks detailed in Chapter 5 established confidence in the assumption of an axisymmetric flow structure.

As described earlier, a traverse was performed by winding outwards from the flare surface. The Coanda was locked into position at the required angle and the beams wound in until impinging upon the surface. Zeroing was achieved by winding the beams further into the model and then winding back out to take up the backlash in the traversing mechanism.

Traverses were performed at each of the angular positions shown in Fig. 5.4 :- the slot plane, 5°, 20°, 30°, 45°, 60°, 75°, 90°, 100° and 100° + 20mm along the flat portion of the Coanda. The sign convention used throughout the study is also drawn.

The radial spacing at each individual angular location was chosen after careful consideration of Morrison's hot wire probe results. This was an attempt to gain maximum data at points of greatest interest whilst maintaining a reasonable time limit for the recording of a complete traverse and the subsequent data analysis.

At each radial position along a traverse, the diffraction grating assembly was rotated to four positions about the optical axis. The plane of the laser beams was thus positioned in four separate orientations.

For each beam orientation, 4000 samples were collected with the window length maintained at $10^4 \mu$s. All four beam orientations and their corresponding components of velocity were recorded at a point before moving to a new position along the traverse radius.

Throughout the survey, the laser power was maintained at 0.3W and the PM tube voltage at 610v. The DISA processor operated with the 5:8 cycle comparator setting for validating signals.

The data for a complete traverse was collected onto discs and stored for later analysis. The analysed results were then transferred onto the mainframe

computer for further analysis and data reduction and display. The graphics package, GHOST80, routines were used for all plotting requirements.

6.2 RESULTS AND DISCUSSION

6.2.1 Mean Velocity Profiles

Fig. 6.1 shows the streamwise mean velocity profiles for all angular positions. All data has been analysed as decribed in detail in Chapter 5. The measurements from all beam orientations at each radial position were statistically combined and fitted with a least squares curve (the latter was not done for the slot and 5° locations). The fitted curves were interpolated for values of the maximum streamwise velocity, U_m, the corresponding radial location, ym and the radial position at which the streamwise velocity has fallen to half its maximum value, $y_{1/2}$.

All the plots presented are of the fitted curves and the symbols are for identification purposes, included for clarity. The symbols do not indicate measurement data points or locations; this information may be obtained by reference to the diagrams presented in Chapter 5.

Some inconsistencies are shown in the curves near the origin e.g. Figs. 6.4, 6.7. Although the velocities are zero at the wall, the curves have been plotted through points at which data was recorded and not extrapolated to the origin. The inconsistencies are solely a function of the graphics curve fitting.

Within the first 5° from the slot exit, the flow has accelerated due to the low pressure at the surface caused by the jet curvature. The jet narrows with radial fluid outflow. Continuity considerations demand a narrowing of the jet and this is readily apparent from comparison of the slot and 5° profiles.

These processes continue up to 20° but by 30° the maximum velocity has nearly returned to the slot value. Between 45° and 60° there is very little change in streamwise velocities but the jet width increases. Thereafter, as U_m falls the width of the jet increases as more fluid is entrained and the jet spreads radially outwards. The radial position of the maximum velocity, y_m, obtained from Fig. 6.1, rises steadily around the flare.

Growth and velocity decay rates are shown in Fig. 6.2. The growth rate plot also shows an experimental best fit line for a wall jet on a circular cylinder, obtained from the work of Wilson & Goldstein (1976). The lack of agreement between the two situations indicates the effect of the increase in the potential core size of the jet for the larger slot used in this study (t/R = 0.06 and 0.17 resp.). This increase has the effect of increasing the length over which the jet attains its fully developed jet status.

The growth rate decreases in the early stages of development, up to 60°, illustrating the axisymmetric nature of the model flow. Unfortunately, no transverse traverse data is available for the initial jet growth to confirm this feature.

Integration over the velocity profiles was performed to estimate entrainment rates, shown in Fig. 6.2(a). The maximum entrainment, at 100° is three times the slot mass flowrate. This compares with Kaldair estimates of twenty for the Coanda in-air operation. The latter was for configurations with smaller relative slot widths. The gradient of Fig. 6.2(a) is significantly greater than that expected for a radial wall jet, highlighting the effect of curvature.

Comparable mean radial velocity plots are given in Fig. 6.3. Initially, the flow is strongly radially inwards, due to jet thinning. By 20°, the boundary layer is growing so flow is radially outward close to the Coanda

surface but changes to inward flow at the edge of the jet where entrainment of the surrounding fluid is occurring. The profiles again show how the jet grows and gains increasing velocity uniformity across its width.

The mean transverse velocity profiles are shown in Fig. 6.4. They are consistently of a very small magnitude, especially when the error bars associated with this data are considered.

Non-dimensionalised mean velocity data is shown in Figs. 6.5–6.7. Fig. 6.5 shows U/U_m collapsing fairly well to a single line. This may give the incorrect impression of similar velocity profiles. The constant surface curvature in this work does not, however, satisfy the log–spiral criterion necessary for similarity (Ref. Irwin (1973)). The V/U_m plots in Fig. 6.6 confirm this by being distinctly non-similar. Wilson & Goldstein (1976) suggest that the apparent similarity of the mean streamwise velocity profile can be regarded as an indication of its insensitivity to departures of the entire velocity field from self-preservation.

The data for the traverses conducted at 100° and 100° + 20mm, on the flat portion of the Coanda, show thicker non-dimensional profiles for the region $0.2 < \xi < 1.0$. Larger values of $\partial U/\partial y$ on either side of the velocity maximum results, implying strongly perturbed mean flow in this region.

Fig. 6.7 shows the values of W/U_m to have collapsed onto closely similar plots around zero. The maximum deviation is shown by the 75° traverse data.

6.2.2 Second Order Correlations - Normal Stresses

Normal stresses have been plotted in Figs. 6.8 - 6.10 as e.g. $\sqrt{\overline{u'^2}}/U_m$ so are displayed as turbulence intensities relative to the maximum streamwise

velocity.

Again, 'best fit' curves were derived for the analysed data at all locations except the slot and 5°.

The data for velocities and turbulence data is similar to that recorded by Morrison (1982). The LDA technique has provided much more consistent data generally than by intrusive techniques e.g. Morrison's hot wire data, and this is very apparent, especially in the quality of the normal stress profiles. The present survey therefore provides a more detailed survey with data of higher quality.

The results are discussed in terms of the effect of streamline curvature and divergence upon the turbulence structure. The presence of large cross–stream and streamwise mean pressure gradients do not affect the turbulence structure directly; they do not appear explicitly in the Reynolds stress transport equations but only affect the structure via the mean momentum equation.

Considering streamwise curvature effects, the jet undergoes transition and recovery after 90°, encountering a sudden change in surface curvature at 100° with dr/dx= ∞ to which the jet responds. At 90°, the geometry changes from diverging to converging. Unlike the steamwise curvature, this is not a sudden change since dR/dx changes sign after passing through zero and then maintains a constant value.

The streamwise intensities at the slot and 5° locations show a peak coinciding with the position of high negative gradient on the streamline velocity profile, due to the high shear stress generating high turbulence.

Fig. 6.8 also shows that the intensities rise steadily and are all very high, being over 15% by 20° and reaching a maximum of 36% at 100° + 20mm. Profiles for 45° and higher all lie very close together, and are all within 5%. They reach a maximum at 75°, then the turbulence intensity drops at 90° but recovers again at both 100° and 100° + 20mm. positions.

The values are fairly constant over the jet width out to $\xi = 0.9$ and decrease thereafter. Morrisons x-component normal stress data showed peaks at ξ=0.6 in the early stages of jet development, subsequently moving inwards; at 75° and 90° the intensity reached a maximum and was fairly constant across the jet width. The LDA data is far more constant across the jet width, only falling off outboard of ξ=1.0; the intensities are of a similar magnitude but, whereas Morrisons showed a marked decrease at 100° and a non-monotonic response to the removal of curvature, recovering to near 90° values by 100° + 20mm., the decrease is now apparent at 90° with the data for 100° + 20mm being similar to that at 75°.

Fig. 6.10 includes plots of the z–component normal stresses, less uniform across the jet width than the x–equivalents. They show similarity to the x–component values, at 75° and 90° angular locations, across the jet out to approx ξ=0.8. Indeed, the data at 90° is almost identical (the position at which there was greatest confidence in re–locating for the z–traverse).

The normal stresses in the radial direction display rather different behaviour. The plots all show the strong influence of the presence of the wall. Whereas the u and w are still uniform to within ξ=0.15, the v profiles fall inboard of ξ=0.4, increasingly rapidly around the Coanda.

The hot wire results of y–component normal stresses obtained by Morrison are very scattered and show no definite peak in the profiles. Unlike

Morrison's hot wire results, v intensity profiles here show even more pronounced peaks in their profiles. They indicate increasing values up to 100°, where the maximum value reaches 37%, decreasing to 32% by 100° + 20mm. The profile peaks move inwards towards the Coanda surface.

Some disagreement is shown in the reaction to the sudden change in curvature : Morrison's data shows the v intensity profiles to be very sensitive and first shown at 90° displaying a non-monotonic response to its removal; here, the first indication of a response shown by the y–component normal stresses is at 100° + 20mm.

The normal stresses are up to three times those for a plane wall jet, as given in Wilson & Goldstein (1976), showing the effect of streamline curvature. All three components increase around the flare. The three components show differing response to the removal of curvature and the continued application of the extra rate of strain induced by a constant rate of convergence. The streamwise component is, perhaps, more sensitive to these effects since there is a noticable drop in the 90° profile before recovery at 100° and 100° +20mm.

Smits et al (1979b) suggest that a likely effect of divergence is to increase the fluctuating radial component of vorticity. This would increase the fluctuating rate of strain in the radial direction which would, in turn, increase all three turbulence intensities without preference.

Comparison with the data for convex streamline curvature jets presented by Wilson & Goldstein (1976) and Dakos et al (1984) reveals that the present study displays much higher levels. This can be attributed to the effect of divergence in addition to that of streamline curvature.

The data of Alcaraz et al (1977), although over only 20° of arc, indicated large increases in x– and y–component normal stresses, as seen in the present survey. The data of Wilson & Goldstein (1976) for the locations at 60° and 130° show only a small increase in x–component stress but a more pronounced change in the value of maximum y–component normal stress.

6.2.3 Shear Stresses

The x–y shear stresses are shown in Fig. 6.11. They are fairly closely grouped above 45° as more fluid is entrained by the jet, in agreement with Morrisons data. They become increasingly sharply curved with angular location. There appears to be some inconsistency in the data for the 60° traverse which is seen to fall below both lower and higher angular position plots. A maximum value of 0.065 is shown on the 75° profile with a decrease at 90° and subsequent rise at 100°.

Sharp peaks in the slot and 5° shear stress profiles correspond to high negative gradients of the streamline velocity in the mixing layer where high shear stresses would be expected. For the remainder of the profiles at the slot and 5° the shear stress is nearly zero.

The position of zero shear stress can be found by extrapolating the curves. From 30°, this position moves inwards up to 100° and then sharply outwards again at 100° + 20mm. It consistently lies closer to the wall than the corresponding velocity maximum and approaches the wall as x/t increases. The interaction of the outer and inner layers of the jet is shown by the movement of the position of zero shear stress in towards the wall with increasing downstream distance.

Shear stresses show an inward–moving peak up to 100°. By 100°+ 20mm. the distribution has altered significantly, the maximum value has decreased slightly and the peak has moved outwards. Shear stress data obtained by Smits et al (1979) revealed an outward going peak in the shear stress profiles as downstream distance increased but their data was for a convex curvature boundary layer not a full jet as in the present study.

The departure from self-preservation for the curved jet flow is evident from the shear stress plots. The large increase in turbulent mixing due to convex curvature is readily apparent as the Reynolds stress is several times higher than the plane flow value. The values are again generally higher than those from the studies of Dakos et al (1984) and Wilson & Goldstein (1976) highlighting the effect of divergence in addition to streamline curvature influences.

The transverse shear stresses for the locations studied are satisfactorily close to zero, as plotted in Fig. 6.12.

6.2.4 Structural Parameters

In order to characterise the structural changes indicated by the turbulent intensity and shear stress plots, dimensionless ratios are required and these are plotted in Figs. 6.13 – 6.16 for the x–y and y–z traverse data.

The dimensionless quantities considered are

$$R_{uv} = \overline{u'v'}/\sqrt{u'^2 v'^2}$$

$$a_1 = \overline{u'v'}/q^2$$

and isotropy indicators

$\overline{v'^2}/\overline{u'^2}$ and $\overline{w'^2}/\overline{u'^2}$.

The first structural parameter considered, shown in Fig. 6.13, $\overline{v'^2}/\overline{u'^2}$ gives an indication of the isotropy of the flow. Initially, the flow is far from isotropic but by 20° the central section of the jet shows $v'^2/u'^2 = 1.0$. This profile is repeated except at 45° where it falls below 1.0 and 60° where values in the central portion rise above 1.0. It falls again at 100° +20mm. to approximately 0.7. All locations show a sharp decline inboard of ξ=0.4 a clear indication of the effect of the presence of the wall on the radial component of normal stresses. They also show a rise above 1.0 far away from the jet for $20°to90°$ with the exception of 60°. Morrison's data (1982) showed very high peaks for $\overline{v'^2}/\overline{u'^2}$ of 4.5 and 3.5 at 45° and 60° positions respectively. The present data is in far greater agreement with that of Guitton (1970) whose data showed 0.37 for uncurved and 0.7 for curved surfaces, both recorded at y=$y_{1/2}$. Guitton & Newman (1977) also report a value of $\overline{v'^2}/\overline{u'^2}$ =1.0 for their log-spiral surface, x/R=1.

Comparable plots of $\overline{w'^2}/\overline{u'^2}$ are given in Fig. 6.14. For $75°and90°$ they indicate the jet is uniform and nearly isotropic across its width. At 100° and 100° + 20mm, $\overline{w'^2}/\overline{u'^2}$ has dropped to approximately 0.7.

$R_{uv} = \overline{u'v'}/\sqrt{\overline{u'^2}\overline{v'^2}}$ shows little variation away from the wall from one angular position to another except at 0° and 5°. It maintains a fairly constant value of 0.5-0.55, similar to that found by Guitton and Wilson & Goldstein, who reported nearly constant values of R_{uv} = 0.55 with streamwise distance, decreasing near the wall. At all locations, here too is seen a rapid decrease

below ξ=0.5. Alcaraz et al (1977) display data showing R_{uv} of 0.45 at the maximum and Morrison (1982) also indicates 0.45 up to 100°, the position at which there is a sudden change in the surface curvature.

Another dimensionless ratio considered, $a_1 = \overline{u'v'}/q^2$ is plotted in Fig. 6.16. Direct values are only attainable at the four final locations where both traverses were performed. The data for earlier positions have been obtained by assuming $\overline{w'^2} = \overline{u'^2}$. This seems a reasonable approximation when the plots of x and z normal stresses and $\overline{w'^2}/\overline{u'^2}$ are reviewed.

Wilson & Goldstein (1976) cite work proposing that, for non-equilibrium turbulent flows, parameters scaled relative to each other, rather than to U_m, would produce a turbulent field showing a much higher degree of self–preservation. They investigated this hypothesis for their curved wall jet by plotting Reynolds stress scaled with the local turbulent kinetic energy i.e.a_1. Comparable plots for the Coanda jet flow are shown in Fig. 6.17 as a superimposition of the values of a_1 and are very similar to those plotted by Wilson & Goldstein. They confirm their conclusions that the non-equilibrium nature of the curved jet is still apparent using this type of scaling.

The profiles for 30° – −90° are fairly uniform over the centre section of the jet, outwards of ξ=0.5, at 0.18 – 0.20, falling slightly at 100° and 100° +20mm. Morrison's data for a_1 is in agreement with that of Wilson & Golstein (1976) who realised a value of 0.13, constant for much of the jet width. Wilson & Golstein show, however, for the 45° location that a_1 rises to 0.16, which is closer to the present data.

Morrison (1982) identified non-monotonic recovery of the stress components and all structural parameters with the removal of curvature. This

was in direct contrast to Castro & Bradshaw (1976) and Smits et al (1979a) for whom a_1 returned monotonically to its equilibrium value. The ratios recorded in the present study appear to be in general agreement with the former survey, showing themselves to be affected by the streamline curvature removal in a non-monotonic manner.

6.2.5 Turbulence Data

Presented in Fig. 6.18 are plots of the non-dimensionalised turbulent kinetic energy and eddy viscosity levels.

Wilson & Goldstein (1976) computed values of eddy viscosity from their curved jet measurements between 60° and 130°. They corrected their data to take account of streamline curvature and, when the present data was similarly analysed, the data showed close similarity.

The kinetic energy profiles show that, after 30°, values are fairly close. Maximum values are shown at 100°, where kinetic energy levels are approximately 0.17.

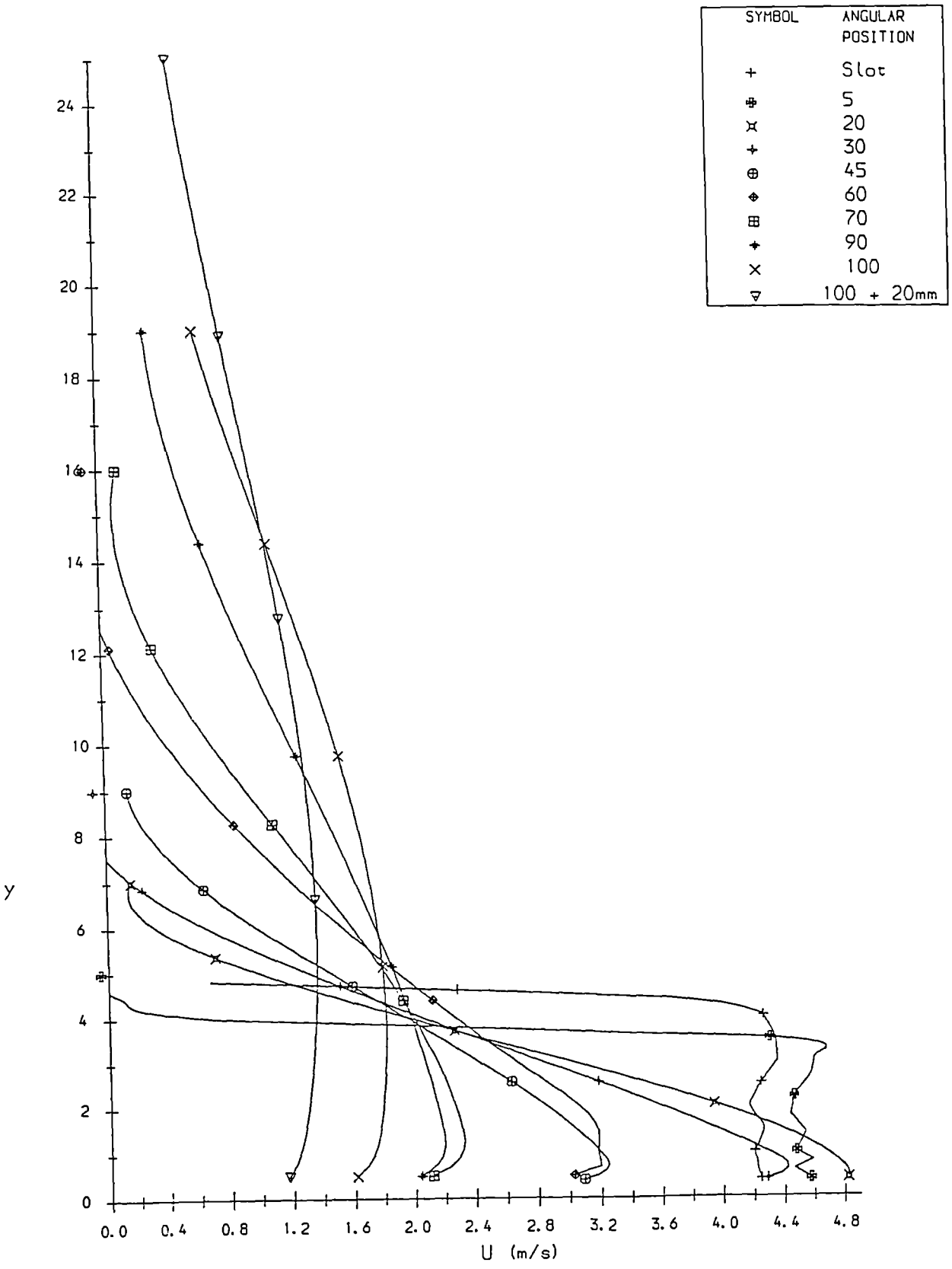
SYMBOL
ANGULAR POSITION
Slot
5
20
30
45
60
70
90
100
100 + 20mm
y
U (m/s)
0
2
4
6
8
10
12
14
16
18
20
22
24
0.0
0.4
0.8
1.2
1.6
2.0
2.4
2.8
3.2
3.6
4.0
4.4
4.8

Fig. 6.1 U vs. y

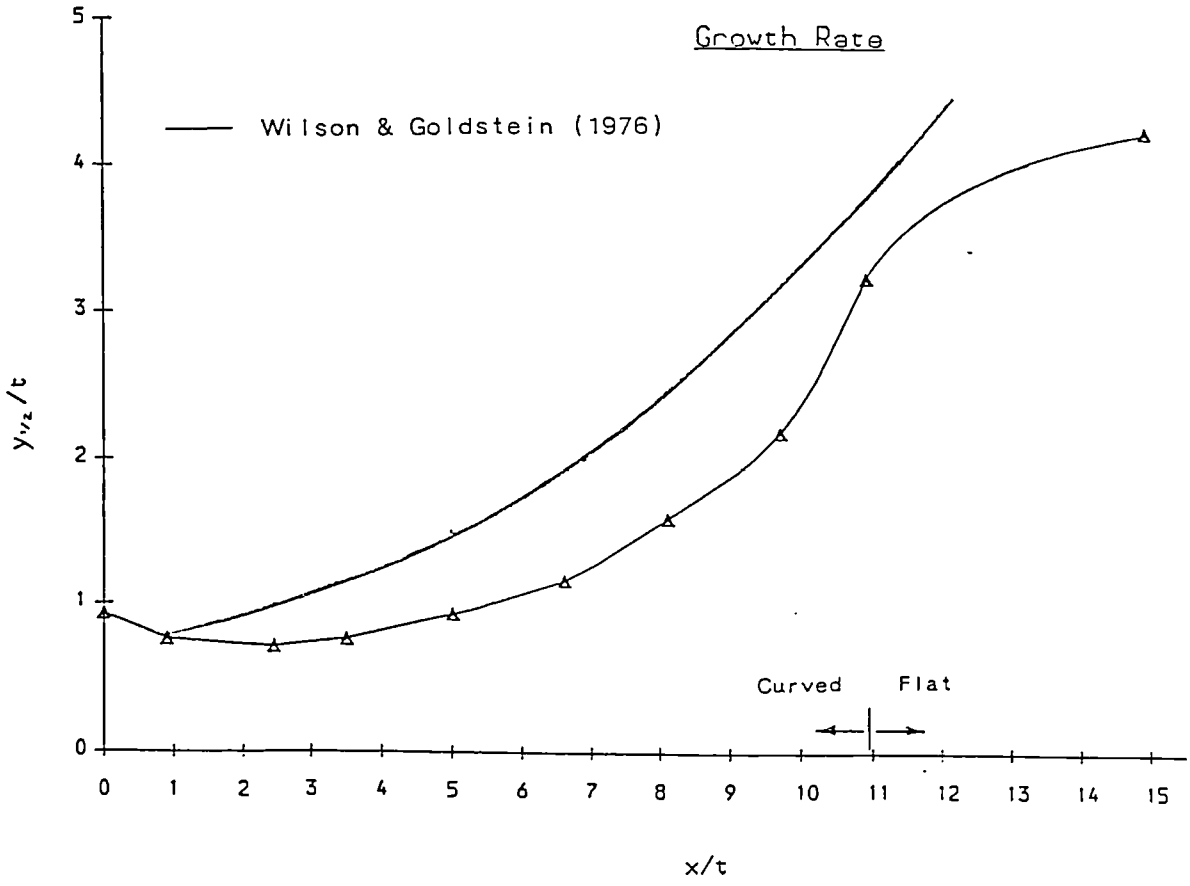

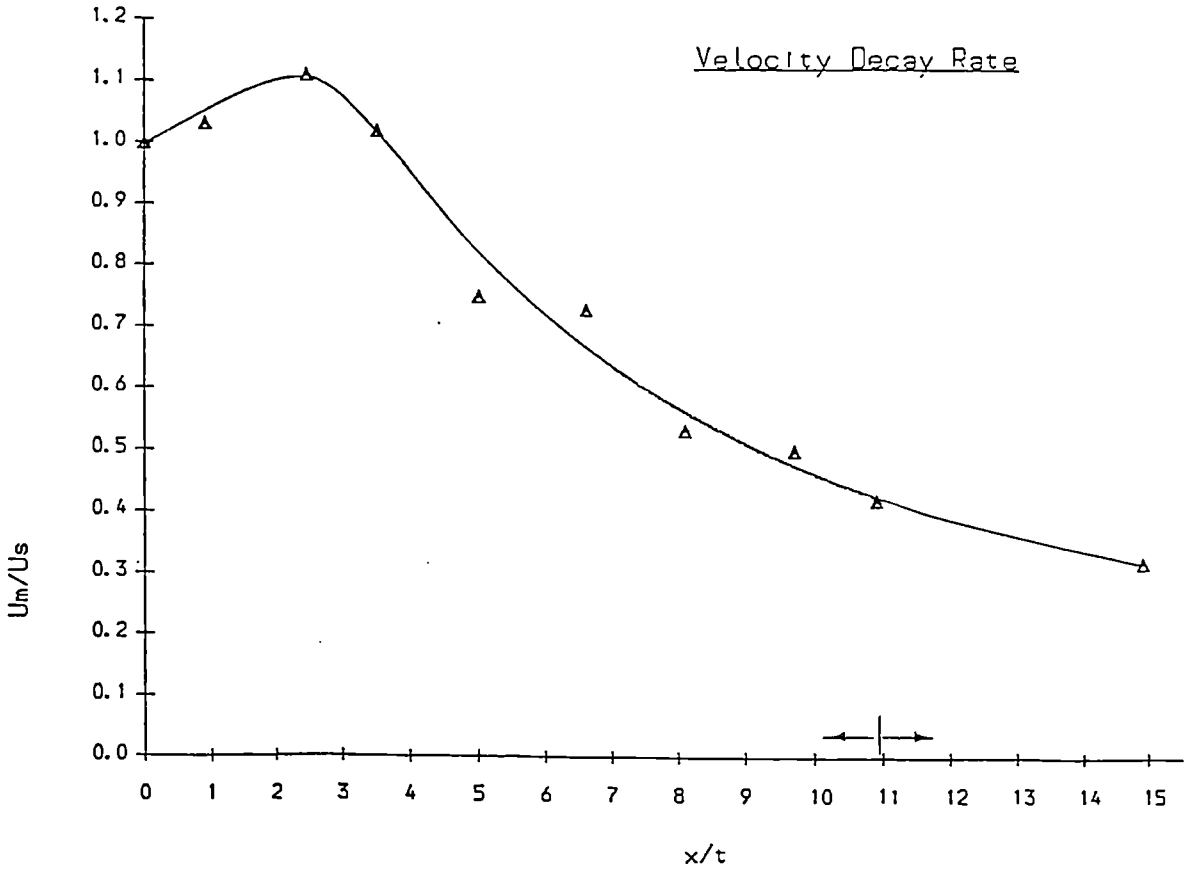

Fig. 6.2 Coanda Jet Growth & Velocity Decay Rates

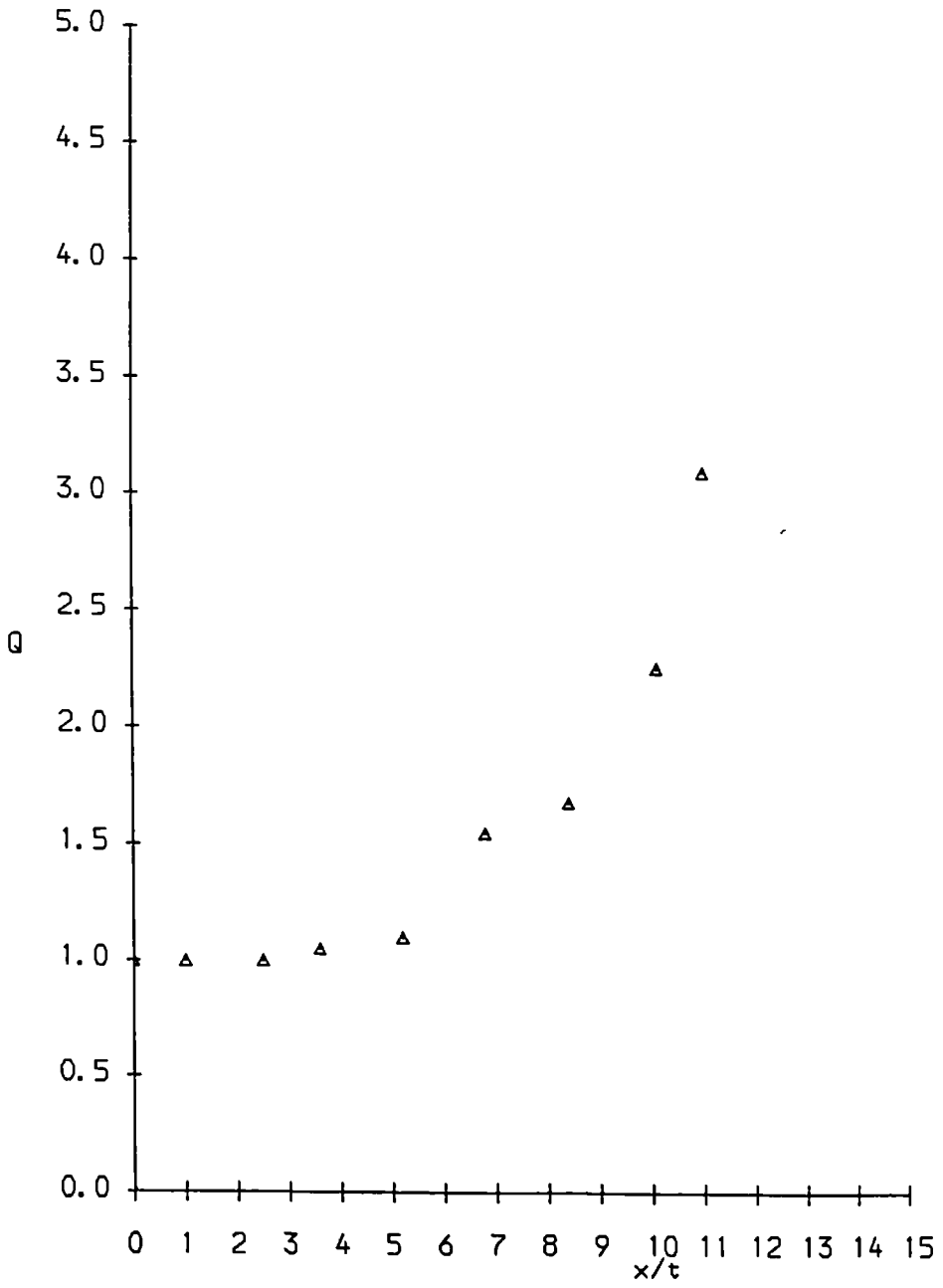

Fig. 6.2(a) Coanda Flare Entrainment Rates

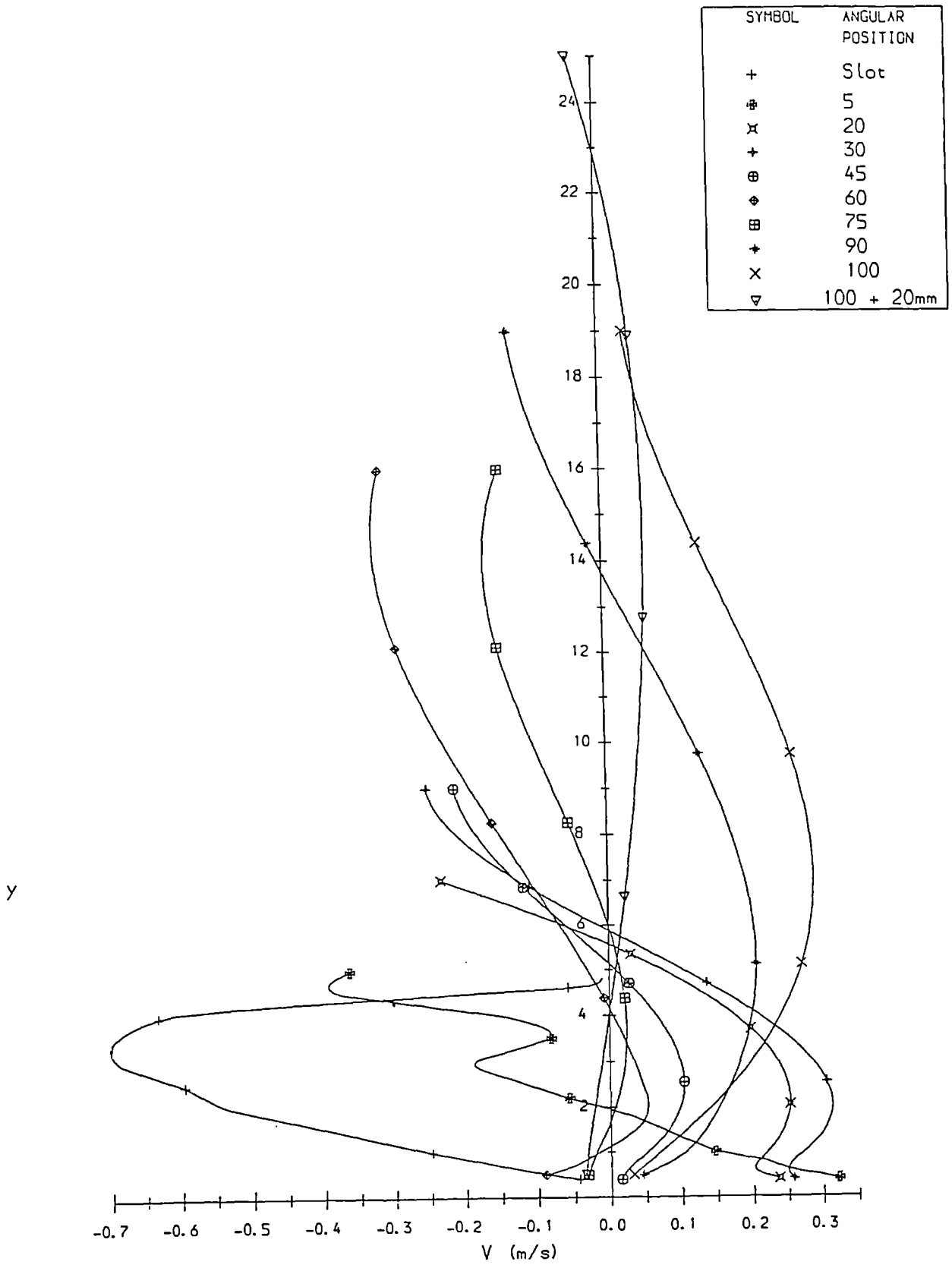
SYMBOL
ANGULAR POSITION
Slot
5
20
30
45
60
75
90
100
100 + 20mm
y
24
22
20
18
16
14
12
10
8
6
4
2
-0.7
-0.6
-0.5
-0.4
-0.3
-0.2
-0.1
0.0
0.1
0.2
0.3
V (m/s)

Fig. 6.3 V vs. y

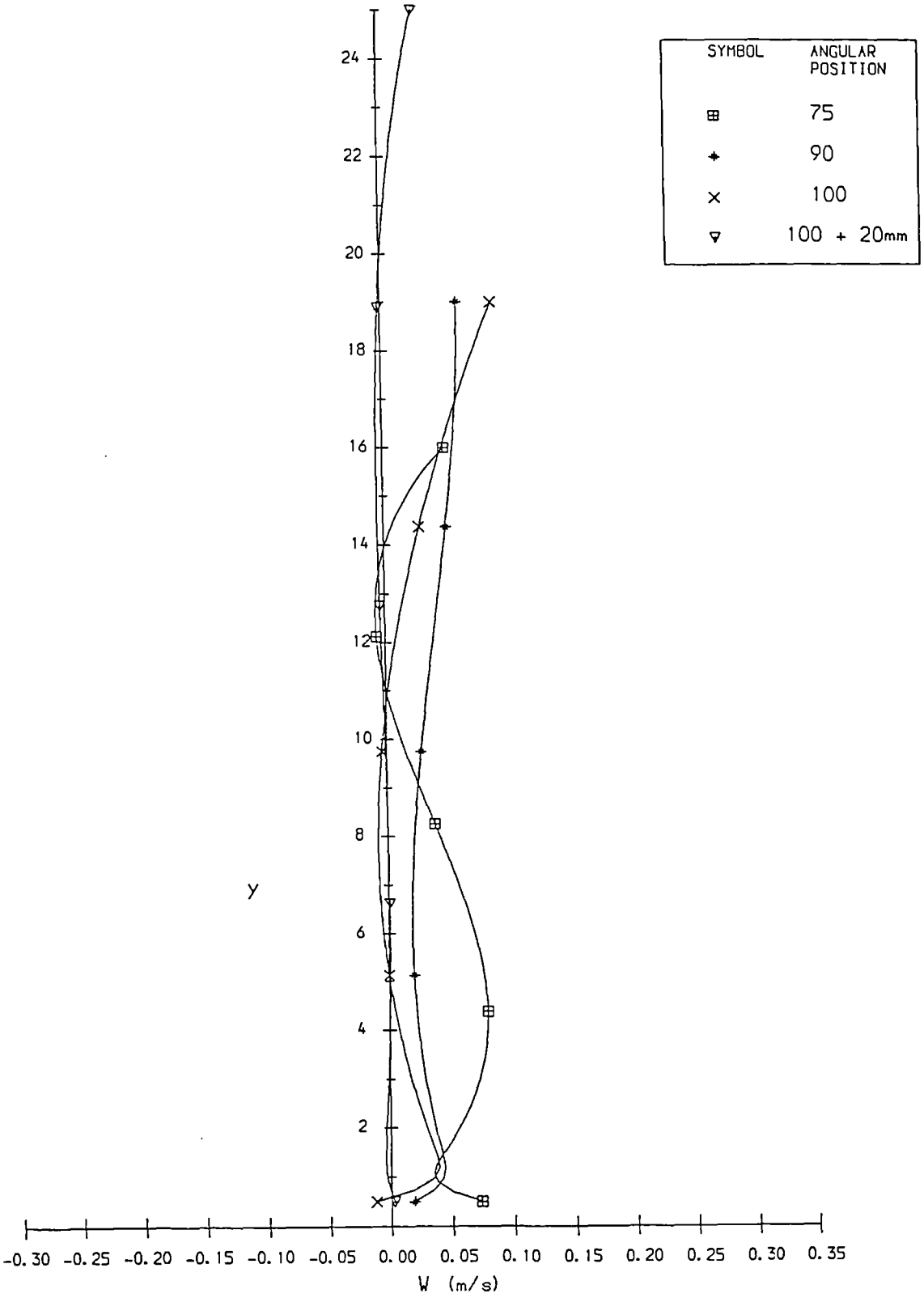
SYMBOL
ANGULAR POSITION
75
90
100
100 + 20mm
y
24
22
20
18
16
14
12
10
8
6
4
2
-0.30 -0.25 -0.20 -0.15 -0.10 -0.05 0.00 0.05 0.10 0.15 0.20 0.25 0.30 0.35
W (m/s)

Fig. 6.4 W vs. y

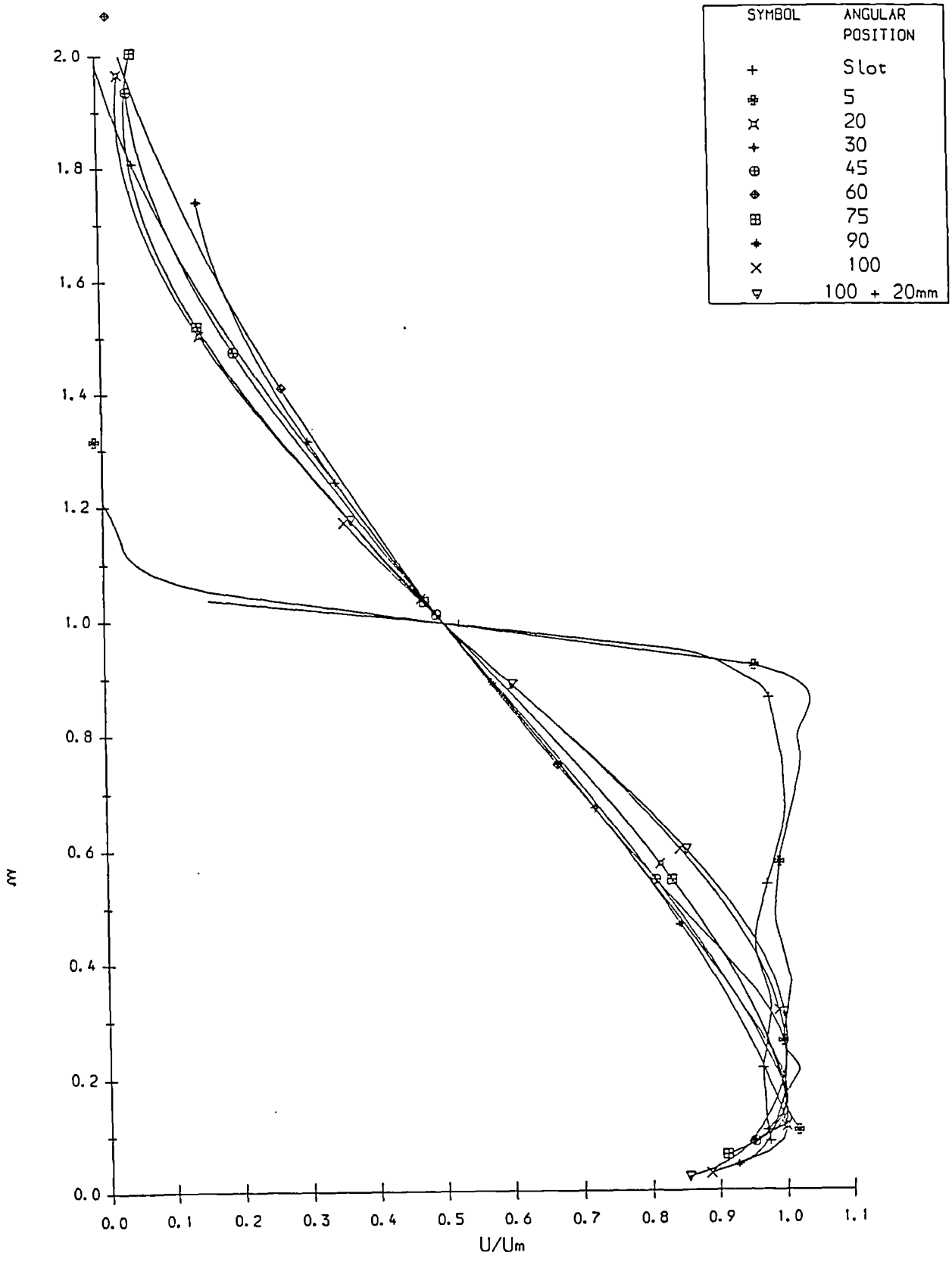

Fig. 6.5 U/Um vs. $y/y_{1/2}$

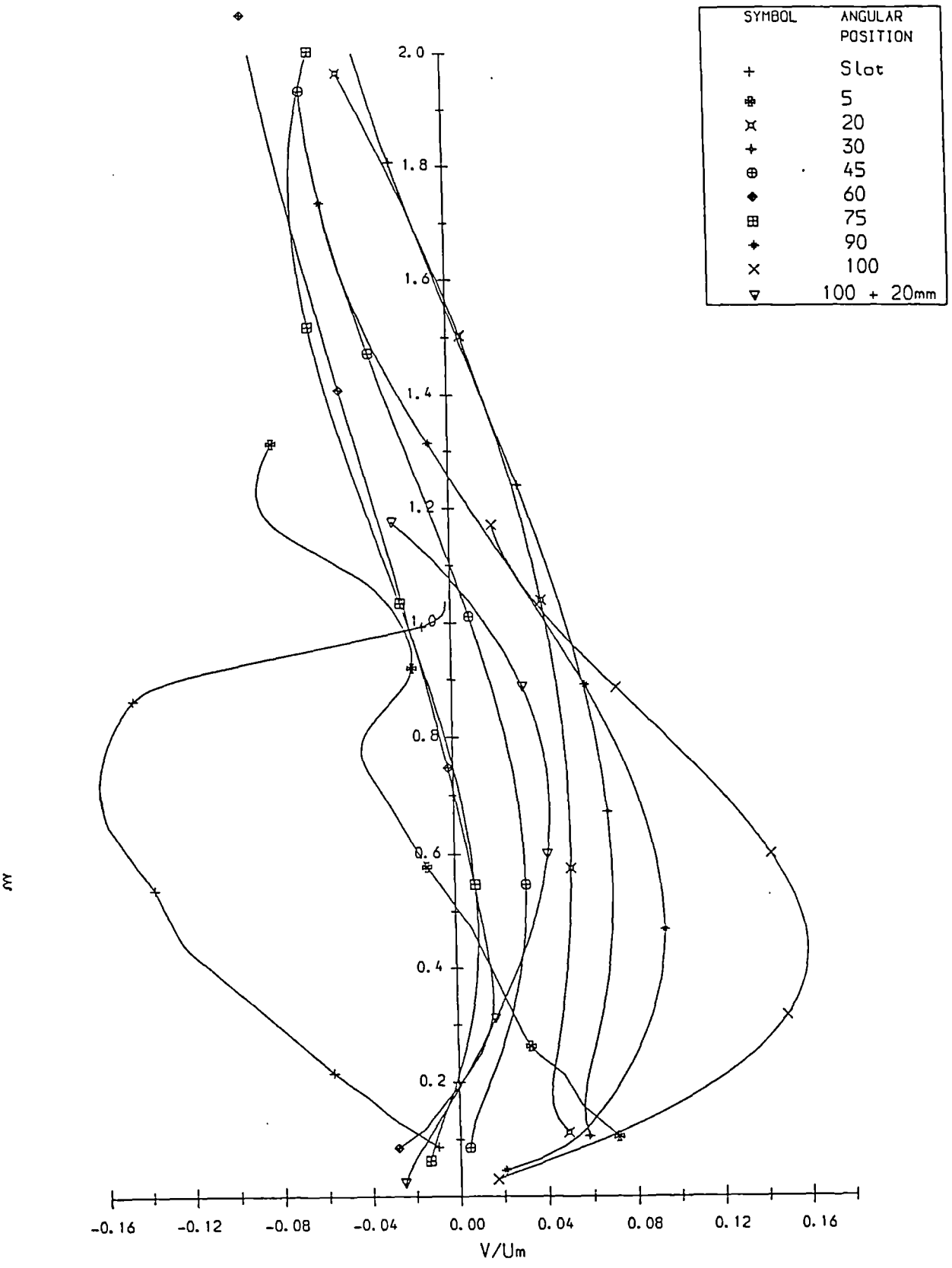

Fig. 6.6 V/Um vs. $y/y_{1/2}$

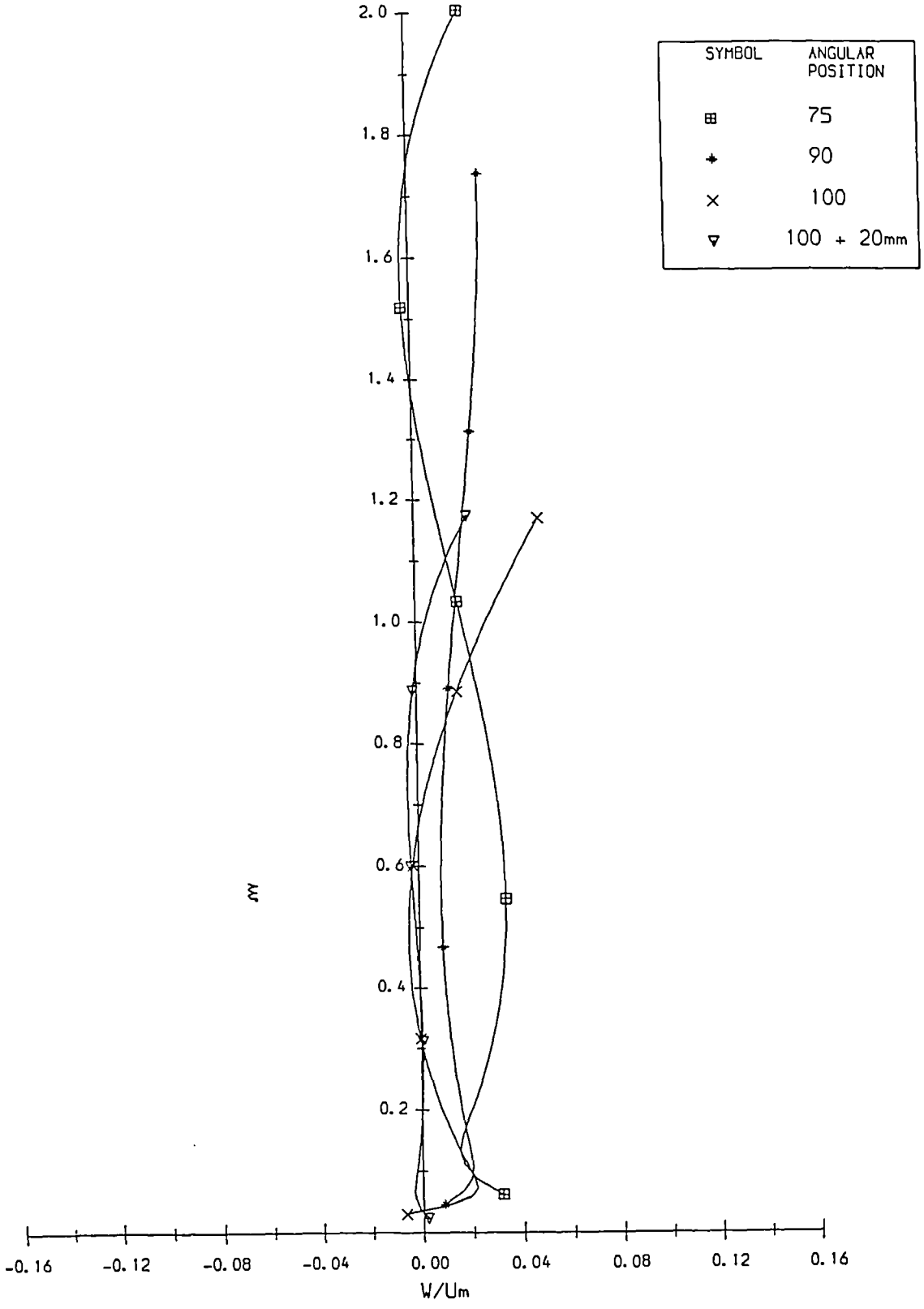

Fig. 6.7 W/Um vs. $y/y_{1/2}$

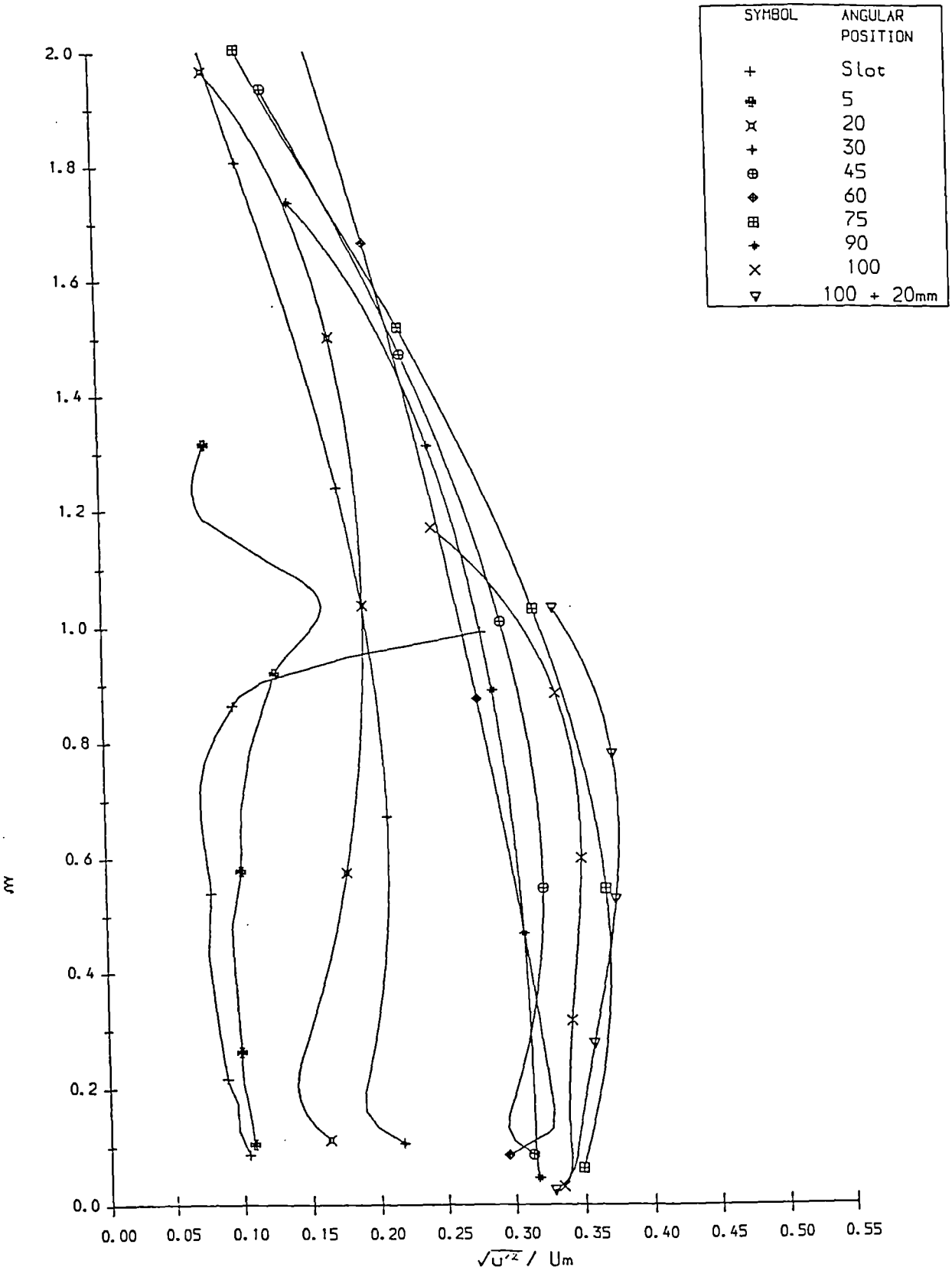

Fig. 6.8 x - Component Normal Stress

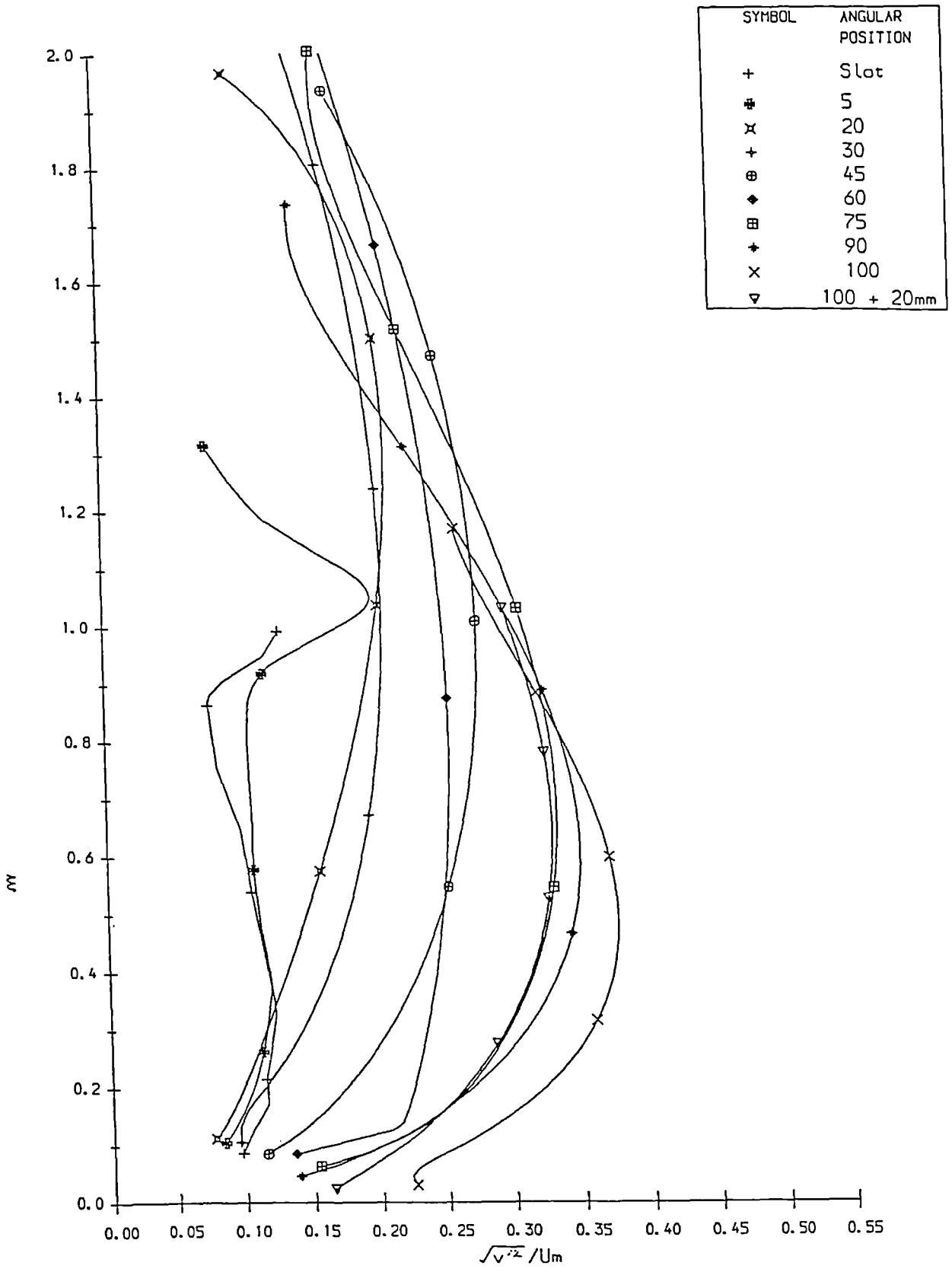

Fig. 6.9 Y - Component Normal Stresses

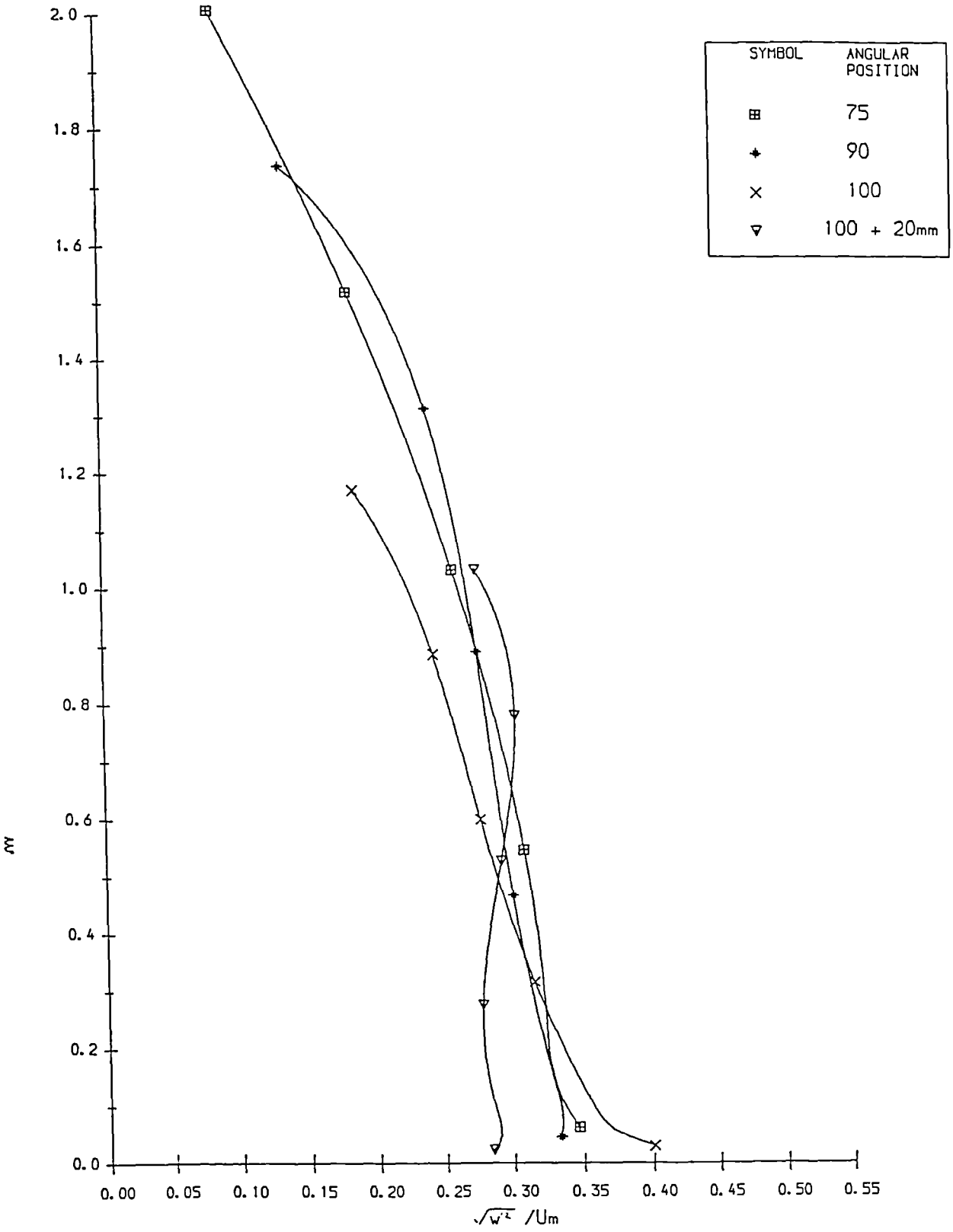

Fig. 6.10 Z - Component Normal Stresses

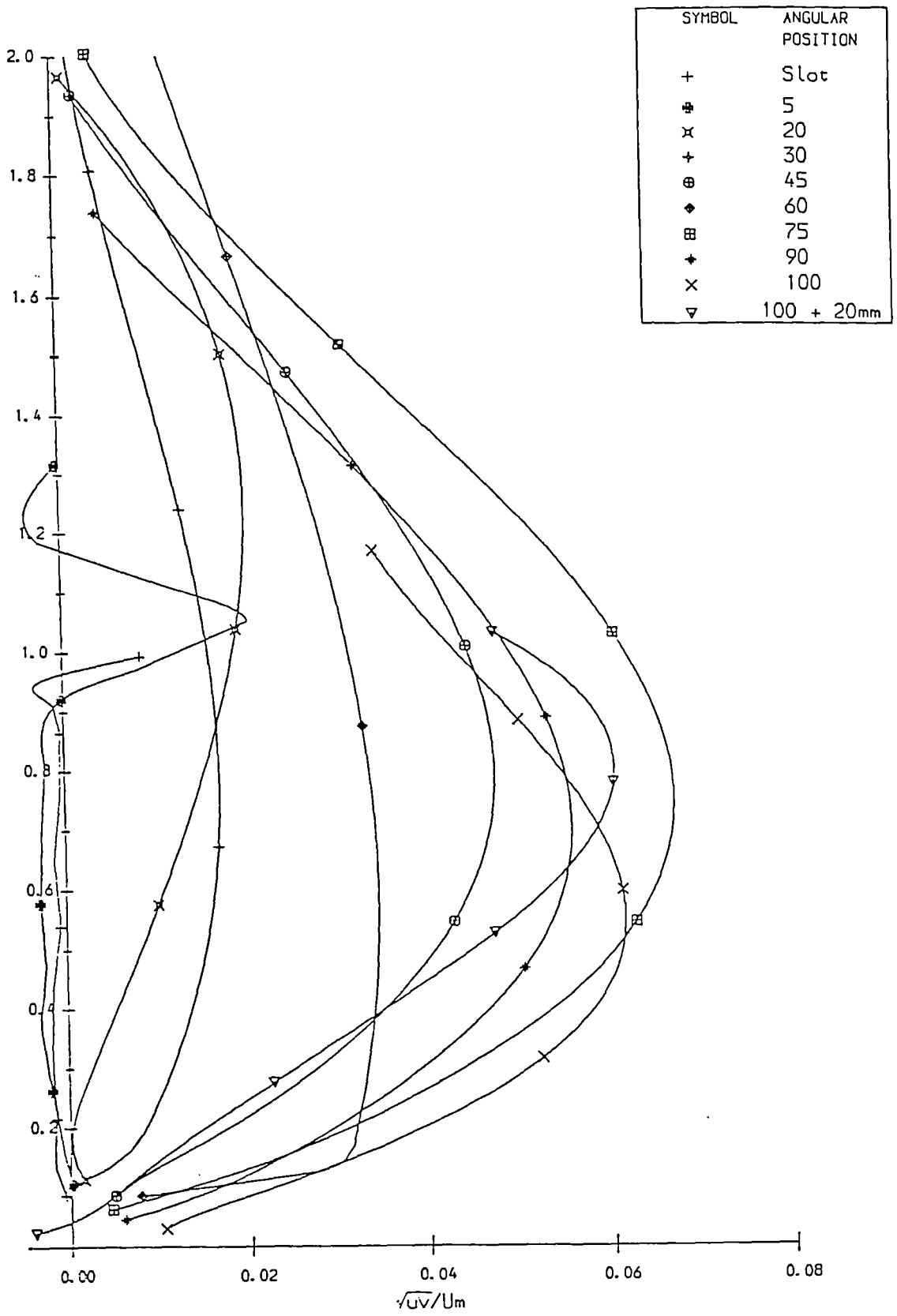

Fig. 6.11 Shear Stresses

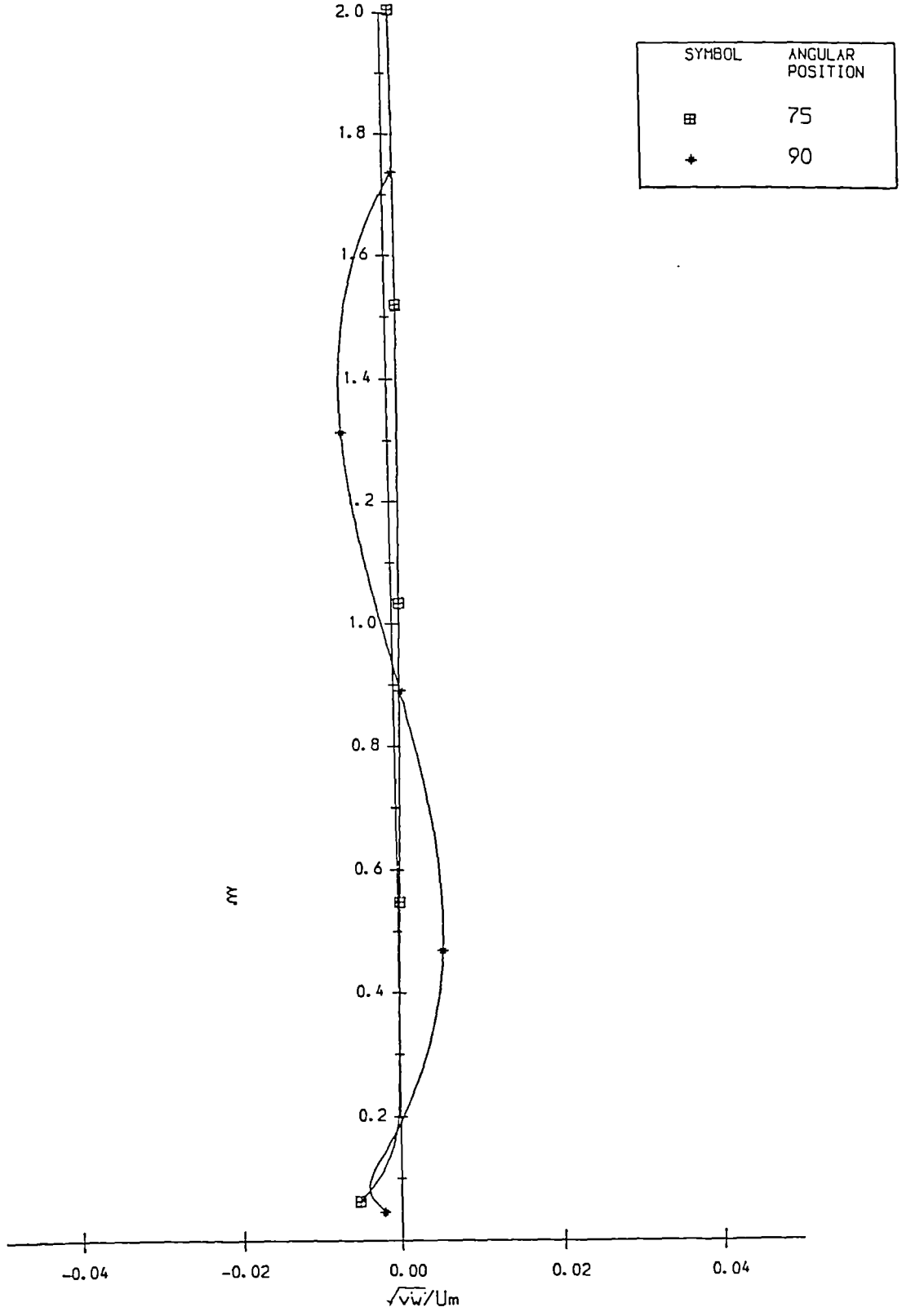

Fig. 6.12 Shear Stresses

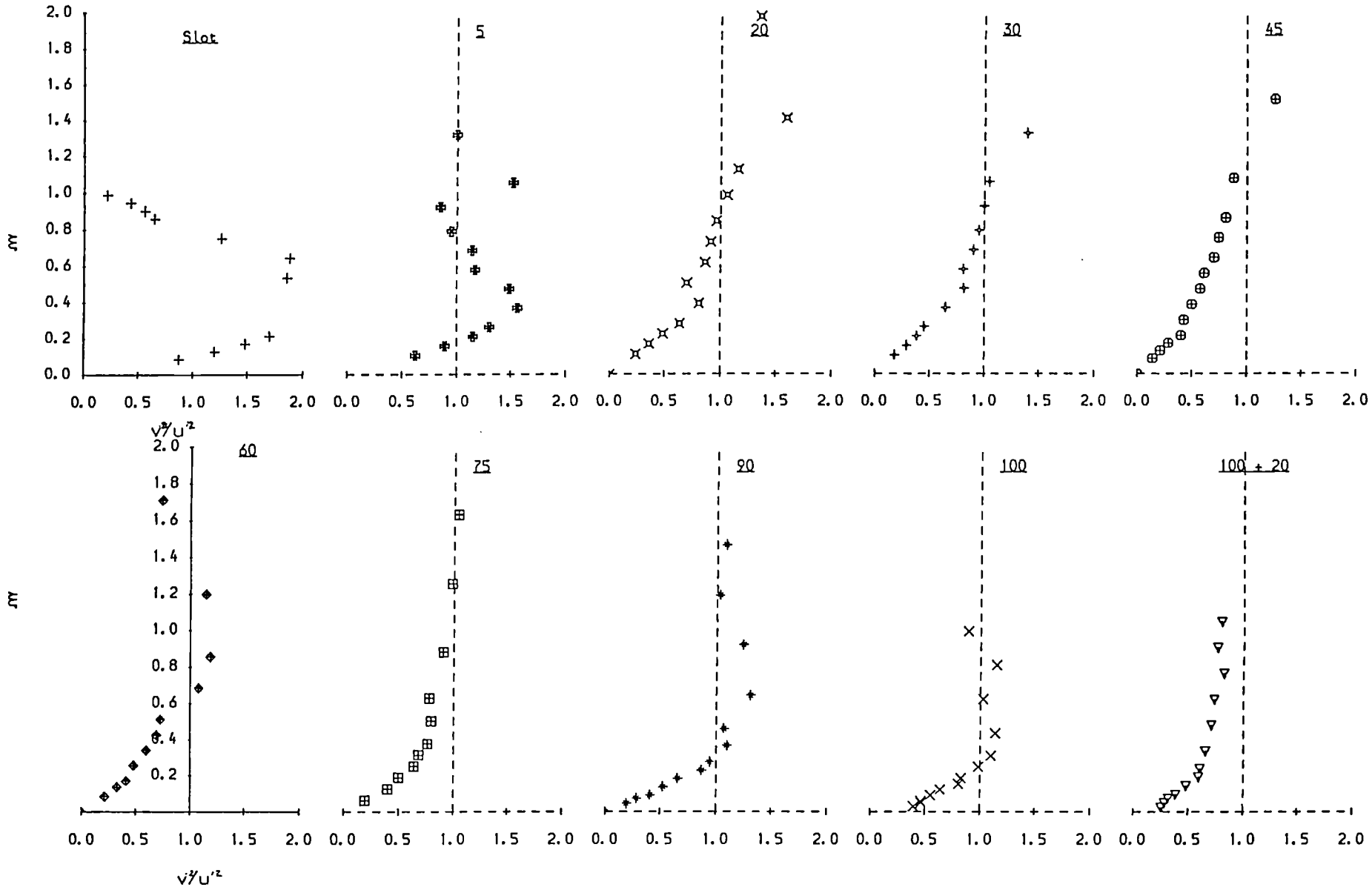

Fig. 6.13 Structural Parameter v'^2/u'^2

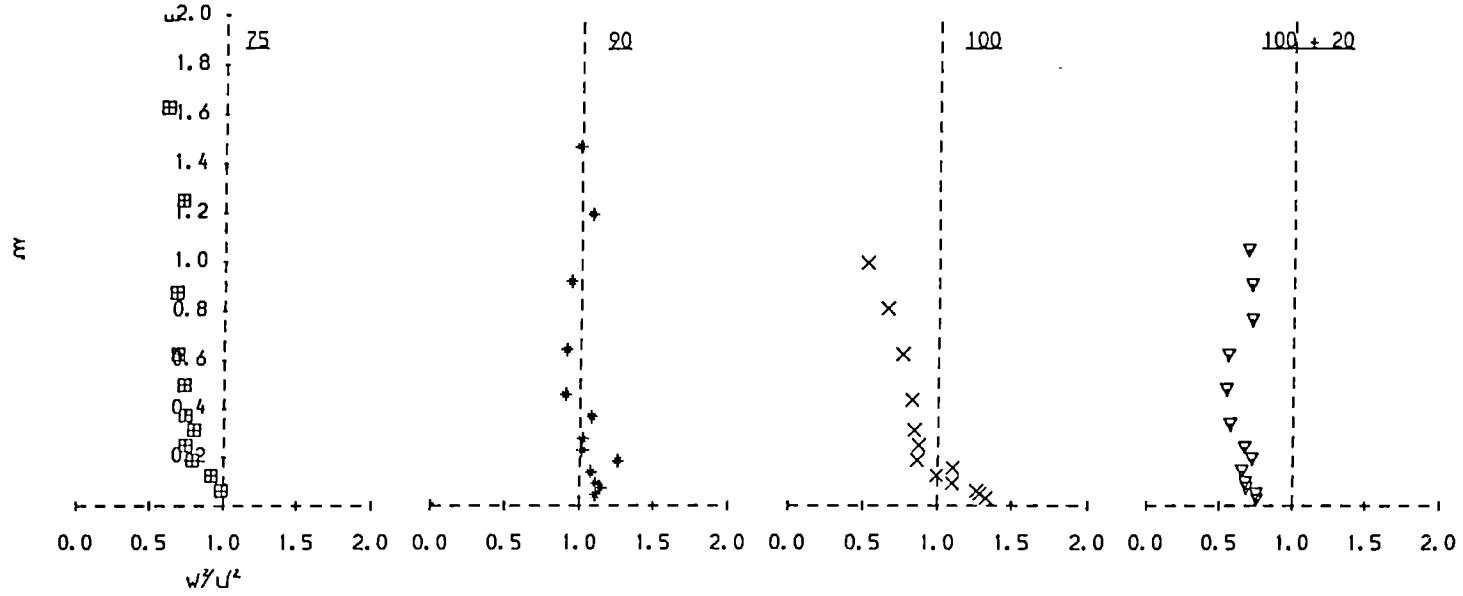

Fig. 6.14 Structural Parameter w'^2/u'^2

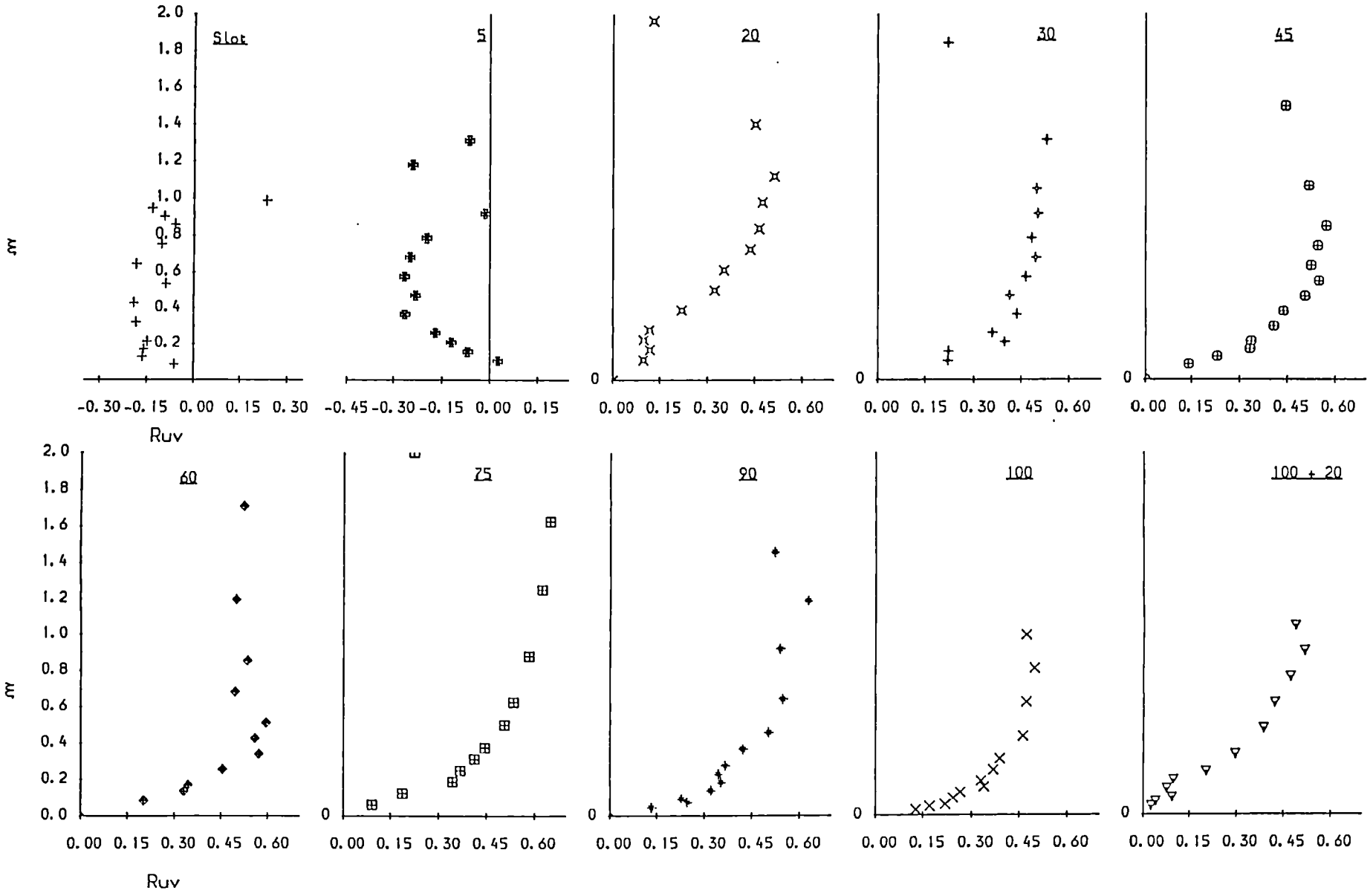

Fig. 6.15 Structural Parameter Ruv

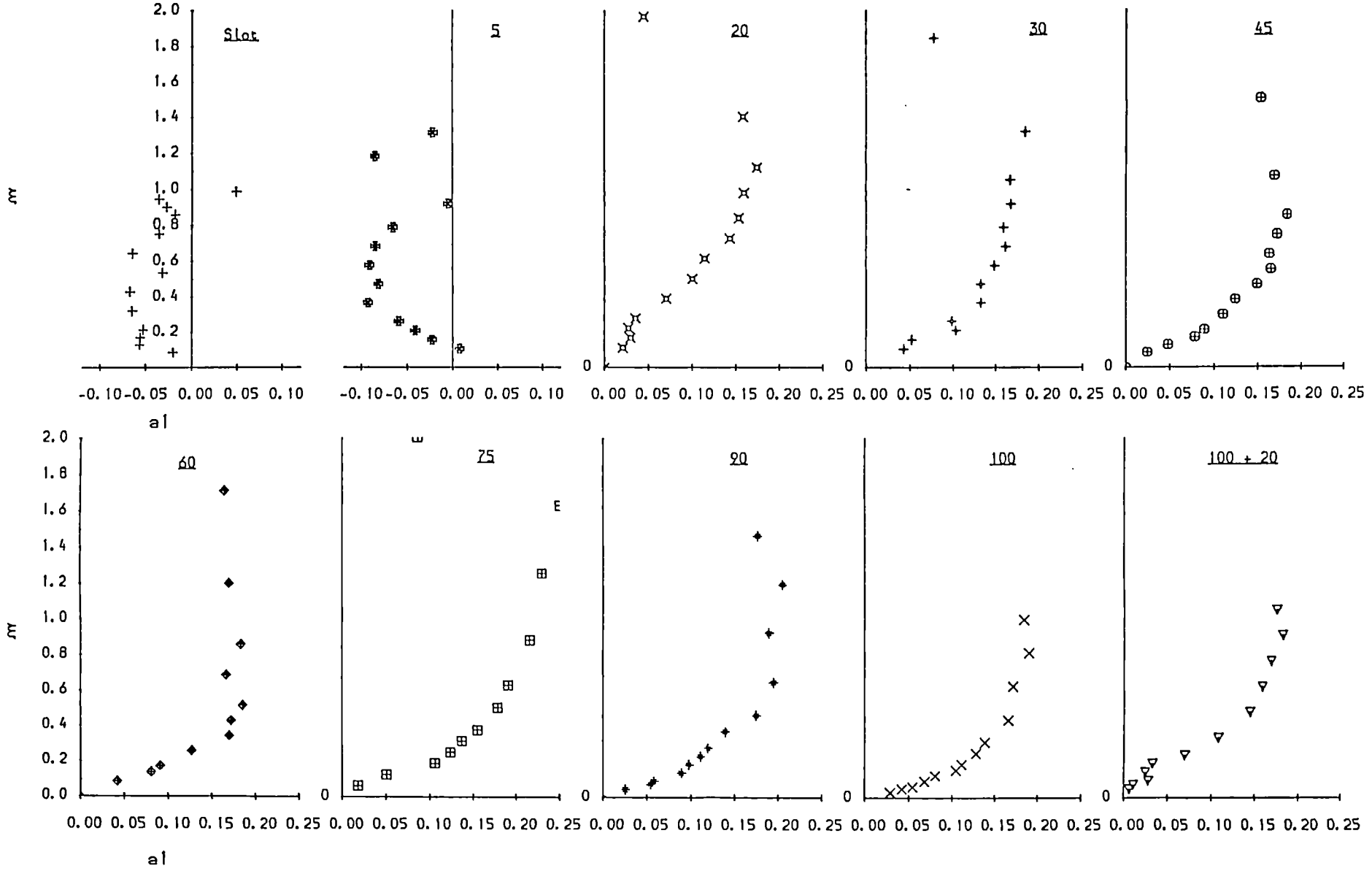

Fig. 6.16 Structural Parameter al

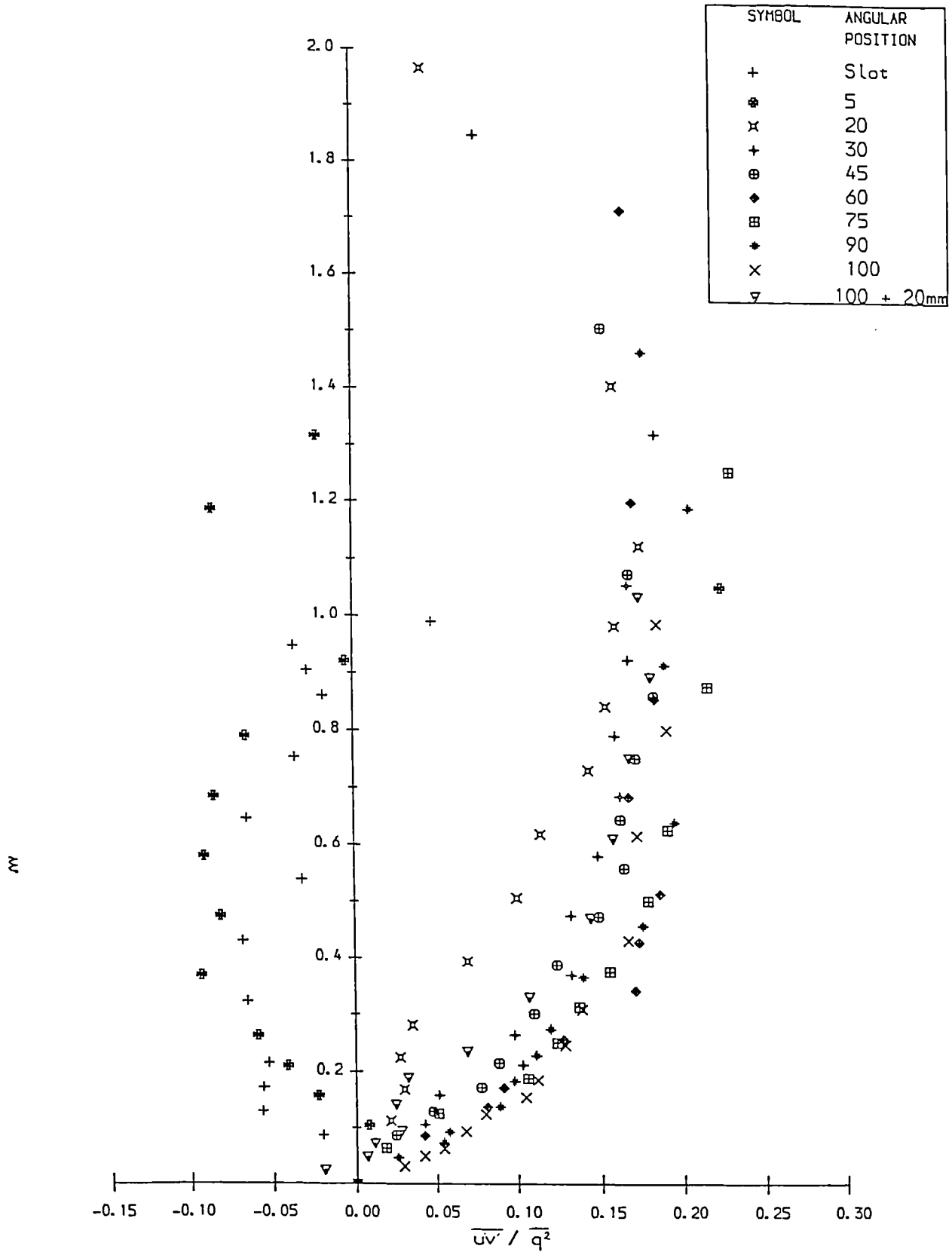
SYMBOL
ANGULAR POSITION
Slot
5
20
30
45
60
75
90
100
100 + 20mm
2.0
1.8
1.6
1.4
1.2
1.0
0.8
0.6
0.4
0.2
W
-0.15
-0.10
-0.05
0.00
0.05
0.10
0.15
0.20
0.25
0.30
$\overline{uv}$ / $\overline{q^2}$

Fig. 6.17 a1

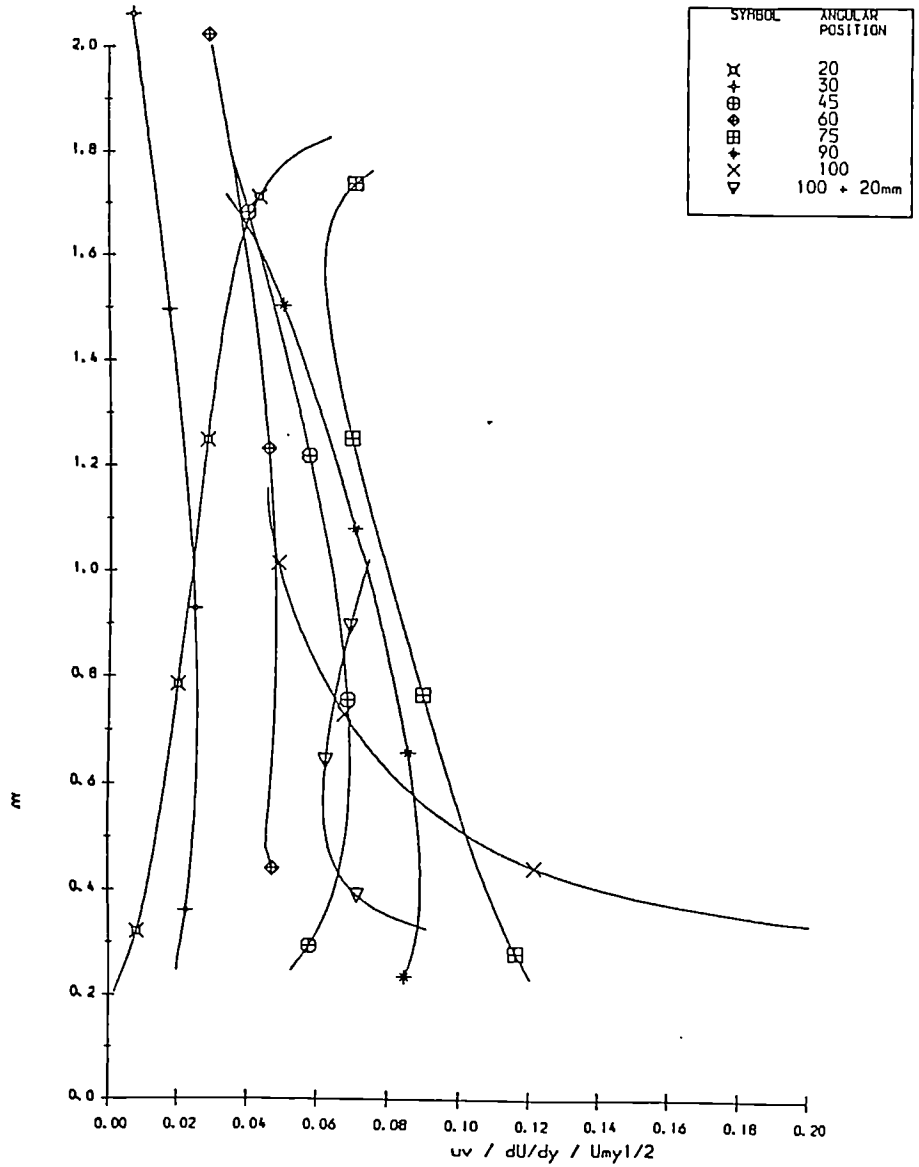

Eddy Viscosity Levels

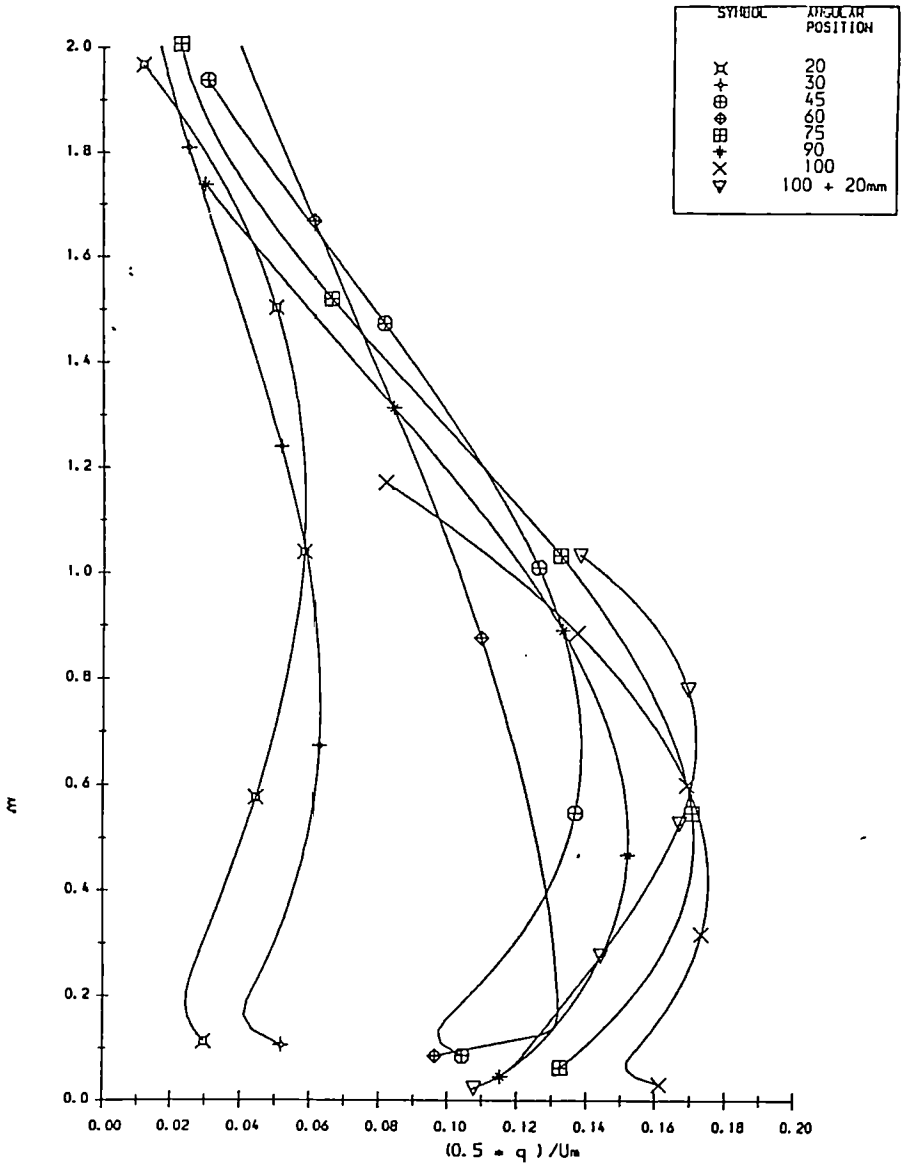

Kinetic Energy

Fig. 6.18

CHAPTER 7

COMPUTER MODELLING

7.1 OBJECTIVES

The opportunity was taken to make a comparison between the newly-acquired experimental data and the predictions given by Morrison's (1982) model.

The intention of the computer modelling section of the project was also to perform development studies on the flow calculation program PHOENICS and attempt to advance predictive techniques. The acquisition of high quality LDA data for the sudden expansion and curved jet flow situations provided ideal test cases. They furnished the opportunity to discover the potentials and limitations of available turbulence models.

7.2 COMPUTER MODEL

Details of the model produced by Morrison are given in his PhD thesis (1982) and the results summarised in Morrison & Gregory-Smith (1984).

The calculation method is similar to that of Patankar & Spalding (1972) using a simple mixing length turbulence closure. It was made more specific to the case of a jet emerging from an annular slot ; such effects as heat transfer, chemical reaction and surface porosity were omitted, and the geometry was made more relevant.

The two-dimensional form of the Patankar & Spalding (1972) method expresses the equation of motion in finite difference form by the use of four nodes. Central differences are used in the streamwise direction. The streamwise and cross-stream pressure gradients in the mean momentum equations (in the x and y directions) are uncoupled by assuming dp/dx=0. This ensures a parabolic system of equations which can be 'marched'. Near-wall grid positions and wall shear stresses were calculated by the use of a modified form of the law of the wall, including the effect of an adverse pressure gradient.

The turbulence model is basically a second order mixing length calculation. Turbulence modelling of the extra rates of strain due to streamline curvature and divergence, was achieved by empirical modifications to the mixing length model. The relevant nomenclature is shown in Fig. 7.1. Algebraic expressions derived for the changes in mixing length, due to these extra strain rates, are as follows :-

(a) Streamline Curvature

$$-\overline{u'v'} = l_o^2(1 - \alpha_1 Ri - \alpha_2 Ri^2)^{3/2}(1 - K)^2\left(\frac{du}{dy}\right)^2 \qquad 7.1$$

where

$$K = \frac{U}{(y + r)(dU/dy)} \qquad 7.2$$

and

$$Ri = \frac{2K(1 + K)}{(1 - K)^2} \qquad 7.3$$

The constants α_1 and α_2 are not universal but are geometry-dependent, accounting for the neglect of transport terms, which are significant to differing degrees, and for the neglect of wall influence on pressure-strain modelling.

(b) Divergence

$$l_c = l_o\left(1 - \sigma\frac{(U sin\alpha + V cos\alpha)}{R(dU/dy)}\right) \qquad 7.4$$

where l_o is the mixing length for a plane wall jet without divergence.

No allowance was made for history effects i.e. changes in terms in the transport equations which do not occur immediately with a change in the mean rate of strain. Any such associated time constants for a shear layer responding to a sudden change in surface curvature were considered to be small for the cases modelled.

Normal stress terms were modelled by simple proportionality to the shear stress and were assumed isotropic. No correction was made to account for the preferential effect of streamline curvature on $\overline{v'^2}$. This choice was made because of repercussions on the model's stability.

The calculation method was used to predict a number of different geometries, including the Coanda flare for two different conditions. Case 6 corresponds to the situation investigated experimentally in the present project.

From testing the predictions against various experimental studies, values were obtained for the longitudinal curvature constants, α_1 and α_2, and the streamline divergence constant, σ. These were taken as 3.26, 3.09

and 9.0 respectively. The model made the assumption that the effects of streamline curvature and divergence were linearly additive. This was considered satisfactory to a first order.

An alternative approach to assessing the validity of the correction factors was achieved by applying them directly to the values of mixing-length deduced from the Coanda experimental data. The factors were applied individually and then combined, as in Morrison's model.

7.3 RESULTS

Fig. 7.2 shows comparisons of Morrison's (1982) predicted and the measured jet growth rate and velocity decay rate. The growth rate of the jet is predicted fairly well initially when compared to the LDA data. The decay of maximum velocity is less-well predicted, showing underestimation of the velocity decay rate. In practice, the relatively thick potential core which persists for a significant distance downstream from the slot makes the simple assumptions for the modelling of shear stress inadequate.

The mean velocity profiles are shown in Fig. 7.3 where the 50° profile is compared with the data recorded at 60°. The predicted profile for 50° is still developing but at 100° the prediction shows a too narrow velocity peak too close to the wall.

The radial velocity profiles, shown in Fig. 7.4, indicate fair agreement, the trend towards an outward–flowing profile at 100° is predicted correctly, but insufficient inward–flowing behaviour is demonstrated at 50°.

Fig. 7.5 plots the comparison of turbulent shear stresses. These are under-predicted across the jet width. The uneven predictions at 50° are reported by Morrison to be associated with the development of the velocity profile and the positions of the assumed mixing region boundaries.

Superior agreement has been found to that previously shown by Morrison (1982). He noted that his experimental data suffered from three-dimensionality, notably base-plate boundary-layer development and some unsteady spanwise periodicity of the flow.

Fig. 7.6 shows the derived values of mixing-length, evaluated directly from the data collected around the Coanda model. During the data analysis detailed in Chapter 5, values of velocity gradients were computed by NAG subroutine E02BCF. These values were accessed by a further analysis programme which then computed the basic mixing-lengths. Additional programming calculated the correction factors for curvature and divergence and applied them to the basic mixing-length values. Also shown in Fig. 7.6 are the plots of 'corrected' mixing-lengths, when the factors had been applied. The values of mixing-length are seen to be fairly constant across the jet width, the only serious deviations being at 100° and 100° + 20mm.

If the streamline curvature factors fully accounted for the physical situation, the mixing-length data should, when corrected, collapse onto a single line. It is clear from the second plot in Fig. 7.6 that the spread of values has been significantly reduced but there is still some variation between angular locations. The effect of the divergence term is seen to have a smaller effect upon the mixing-length values.

7.4 PHOENICS

PHOENICS is an acronym for Parabolic, Hyperbolic Or Elliptic Numerical Integration Code Series. It is a general-purpose code for simulating single- and multi-phase flow, heat- and mass- transfer and chemical reaction phenomena. It has been supplied by the computer programming firm Concentration, Heat And Momentum Ltd. (CHAM). It solves the finite-domain equations of mass, momentum and energy conservation etc. and has the capability to apply them to both steady and unsteady flow, for one-, two- or three- dimensional geometries.

PHOENICS is written in standard FORTRAN programme language and is run on the School's Apollo computer, with a link into the mainframe system for data transfer to and from the mainframe computer network. Version 1.3 of PHOENICS, first issued in 1984, was used throughout the studies detailed below.

7.4.1 Programme Organisation

PHOENICS is designed to be operable with very little knowledge of the computing processes involved in the specific problem's solution. It is, however, helpful to understand its organisation and the main points are listed below.

PHOENICS has a *planetary* arrangement, the essentials of its operational layout being shown in Fig. 7.7. A central core of subroutines called EARTH exist and there is a satellite programme. This accepts inputs corre-

sponding to a particular flow simulation. The satellite is a data-preparation programme, writing a data file which is then read by EARTH.

EARTH calls a subroutine GROUND at pre-set points of the solution cycle. EARTH starts with a MAIN programme and contains sequences for storage allocation, formulation and solution of finite difference equations, (FDE's), termination of iteration sequences, output of results and calling GROUND when required.

The file named GROUND contains not only program MAIN but also subroutines GROSTA and GROUND. The 'ground-station' subroutine GROSTA acts as a junction box for PHOENICS; it is called by the EARTH and itself calls a series of user-accessible subroutines, one of which is GROUND. The calls to the subroutines are activated to access such items of information as fluid properties, turbulence models and wall function formulations. If the opportunity is taken by the user to make changes to MAIN or GROUND, recompilation of the file and relinking of the load module are then necessary for the changes to take effect.

Data inputs are organised into 24 groups, covering such items as grid definition, material properties, initial values, boundary conditions, iterations, output and terms in their differential equations. A library of prepared input files, covering various flow phenomenon, serve as convenient starting points for fluid-flow simulations.

7.4.2 Grid

Grid cell nomenclature is shown in Fig. 7.8. Temperatures and pressures are evaluated within the cells e.g. P, N, S, E, W. West-to-east

velocities are calculated at cell-wall locations e.g. w and e. South-to-north velocities are calculated at cell-wall locations e.g. s and n.

PHOENICS can employ one of three distinct kinds of grid:-

Cartesian : this is composed of cells formed by the intersection of three sets of mutually perpendicular parallel planes.

Cylindrical-Polar : this consists of cells formed by the intersection of (a) planes of constant z, perpendicular to the axis of rotation (b) planes of constant x (representing angle), intersecting that axis and (c) concentric cylindrical surfaces of constant radial coordinate y.

Curvilinear : this consists of a distorted regular cartesian grid. A *Body Fitted Coordinate* grid can be imagined as a cartesian grid which has been stretched, bent or twisted. Cells retain six faces and cells originally in contact remain so. They are recommended by CHAM for internal or external flows with smoothly-varying non-regular boundaries. PHOENICS can handle curvilinear grids of any shape. It performs best, however, with those which are nearly or wholly orthogonal. The greater flexibility of curvilinear grids necessitates the input of more information for their definition. The three coordinates of the corners of all cells are required.

In all cases, the grid definitions are as follows :-

x measures distance (or angle) in west-to-east direction

y measures distance in south-to-north direction

z measures distance in low-to-high direction.

7.4.3 Solution Techniques

The values of temperature, pressure, velocity etc. produced by PHOENICS represent solutions to a set of algebraic equations representing the relevant laws of physics for the chosen set of cells. These laws are those governing the 'conservation' of mass, momentum and energy, coupled with the 'transport' laws describing heat conduction, diffusion of matter and viscous action.

The algebraic equations are numerous and strongly coupled. PHOENICS, therefore, solves them in an iterative 'guess and correct' manner. The iterative process can involve slabwise, sweep, whole-field or parabolic solution. Slabs are arrays of cells with the same Z coordinate. Slabwise solutions indicate when PHOENICS performs mathematical operations on one slab before tranferring attention to the next slab. A sweep is a set of slabwise operations conducted in sequence from the lowest slab to the highest.

The parabolic option implies that, although gradients in solution variables exist in the low-to-high direction, higher-slab values do not appear in the lower-slab equations. In this case, a single sweep through the integration domain suffices and provides great reductions in computer storage.

7.4.4 Output

A variety of output facilities are available within the PHOENICS system. The PHOTON program (PHoenics OuTput OptioN) plots graphical displays on the VDU screen. Options include plotting the grid, flow vectors or contours.

File transfer to the University mainframe computer is also possible, using the KERMIT data transfer facility. This enables analysis of the prediction results and their plotted display to be produced in comparable form to those of the measurements.

7.5 SUDDEN EXPANSION TEST CASE

7.5.1 Grid Details

The grid was defined using cylindrical coordinates in the Y-Z plane. The final form of the grid, for which all results are presented are as follows:-

The Z-direction comprised 40 cells each of 10mm length.

In the Y-direction, three separate groups of cell definitions were used in order adequately to define the regions of the small pipe diameter, the main shear layer region and the near-wall area. The requirements were to cover the model in sufficient detail but to minimise the number of grid points if possible, in order to maintain computer time at a minimum.

The grid y- definition then comprised 7 cells, each of 0.9mm width, covering the small, inlet pipe half-diameter, 20 cells in the shear layer, each of 0.6mm width, and 10 cells in the 1mm out to the large diameter pipe wall.

7.5.2 Boundary Conditions

Use was made of the library cases for a 2:1 in air sudden expansion and an in air backward facing step to gain guidance in setting appropriate

boundary conditions. The inlet was given a fixed mass inflow boundary to represent the width of the small pipe. Expressions for the inlet turbulent kinetic energy were also provided.

Refinements to the library case conditions included changing from a single, mean velocity value for the inlet to an inlet profile, matching the measured values. Outlet conditions and the free inner boundary were specified as a fixed pressure situation. Parameters were set at the wall to access the routines calculating skin-friction factors deduced from the log-law.

7.5.3 Turbulence Modelling

The k-ε model programmed within the GROUND subroutine was used directly with no modifications introduced by the user. It is programmed to derive a length-scale from the turbulent kinetic energy and its dissipation rate by the relationship :-

$$l = C_D \frac{KE^{1.5}}{EP} \qquad 7.5$$

where C_D was set to 0.1643.

7.5.4 Permutations Performed

A number of permutations were performed on the basic model to arrive at the final grid definition and boundary conditions. The various modifications were tested for their improvement of the predictions. They were made to ensure grid independence and solution convergence.

The grid definition was changed to include twice the number of cells indicated in (a) above. The number of iterations (number of sweeps) was also increased and its effect upon convergence tested. Both the further refinement of the grid and the increased number of iterations were found to have negligible effect upon the results.

7.5.5 Results

Shown in Figs. 7.9 and 7.10 are the comparable plots of velocities and streamlines for measured and predicted values.

The overall features of the flow are predicted very successfully. Both velocity and streamline plots are closely similar in form and the recirculation region is reproduced by the model. There is, however, some shortfall in the PHOENICS model predictions. The main deficiencies are apparent at the wall, where reattachment occurs approximately 20% too soon, the extent of the recirculation zone consequently being underestimated. A similar situation was found in the library cases and was not unexpected since CHAM warn of this attribute of their k-ε model in the comment statement at the introduction of the step model!

7.6 COANDA MODELS

Experience with PHOENICS was gained by modelling the relatively simple configuration of the sudden expansion flow situation. The skills thereby acquired were then applied and extended when tackling the far more

complex problem of the Coanda flare flowfield. This was complicated both in the geometry and the modelling requirements.

The programme documentation proved disappointingly inadequate or badly organised and presented. In some instances it was incorrect and these inadequacies imposed severe limitations on initial progress in the study. The implications of choosing alternative options in the modelling were not apparent and little help was given in the manuals to decide which might be the appropriate approach. Recourse to the FORTRAN coding sequences was frequently necessary; this proved a laborious and inefficient method of problem-solving. It is perhaps difficult, with such a complex package as PHOENICS, to provide an easy introduction for a first-time user but revision of the documentation would be beneficial.

7.6.1 Grid Details

The models used the *body-fitted coordinate* (BFC) system option in their grid definitions. The grid from which the predictions are presented is shown in Fig. 7.11. Variations on the grid definition and the number of iterations were performed as for the sudden expansion to check model convergence.

The final form of the BFC grid for the Coanda flare comprised:-

14 cells were spaced at 10° intervals around the Coanda beyond 100°.

29 cells emanated radially with their spacing varying exponentially. Different formulations were necessary to produce the curved and flat sections. This resulted in a small discontinuity at 100°. It occurs at such a large distance from the wall as to have no effect upon the jet calculations.

Fig. 7.11 also shows a section in the X-Y plane through the cells at the ninth slab. This shows the small wedge shape produced to account for the divergence of the Coanda structure.

7.6.2 Boundary Conditions

The library cases studied for guidance in establishing appropriate boundary conditions were the Wall Jet (parabolic k-ε model), Free Jet (parabolic mixing-length model) and the Boundary-Layer Flat Plate (parabolic M-L model).

Nozzle conditions were simulated by taking the jet as issuing from a slot of width 5mm. This was treated as a fixed mass inflow boundary. Uniform values of streamline velocity were input, set to the LDA slot measurement value. The fixed flux situation was indicated by setting the pressure source to the appropriate value of mass flow/unit area.

The remainder of the inlet plane and the free, outer edge of the jet were treated as fixed external pressure boundaries. An in/outflow boundary condition was used to describe the streamline velocity at the outer edge of the jet.

The downstream exit boundary was specified as an outflow boundary. This was achieved by the appropriate allocation for the streamline velocity parameter. The pressure source was set to zero i.e. ambient conditions.

Conditions at the wall were input to give a skin-friction factor deduced from the log-law relationship.

7.6.3 k-ε Model

The version of the k-ε model outlined in section 7.5.3 was used directly without modification of the relevant subroutine coding by the user.

The flow situation required an elliptical form of solution technique to be used. Iterations continued until the solution was considered fully converged. This was adjudged from studying the values of the 'residuals' of the parameters. They are seen to decay, in a converging solution, with increasingly negligible change between iterations.

7.6.4 Mixing - Length Models

The flat plate wall jet library case was taken as a basis for modelling the Coanda flare situation. This was run as programmed, without modification. The basic mixing-length turbulence formulae programmed within the GROUND subroutine comprises the Escudier formulae, allowing the mixing - length multiplication constant to vary with distance out from a surface.

The next run used the same input file but modified the GROUND subroutine. This then contained the user's own programming for mixing-length formulation. The initial listing was identical to that used in the GROUND option and the results were scrutinized to ensure they were identical to those previously obtained.

Introducing the complexity of a BFC grid required additional modifications. Some pre-programmed subroutines were then unavailable and work was done to overcome these problems.

An unmodified mixing-length calculation subroutine was obtained for use with the Coanda BFC grid and appropriate boundary conditions. The programme steps are outlined in Figure 7.21. It was essentially a copy of the original calculations but introduced steps to reproduce the subroutines unavailable for BFC grids.

When this had been fully tested and the results ratified by some hand calculations, the modifications were introduced. The same modifications as used by Morrison (1982) for streamline curvature and divergence were used. Three separate solution files were produced and each run accessed its own special GROUND. As for the basic mixing-length calculation, programming was introduced into Group 9, Section 12 of GROUND. Steps 5 and 7 of Fig. 7.21 contain the additional calculations required to introduce the appropriate modifications to the basic mixing-length model. Limits were necessary for the calculation of Richardson number, Equation 7.3, since the correction factor becomes undefined at certain conditions (i.e. trying to take a square-root of a negative number). The divergence factor was also limited to range between 1.0 and 5.0; these limits were felt to be representative of the physical situation.

Separate runs were thus performed to study the effect of curvature and divergence terms individually. In the final GROUND file, it was assumed that their effects on the shear stress was additive and hence combined the two sources of extra rates of strain, as did Morrison (1982).

For any of the runs, no adjustments were made to the values of the constants in the law of the wall, for the effects of either streamline curvature or divergence. Calculation of jet width, for evaluating mixing-length values,

was defined as the distance from the wall to 99.5% of the jet velocity, no account being taken of the boundary layer segment of the jet profile.

Initial conditions for the variables were input from the basic mixing-length model's output. This should not change the final solutions but appeared to help convergence. The number of iterations was varied to ensure full convergence. Usually 100 iterations was sufficient to produce a converged solution, further iterations having negligible effect upon the predicted results.

7.6.5 Model Results & Discussion

Shown in Figs. 7.12-7.14 are comparative plots for predicted and measured values of velocities and turbulence data from the k-ε run. The data from all the mixing-length models are shown in Figs. 7.15-7.19. Velocity data are given in Figs. 7.15-7.16 and comparable mixing-length values are plotted in Fig. 7.19. PHOTON velocity plots are shown in Figs. 7.17-7.18, for all turbulence models.

The mean velocity profiles for the k-ε model, shown in Figs. 7.12, underestimate U/U_m near the velocity maximum. A peak which is too sharp is, therefore, given. The streamwise velocities show underprediction by the model of the velocity decay and jet width growth. The radial velocities shown in Fig. 7.13 illustrate the marked difference between measured and predicted profiles.

A representative selection of kinetic energy profiles are shown in Fig. 7.14. Comparison of the kinetic energy levels reveals the predictions to be four times lower than the measured values. The smallest discrepancy is at 90° where predictions are approximately 75% of the recorded values. The

PHOTON velocity plots illustrate changes in the jet development as the different turbulence models were introduced.

The basic mixing-length model is seen in Fig. 7.15 to produce predictions in closer agreement with the measurements than those from the k-ε model. The mixing-length model shows more realistic jet growth and velocity decay rates, by improving the initial jet acceleration and concommitant jet contraction. It does, however, fail to achieve close simulation of the jet development in its later stages.

The curvature and divergence terms were treated separately and then combined by simple addition. Morrison (1982) points out that this is unlikely to be realistic, except in cases of small extra rates of strain. The implication of such an assumption is that any interaction between the effects of the two extra rates of strain, present in reality, are not taken into account in this shear stress model. With a simple mixing-length model, however, further sophistication is probably not justifiable.

Examples of mixing-length values computed by the various models is shown in Fig. 7.19. They are of similar magnitude to the values derived from the measured data, shown non-dimensionally in Fig. 7.6.

The effects of the models are summarised by plots of jet growth rate and velocity decay rate in Fig. 7.20. The measurements are shown in addition to all the turbulence models investigated. The streamline curvature modifications made to the mixing-length model resulted in over-acceleration of the flow in the early stages of its development. Consequently, the jet growth rate is reduced. Divergence correction terms increase jet growth rate significantly by 20° and the velocity decay rate is too rapid in the early jet development stages.

The effect of the combination of streamline and divergence correction terms is also shown in Fig. 7.20. In the initial stages, the velocity decay is again too rapid and the growth rate too high. By 60°, predictions and measurements are fairly close. Beyond 90°, however, the predicted velocity decay has flattened off, as has the growth rate, providing inadequate matching to the measurements.

7.6.6 Conclusions

The modelling investigation advanced knowledge of PHOENICS and a selection of the available turbulence models. It proved the adequacy of PHOENICS predictions in turbulent flowfield modelling and indicated the potential advantages of further study.

Software changes precluded further investigations in this project but many interesting aspects of the flow modelling for the Coanda situation remain to be studied. Work could profitably be directed towards investigating a number of avenues :-

1. The latest version of PHOENICS is to be introduced and all runs need verification to this new standard.

2. The Coanda grid could be refined, especially in the initial jet development region. The predictions have indicated over-acceleration of the flow and this may well be improved by a much finer grid definition.

3. The assumptions made in the mixing-length models should be reviewed and refined.

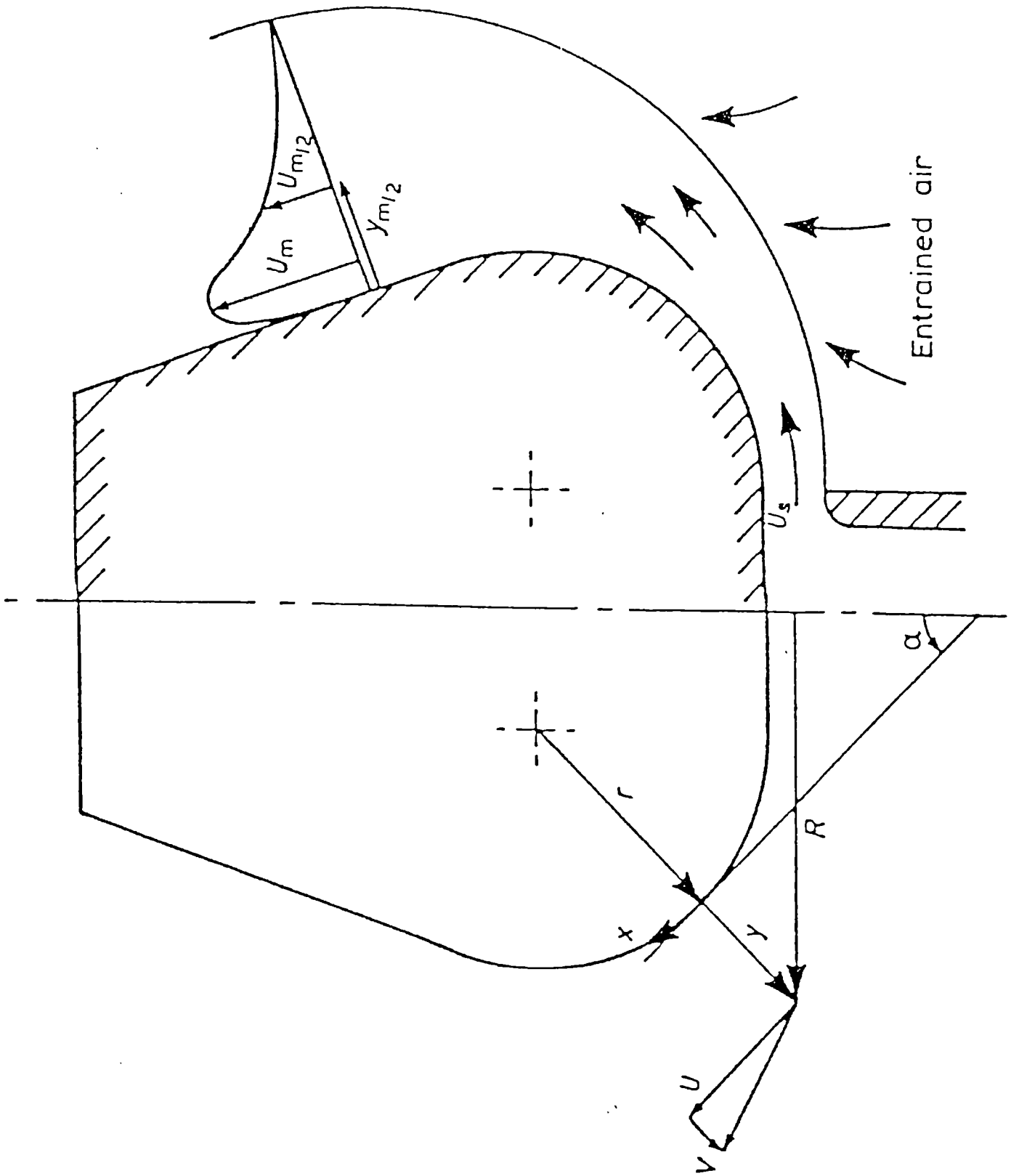

Fig. 7.1 Nomenclature

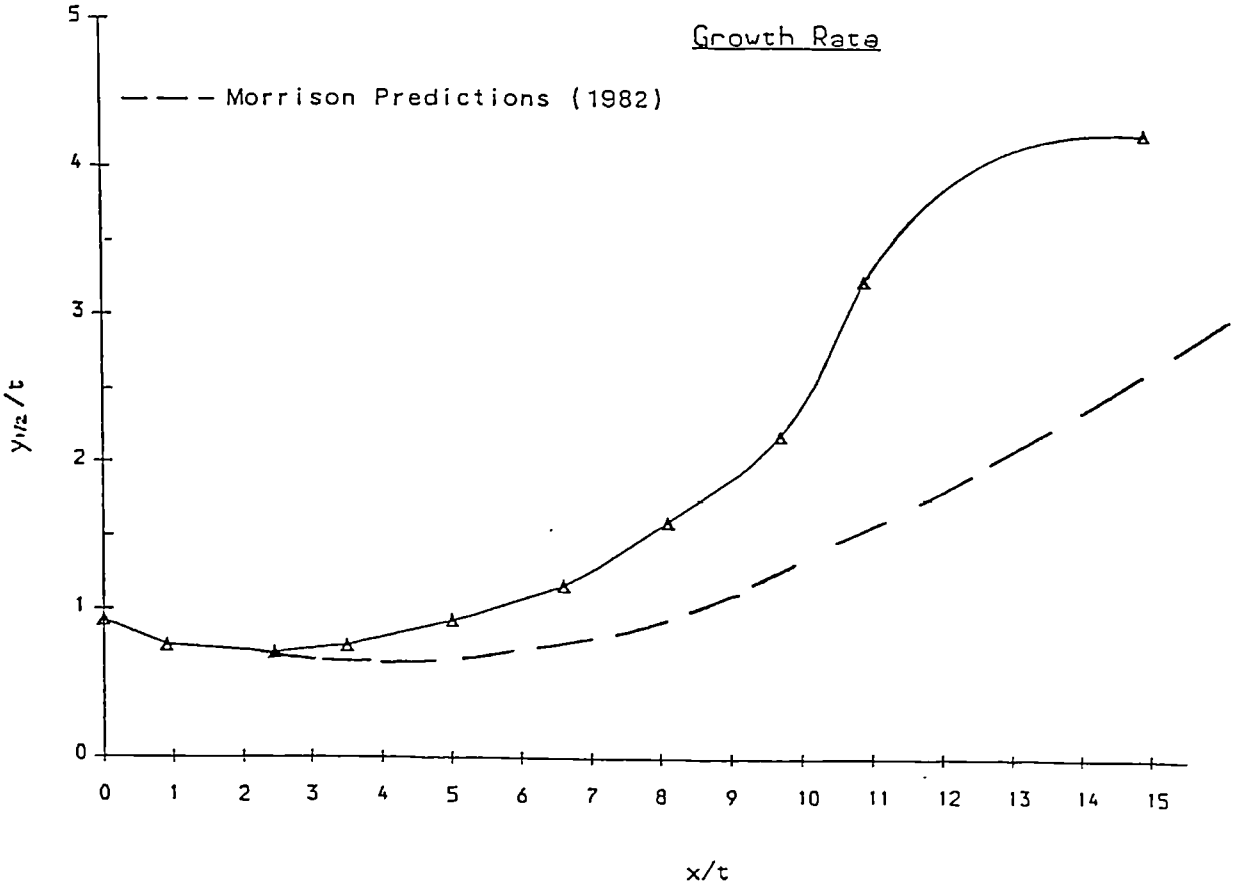

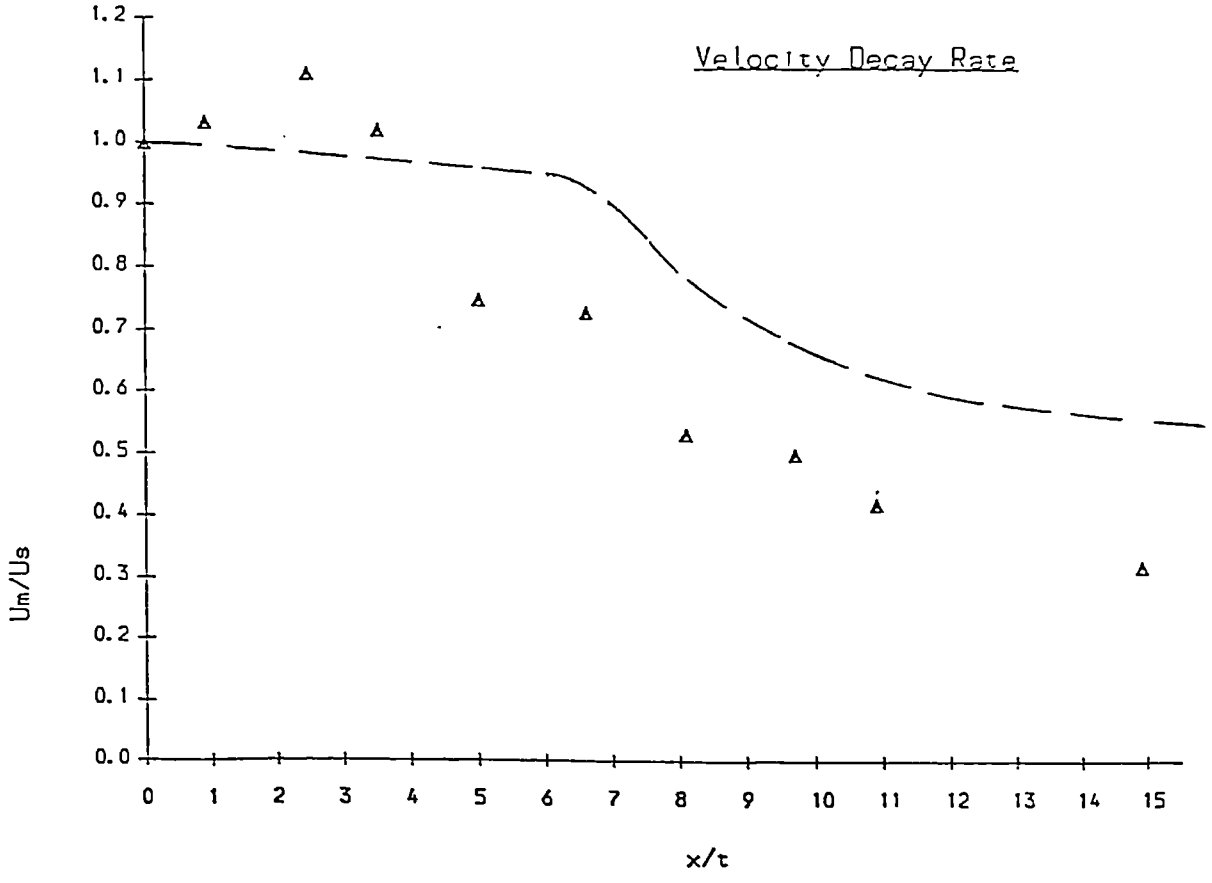

Fig. 7.2 Coanda Jet Growth & Velocity Decay Rates

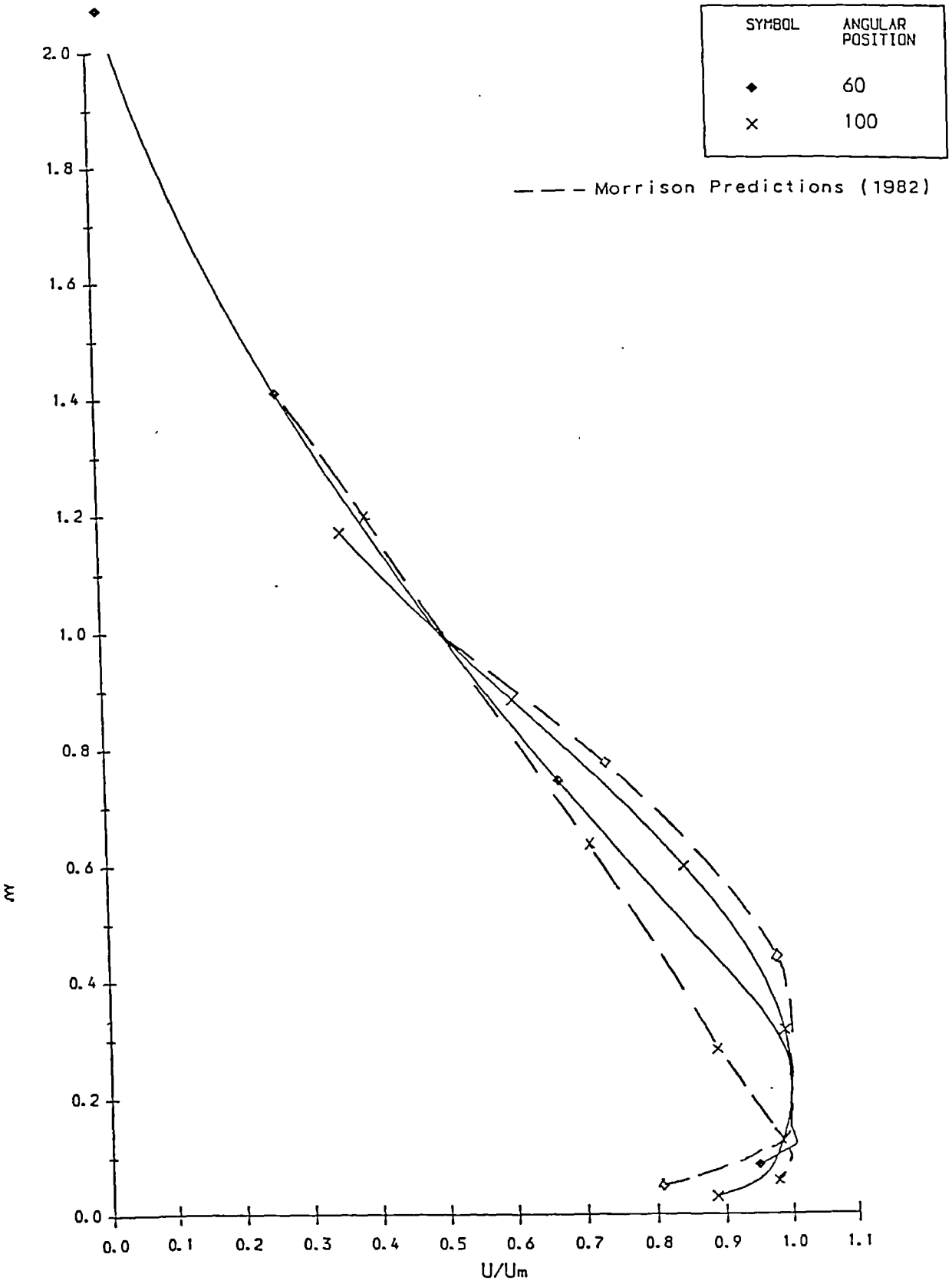

Fig. 7.3 U/Um vs. $y/y_{1/2}$

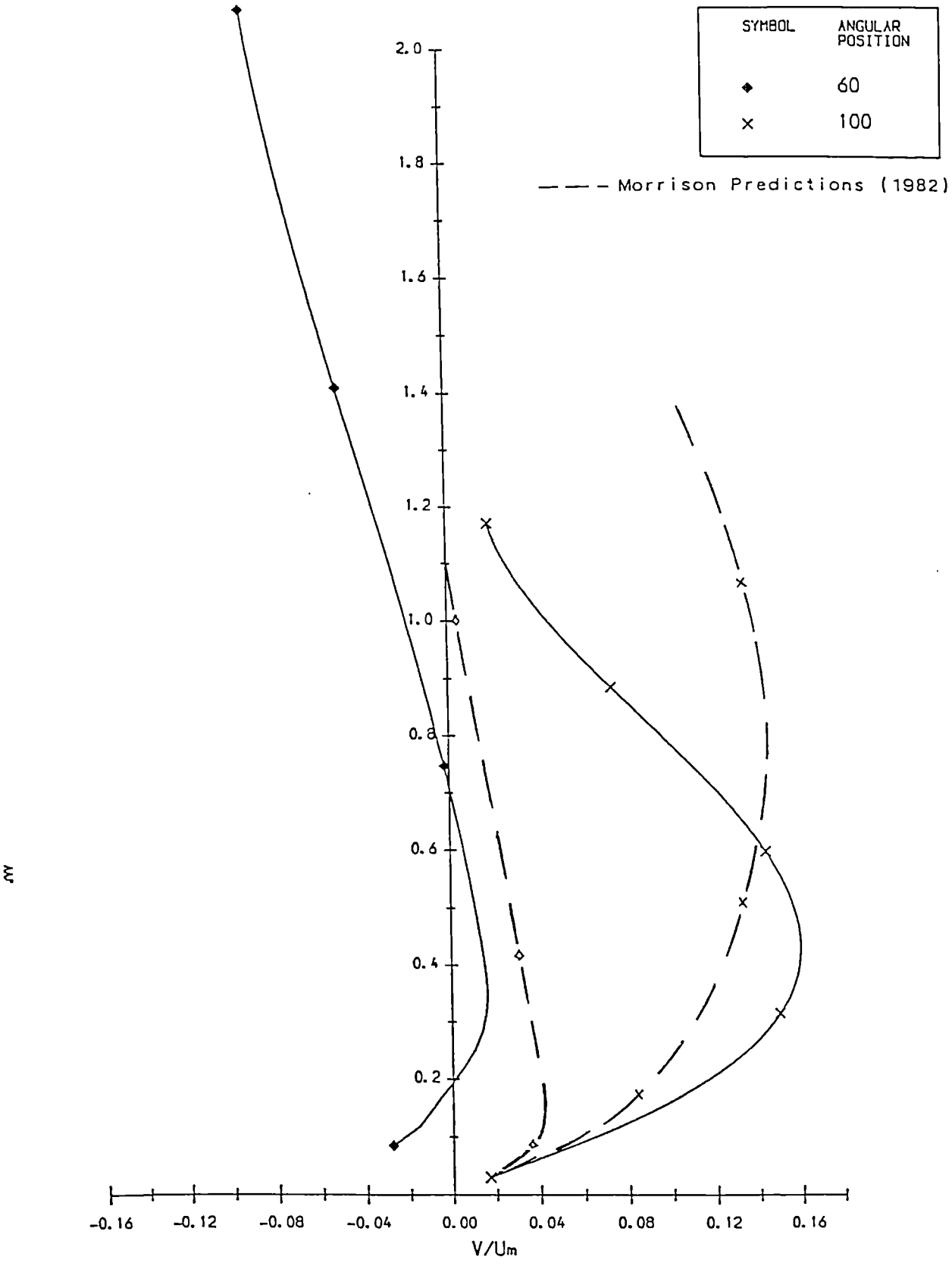

Fig. 7.4 V/Um vs. $y/y_{1/2}$

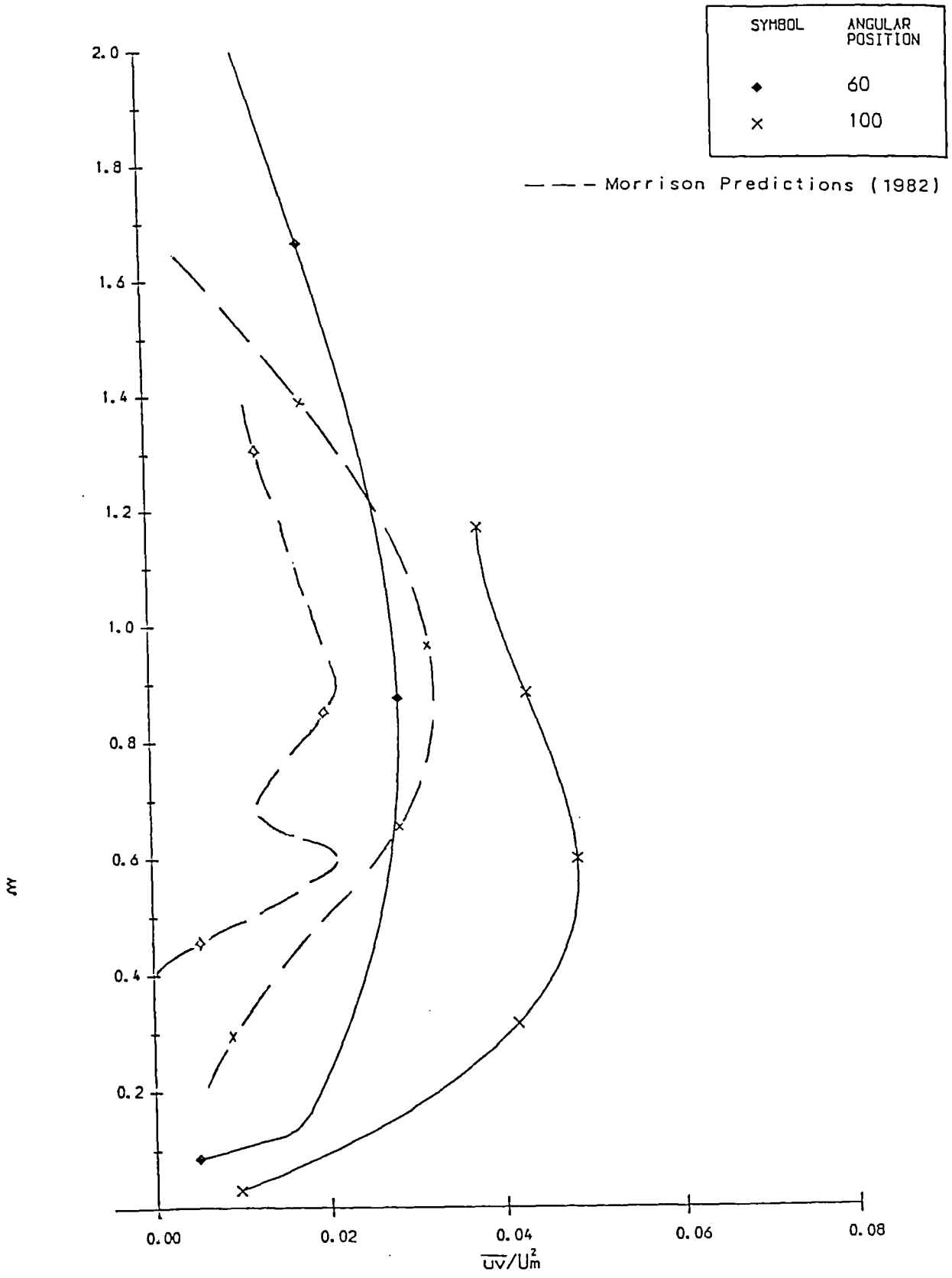

Fig. 7.5 Shear Stresses

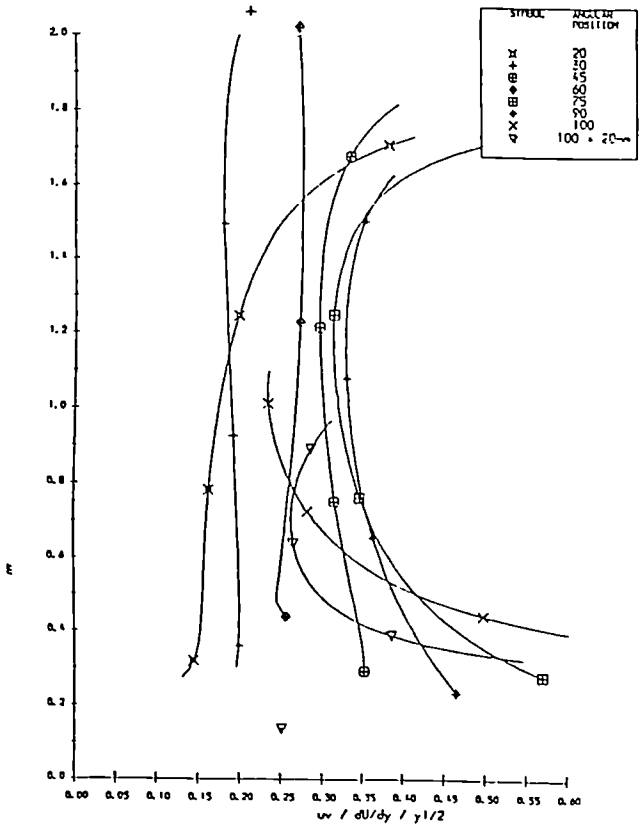

Mixing Length Values

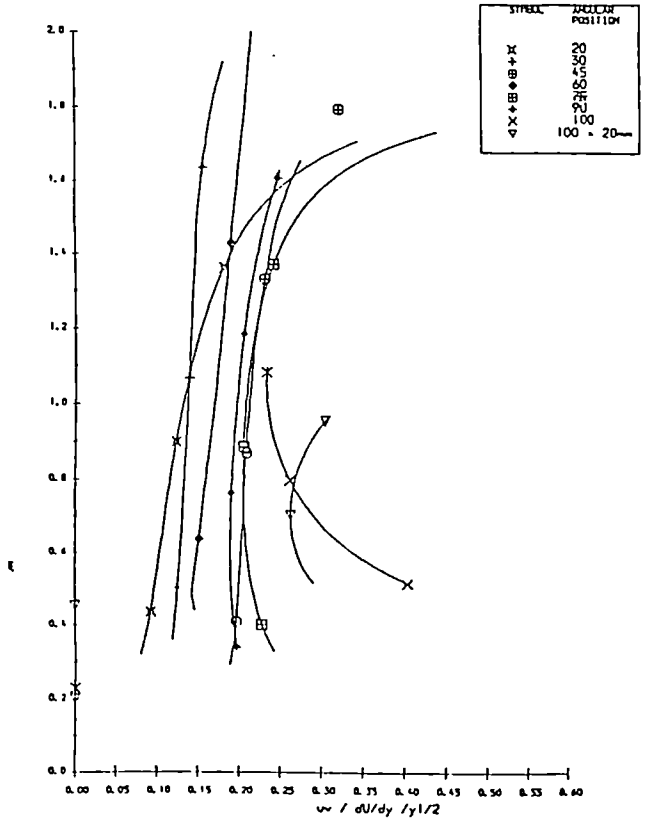

Mixing Length Values
Corrected For S/L Curvature

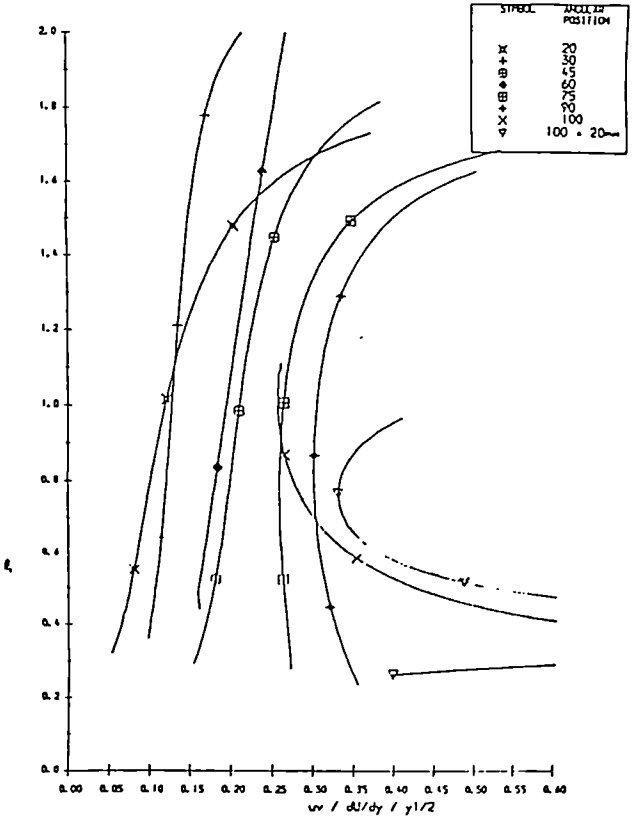

Mixing Length Values
Corrected For Divergence

Fig. 7.6

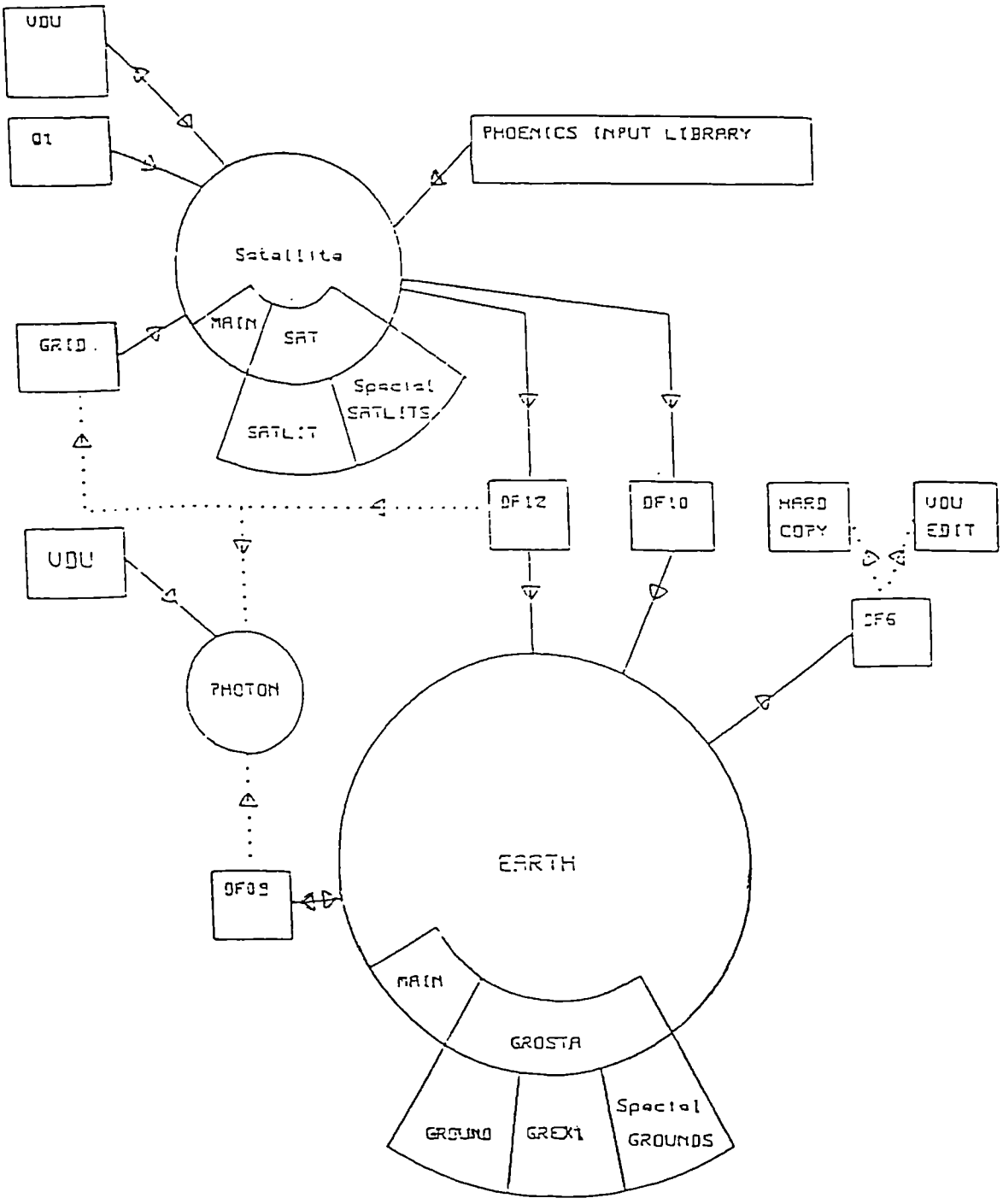

Fig. 7.7 PHOENICS Programme Organisation

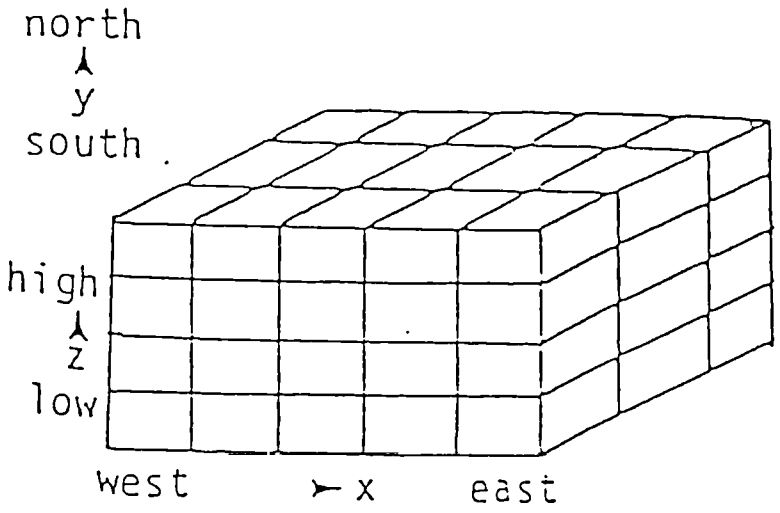

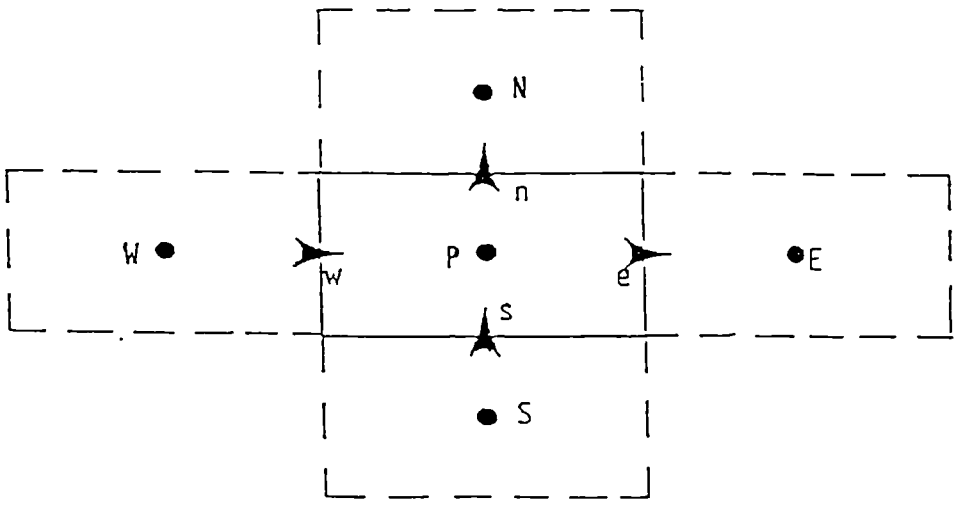

Fig. 7.8 PHOENICS Grid Cell Definitions

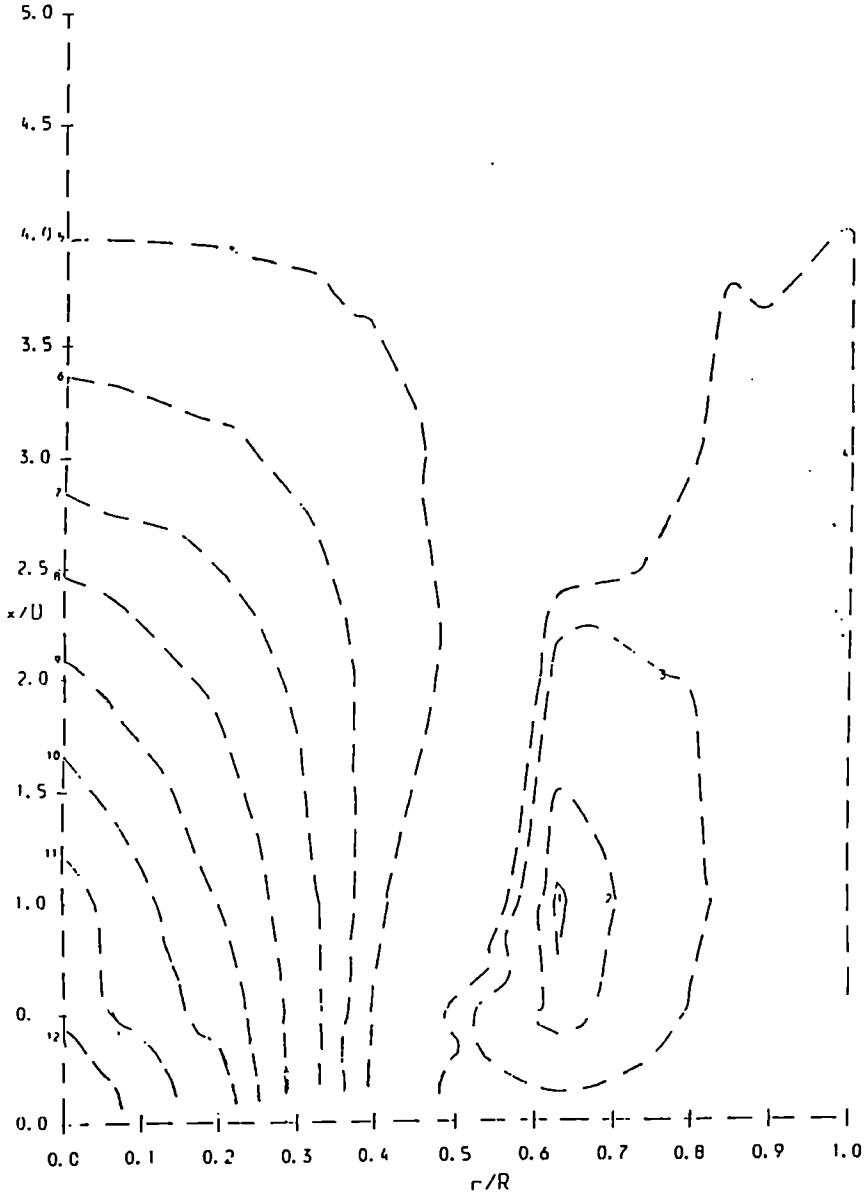

VELOCITY CONTOURS DOWNSTREAM OF EXPANSION - MEASUREMENTS

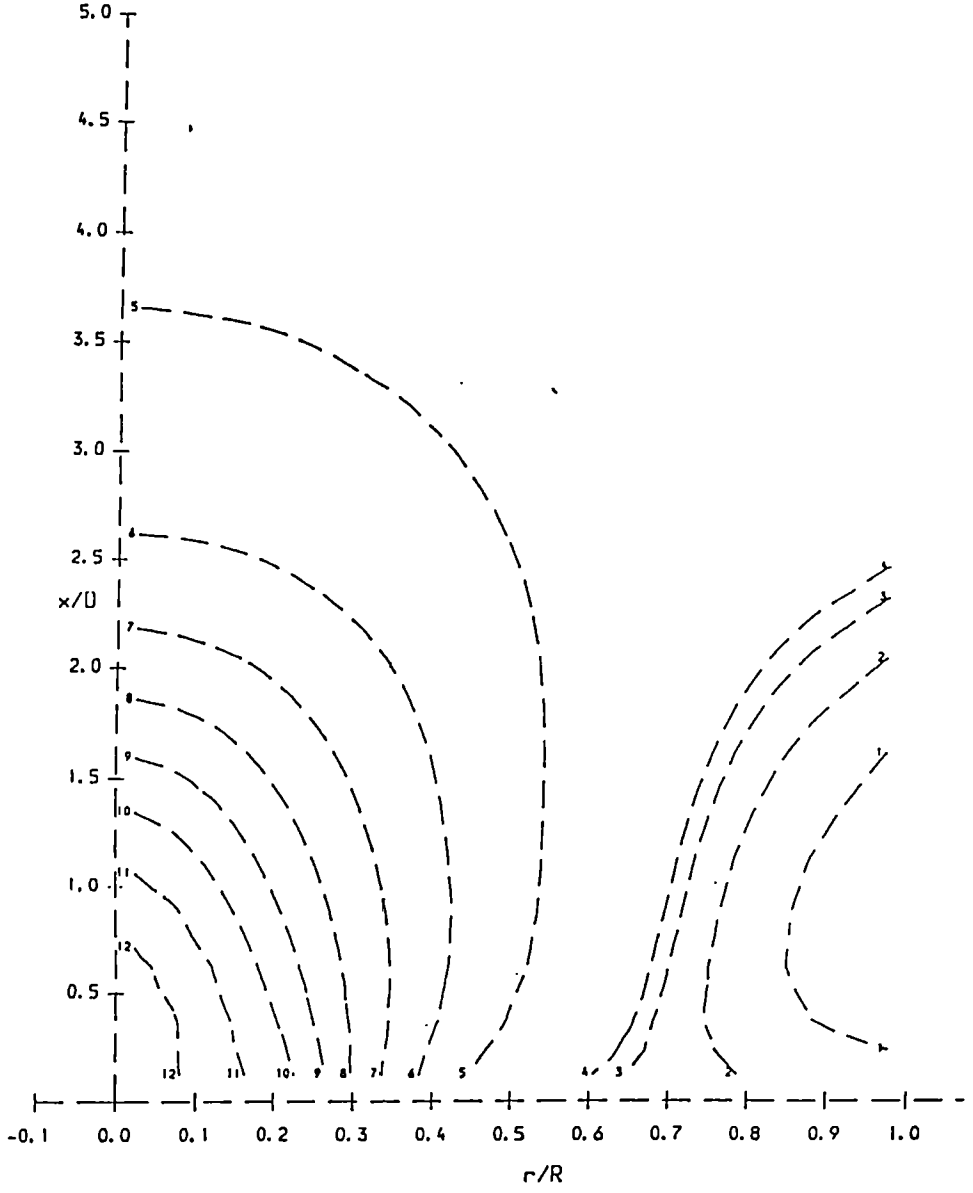

VELOCITY CONTOURS DOWNSTREAM OF EXPANSION - PHOENICS PREDICTI

Fig. 7.9

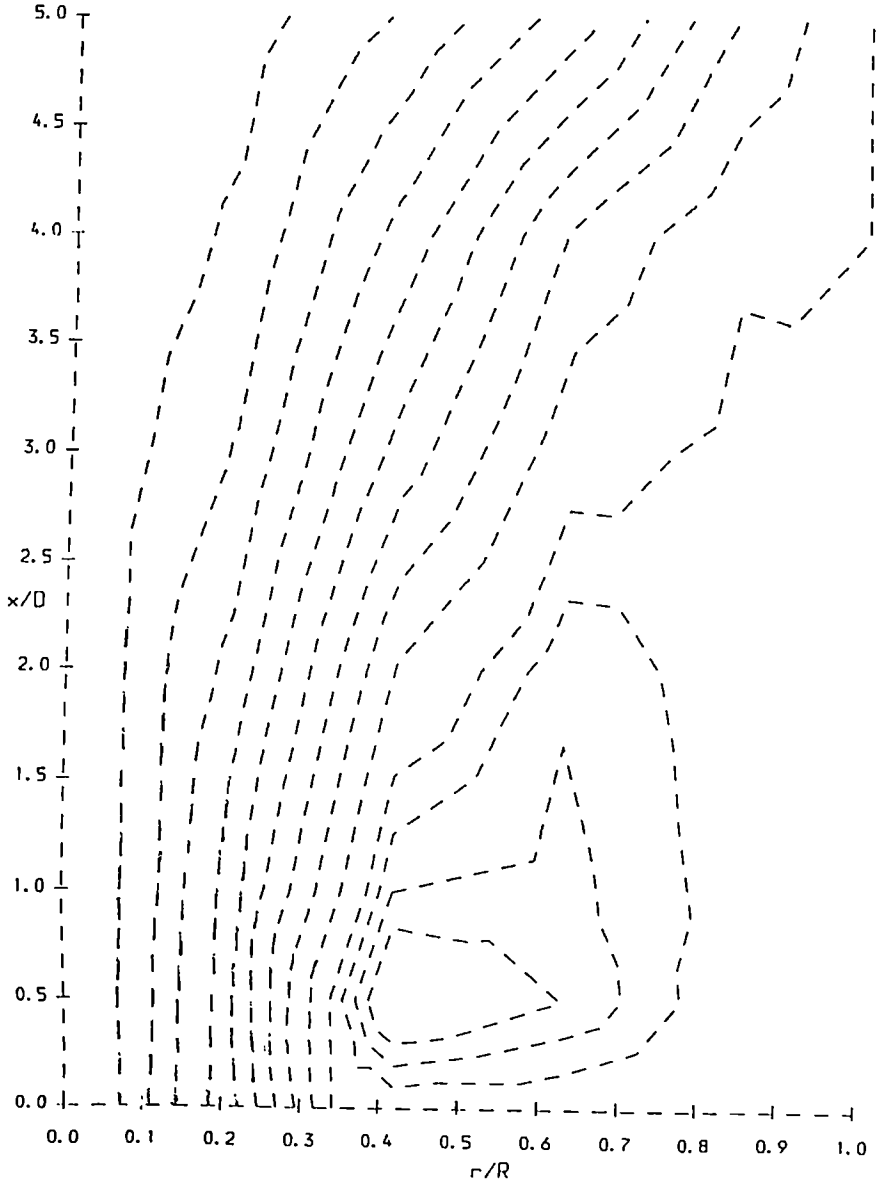

STREAMLINES DOWNSTREAM OF EXPANSION - MEASUREMENTS

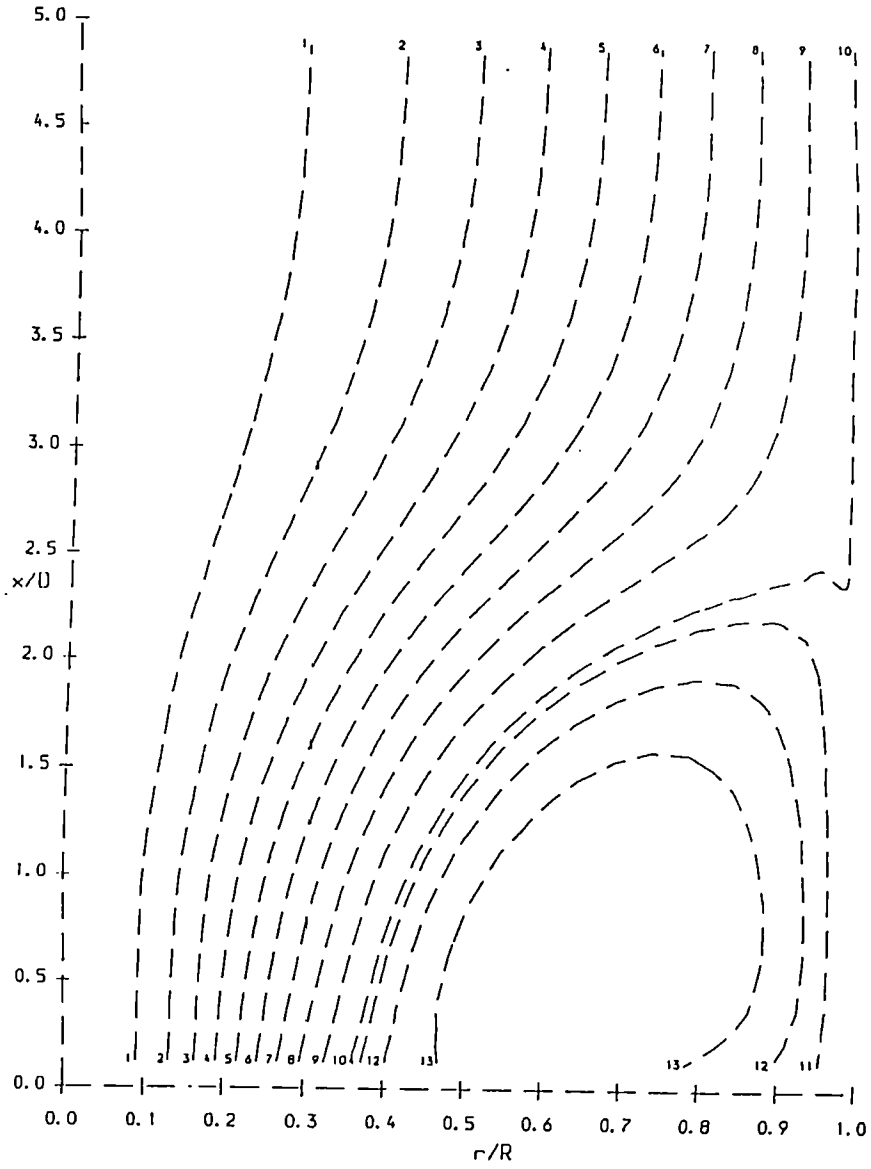

STREAMLINES DOWNSTREAM OF EXPANSION - PHOENICS PREDICTIONS

Fig. 7.10

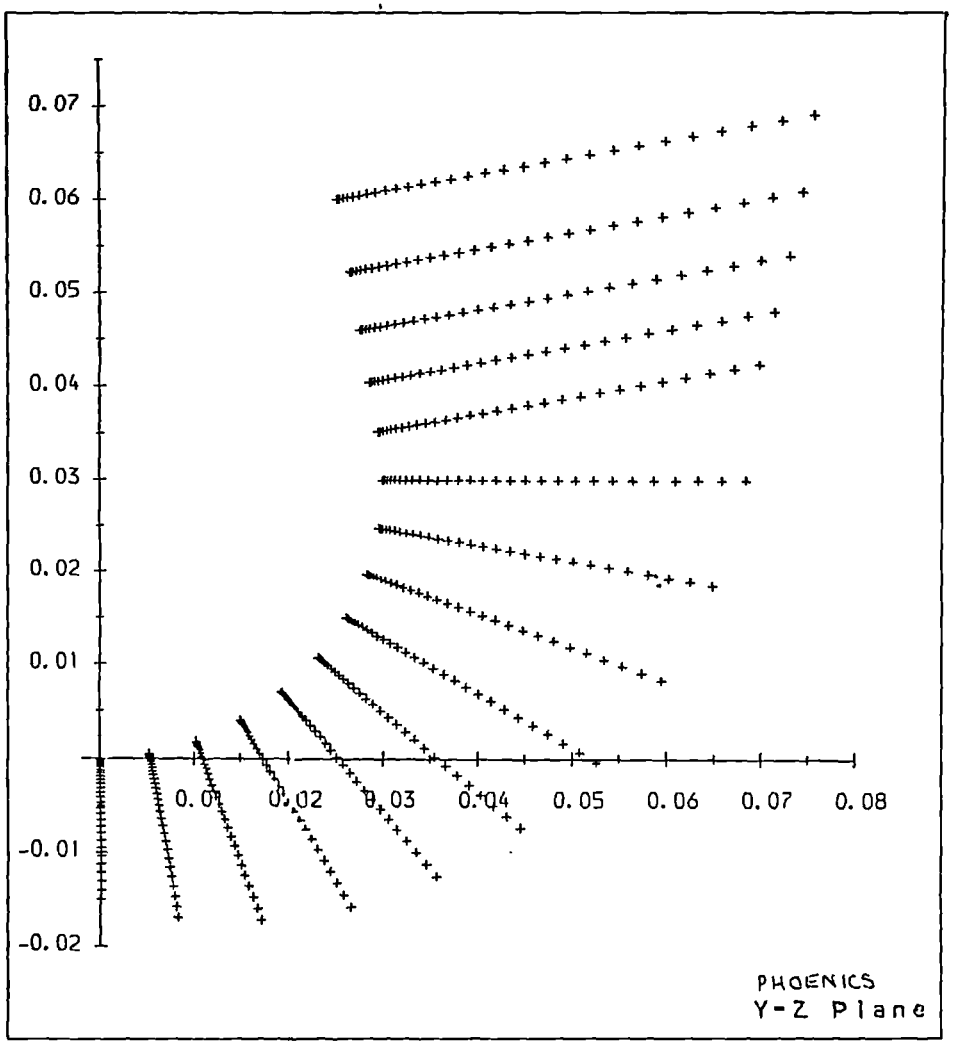

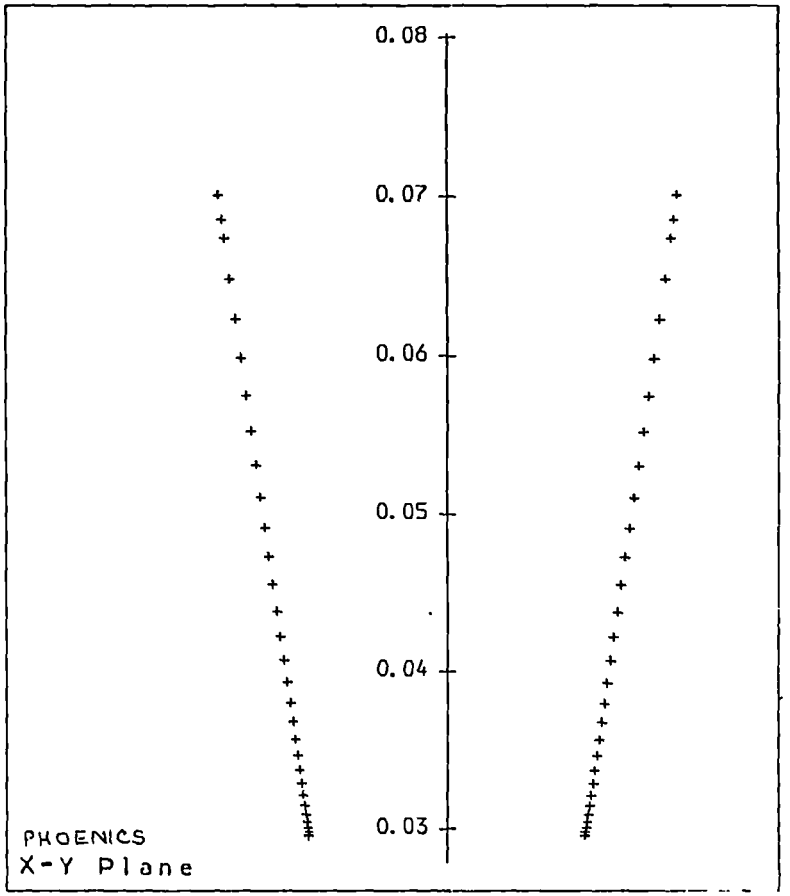

.Fig. 7.11 PHOENICS COANDA GRID

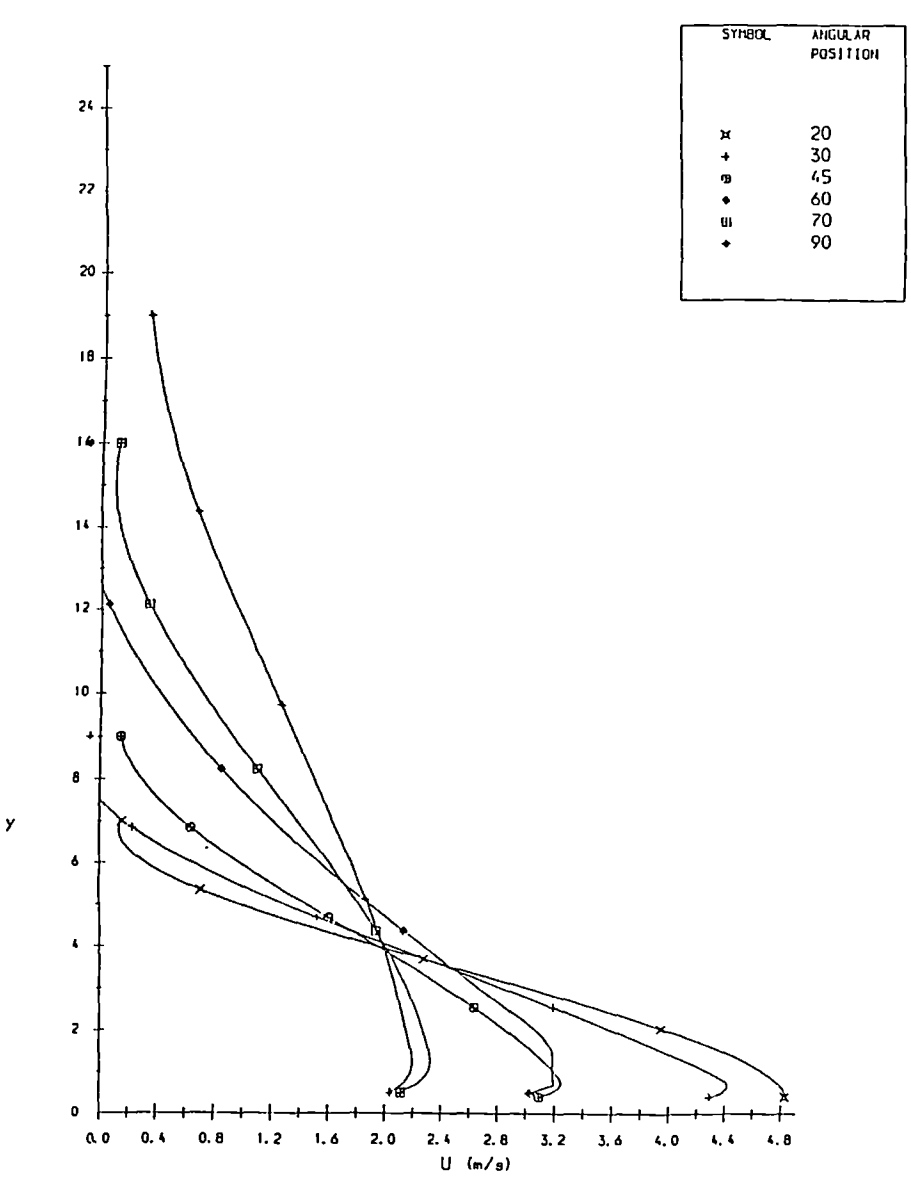

U vs. y

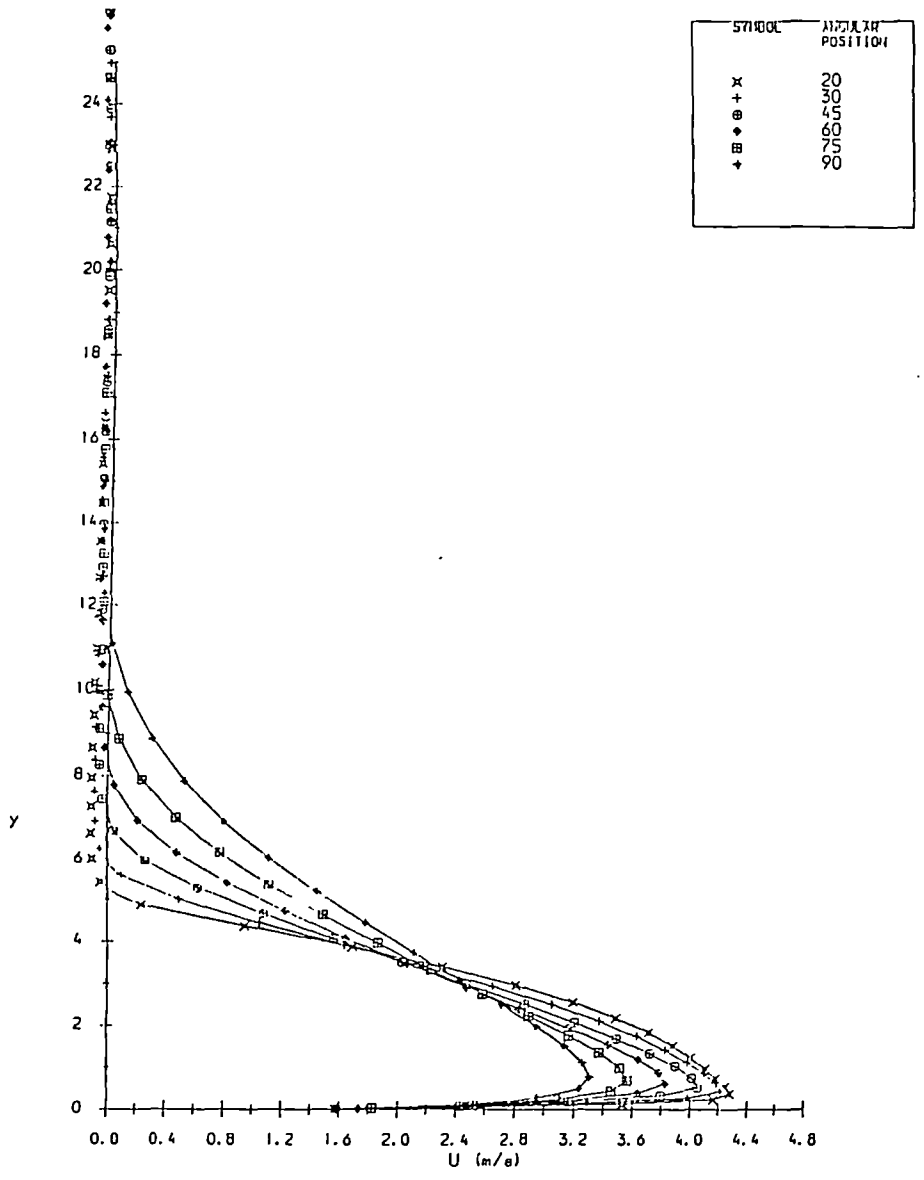

U vs. y - PHOENICS Predictions

Fig. 7.12

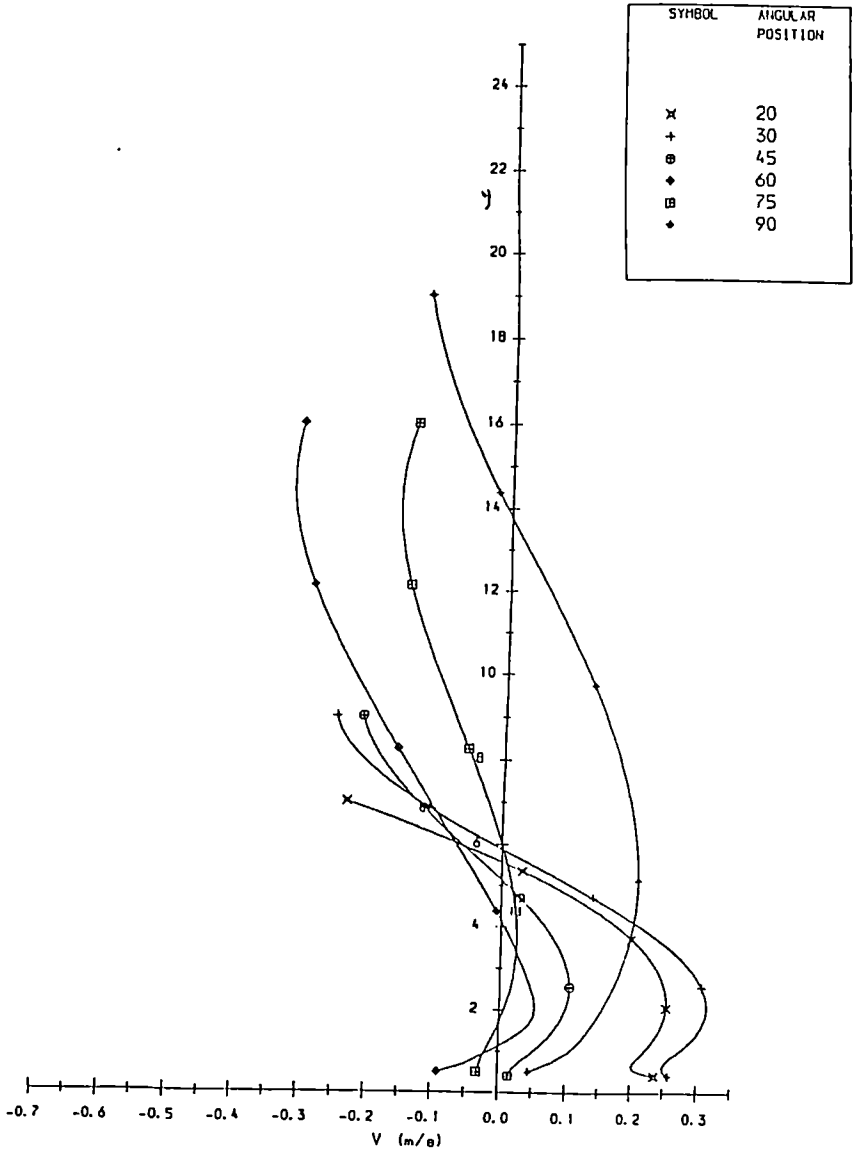

V vs. y

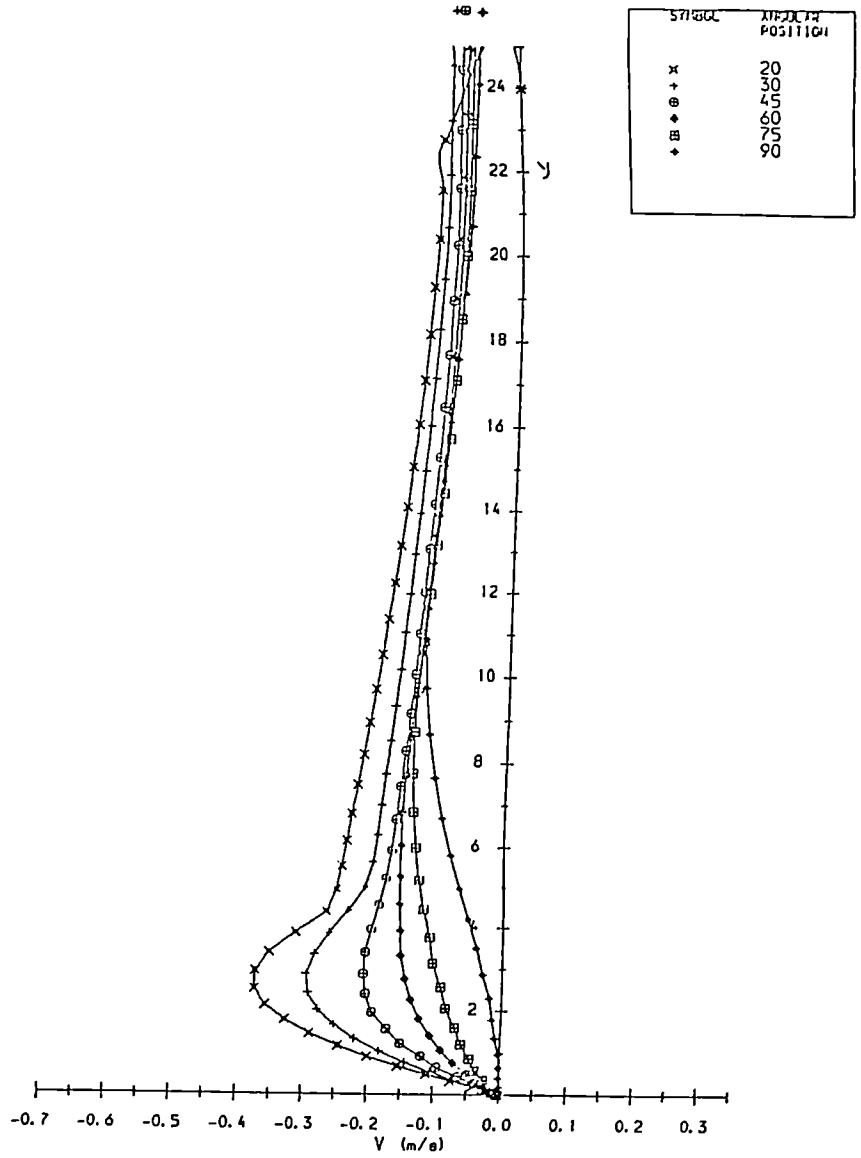

V vs. y - PHOENICS Predictions

Fig. 7.13

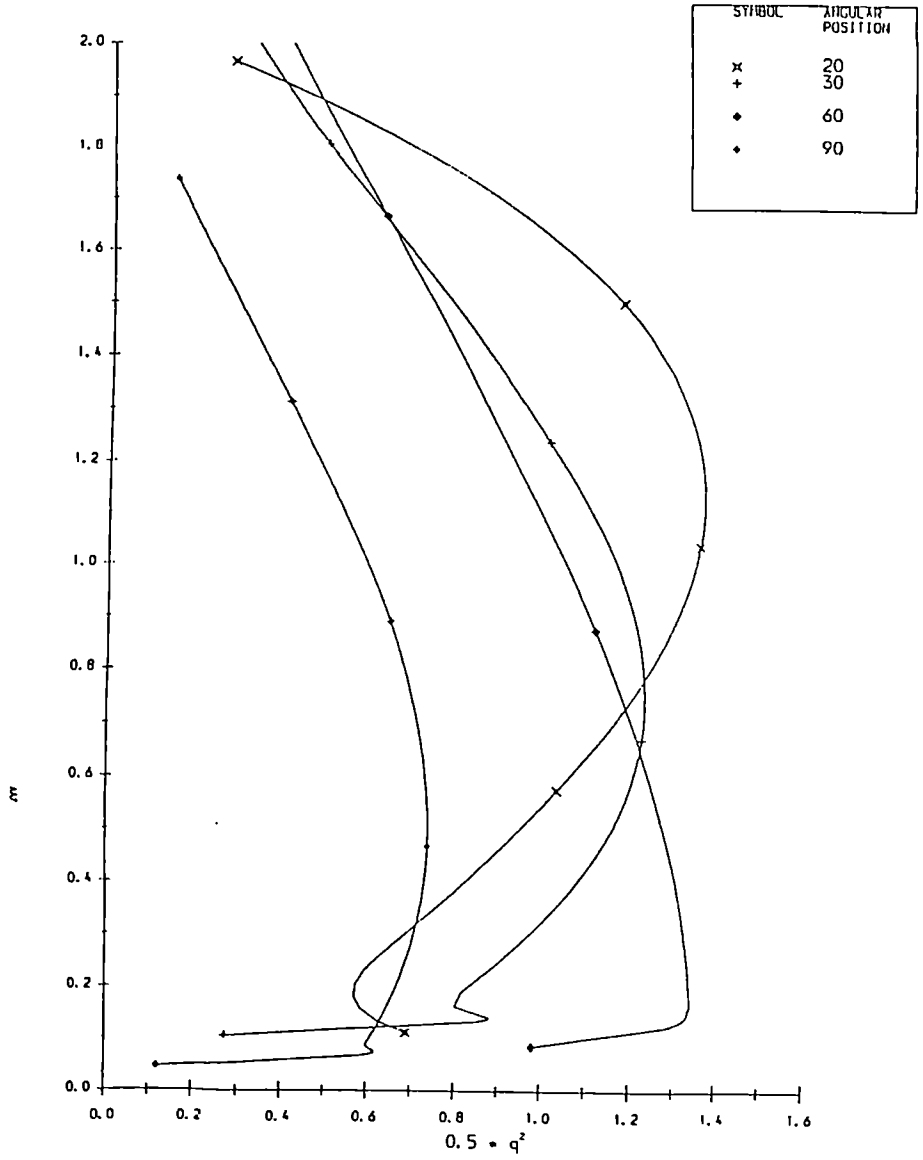

Kinetic Energy

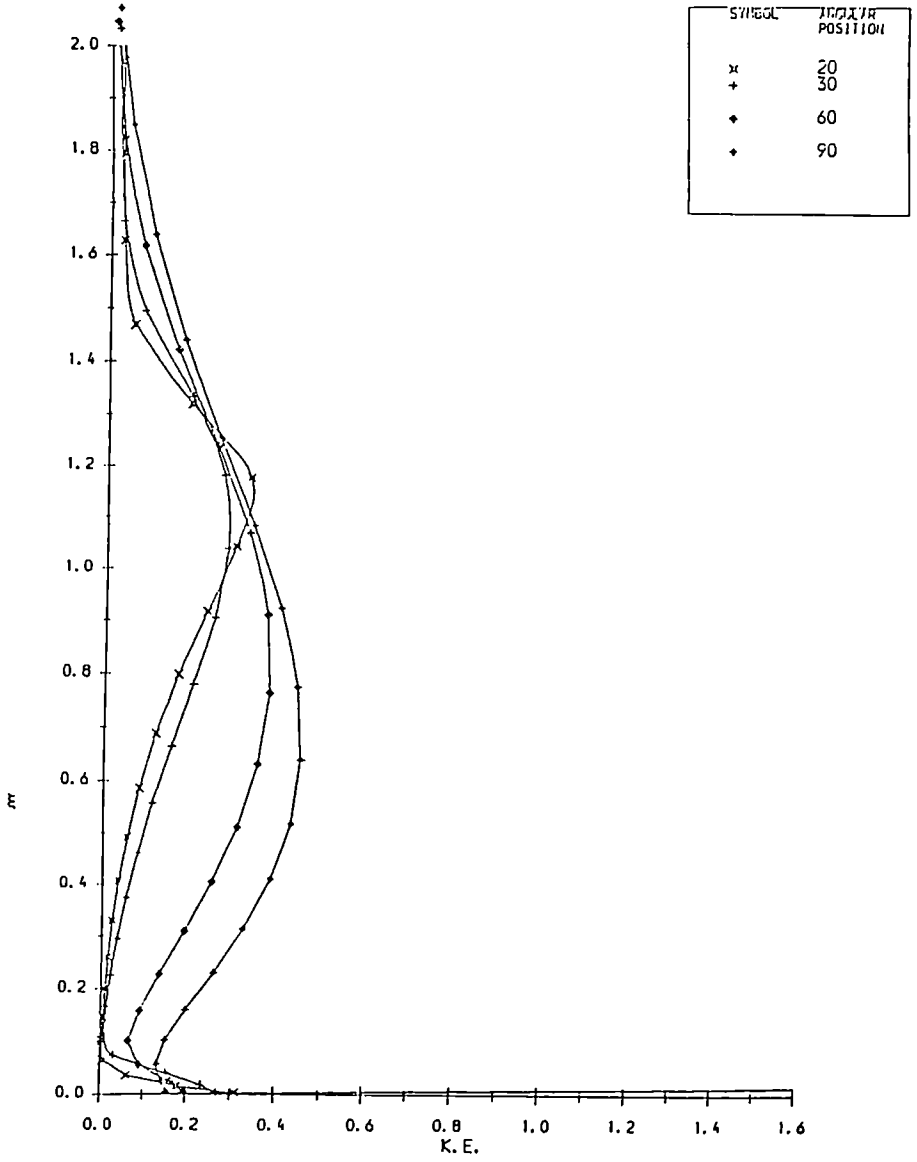

Kinetic Energy - PHOENICS Predictions

Fig. 7.14

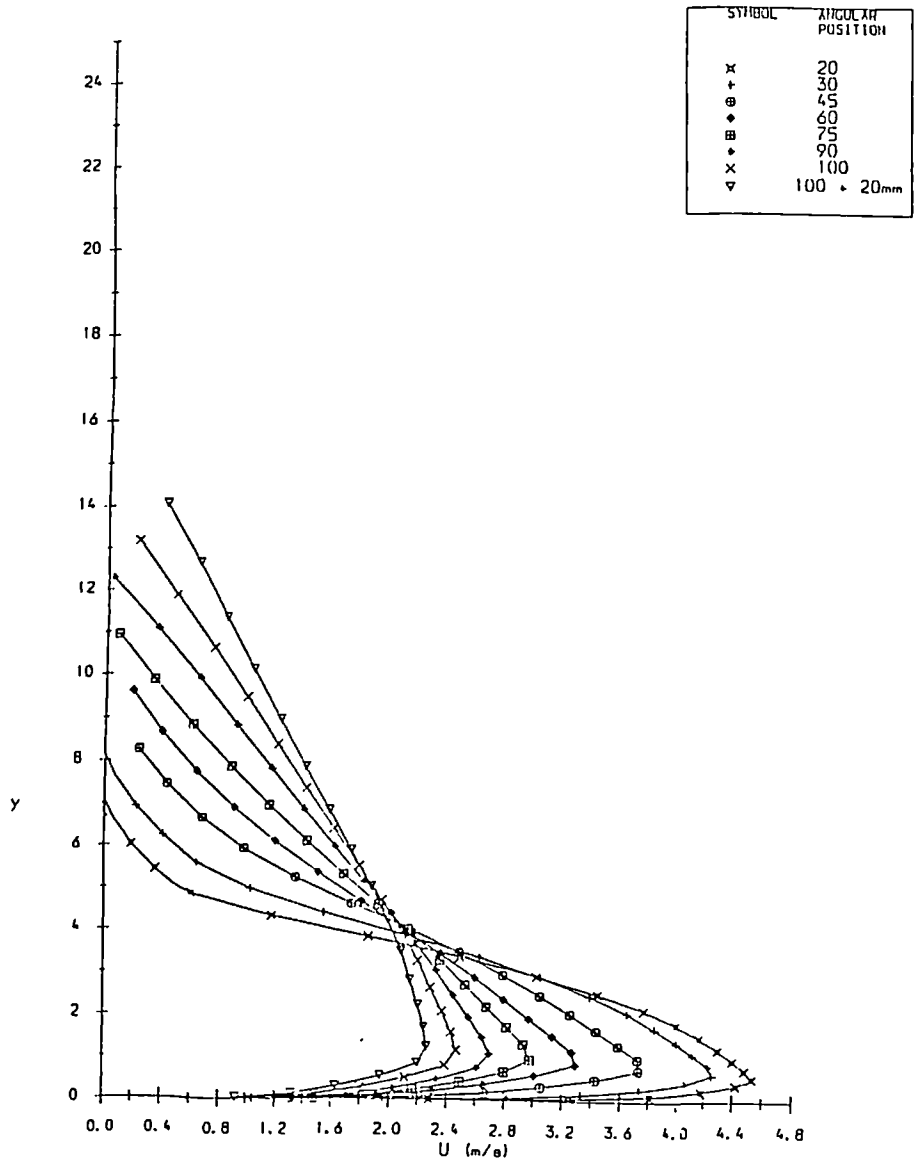

U vs. y - PHOENICS Predictions
Mixing Length Model

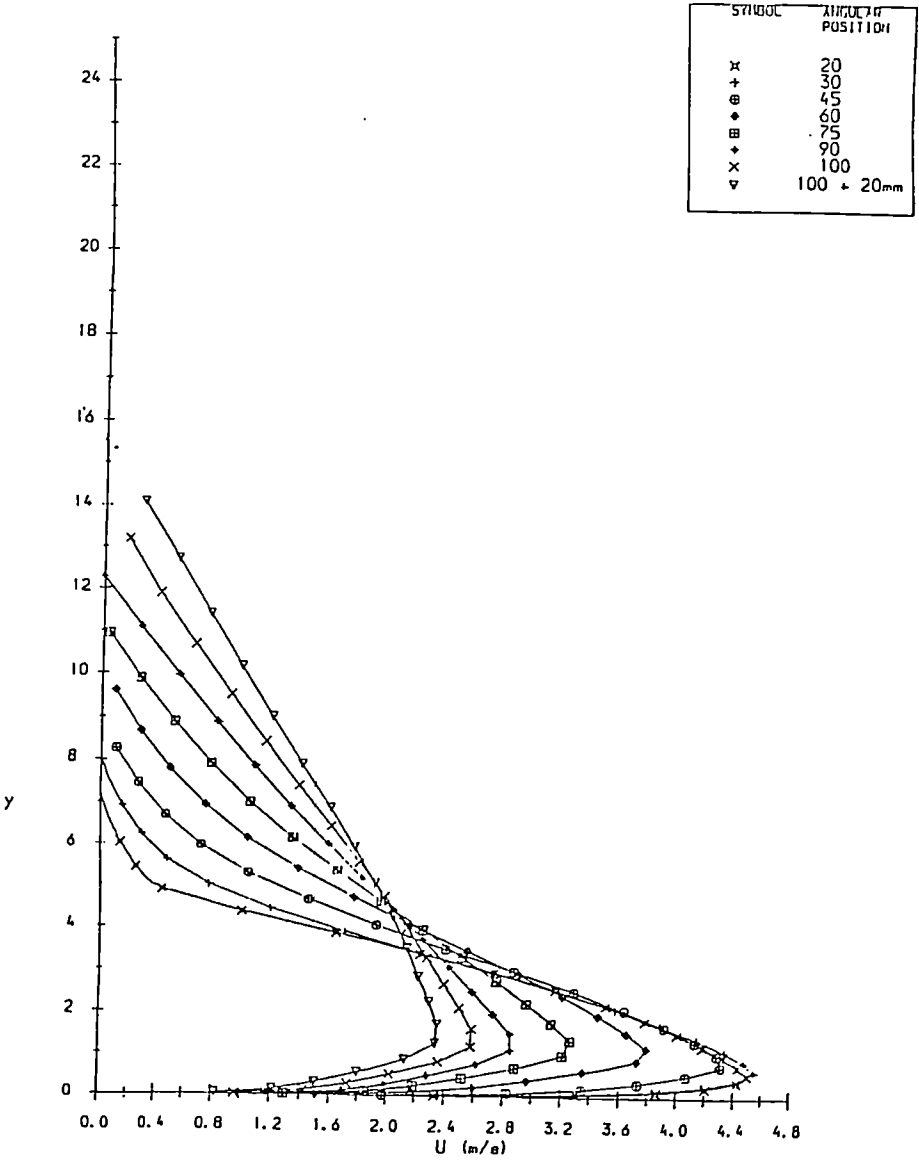

U vs. y - PHOENICS Predictions
M-L S/L C. Mods.

Fig. 7.15

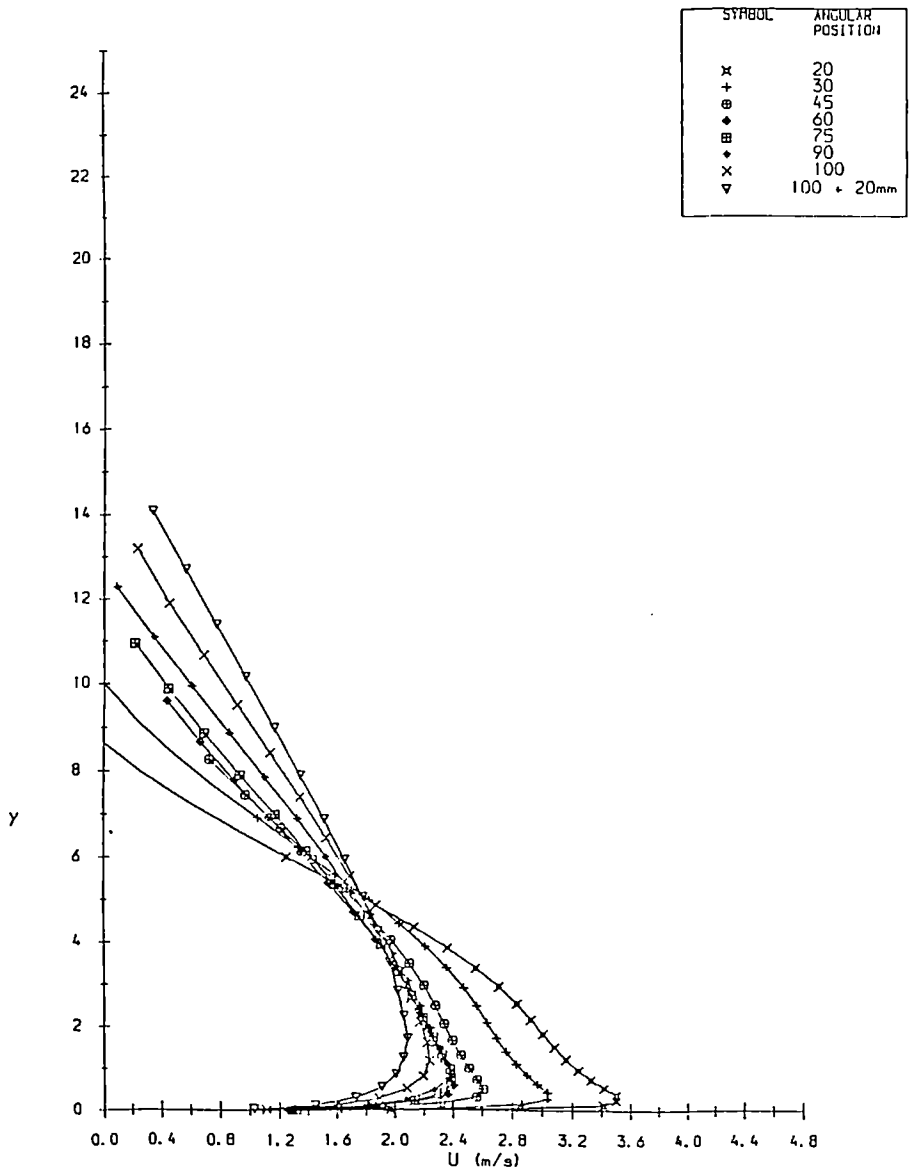

U vs. y - PHOENICS Predictions
M-L - Div. Mods.

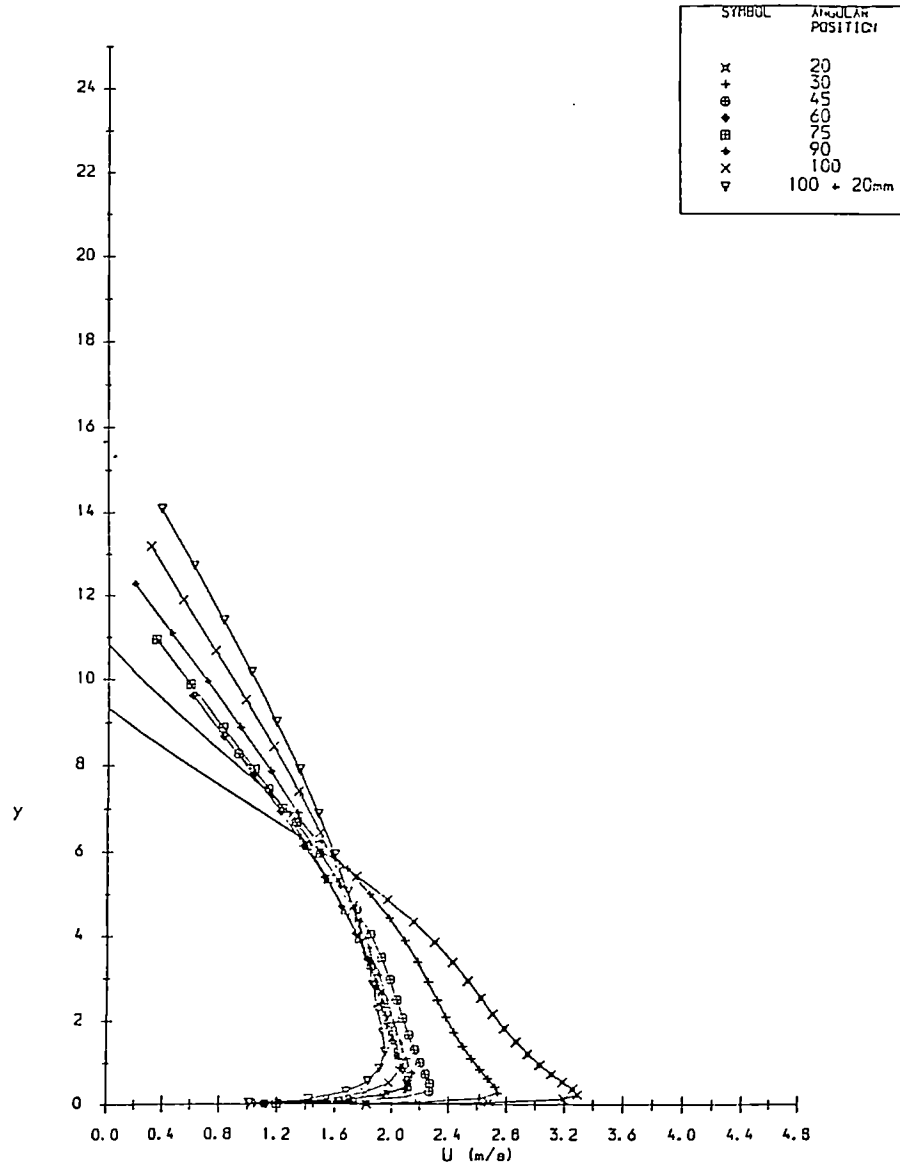

U vs. y - PHOENICS Predictions
M-L - S/L C. & DIV.

Fig. 7.16

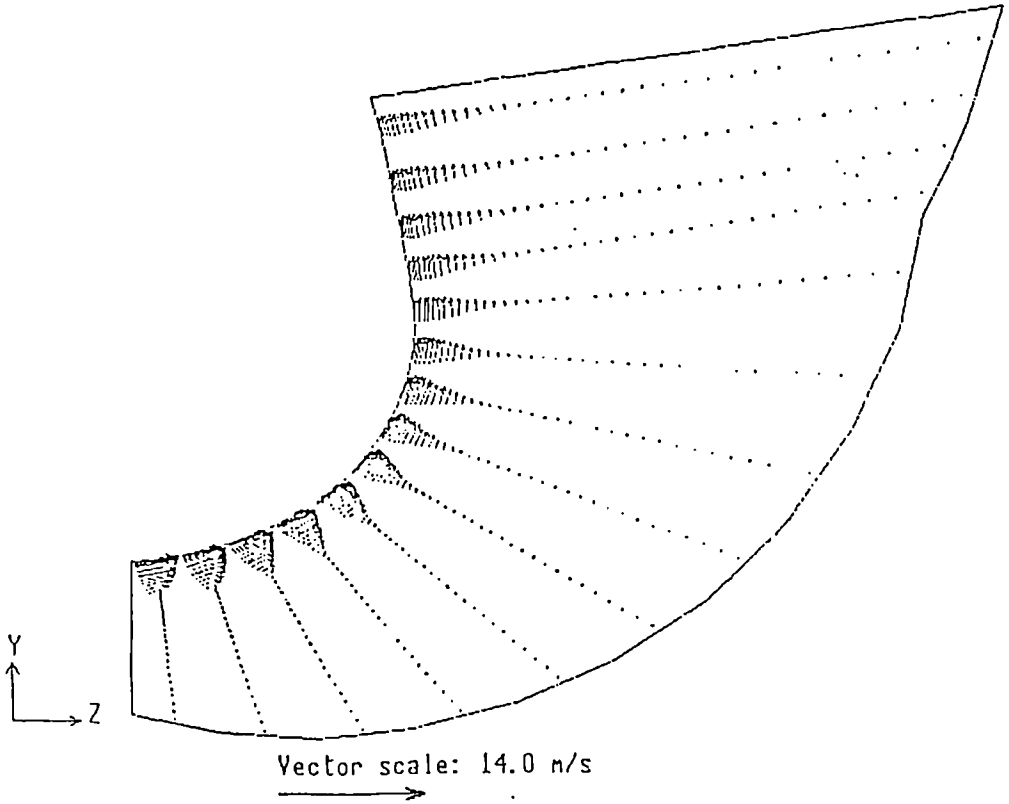

K-ε Model Predictions

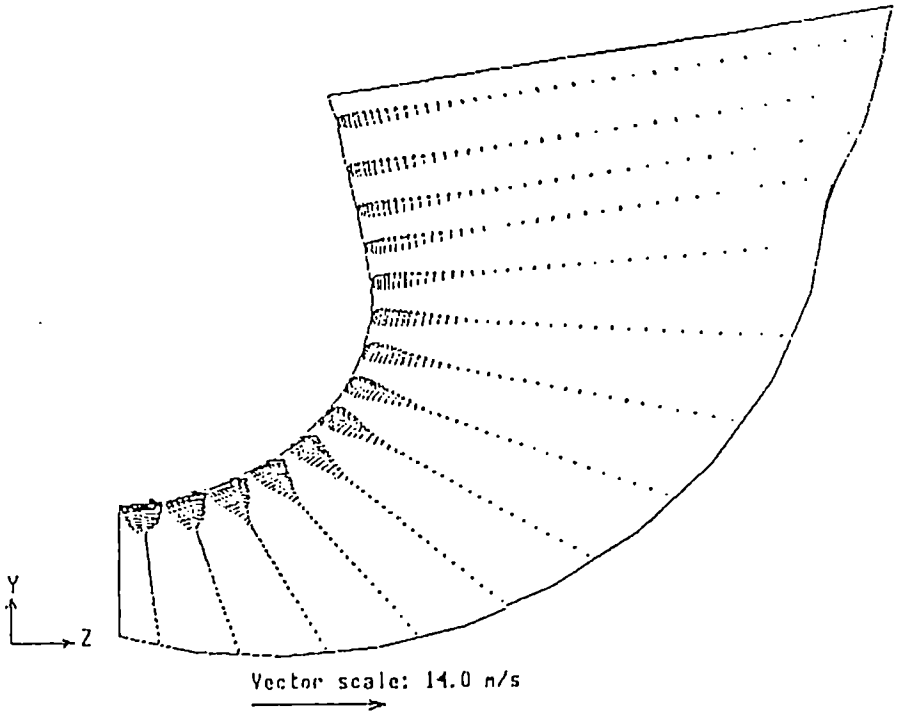

Basic Mixing Length Predictions

Fig. 7.17 PHOTON Velocity PLots

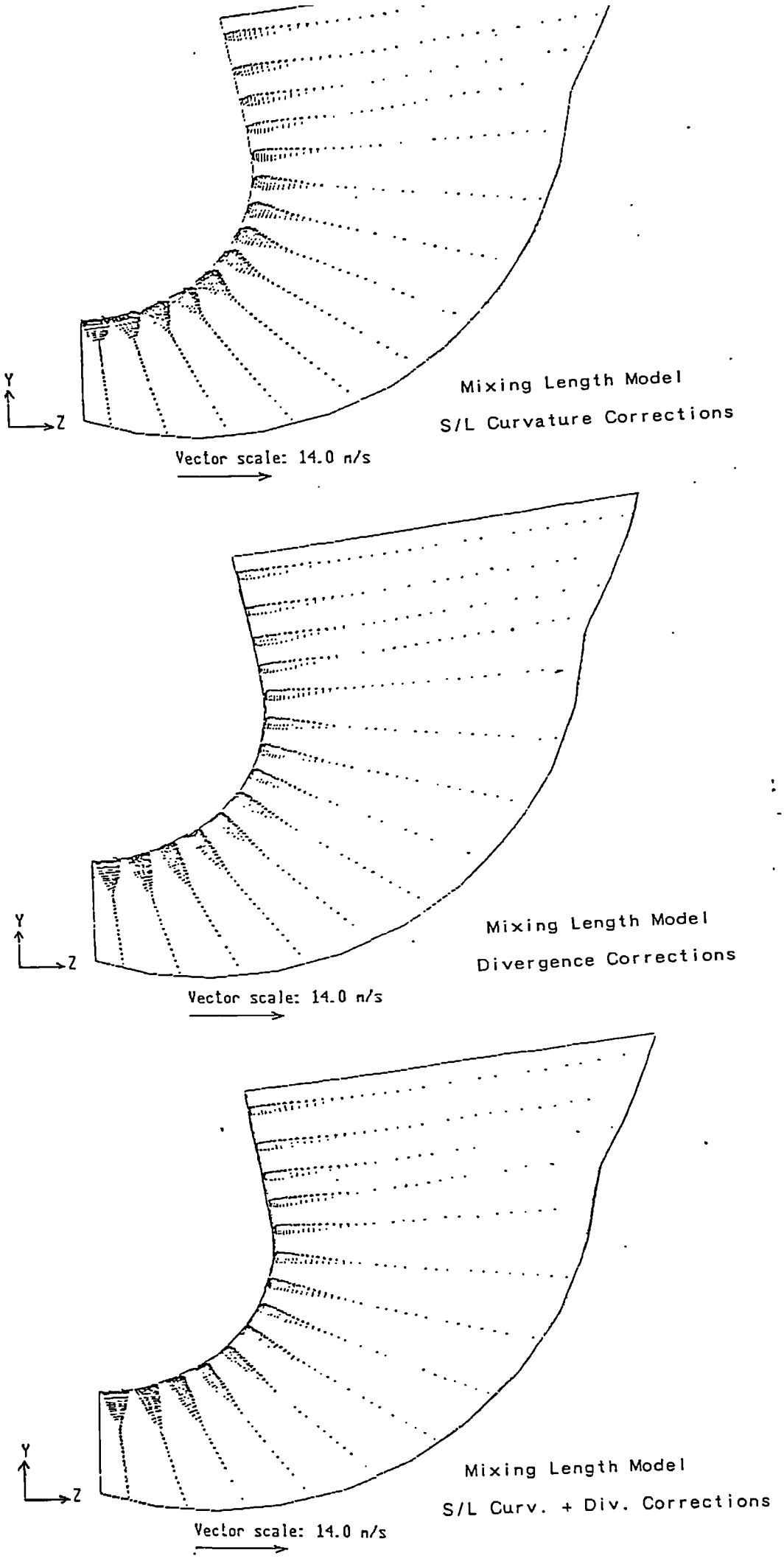

Fig. 7.18 PHOTON Velocity Plots - Mixing Length Models

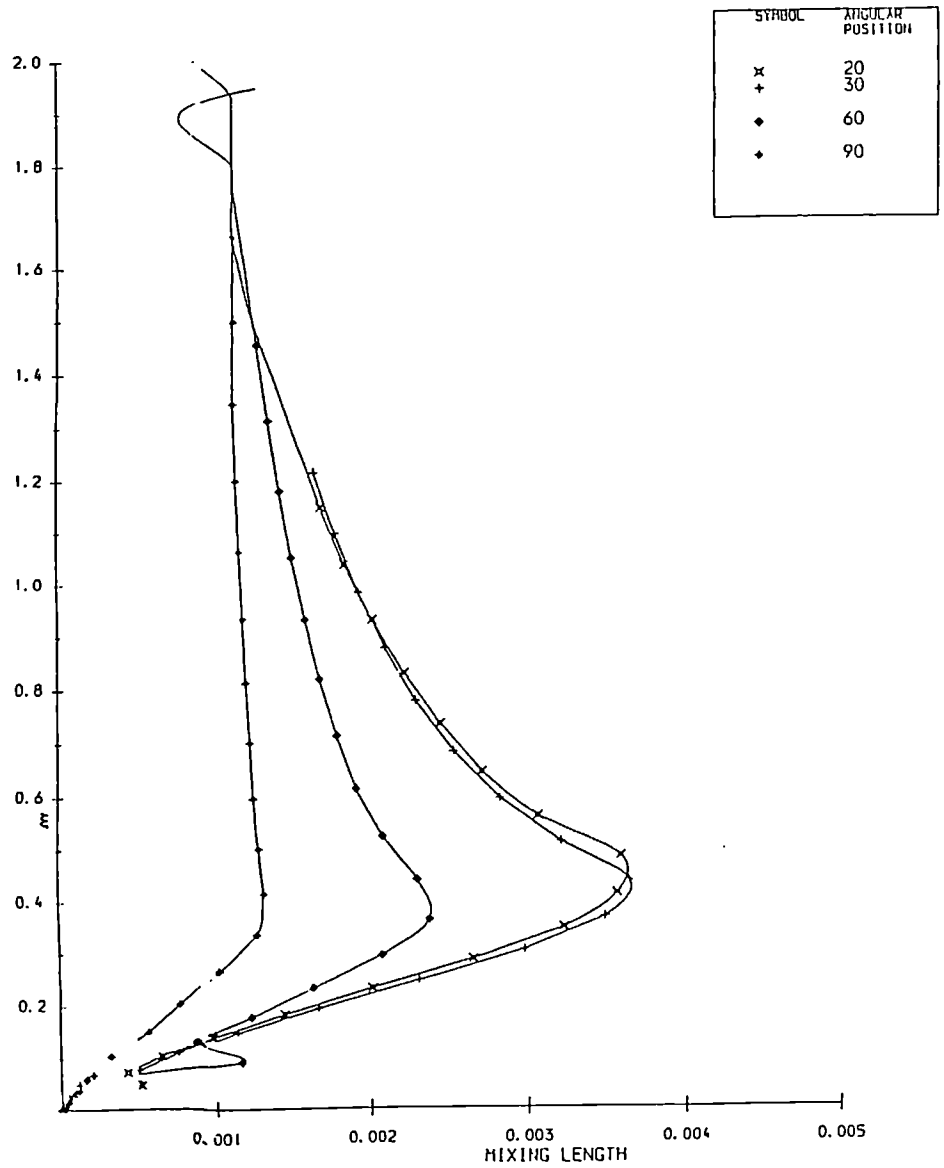

Mixing Lengths - PHOENICS Predictions
M-L - Div. Mods.

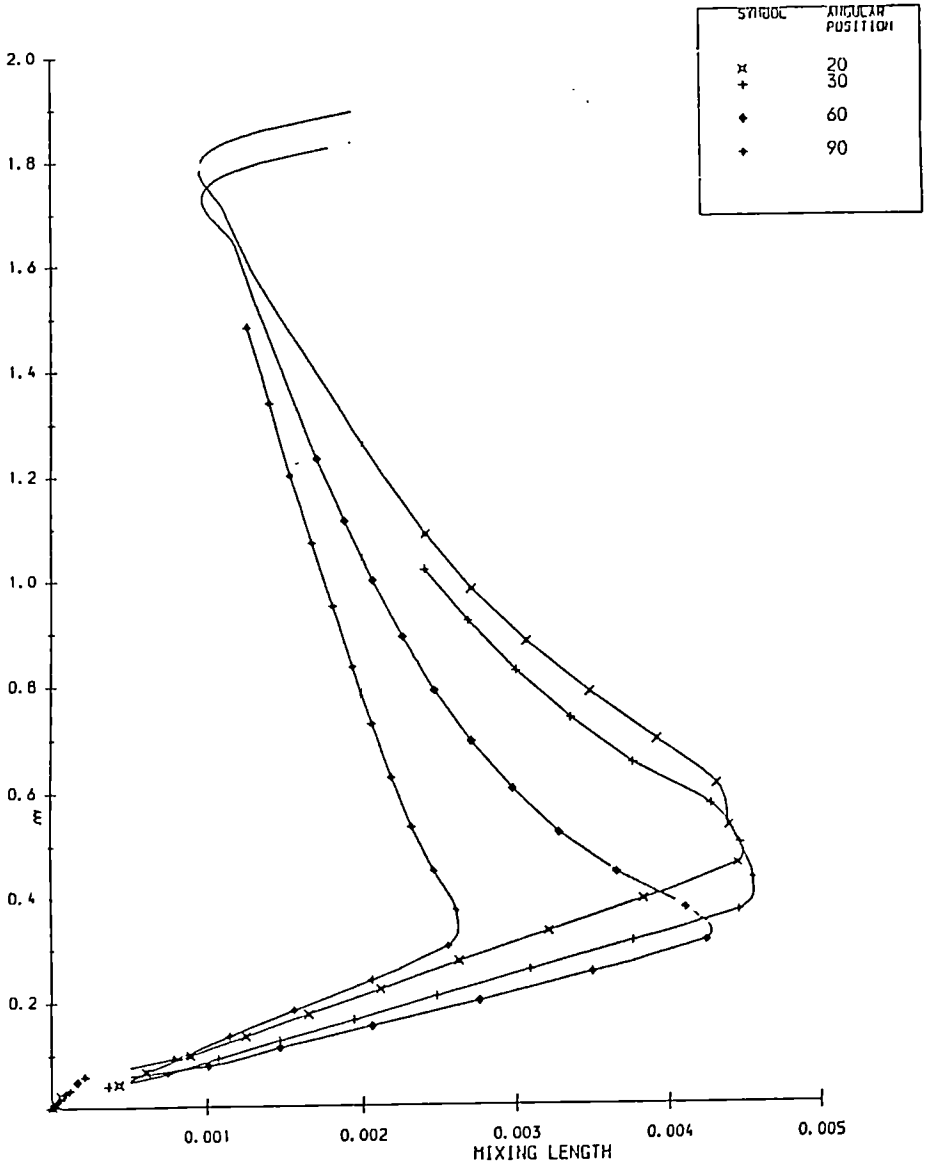

Mixing Lengths - PHOENICS Predictions
M-L - S/L C. & DIV.

Fig. 7.19

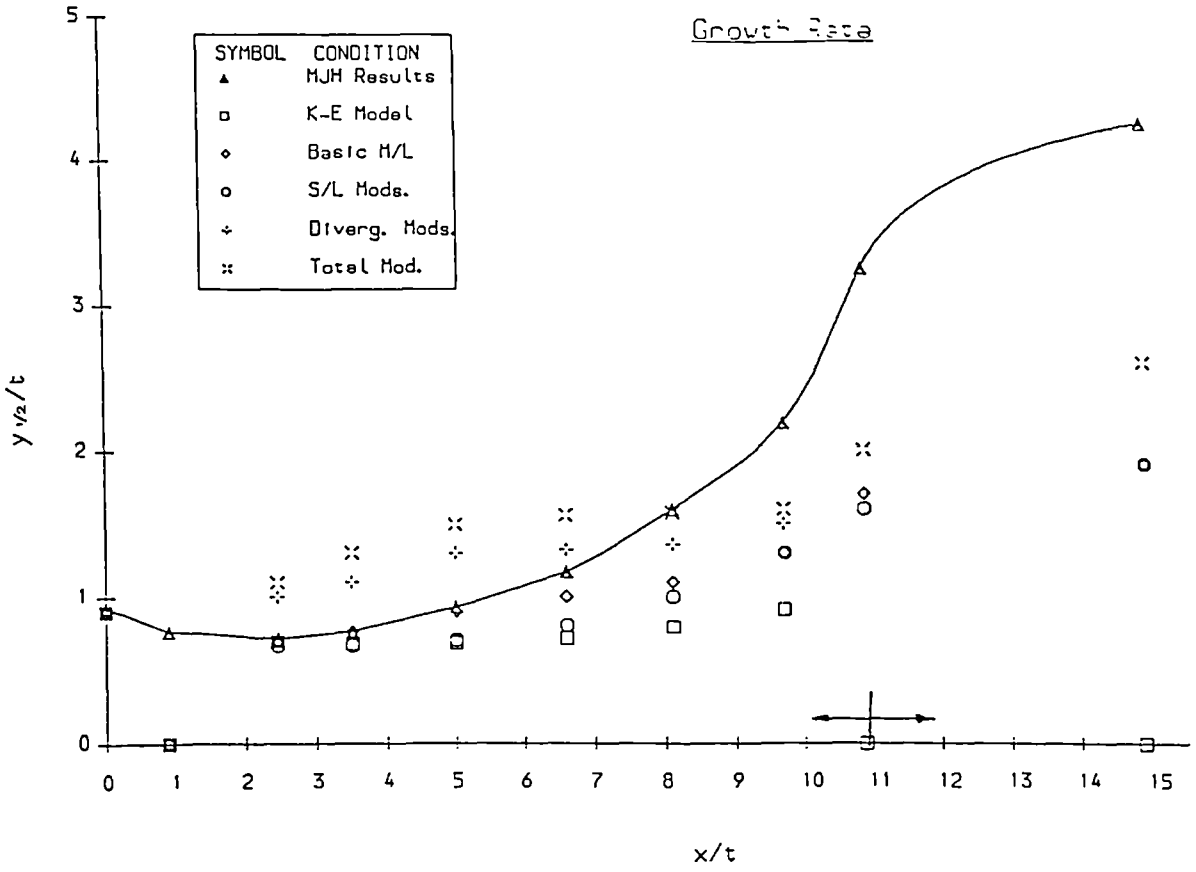

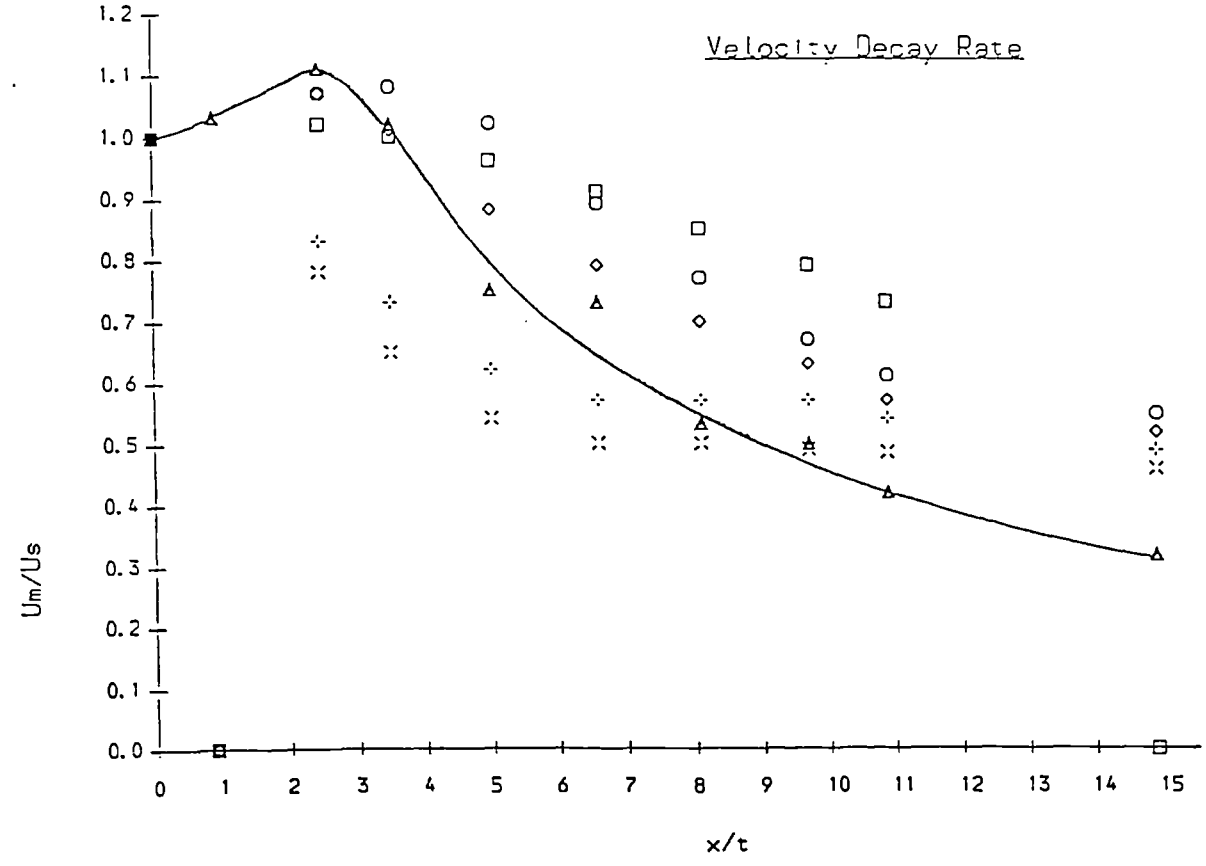

Fig. 7.20 Coanda Jet Growth & Velocity Decay Rates

1. Calculate Distances From Coordinates Y,Z
   $D = \sqrt{Y^2 + Z^2}$

2. M1 = 0.41 * D

3. Jet Width Calculation
   V = 0.995 * Ujet
   VDIF = U(1,1) - U(1,NY)

   IY = 1, NY-1

   WP = U(1,IY) YP = Y(1,IY)
   WN = U(1,IY+1) YN = Y(1,IY+1)

IF VDIF < 0 AND WN ≥ V ≥ WP
OR VDIF ≥ 0 AND WP ≥ V ≥ WN

NO

YES

$$Xratio = \frac{V - WP}{WN - WP}$$

Yratio = 1 - Xratio

WID = (Yratio * YP) + (Xratio * YN)

WIDTH = MAX OF WID AND 0.0
WIDTH = MIN OF WIDTH AND D(1,NY)

4. M2 = 0.09 * WIDTH

5. MODIFICATION CALCULATIONS - EVALUATE CORRECTION FACTORS
   (a) Divergence XD Equation 7.4
      Limits set - if XD < 1.0 XD = 1.0
                   if XD ≥ 5.0 XD = 5.0
   (b) Streamline Curvature XS Equation 7.1
      Limit set - if XS < 0.0 XS = 1.0
   (c) Combined Effects XD + XS

6. MIXING LENGTH = MIN OF M1 AND M2

7. APPLY CORRECTION FACTORS XD, XS or (XD+XS)

Fig. 7.21 Special GROUND Calculation Steps

CHAPTER 8

DISCUSSION

8.1 INTRODUCTION

The present work was envisaged to use to the full the potential of LDA to monitor turbulent velocity fluctuations and, hence, acquire an understanding of curved jet velocity distribution and shear stress components. There are few instances where such detailed turbulence measurements have been obtained. In the present work a particular case was studied in depth experimentally with a view to providing more definitive data than has hitherto been available.

8.2 LDA BIAS STUDIES

The whole field of bias errors associated with LDA data remains a contentious topic, with little agreement over the existence of individual errors or effective correction techniques. Petrie et al (1988) note that the decision on how, or whether, to correct for bias effects is not trivial; it requires careful consideration of the many factors involved, as well as close examination of the results from each individual system.

An evaluation of the effect of biases and the effectiveness of, or need for, any corrective actions was considered essential to these LDV studies because of the controversial nature of the bias problem and the potential affects on the results. Without such an effort, systematic uncertainties and unanswered questions would exist regarding the quality and accuracy of the experimental results.

The experiments on the subsystems indicated the existence of low frequency components in the sudden expansion flowfield. Repeated experiments showed unaccountable data variations were collected when the beam crossover was located in a Perspex block; this may perhaps be due to a lower level of signal to noise ratio in this situation.

Factors considered to influence bias in velocity readings were identified and investigated. The attempts to quantify velocity bias or signal amplitude bias provided inconclusive results. Any trends that exist were effectively masked by the scatter in the data recorded. When operating in a regime that eliminated velocity bias, however, no signal amplitude bias effects were detectable. The lack of any apparent signal amplitude bias may be due to the charateristics of the PM tube employed. These were somewhat different from those of the tubes used by Durao & Whitelaw (1980) in their bias study.

In order to ensure velocity data is recorded in a truly ergodic regime, the acquisition time must be greater than the turbulence persistence time. By fulfilling this condition, arrival rate bias has also been eliminated. In common with many other researchers, this bias study was, unfortunately, unable to provide definitive clarification of the long-running bias controversies. The essential aspect of the initial experiments, however, was to establish operational techniques for this particular LDA system, whereby assurance of bias-free measurement collection could be achieved.

The velocity profiles and turbulence data recorded in the sudden expansion situation agreed well with those of other researchers. The results achieved were especially good considering the relative simplicity of the rig. Greater definition of the flowfield would require a more detailed survey, with a finer measurement grid. It would really need an improved experimental rig

with greater positional accuracy. To eliminate the flare problems encountered when approaching the walls of the tubing one might consider embarking upon the design of a rig incorporating *refractive index matching.* This involves a rig which contains, and also may be surrounded by, fluid of a refractive index tuned to match that of the rig material. This would, however, involve vastly more complex experimental techniques and could only be justified for a detailed survey.

8.3 CURVED JET FLOWS

Because the wall jet has so many important applications in engineering practice, it has received considerable attention from both experimenters and modellers. Launder & Rodi(1981) discovered well over 200 experimental studies published on the turbulent wall jet - half of these, however, looked at heat transfer aspects. Of all the papers only seven concerned detailed study of wall jets on convex walls. Even within these, Launder & Rodi highlighted gaps and inconsistencies in the data reviewed.

For all unstably curved wall shear layers, it was seen from previous studies the necessity of establishing the initial flow conditions as near two-dimensional as possible. Effort was therefore expended in the design and manufacture stages of the Coanda rig to ensure two-dimensionality of the flow. A plenum chamber and a suitable length of feed pipe were incorporated to reduce the propagation of any upstream disturbances. A high quality surface finish was achieved on the slot lip and care was taken to position the assembly within its tank to avoid sidewall effects.

Assessment of the success of these design features in providing flow axisymmetry has been confined to the critical study of the velocity profiles and turbulence data. Launder & Rodi (1983), in their review, did not accept velocity profiles alone as confirmation of two-dimensionality of the flow, but also applied a momentum balance as a test of the data. It was not possible to adopt a similar refinement in this survey due to the absence of any pressure measurements, necessary for the assessment of this axisymmetric curved jet flow.

The results of all the tests to observe flow axisymmetry indicate a high level of conformity. Their quality brings into doubt the potential benefit to be gained from the additional complexity involved in obtaining pressure measurements in this situation. There was no evidence of any periodic variations to indicate the existence of longitudinal vortices, as suggested by Morrison (1982).

The initial experiments involved tuning of the previously validated LDA system to ensure that ergodic sampling was attained and maintained. This was achieved by further use of the windowing circuit, previously validated in the sudden expansion survey. A setting of $10^4 \mu$s for the window length was necessary to provided data repeatable to within the target limit of 2%.

The LDA system proved a robust and versatile arrangement. Full use was made of its versatility in this survey where its design provided a certain degree of data redundancy. The rigorous statistical analysis thus possible for all the curved jet flow measurements, provided confidence intervals for all velocities and higher order data. The results emphasised the high quality of the data obtained with the LDA technique. It was unfortunate that full X-Y and Y-Z traverses were only achievable for the last four angular locations.

It would be beneficial fully to observe the flow during the early stages of the jet's development. The achievement of coincident realigment for the Y-Z traverse proved more difficult then anticipated. Although the results indicate that this drawback was overcome, some redesign of the rig to alleviate this problem would be of use.

The most nearly comparable work is that undertaken by Morrison (1982) - this, however, was carried out in air, and it did not include measurements of all velocity components. The present velocity profiles and turbulence data show similarities to, but also deviations from, the hot-wire anemometry data recorded by Morrison.

Comparison between the present investigation and that of a wall jet on a circular cylinder provides details of the changes occurring in the flow structure. However, conclusions attributing observed effects to either of the extra rates of strain present, or to the changes in these rates of strain, can be tentative only; their effects may well not be additive.

The effect of streamline curvature may be seen by the normal stresses which are up to three times those for a plane wall jet. The levels of normal stress are also much higher than those recorded by Wilson & Golstein (1976) and Dakos et al (1984), thereby indicating the influence of divergence, in addition to streamline curvature. Similar trends are shown by the shear stresses.

The departure from self-preservation for the curved jet flow is readily apparent from the plots of non-dimensionalised radial velocities, shear stresses and the structural parameter, a_1.

8.4 COMPUTER MODELLING

Ultimately, experimental data for mean velocities and turbulence parameters are needed to develop or test turbulence models. The current surveys of a sudden expansion flowfield and a curved jet have provided ideal test material.

8.4.1 Sudden Expansion Flow

The PHOENICS k-ϵ model provided an excellent qualitative picture of the flowfield but fell short of a totally accurate prediction of specific features e.g. the point of reattachment.

8.4.2 Coanda Flare Flow

The present detailed survey of the Coanda flare jet development provided an invaluable database against which to correlate computer models.

The comparison made between the measured data and the modified mixing length model produced by Morrison (1982) revealed satisfactory agreement, considering the fairly crude initial assumptions that had been made and the complexity of the real life flow. The streamline curvature and divergence constants had been tuned individually and the simple addition of their effects on the shear stress proved reasonable.

The k-ϵ model in PHOENICS produced a prediction which significantly underestimated the spreading rate of the jet.

The initial attempts at using modifications applied to mixing-length models within PHOENICS produced good results. Although there are obvious

deficiencies, the modelling work indicates the potential of this relatively simple model to be 'tuned' to predict a specific, and complex, curved jet flow situation.

Superior agreement to that of the turbulence model produced by Morrison has already been achieved. Further refinement of the calculation grid is likely to result in significant improvements. Benefits would also be obtained from the incorporation of more precise calculations for the jet width.

Major theoretical work would be required to obtain modification factors applicable to the k-ε model. It is debatable whether this would be the most profitable route of research. A preferable alternative may well be to embark upon the use of higher order models. Their greater sophistication would preclude the neccessity of making assumptions and approximations for physical features such as streamline curvature and divergence.

CHAPTER 9
CONCLUSIONS AND RECOMMENDATIONS

9.1 CONCLUSIONS

1. A systematic survey to identify sources of error and bias in LDA hardware and operating system has been performed.

The prime limitation on repeatability of data was found to be sampling mode. To ensure ergodic sampling of data, sample periods had to be long by comparison with the lowest frequency present in the system.

All other sources of error and bias were eliminated or were negligible for the present system.

2. Plots of velocity and turbulence intensities obtained for a sudden expansion situation confirmed the validity of the technique adopted.

3. Initial tuning was required for data acquisition for the Coanda flare flowfield. An extensive survey of the Coanda flare flowfield was performed. Velocity and turbulence data were recorded.

Redundancy of data enabled a rigorous error analysis to be undertaken. The results vindicated the LDA hardware and acquisition procedure, confirming the quality of the data.

4. Entrainment rates of three times slot mass flowrate were calculated.

5. Computer modelling was performed of both the sudden expansion and the Coanda flare flow situations and a comparative study of results was effected. The PHOENICS computer package proved to be a versatile tool. Reasonable agreement of the sudden expansion situation was obtained with a basic k-ε model.

Neither the k-ε nor mixing-length model produced very good results for the Coanda situation. Modifications introduced to the latter, however, indicated the potential of PHOENICS to be tuned to a specific situation.

9.2 FUTURE WORK

1. A more suitable rig for studying arrival rate and velocity bias effects may be a pipe of channel flow through a gauze followed by a series of small bars. This should produce high levels of turbulence intensity without the low frequency components seen in the sudden expansion situation.

2. Additional data should be attained with the present Coanda flare rig, especially X-Y plane traverses between 5° and 20°.

3. The limitation on full 3-D traverses for angular locations below 75° was beam impingement on the feed tube harware. The plenum chamber and inlet pipe could be redesigned to lie behind the body of the flare. This would not only provide greater access but should result in an improvement in the initial, slot velocity profile.

4. Since the LDA data acquisition system has proved so successful, it would be of benefit to apply it to a number of flow situations. Of immediate interest might be flow in two-dimensional models of simple convex and concave curvature, the draft designs of which have been prepared.

5. For future LDA systems, recent innovations such as BSA should be evaluated for inclusion.

6. Much interesting additional work on modelling of the flowfields remains to be studied. Among other potentially profitable routes of enquiry, refinement of the present Coanda grid and reassessment of the correction factors applied to the mixing-length model are recommended.

7. More work should be directed towards studying the modifications applied to the mixing-length model. Assumptions to simulate the physical situation and an alternative to their direct addition could improve this relatively simple model.

8. Other areas for computing investigations should involve the use of higher order models.

REFERENCES

Adams, E.W. & Eaton, J.K. (1985) *An LDA Study Of The Backward-Facing Step Flow, Including The Effects Of Velocity Bias* Proceedings of International Symposium On LA, ASME WAM, FED-Vol. 33, Florida

Alcaraz, E. ,Charnay, G. & Mathieu, J. (1977) *Measurements In A Wall Jet Over A Convex Surface* Physics Fluids 20,203

Bakke, P. (1957) *Experimental Investigation Of A Wall Jet* J.Fl.Mech.,2,467

Barnett, D.O. & Bentley, H.T. (1974)*Statistical Bias Of Individual Realisation Laser Velocimetry* 2nd. International Workshop On LV, Purdue University

Bogard, D.G. & Tiederman, W.G. (1978)*Experimental Evaluation Of Sampling Bias In Naturally Seeded Flows* Hemisphere Publishing Corp.

Bradshaw, P., Cebici, T. & Whitelaw, J.H. (1981) *Engineering Calculation Methods For Turbulent Flow* Academic Press, London

Bradshaw, P. & Ferris, D.H. (1971) *Calculation Of Boundary Layer Development Using The Turbulent Energy Equation : Compressible Flow On Adiabatic Walls* J.Fl.Mech., 46

Bradshaw, P. & Gee, M.T. (1960) *Turbulent Wall Jets With & Without An External Stream* A.R.C. R & M 3252

Bradshaw, P., Ferris, D.H. & Atwell, N.P. (1967) *Calculation Of Boundary Layer Development Using The Turbulent Energy Equation* J. Fl. Mech., 28,593

Bradshaw, P. (1971) *An Introduction To Turbulence And Its Measurement* Pergamon Press, 2nd. Ed.

Bradshaw, P. (1972) *The Understanding And Prediction Of Turbulent Flow* Aero. J. 76,403

Bradshaw, P. (1973) *Effects Of Streamline Curvature On Turbulent Flow* AGARDograph No. 169

Buchhave, P. (1975) *Biasing Error In Individual Particle Measurements With The LDA-Counter Signal Processor* Proceedings Of The LDA-Symposium, Copenhagen

Buchhave, P. (1979) *Measurements Of Turbulence With The Burst-Type LDA* Report TRL-196, Turbulence Research Laboratory, State University Of N.Y., Buffalo

Buchhave, P. & George, W.K. (1978) *Bias Corrections In Turbulence Measurements By The LDA* Hemisphere Publ. Corp.

Castro, I.P. & Bradshaw, P. (1976) *The Turbulent Structure Of A Highly Curved Mixing Layer* J.Fl.Mech., 73

Catalano, G.D., Morton, J.B. & Humphriss, R.R. (1977) *An Experimental Investigation Of A Three-Dimensional Wall Jet* AIAA 15,1146

Cebici, T. & Smith, A.M.O. (1974) *Analysis Of Turbulent Boundary Layers* Academic Press, London

Chatfield, C. (1980) *The Analysis Of Time Series* Chapman & Hall

Chow, C-Y (1979) *An Introduction To Computational Fluid Mechanics* Wiley, New York

Craig, R.R., Nejad, A.S., Hahn, E.Y., & Schwartzkopf, K.G. (1984) *A General Approach For Obtaining Unbiased LDV Data In Highly Turbulent Non-Reacting And Reacting Flows* AIAA-84-0366, AIAA 22nd. Aerospace Sciences Meeting, Reno, Nevada

Dakos, T., Verriopoulos, C.A. & Gibson, M.M. (1984) *Turbulent Flow With Heat Transfer In Plane And Curved Wall Jets* J.Fl.Mech., 145,339

Davies, J.T. (1972) *Turbulence Phenomenon* Academic Press

DISA *DISA 55L90a LDA Counter Processor, Service Manual, Circuit Boards And Diagrams And Instruction Manual* DANTEC Documentation Dept., Scientific Research Division

Donaldson, C. duP. & Sullivan, R.D. (1972) *An Invariant Second-Order Closure Model Of The Compressible Turbulent Boundary Layer On A Flat Plate* ARAP Inc. Rep. 178

Drain, L.E. (1980) *The Laser Doppler Technique* J.Wiley & Sons

Durao, D.F.G., & Whitelaw, J.H. (1975) *The Influence Of Sampling Procedures On Velocity Bias In Turbulent Flows* Proceedings Of The LDA-Symposium, Copenhagen

Durao, D.F.G., & Whitelaw, J.H. (1979) *Relationship Between Velocity Ans Signal Quality In LDA* J.Phys.E.: Sci. Inst., Vol. 12

Durao, D.F.G., Laker, J., & Whitelaw, J.H. (1980) *Bias Effects In LDA* J.Phys.E.: Sci. Inst., Vol.13

Durao, D.F.G., Founti, M.A., Laker, J., Pita, G., Velho, A. & Whitelaw, J.H. (1982) *Some Consequences Of Bias Effects In LDA* Proceedings of The First International Symposium on Applications of LA to Fluid Mechanics, Lisbon, Portugal

Durst, F., Melling, A. & Whitelaw, J.H. (1981) *Principles & Practice Of LDA* Academic Press, 2nd.Ed.

Durst, F. & Zare, M. (1972) *Removal Of Pedestals And Directional Ambiguity Of Optical Anemometry Signals* App. Optics, Vol.13, No. 11

Edwards, R.V. (1981) *A New Look At Particle Statistics In LA Measurements* J.Fl.Mech., Vol.105

Edwards, R.V. (1987) *Report Of The Special Panel On Statistical Particle Bias Problems In Laser Anemometry* J. Fluids Eng., Vol.109

Edwards, R.V. & Jensen, A.S. (1983) *Particle-Sampling Statistics In L.A.* J.Fluid Mech., Vol.133

Erdmann, J.C., & Tropea, C.D. (1982) *Statistical Bias Of The Velocity Distribution Function In LA* Proceedings Of International Symposium On Applications Of LA To Fluid Mechanics, Lisbon

Fekete, G.I. (1963) *Coanda Flow Of A Two-Dimensional Wall Jet On The Outside Of A Circular Cylinder* McGill Univ. MERL Rep. No. 63-11

Fernholz, H.H. (1971) *Deflection Of Free Jets At Convexly Curved Walls (Coanda Effect)* Can. NRC-TT-1504

Freeman, A.R. (1975) *Laser Anemometer Measurements In The Recirculating Region Downstream Of A Sudden Pipe Expansion* Proceedings of the LDA Symposium, Copenhagen

George, W.K. (1975) *Limitations To Measuring Accuracy Inherent In The Laser Doppler Signal* Proceedings Of The LDA Symposium, Copenhagen

Gibson, M.M. & Rodi, W. (1981) *A Reynolds-Stress Closure Model Of Turbulence Applied To The Calculation Of A Highly Curved Mixing Layer* J. Fl. Mech., Vol.103, 161

Giel, T.V. & Barnett, D.O. (1978) *Analytical & Experimental Study Of Statistical Bias In L.V.* L.V. & Particle Sizing, Hemisphere Publishing Corp.

Gilchrist, A.R. (1985) *The Development & Breakaway Of A Compressible Air Jet With Streamline Curvature & Its Application To The Coanda*

Flare PhD Thesis, Durham University

Gillis, J.C., Johnston, J.P., Kays, W.M. & Moffat, R.J. (1981) *Turbulent Boundary Layer On A Convex Curved Surface* NASA CR 3391

Glauert, M.B. (1956) *The Wall Jet* J. Fl. Mech., 1, 625

Gould, R.D., Stevenson, W.H., & Thompson, H.D. (1988) *A Parametric Study Of Statistical Bias In LDV* To Be Published, AIAA

Gregory-Smith, D.G. & Robinson, C.J. (1982) *The Discharge From A Thin Slot Over A Surface Of Convex Curvature* Int. J. Heat Mass Transfer, Vol. 24

Guitton, D.E. (1970) *Some Contributions To The Study Of Equilibrium & Non-Equilibrium Wall Jets Over Curved Surfaces* Ph.D. Thesis, McGill Univ., Montreal

Guitton, D.E. & Newman, B.G. (1977) *Self-Preserving Turbulent Wall Jets Over Convex Surfaces* J.Fl.Mech., 81, 155

Hanjalic, K. & Launder, B.E. (1972) *A Reynolds Stress Model Of Turbulence And Its Application To Thin Shear Flows* J. Fl. Mechs., 52, 609

Hartis, G. & King, C.F. (1983) *An Optical System For LDV* Colloquium On LDA Counter System Applications, Durham University

Hartis, G. & King, C.F. (1983) *Data Collection From A Counter Based LDA Used In A Time-Varying Swirling Flow* Colloquium On LDA Counter System Applicatins, Durham University

Hawkins, M.J. & King, C.F. (1987) *LDA Studies In A Sudden Expansion Water Flowrig* Proceedings of The International Conference on LA Advances & Applications, Strathclyde, Paper 28

Head, M.R. (1960) *Entrainment In The Turbulent Boundary Layer* ARC R & M 3152

Hinze, J.O. (1975) *Turbulence* McGraw-Hill, 2nd. Ed.

Hoesel, W. & Rodi, W. (1977) *New Biasing Elimination Method For LDV Counter Processing* Rev. Sci. Inst., Vol. 48, No. 7

Hong, S.K. & Murthy, S.N.B. (1986) *Effective Velocity Of Transport In Curved Wall Boundary Layers* AIAA, Vol.24, No.3

Irwin, H.P.A. (1973) *Measurements In A Self-Preserving Plane Wall Jet In A Positive Pressure Gradient* J. Fl. Mech., 61, 33

Irwin, H.P.A. & Smith, P.A. (1975) *Prediction Of The Effect Of Streamline Curvature On Turbulence* Physics Fluids, 18, 624

Johnson, D.A. Modarress, D. & Owen, F. (1984) *An Experimental Verification Of Laser-Velocimeter Sampling Bias And Its Correction* J. Fluids Eng.,Vol.106

King, C.F. (1983) *Elimination Of Arrival Rate Bias In LDA Counter Systems* Colloquium On LDA Counter Sytem Applications, Durham University

King, C.F. & Watson, S. (1985) *A Hardware Windowing Circuit For LDA In Periodic & Aperiodic Flows* International Conference On LA, Manchester

Kline, S.J., Morkovin, M.V., Sovran, G. & Cockrell, D.G. (1969) Proceedings of Computational Turbulent Boundary Layers, 1968 AFOSR-IFP-Stanford Conference, Stanford University, California

Lading, L. (1987) *Spectrum Analysis Of LDA Signals* Dantec Information, Measurement And Analysis, Vol. 5

Launder, B.E., Reece, G. & Rodi, W. (1975) *Progress In The Development Of A Reynolds Stress Turbulence Closure* J. Fl. Mech., 68, 537

Launder, B.E. & Rodi, W. (1981) *The Turbulent Wall Jet* Prog. Aerospace Sci., Vol. 19, Pergamon Press Ltd.

Launder, B.E. & Rodi, W. (1983) *Turbulent Wall Jet - Measurements & Modelling* Ann. Rev. Fl. Mech.

Launder, B.E. & Spalding, D.B. (1972) *Lectures In Mathematical Models Of Turbulence* Academic Press, London

Launder, B.E. & Spalding, D.B. (1974) *The Numerical Computation Of Turbulent Flows* Comp. Methods Appl. Mech. & Eng., 3, 269

Love, E.S., Grigsby, C.E., Lee, L.P. & Woodling, M.J. (1959) *Experimental & Theoretical Studies Of Axisymmetric Free Jets* NASA Tech. Report, R-6

McDougall, T.J. (1980) *Bias Correction For Individual Realisation LDA Measurements* J.Phys.E.:Sci. Inst., Vol. 13

McLaughlin, D.K. & Tiederman, W.G. (1973) *Biasing Correction For Individual Realisation LA Measurements In Turbulent Flows* Physics Of Fluids, Vol.16 No.2

Mellor, G.L. & Herring, H.J. (1973) *A Survey Of The Mean Turbulent Field Closure Models* AIAA J., 11, 590

Meroney, R.N. & Bradshaw, P. (1975) *Turbulent Boundary Layer Growth Over A Longitudinally Curved Surface* AIAA J., 13, 1448

Morrison, J.F. (1982) *Axisymmetric Wall Jet With Streamline Curvature* PhD Thesis, Durham University

Nagano, Y. & Hishida, M. (1987) *Improved Form Of The k-e Model For Wall Turbulent Shear Flows* J.Fl.Eng., 109

Newman, B.G. (1961) *Deflexion Of Plane Jets By Adjacent Boundaries - Coanda Effect* B.L. Theory & Flow Control, Ed. Zachmann C.V., Pergamon Press

Newman, B.G. (1969) *The Prediction Of Turbulent Jets & Wall Jets* Can. Aeronaut. J., 15, 288

Ng, K.H. & Spalding, D.B. (1970) *Predictions Of Two- Dimensional Boundary Layers On Smooth Walls With A Two-Equation Model Of Turbulence* Imperial College, Mechanical Engineering Department Report BL/TN/A/25

Patankar, S.V. & Spalding, D.B. (1970) *Heat And Mass Transfer In Boundary Layers* Intertext Books London, 2nd. Ed.

Petrie, H.L., Samimy, M. & Addy, A.L. (1988) *LD Velocity Bias In Separated Turbulent Flows* Expts. In Fl., Vol. 6

Ramaprian, B.R. & Shivaprasad, B.G. (1977) *Mean Flow Measurements In Turbulent Boundary Layers Along Mildly Curved Surfaces* AIAA, Vol.15

Rayleigh (1916) *On The Dynamics Of Revolving Fluids* Proc. Royal Soc. Series A, 113, 148

Reynolds, O. (1870) *Suspension Of A Ball By A Jet Of Fluid* Proc. Man. Lit. Phil. Soc., 9, 114 & 133

Reynolds, W.C. (1976) *Computation Of Turbulent Flows* Ann. Rev. Fluid Mech., 8, 183

Roesler, T.C., Stevenson, W.H. & Thompson, H.D. (1980) *Investigation Of Bias Errors In LDV Measurements* AFWAL-TR-80-2105

Ruck, B. & Durst, F. (1982) *Influence Of Signal Detection & Signal Processing Electronics On Mean Property Measurements Of LDA Frequencies* Proceedings of The First International Symposium on Applications of LA To Fluid Mechanics, Lisbon, Portugal

Sawyer, R.A. (1963) *Two-Dimensional Reattaching Jet Flows Including The Effects Of Curvature On Entrainment* J.Fl.Mechs., 17

Schlichting, H. (1979) *Boundary-Layer Theory* 7th. Edition, McGraw-Hill Book Co., New York

Schwarz, W.H. & Cosart, W.P. (1960) *Two-Dimensional Turbulent Wall Jet* J.Fl.Mech., 10

Sharma, R.N. (1981) *Experimental Investigation Of Conical Wall Jets* AIAA J., 19

Shivaprasad, B.G. & Ramaprian, B.R. (1978) *Turbulent Measurements In Boundary Layers Along Mildly Curved Surfaces* J.Fluids Eng.,Vol. 100

Simpson, C.J. (1985) *An Investigation Of Velocity Bias In LDA* Durham University Final Year Report

Smith, P.A. (1973) PhD Thesis, McGill University

Smits, A.J., Young, S.T.B. & Bradshaw, P. (1979a) *The Effect Of Short Regions Of High Surface Curvature On Turbulent Boundary Layers* J.Fl. Mechs., 94, 209

Smits, A.J., Eaton, J.A., & Bradshaw, P. (1979b) *The Response Of A Turbulent Boundary Layer To Lateral Divergence* J.Fl.Mech., 94

So, R.M.C. & Mellor, G.L. (1972) *An Experimental Investigation Of Turbulent Boundary Layers Along Curved Surfaces* NASA CR-1940

Starr, J.B. & Sparrow, E.M. (1967) *Experiments On A Turbulent Cylindrical Wall Jet* J.Fl.Mech., 29

Stevenson, W.H., Thompson, H.D. & Craig, R.R. (1984) *Laser Velocimeter Measurements In Highly Turbulent Recirculating Flows* J.Fl.Eng., Vol. 106

Stevenson, W.H., Thompson, H.D. & Roesler, T.C. (1982) *Direct Measurement Of LV Bias In A Turbulent Flow* AIAA Vol.20,No.12

Szczepura, R. (1985) *Flow Characteristics Of An Axisymmetric Sudden Pipe Expansion : Results Obtained From The Turbulence Studies Rig. Part 1 Mean And Turbulence Velocity Results* CEGB Report No. TPRD/B/0702/N85

Szczepura, R. (1986) *Flow Characteristics Of An Axisymmetric Sudden Pipe Expansion : Results Obtained From The Turbulence Studies Rig. Part 2 Spectral Measurements* CEGB Report No. TPRD/B/0703/R86

Thompson, H.D. & Flack, R.D. (1976) *An Application Of LV To The Interpretation Of Turbulent Structure* Proceedings Of ISL/AGARD Workshop On LA, St.-Louis, France

Titcombe, C.G. (1980) *Mathematical Model Of Coanda Flares* Unpublished report, B.P. Research Centre, Sunbury-on-Thames

Townsend, A.A. (1961) *Equilibrium Layers & Wall Turbulence* J. Fl. Mechs., 11, 97

Townsend, A.A. (1976) *The Structure Of Turbulent Shear Flow* Cambridge University Press, 2nd. Edition

Wang, J.C.F. (1975) *Measurement Accuracy Of Flow Velocity Via A Digital-Frequency-Counter Laser Velocimetry Processor* LDA Symposium Proceedings, Copenhagen

Wille, R. & Fernholz, H. (1956) *Report On The First European Mechanics Colloquium On The Coanda Effect* J. Fl. Mechs., 23, 801

Wilson, D.J. & Goldstein, R.J. (1976) *Turbulent Wall Jets With Cylindrical Streamwise Surface Curvature* J. Fl. Eng., Trans ASME, 98, 550

Wright, A. (1984) *Statistical Analysis Of Turbulent Velocities* Internal Report, Durham University

Young, T. (1800) *Outlines Of Experiments & Inquiries Respecting Sound & Light* J. Royal Soc., 61, 157